Doctoral Thesis: Massive MIMO in Real Propagation Environments

Gao, Xiang

2016

Document Version:
Publisher's PDF, also known as Version of record

Massive MIMO in Real Propagation Environments

—

Xiang Gao

Lund 2016

Department of Electrical and Information Technology
Lund University
Box 118, SE-221 00 LUND
SWEDEN

This thesis is set in Computer Modern 10pt
with the LaTeX Documentation System

Series of licentiate and doctoral theses
ISSN 1654-790X; No. 80
ISBN 978-91-7623-646-8 (print)
ISBN 978-91-7623-647-5 (digital)

Printed in Sweden by *Tryckeriet i E-huset*, Lund.
January 2016.

Abstract

Mobile communications are now evolving towards the fifth generation (5G). In the near future, we expect an explosive increase in the number of connected devices, such as phones, tablets, sensors, connected vehicles and so on. Much higher data rates than in today's 4G systems are required. In the 5G visions, better coverage in remote regions is also included, aiming for bringing the current "4 billion unconnected" population into the online world. There is also a great interest in "green communications", for less energy consumption in the ICT (information and communication technology) industry.

Massive MIMO is a potential technology to fulfill the requirements and visions. By equipping a base station with a large number, say tens to hundreds, of antennas, many terminals can be served in the same time-frequency resource without severe inter-user interference. Through "aggressive" spatial multiplexing, higher data rates can be achieved without increasing the required spectrum. Processing efforts can be made at the base station side, allowing terminals to have simple and cheap hardware. By exploiting the many spatial degrees of freedom, linear precoding/detection schemes can be used to achieve near-optimal performance. The large number of antennas also brings the advantage of large array gain, resulting in an increase in received signal strength. Better coverage is thus achieved. On the other hand, transmit power from base stations and terminals can be scaled down to pursue energy efficiency.

In the last five years, a lot of theoretical studies have been done, showing the extraordinary advantages of massive MIMO. However, the investigations are mainly based on theoretical channels with independent and identically distributed (i.i.d.) Gaussian coefficients, and sometimes assuming unlimited number of antennas. When bringing this new technology from theory to practice, it is important to understand massive MIMO behavior in real propagation channels using practical antenna arrays. Not much has been known about real massive MIMO channels, and whether the claims about massive MIMO still hold there, until the studies in this thesis were done.

The thesis study connects the "ideal" world of theory to the "non-ideal"

reality. Channel measurements for massive MIMO in the 2.6 GHz band were performed, in different propagation environments and using different types of antenna arrays. Based on obtained real-life channel data, the studies include

- channel characterization to identify important massive MIMO properties,
- evaluation of propagation conditions in real channels and corresponding massive MIMO performance,
- channel modeling for massive MIMO to capture the identified channel properties, and
- reduction of massive MIMO hardware complexity through antenna selection.

The investigations in the thesis conclude that massive MIMO works efficiently in real propagation environments. The theoretical advantages, as observed in i.i.d. Rayleigh channels, can also be harvested in real channels. Important propagation effects are identified for massive MIMO scenarios, including channel variations over large arrays, multipath-component (MPC) lifetime, and 3D propagation. These propagation properties are modeled and included into the COST 2100 MIMO channel model as an extension for massive MIMO. The study on antenna selection shows that characteristics in real channels allow for significant reductions of massive MIMO complexity without significant performance loss.

As one of the world's first research work on massive MIMO behavior in real propagation channels, the studies in this thesis promote massive MIMO as a practical technology for future communication systems.

Preface

This thesis concludes my work as a Ph.D. student, and is comprised of two parts. The first part gives an overview of the research field in which I have been working during my Ph.D. study and a brief summary of my contribution in it. The second part is composed of six included papers that constitute my main scientific work:

[1] X. Gao, O. Edfors, F. Rusek, F. Tufvesson, "Linear Precoding Performance in Measured Very-Large MIMO Channels," in *Proc. IEEE Vehicular Technology Conference (VTC Fall)*, San Francisco, California, U.S., Sept. 2011.

[2] X. Gao, O. Edfors, F. Rusek, F. Tufvesson, "Massive MIMO Performance Evaluation Based on Measured Propagation Data," in *IEEE Transactions on Wireless Communications*, vol. 14, no. 7, pp. 3899-3911, July 2015.

[3] J. Flordelis, X. Gao, G. Dahman, F. Rusek, O. Edfors, F. Tufvesson, "Spatial Separation of Closely-Spaced Users in Measured Massive Multi-User MIMO Channels," in *Proc. IEEE International Conference on Communications (ICC)*, London, UK, June 2015.

[4] X. Gao, F. Tufvesson, O. Edfors, "Massive MIMO Channels – Measurements and Models," in *Proc. Asilomar Conference on Signals, Systems, and Computers (ASILOMAR)*, Pacific Grove, California, U.S., Nov. 2013.

[5] X. Gao, J. Flordelis, G. Dahman, F. Tufvesson, O. Edfors, "Massive MIMO Channel Modeling – the COST 2100 Extension," Updated version of TD(15)W1025 in *European Cooperation in Science and Technology (COST) Action IC1004*, Barcelona, Spain, Oct. 2015.

[6] X. Gao, O. Edfors, F. Tufvesson, E. G. Larsson, "Massive MIMO in Real Propagation Environments: Do All Antennas Contribute Equally," in *IEEE Transactions on Communications*, vol. 63, no. 11, pp. 3917-3928, Nov. 2015.

During my Ph.D. study, I have also contributed to the following publications. However, these publications are not included in the thesis:

[7] X. Gao, A. Alayon Glazunov, J. Weng, C. Fang, J. Zhang, F. Tufvesson, "Channel Measurement and Characterization of Interference Between Residential Femto-Cell Systems," in *Proc. European Conference on Antennas and Propagation (EuCAP)*, Rome, Italy, Apr. 2011.

[8] X. Gao, B. K. Lau, X. Wang, T. Bolin, "On Simplifying WINNER II Channel Model for MIMO OTA Performance Evaluation," in *Proc. European Conference on Antennas and Propagation (EuCAP)*, Rome, Italy, Apr. 2011.

[9] X. Gao, F. Tufvesson, O. Edfors, F. Rusek, "Measured Propagation Characteristics for Very-Large MIMO at 2.6 GHz," in *Proc. Asilomar Conference on Signals, Systems, and Computers (ASILOMAR)*, Pacific Grove, California, U.S., Nov. 2012.

[10] X. Gao, O. Edfors, J. Liu, F. Tufvesson, "Antenna Selection in Measured Massive MIMO Channels Using Convex Optimization," in *Proc. IEEE Global Communications Conference (GLOBECOM) Workshop on Emerging Technologies for LTE-Advanced and Beyond-4G*, Atlanta, Georgia, U.S., Dec. 2013.

[11] X. Gao, M. Zhu, F. Rusek, F. Tufvesson, O. Edfors, "Large Antenna Array and Propagation Environment Interaction," in *Proc. Asilomar Conference on Signals, Systems, and Computers (ASILOMAR)*, Pacific Grove, California, U.S., Nov. 2014.

[12] X. Gao, O. Edfors, F. Tufvesson, E. G. Larsson, "Multi-Switch for Antenna Selection in Massive MIMO," in *Proc. IEEE Global Communications Conference (GLOBECOM)*, San Diego, California, U.S., Dec. 2015.

[13] Z. Zhou, X. Gao, J. Fang, Z. Chen, "Spherical Wave Channel and Analysis for Large Linear Array in LoS Conditions," in *Proc. IEEE Global Communications Conference (GLOBECOM) Workshop on Massive MIMO: From Theory to Practice*, San Diego, California, U.S., Dec. 2015.

Furthermore, I have contributed to the following Temporary Documents (TDs) in the European Cooperation in Science and Technology (COST) Action IC1004 on Cooperative Radio Communications for Green Smart Environments:

[14] X. Gao, O. Edfors, F. Rusek, F. Tufvesson, "Linear Precoding Performance in Measured Very-Large MIMO Channels," TD(11)01047 in *COST IC1004*, Lund, Sweden, June 2011.

[15] X. Gao, F. Tufvesson, O. Edfors, F. Rusek, "Channel Behavior for Very-Large MIMO Systems – Initial Characterization," TD(12)05075 in *COST IC1004*, Bristol, UK, Sept. 2012.

[16] X. Gao, F. Tufvesson, O. Edfors, F. Rusek, "Measured Propagation Characteristics for Very-Large MIMO at 2.6 GHz," TD(13)06060 in *COST IC1004*, Malaga, Spain, Feb. 2013.

[17] X. Gao, M. Zhu, F. Tufvesson, F. Rusek, O. Edfors, "Extension of the COST 2100 Channel Model for Massive MIMO," TD(15)12083 in *COST IC1004*, Dublin, Ireland, Jan. 2015.

[18] J. Flordelis, X. Gao, G. Dahman, O. Edfors, F. Tufvesson, "Initial Characterization of Massive Multi-User MIMO Channels at 2.6 GHz in Indoor and Outdoor Environments," TD(15)W1023 in *COST IC1004*, Barcelona, Spain, Oct. 2015.

Besides, I have also contributed to the following deliverables for the EU project MAMMOET – Massive MIMO for Efficient Transmission (http://mammoet-project.eu/):

[19] "MaMi Channel Characteristics: Measurement Results", Technical Report, MAMMOET D1.2 V1.0, June 2015.

[20] "MaMi Channel Characteristics: MAMMOET Channel", Technical Report, MAMMOET D1.3 V1.0, June 2015.

Acknowledgements

Here I take the opportunity to express my very sincere thanks to my teachers, colleagues, family and friends.

First and foremost, I would like to thank my doctoral supervisor and co-supervisors – Prof. Ove Edfors, Prof. Fredrik Tufvesson, Prof. Fredrik Rusek and Prof. Buon Kiong Lau, for all the helpful discussions and guidance during my Ph.D. study. Special thanks to Ove Edfors and Fredrik Tufvesson, who guided me step by step into the research area and advised me with their expertise and insights. From them I have learnt many things, not only professional knowledge, but also methodologies of scientific research as well as analytical and critical thinkings. All these, for sure, will benefit me throughout my life and career.

I would like to thank my colleagues in the Communication Engineering Group, some of whom have left Lund University but still own my gratefulness. This includes but is not limited to: Jose Flordelis, Dr. Ghassan Dahman, Dr. Zhu Meifang, Dr. Li Hui, Dr. Carl Gustafson, Dr. Taimoor Abbas, Dr. Rohit Chandra, Muhammad Atif Yaqoob, Nafiseh Seyed Mazloum, Joao Vieira, Muris Sarajlic, Saeedeh Moloudi, Dimitrios Vlastaras, Dr. Ivaylo Vasilev, Zachary Miers, Hu Sha and Li Xuhong. I am also grateful to my co-authors, including Prof. Erik G. Larsson from Linköping University and Liu Jianan from Ericsson, for the fruitful discussions through emails and phone calls.

I acknowledge the financial support in my research projects, from ELLIIT – an Excellence Center at Linköping-Lund in Information Technology, the Swedish Research Council (VR), the Swedish Foundation for Strategic Research (SSF) and the EU-Project MAMMOET – Massive MIMO for Efficient Transmission.

Further, I would like to thank the teachers in the Networking Group and the Broadband Communication Group, including Prof. Ulf Körner, Prof. Maria Kihl and Jens A Andersson, with whom I had nice experience as a teaching assistant. Also many thanks to Pia Bruhn, for her help in all administrative things.

I am happy to mention the dear friends who I met in Sweden: Xu Dandan, Luo Cong, Luo Tingting, Yuan Song, Zhu Qiushi, Zhong Yang, Liu Jiayin, for the joy and fun we had together in every bright summer and dark winter.

I must thank my parents, with whom I have developed the curiosity for all kinds of knowledge, the habit of thinking, and the courage of travelling around the world. To all my old friends from Chengdu Shishi High School and University of Electronic Science and Technology of China (UESTC), no matter where I am, I treasure our friendship ever since teenage years.

Finally, I would like to pay my last respects to two Chinese scholars, Prof. Lin Weigan and Prof. Li Xiaowen, who passed away in January 2015. As my family friends, renowned scientists and educators, their stories have inspired me since my childhood. Rest in Peace.

Gao Xiang

List of Acronyms and Abbreviations

5G fifth generation

ACF auto-correlation function

ADC analog-to-digital converter

AOA angle of arrival

AOD angle of departure

APS angular power spectrum

CDF cumulative distribution function

CDMA code division multiple access

COST European Cooperation in Science and Technology

CSI channel state information

DAC digital-to-analog converter

DMC diffuse multipath component

DoF degree of freedom

DPC dirty-paper coding

DSD Doppler spectral density

EKF extended Kalman filter

EM electromagnetic

ETSI European Telecommunications Standards Institute

FDD frequency-division duplexing

FD-MIMO full-dimension MIMO

FMCW frequency modulated continuous wave

GMM Gaussian mixture model

GPRS general packet radio service

GPS Global Positioning System

GSCM geometry-based stochastic channel model

GSM Global System for Mobile Communications

ICT information and communication technology

IEEE Institute of Electrical and Electronics Engineers

IF intermediate frequency

i.i.d. independent and identically distributed

IO interacting object

IoT internet of things

IQR inter-quartile range

ISI inter-symbol interference

LAN local area network

LNA low-noise amplifier

LOS line-of-sight

LSF local scattering function

LTE long-term evolution

MAMMOET massive MIMO for efficient transmission

MCD multipath component distance

MF matched filtering

MIMO multiple-input multiple-output

MSE mean-squared error

MMSE minimum mean-squared error

MPC multipath component

MRC maximum ration combining

MRT maximum ratio transmission

MU-MIMO multi-user MIMO

M2M mobile-to-mobile

NLOS non-line-of-sight

OFDM orthogonal frequency division multiplexing

PAR peak-to-average-ratio

PDP power delay profile

PDF probability density function

QoS quality of service

RCM Random Cluster Model

RF radio frequency

RMS root mean square

RF radio frequency

RX receiver

SAGE space-alternating generalized expectation maximization

SCM Spatial Channel Model

SCME Spatial Channel Model Extended

SINR signal-to-interference-plus-noise ratio

SIR signal-to-interference ratio

SISO single-input single-output

SNR signal-to-noise ratio

s.t. subject to

SU-MIMO single-user MIMO

SVD singular value decomposition

TDD time-division duplexing

TX transmitter

US uncorrelated scattering

VR visibility region

WCDMA wide-band code division multiple access

WLAN wireless local area network

WSS wide-sense stationary

WSSUS wide-sense stationary uncorrelated scattering

ZF zero-forcing

Contents

Part I

Overview of Research Field

Chapter 1

Introduction

This chapter briefly reviews the technology of multiple-input multiple-output (MIMO) wireless communication, and then discusses the rationale behind that MIMO evolves towards massive MIMO. Massive MIMO is the research topic of this thesis, and its structure is outlined at the end of this chapter.

1.1 MIMO Review

As a physical-layer performance booster for wireless communications, the technology of MIMO has been incorporated into wireless broadband standards, such as IEEE 802.11n, IEEE 802.11ac, HSPA+, WiMAX and Long-Term Evolution (LTE) [1]. Among these, the current LTE standard allows for up to eight antennas on base stations and on terminals [2]. Figure 1.1 shows examples of a cellular base station and a WiFi access point, both equipped with multiple antennas. Compared to single-antenna systems, the performance gain brought by the use of multiple antennas is due to the spatial degrees of freedom (DoF) that expand the dimensions available for signal processing. As wireless spectrum has become a precious resource, MIMO technology exploiting the spatial domain offers the opportunity of improving system performance without increasing the required spectrum.

Let us briefly review MIMO systems. Generally, MIMO systems are divided into two categories: single-user MIMO (SU-MIMO) and multi-user MIMO (MU-MIMO). Figure 1.2 illustrates the two categories. In SU-MIMO, the transmitter and receiver are equipped with multiple antennas. Performance gain in terms of coverage, link reliability and data rate can be achieved through techniques such as beamforming, diversity-oriented space-time coding, and spatial

(a) (b)

Figure 1.1: Examples of MIMO technology used in our everyday life. (a) A cellular base station tower with multiple antennas. (b) A Linksys wireless router with multiple antennas (source: www.linksys.com).

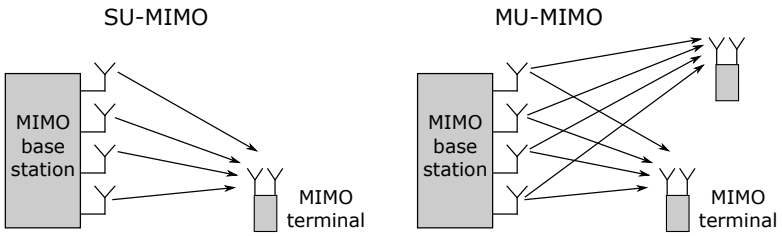

Figure 1.2: Single-user MIMO and multi-user MIMO.

multiplexing of several data streams. These techniques cannot be fully used at the same time, thus we typically find a tradeoff between them. For example, adaptive switching between spatial diversity and multiplexing schemes is adopted in LTE [3].

The situation with MU-MIMO [4] is radically different. The wireless channel is now spatially shared by different users, and the users transmit and receive without joint encoding and detection among them. By exploiting differences in spatial signatures at the base station antenna array induced by spatially-dispersed users, the base station communicates simultaneously to the users. As a result, performance gains in terms of sum-rates of all users can be impressive. A major challenge is, however, the interference among the co-channel users. Signal processing in MU-MIMO often aims at suppressing inter-user interference, so spatial channel knowledge becomes more crucial compared to SU-MIMO.

In general, by exploiting the spatial domain of wireless channels, MIMO

has the following key advantages compared to single-antenna systems:

- better coverage, through beamforming that results in higher received signal power,
- improved link reliability, through diversity schemes that combat fading effects in propagation channels and eventually reduce communication error probabilities,
- higher capacity, through spatial multiplexing that transmits and receives several data streams in the same time-frequency resource,
- decreased delay dispersion, due to channel shortening effect in beamforming, and
- improved estimation of directional information, due to the ability of antenna arrays to resolve the spatial domain.

1.2 MIMO Goes Massive

In both SU-MIMO and MU-MIMO, theoretically, the more antennas the transmitter and/or receiver are equipped with, the larger the scale on which the spatial domain can be exploited. This leads to better performance in terms of the above-mentioned MIMO advantages. When MIMO technology with up to eight antennas has become mature, we may ask: Has the potential of MIMO been fully exploited?

Dr. Thomas L. Marzetta from Bell Labs published a paper in 2010 – "Noncooperative Cellular Wireless with Unlimited Numbers of Base Station Antennas" [5], on what can be seen as an attempt to make full use of MIMO. Let the number of base station antennas grow without limit in MU-MIMO scenarios, the first important phenomenon is that the effects of additive receive noise and small-scale fading disappear, as does intra-cellular interference among users. The only remaining impediment is inter-cellular interference from transmissions that are associated with the same pilot sequence used in channel estimation. The paper concludes that the throughput per cell and the number of terminals per cell are independent of the cell size, the spectral efficiency is independent of the system bandwidth, and required transmit energy per bit vanishes. Although these very impressive results are subject to the system model and propagation assumptions used in the paper, Dr. Marzetta pointed out an important direction in which cellular systems may evolve.

Scaling up MIMO provides many more degrees of freedom in the spatial domain than any of today's systems. This rescues us from the situation that

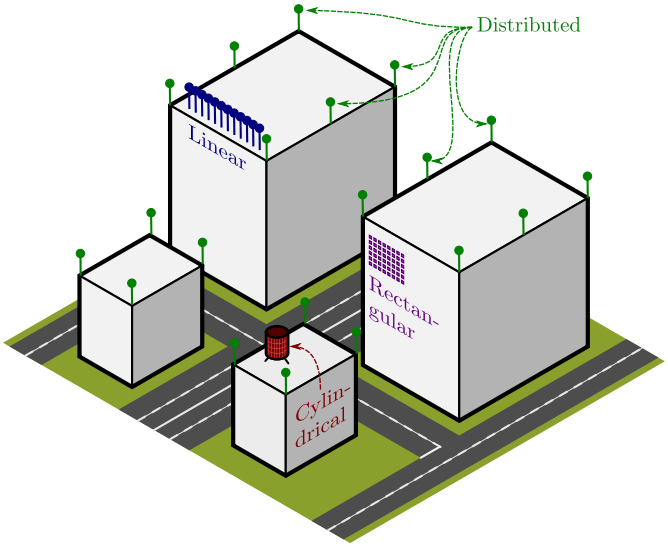

Figure 1.3: Illustration of possible deployments of massive MIMO antenna arrays [6].

wireless spectrum has become congested and expensive, especially in frequency bands below 6 GHz. In contrast to conventional MU-MIMO with up to eight antennas, we call MIMO with a large number of antennas "massive MIMO", "very-large MIMO" or "large-scale MIMO". As a simple illustration, Figure 1.3 shows possible deployments of massive MIMO antenna arrays. Antennas can be co-located in a linear, planar or cylindrical structure, or can be placed in a distributed manner.

In massive MIMO operation, we consider an MU-MIMO scenario, where a base station equipped with a large number of antennas serves many terminals in the same time-frequency resource. Processing efforts can be mostly made at the base station side, and terminals have simple and cheap hardware. Until now, many theoretical and experimental studies have been done in the massive MIMO context, e.g., [7–18] and the included papers I-VI in this thesis. These studies have shown that massive MIMO can greatly improve spectral efficiency while decreasing radiated output power by at least an order of magnitude. In addition, real-time massive MIMO testbeds are being implemented and demonstrations reported [19–22]. Among these contributions, the research work in this thesis has a focus on real massive MIMO channels.

During the five years of the thesis work, massive MIMO has become one of

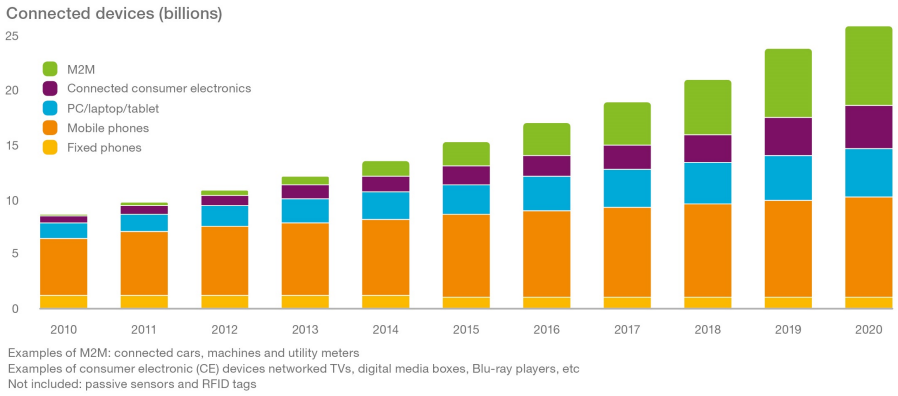

Figure 1.4: Growth in the number of connected devices. Around 25 billion connected devices are expected by 2020, of which 15 billion will be phones, tablets, laptops and PCs [26].

the most promising directions towards future 5G (the fifth generation) systems and beyond [23–25]. In the near future, we expect an explosive increase in connected devices, including phones, tablets, wearable devices, sensors, internet of things (IoT), connected vehicles and so on. Figure 1.4 shows the growing trend and a prediction of the number of connected devices from 2014 to 2020. Much higher data rates than today's 4G systems are required due to, e.g., high-quality video streaming and cloud computing [26]. As shown in Figure 1.5, by 2020 the amount of mobile data traffic due to video streaming is predicted to be 13 times more than that in 2014. Massive MIMO has the potential to meet these future requirements. In frequency bands below 6 GHz, massive MIMO is a candidate for smooth evolution from LTE to pre-5G or so called 4.5G. In high frequency bands, e.g., in millimeter-wave transmission, using many antennas is a potential solution to overcome high propagation losses [27]. Thanks to the large array gain, massive MIMO is also considered a technique to improve wireless network coverage. It can be potentially used for remote regions, e.g., in the Internet.org project [28] initiated by Facebook (www.facebook.com), aiming to provide the unconnected world affordable access to the Internet. From another point of view, radiated power from both base stations and terminals can be scaled down, making massive MIMO a candidate also for "green communications" [29]. At the writing of this thesis, 5G standardization has started. We will see in the near future, whether or not massive MIMO will be adopted for 5G radio access network (RAN) standards.

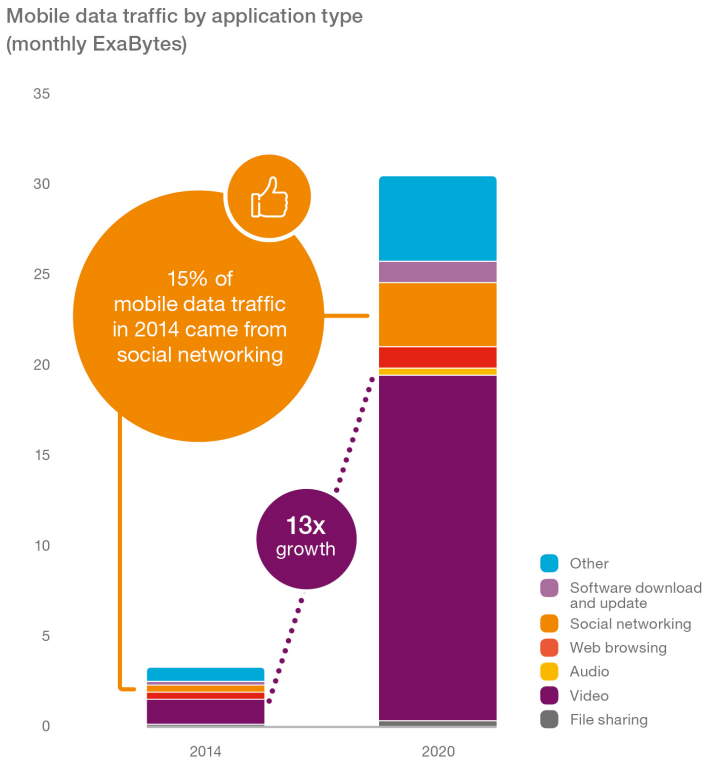

Figure 1.5: Growth in mobile data traffic. In 2014, video accounted for around 45% of mobile data traffic. By 2020, it is expected that 60% of all mobile data traffic will be from video [26].

1.3 Structure of the Thesis

The studies in this thesis are based on channel measurements for massive MIMO in real propagation environments. With the measurement capability of Lund University, several massive MIMO measurement campaigns were conducted. The obtained real-life channel data are used for performance evaluation, channel characterization and modeling. The thesis summarizes and concludes this research work. Part I contains an overview of the research field and puts the included papers in Part II into context. Some ongoing work and unpublished results are also included to complete the story of massive MIMO in real channels.

The structure of the thesis is as follows. Chapter 2 reviews the massive MIMO concept, including the advantages and challenges. In Chapter 3, massive MIMO channel measurements are described. With the obtained channel data, Chapter 4 reviews data processing methods used in this thesis work. After proper data processing, important channel properties in massive MIMO are observed, and Chapter 5 gives a summary of these properties. Based on measured channels, evaluations of massive MIMO performance are reviewed in Chapter 6. Then, in Chapter 7, channel modeling for massive MIMO characteristics is discussed, and different approaches are reviewed. Chapter 8 introduces antenna selection as a potential method to simply massive MIMO hardware. Finally, Chapter 9 summarizes the contributions of the thesis work, draws conclusions, and discusses future work.

Chapter 2

The Massive MIMO Concept

To understand what massive MIMO is, as a new technology for wireless access, let us first overview the massive MIMO concept. This chapter describes the system model used throughout the thesis work, the theoretical advantages brought by scaling up MIMO, and the challenges we encounter in practice. The investigations in this thesis work are then introduced.

2.1 System Description

Generally, a system can be called "massive MIMO" if a large number of antennas are deployed at one or both ends of the communication link. The number of antennas and communication schemes vary in different systems and applications. It is thus difficult to agree on a specific definition of "massive MIMO". In this thesis, we consider massive MIMO an MU-MIMO technology in cellular systems, where a base station is equipped with tens to hundreds of antennas, and communicates with many users simultaneously through spatial multiplexing. Figure 2.1 illustrates the MU-MIMO system model in both downlink and uplink transmissions, for a single cell. MIMO with a large number of antennas, however, should not be limited to multi-user scenarios. It can also be used in single-user scenarios, e.g., backhaul links between base stations in millimeter-wave communications [30].

As this thesis work is, to my best knowledge, one of the first studies of massive MIMO based on channel measurements in real-life environments, we start with relatively simple scenarios and make the following operation assumptions.

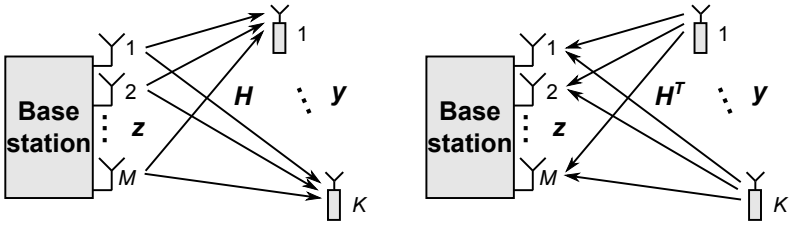

(a) Downlink (b) Uplink

Figure 2.1: An MU-MIMO system model, in the (a) downlink and (b) uplink. An M-antenna base station serves K single-antenna users in a spatial-multiplexing manner. Channel reciprocity is assumed, so the relation between the downlink and uplink channel matrices is simply the matrix transpose.

- *Single-cell systems.* Due to the present capability of conducting channel measurements, only single-cell scenarios can be investigated. Multi-cell measurements require greater efforts and more equipment, since channels in different cells need to be measured in a synchronized manner.
- *MIMO-OFDM.* We primarily approach MIMO assuming the same type of modulation as frequently used in LTE and WLANs, namely OFDM [31].
- *Single-antenna terminals.* Since processing that "massively" exploits the spatial domain can be made at the base station side, multiple antennas at the terminals become less important.
- *Perfect channel state information (CSI).* We assume that the base station perfectly knows the instantaneous channel matrix, and uses the knowledge for precoding and detection. In practice, however, we have imperfect CSI and this may lead to a performance degradation. We do not focus on channel estimation in this thesis, therefore, we assume an ideal situation.
- *Time-division duplexing (TDD).* In frequency-division duplexing (FDD), downlink CSI is estimated by the users and fed back to the base station. CSI estimation and feedback may become very complex, when there are a large number of base station antennas. TDD operation does not rely on CSI feedback, as propagation channels are reciprocal for uplink and downlink. The only challenge is to calibrate the transmit and receive RF chains at the base station [32].

Massive MIMO, of course, is not restricted to the above scenarios and assumptions. Scenarios with, e.g., inter-cellular interference, multi-antenna terminals,

non-orthogonal waveforms, and imperfect CSI, are all important aspects to investigate but are beyond the scope of this thesis.

Let us return to Figure 2.1, where an M-antenna base station multiplexes K single-antenna users in the spatial domain. The downlink signal model, for each time-frequency resource, is

$$\boldsymbol{y} = \sqrt{p_{\mathrm{dl}}}\boldsymbol{H}\boldsymbol{z} + \boldsymbol{n}, \tag{2.1}$$

where $\boldsymbol{H}$ is the propagation channel matrix, $\boldsymbol{z}$ is the vector of precoded transmit signals across the M antennas, $\boldsymbol{y}$ is the receive signal vector at the K users, and $\boldsymbol{n}$ is the white-noise vector with i.i.d. circularly-symmetric complex Gaussian, $CN(0, \sigma_{\mathrm{n}}^2)$, elements. Assume that $\mathbb{E}\{\|\boldsymbol{z}\|^2\} = 1$, so p_{dl} contains the total transmit power in the downlink. Two power-scaling schemes are used in the thesis, 1) $p_{\mathrm{dl}} = \rho K$ and 2) $p_{\mathrm{dl}} = \frac{\rho K}{M}$, where ρ is an SNR factor. We scale up the transmit power with the number of users K, and choose to 1) keep it constant or 2) scale it down with the number of antennas M. Note that in the included papers we usually assume that the noise has unit variance, $\sigma_{\mathrm{n}}^2 = 1$, so the noise power is absorbed into p_{dl} which reflects the SNR. Here and in the following we keep the noise variance σ_{n}^2 as it is, for a better understanding of the signal, noise and inter-user interference.

Due to reciprocity, the uplink channel matrix is $\boldsymbol{H}^T$, and the signal model becomes

$$\boldsymbol{z} = \sqrt{p_{\mathrm{ul}}}\boldsymbol{H}^T\boldsymbol{y} + \boldsymbol{n}. \tag{2.2}$$

The total transmit power from all users is p_{ul}, and $p_{\mathrm{ul}} = \rho K$ or $p_{\mathrm{ul}} = \frac{\rho K}{M}$ depending on used power-scaling scheme. The downlink and uplink signal models are used throughout the thesis, and in the included papers there are subscripts indicating OFDM subcarriers. For simplicity, we drop the subcarrier notation here.

In massive MIMO, we usually assume $M \gg K$, for achieving good spatial separation of user signals. This is, however, as pointed out in [33], not necessarily a requirement for massive MIMO.

2.1.1 Precoding and Detection

In MU-MIMO, precoding and detection are designed for separating data streams with as little inter-user interference as possible. In the downlink, the base station pre-filters signals to the intended users, and in the uplink, the base station post-filters the received signals from all users. CSI is required at the base station to perform the processing, while not necessarily needed at the terminals that perform relatively simple processing, e.g., OFDM modulation/demodulation in our case.

In the downlink, dirty-paper coding (DPC) is optimal in the sense that it achieves sum-rate capacity [34], and in the uplink, successive interference cancellation (SIC) detection achieves capacity [35]. However, the two non-linear schemes are highly complex in practice. Linear schemes, such as matched-filtering (MF) and zero-forcing (ZF), are simple but have suboptimal performance in terms of sum-rates. In massive MIMO, what happens is that linear schemes become nearly-optimal as the number of antennas grows. In the following, we review the precoding/detection schemes used in the thesis work, for evaluating massive MIMO performance in real channels (see papers I-III and VI).

Dirty-Paper Coding

In MU-MIMO downlink channels, sum-rate capacity can be achieved by using DPC [34, 36, 37]. The base station chooses codewords for user signals so that the inter-user interference can be avoided, as if they do not exist.

DPC was originally proposed in [38], dealing with additive interference in a channel. The name comes from the analogy that sending information through a channel with additive interference is like writing a message on a paper with dirt spots. Figure 2.2 illustrates this analogue, where we try to write "MASSIVE MIMO" on a dirty paper. The situation is, we know the location and intensity of the dirt spots, but our reader cannot distinguish the dirt from the ink marks written by us. To convey the message, one way of writing is to get around the dirt as much as possible, see Figure 2.2(c). The dirt will behave as "additive noise" to the reader if some overlap the message. However, this is not the optimal solution. A more clever way is shown in Figure 2.2(d), where we "encode" the message and make it adaptive to the dirt. Before writing, the set of possible "codewords" should also be known to the reader so that he/she can "decode" the message.

Instead of attempting to fight the interference, DPC adapts to it by choosing codewords in the direction of the interference. This technique has been applied to MU-MIMO downlink transmission since [36]. However, the implementation of DPC requires significant additional complexity, and the practical approach remains unsolved. Alternatively, low-complexity but suboptimal schemes, such as linear filtering, are used in practice.

Linear Schemes

Commonly-used linear schemes include matched-filtering (MF), zero-forcing (ZF) and minimum-mean-squared-error (MMSE) filtering. We focus on linear precoding in the downlink, and corresponding linear detection in the uplink can

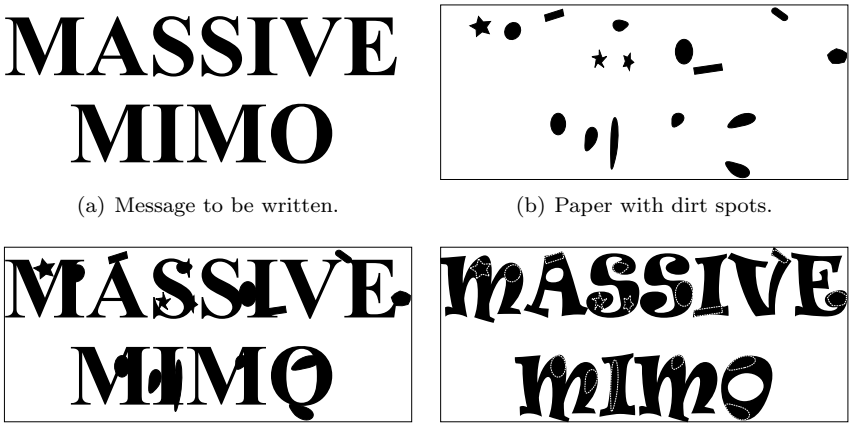

(a) Message to be written.

(b) Paper with dirt spots.

(c) Writing to get around the dirt.

(d) Writing to adapt to the dirt.

Figure 2.2: Illustration of "writing on dirty paper". (a) "MASSIVE MIMO" is the message to be written to the reader. (b) The paper with dirt spots. (c) The writer writes the message with an attempt to avoid the dirt as much as possible, however, some dirt may still interfere with the message. (d) The writer and reader agree upon a code book, where the writer encodes the message so that it adapts to the dirt. The area marked by the dash lines are the dirt, and the writer applies ink around the dirt to form the encoded "MASSIVE MIMO".

be derived in a similar way. A comparison of linear precoding and detection can be found in [39].

With linear precoding, we have the transmit vector

$$\boldsymbol{z} = \boldsymbol{W}\sqrt{\boldsymbol{P}}\boldsymbol{x}, \tag{2.3}$$

where $\boldsymbol{W}$ denotes the precoding matrix, $\boldsymbol{P}$ the power allocation matrix for different users, with P_i, $i=1,2,\ldots,K$, on its diagonal, and $\boldsymbol{x}$ is the vector of transmit symbols for the K users and each entry has unit energy. The transmit signals for the users are $\boldsymbol{s}=\sqrt{\boldsymbol{P}}\boldsymbol{x}$, and $\boldsymbol{W}$ maps $\boldsymbol{s}$ to the M antennas.

We can design $\boldsymbol{W}$ with different objectives, such as SNR maximization and interference cancellation, subject to the sum-power constraint $\mathbb{E}\{\|\boldsymbol{z}\|^2\} = 1$. The constraint can be written as

$$\mathrm{Tr}\left\{\boldsymbol{P}\boldsymbol{W}^H\boldsymbol{W}\right\} = 1, \tag{2.4}$$

where $\mathrm{Tr}\{\cdot\}$ represents the trace of a matrix. In the downlink signal model, the total transmit power is p_{dl}.

Matched-Filtering We start with the simplest linear precoding. MF precoding, also known as maximum ratio transmission (MRT), aims at maximizing the receive SNR at each user. It can be obtained by solving the following optimization problem [39],

$$\boldsymbol{W}_{\mathrm{MF}} = \arg\max_{\boldsymbol{W}} \frac{\mathbb{E}\left\{\left|\boldsymbol{s}^H\boldsymbol{y}\right|\right\}}{\sigma_{\mathrm{n}}^2} \quad \text{s.t. } \mathrm{Tr}\left\{\boldsymbol{P}_{\mathrm{MF}}\boldsymbol{W}^H\boldsymbol{W}\right\} = 1. \tag{2.5}$$

The solution is the Hermitian transpose of the channel matrix,

$$\boldsymbol{W}_{\mathrm{MF}} = \boldsymbol{H}^H, \tag{2.6}$$

for an arbitrary $\boldsymbol{P}_{\mathrm{MF}}$. The effective signal model for the i-th user becomes

$$y_i = \sqrt{p_{\mathrm{dl}}}\left[\boldsymbol{H}\boldsymbol{H}^H\right]_{i,i} s_i + \sqrt{p_{\mathrm{dl}}}\sum_{\substack{j=1\\ j\neq i}}^{K}\left[\boldsymbol{H}\boldsymbol{H}^H\right]_{i,j} s_j + n_i, \tag{2.7}$$

where we see a maximized receive signal for this user but cross-talk exists.

Due to the maximization of the receive SNR at each user, MF is suitable for noise-limited scenarios. At high SNRs, MF performance will be limited by inter-user interference, in which case, ZF precoding is superior to MF.

Zero-Forcing ZF precoding nulls out inter-user interference. It can be obtained through the optimization [39]

$$\boldsymbol{W}_{\mathrm{ZF}} = \arg\min_{\boldsymbol{W}} \mathbb{E}\left\{\|\boldsymbol{W}\boldsymbol{s}\|^2\right\} \quad \text{s.t. } \boldsymbol{H}\boldsymbol{W} = \boldsymbol{I}. \tag{2.8}$$

We look for $\boldsymbol{W}$ that completely removes the interference with the minimum transmit energy. The solution is the Moore–Penrose pseudoinverse of the channel, i.e.,

$$\boldsymbol{W}_{\mathrm{ZF}} = \boldsymbol{H}^{\dagger} = \boldsymbol{H}^H \left(\boldsymbol{H}\boldsymbol{H}^H\right)^{-1}. \tag{2.9}$$

The effective signal model becomes

$$\boldsymbol{y} = \sqrt{p_{\mathrm{dl}}}\boldsymbol{s} + \boldsymbol{n}, \tag{2.10}$$

where each user receives its signal without cross-talk.

Using ZF, we perfectly cancel inter-user interference. However, "there is no such thing as a free lunch," ZF may suffer a power penalty due to the nulling. Let us examine the sum-power constraint, (2.4) becomes

$$\sum_{i=1}^{K} P_{\mathrm{ZF},i} \left[\left(\boldsymbol{H}\boldsymbol{H}^H\right)^{-1}\right]_{i,i} = 1, \tag{2.11}$$

where $P_{\mathrm{ZF},i}$ is the i-th diagonal element in the power allocation matrix $\boldsymbol{P}_{\mathrm{ZF}}$. How much power can be allocated to the user signals depends on the channel condition. There is no power penalty if $\boldsymbol{H}$ has full rank and the Gram matrix $\boldsymbol{H}\boldsymbol{H}^H$ is diagonal, i.e., the channels from the base station to different users are orthogonal. In this case, the transmit power p_{dl} can be fully used on user signals. However, the power penalty increases, as the Gram matrix becomes ill-conditioned [40], i.e., some user channels are aligned to each other. In this situation, $[(\boldsymbol{H}\boldsymbol{H}^H)^{-1}]_{i,i}$ becomes large, so $P_{\mathrm{ZF},i}$ has to be small. More energy has to be spent on the nulling, and less allocated to the user signals, resulting in very low receive signal power at some users. A similar effect happens in ZF detection, known as *noise enhancement*.

Thinking about the propagation channels, we can have a better understanding of the MF and ZF precodings. Figure 2.3 illustrates the propagation mechanisms of the two schemes, in channels with 100 base station antennas and five users. By tuning the power and phase of the transmit signals across all antennas, MF and ZF make the signals through the multipath channel, e.g., after reflection, diffraction and scattering, arrive at the users in different manners. With MF, the multipath signals add up constructively at the intended user location, but cause interference for the other users, see Figure 2.3(a). With ZF, the multipath signals for the intended user add up destructively to zero at

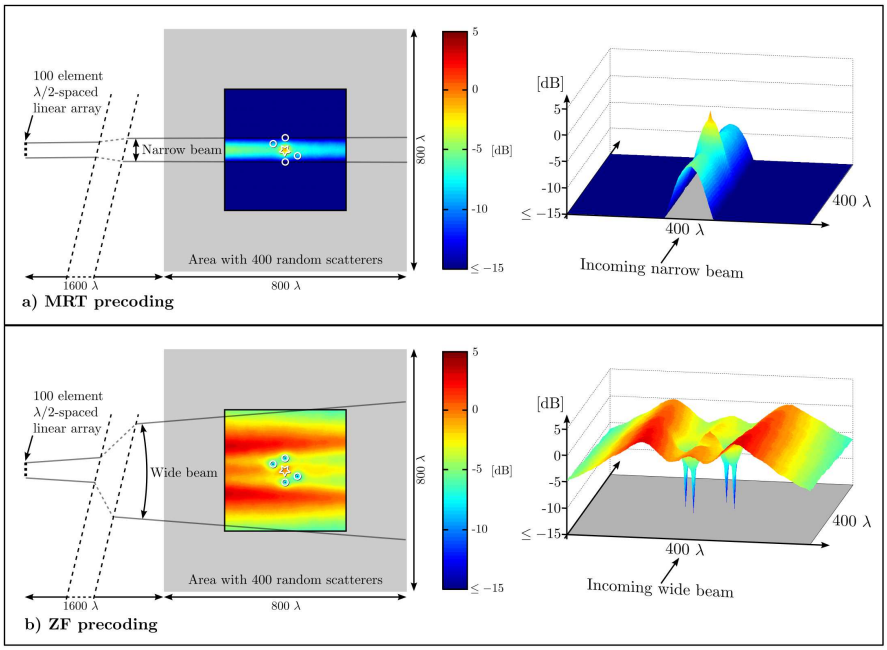

Figure 2.3: Illustration of the ZF and MF mechanisms in propagation channels, with 100 base station antennas, five users and 400 scatterers around [6]. (a) With MF, field strength is maximized at the intended user location. (b) With ZF, field strength is zero at the unintended user locations. The propagation mechanisms are the same for different numbers of antennas. With more antennas, the peak in (a) is higher, and the energy spread in (b) becomes smaller.

the location of the other users, resulting in no interference but a reduction of the receive signal strength for the intended user, see Figure 2.3(b). Comparing the two, we see that energy spreads over a larger area with ZF, which is the power penalty caused by the nulling.

Minimum Mean-Squared Error As mentioned above, ZF is suitable for high SNR scenarios, while MF outperforms at low SNRs. How about the entire SNR range? We turn to schemes that find a tradeoff between the signal strength and the interference reduction. MMSE precoding is one example. The idea is, if the noise covariance is estimated at the receiver and fed back to the transmitter, we can design a better precoder for the entire SNR range.

MMSE is obtained through the optimization [39]

$$\begin{aligned} \boldsymbol{W}_{\text{MMSE}} &= \arg\min_{\boldsymbol{W}} \mathbb{E}\left\{\|\boldsymbol{y} - \sqrt{p_{\text{dl}}}\boldsymbol{s}\|^2\right\} \\ &= \arg\min_{\boldsymbol{W}} \mathbb{E}\left\{\left\|(\boldsymbol{H}\boldsymbol{W} - \boldsymbol{I})\,\boldsymbol{s} + \frac{\boldsymbol{n}}{\sqrt{p_{\text{dl}}}}\right\|^2\right\} \\ &\text{s.t.} \quad \text{Tr}\left\{\boldsymbol{P}_{\text{MMSE}}\boldsymbol{W}^H\boldsymbol{W}\right\} = 1, \end{aligned} \tag{2.12}$$

where we try to minimize the mean-squared error (MSE) between the receive and transmit signals. One possible solution is ZF where $\boldsymbol{H}\boldsymbol{W} = \boldsymbol{I}$, if the transmit power p_{dl} can be arbitrarily high. With limited transmit power, we need to consider the noise covariance, $\sigma_{\text{n}}^2\boldsymbol{I}$ in our case. The MMSE solution is

$$\boldsymbol{W}_{\text{MMSE}} = \boldsymbol{H}^H\left(\boldsymbol{H}\boldsymbol{H}^H + \alpha\boldsymbol{I}\right)^{-1}, \tag{2.13}$$

where $\alpha = \frac{K\sigma_{\text{n}}^2}{p_{\text{dl}}}$ and K is the number of users. The general form in (2.13) is also known as *regularized ZF* (RZF), and α is the regularization parameter. MMSE is a special case of RZF, where $\alpha = \frac{K\sigma_{\text{n}}^2}{p_{\text{dl}}}$ is the result of minimizing the MSE.

MMSE is designed according to the available transmit power at the base station and the noise power measured at the users. It becomes ZF when $\alpha = 0$, i.e., at very high SNRs, and converges to MF when $\alpha \to \infty$, i.e., at very low SNRs. In between the two extremes, MMSE outperforms ZF and MF in terms of sum-rate, since its MSE is smaller than the other two. Back to Figure 2.3, the propagation mechanism of the MMSE works between that of the MF and ZF. The power penalty due to the interference suppression is smaller in MMSE than in ZF.

2.1.2 Capacity and Sum-rate

Based on our signal model in (2.1), MU-MIMO downlink sum-rate capacity, achieved by DPC, is [36, 37]

$$C_{\text{DPC}} = \max_{\boldsymbol{P}_{\text{DPC}}} \log_2 \det\left(\boldsymbol{I} + \frac{p_{\text{dl}}}{\sigma_{\text{n}}^2}\boldsymbol{H}^H\boldsymbol{P}_{\text{DPC}}\boldsymbol{H}\right) \quad \text{s.t.} \sum_{i=1}^{K} P_{\text{DPC},i} = 1. \tag{2.14}$$

The optimization problem of power allocation is convex [41], thus can be easily solved. In addition, an iterative water-filling algorithm is presented in [42] for solving the problem.

With linear precoding, we can treat inter-user interference as additive noise at the receivers. The per-user rate depends on the receive SINR at the user,

which is determined by the used precoding $\boldsymbol{W}$ and the power allocation $\boldsymbol{P}$. The receive SINR at the i-th user can be written as

$$\gamma_i = \frac{p_{\mathrm{dl}} \left| [\boldsymbol{HW}]_{i,i} \right|^2 P_i}{p_{\mathrm{dl}} \left(\sum_{j=1, j\neq i}^{K} \left| [\boldsymbol{HW}]_{i,j} \right|^2 P_j \right) + \sigma_{\mathrm{n}}^2}, \tag{2.15}$$

where the numerator is the desired signal power at the user, and the denominator is the sum of the interference from other users and the noise power. Under the sum-power constraint in (2.4), we can maximize the sum-rate of all users,

$$C = \max_{\boldsymbol{P}} \sum_{i=1}^{K} \log_2 (1 + \gamma_i) \quad \text{s.t.} \ \sum_{i=1}^{K} P_i \left[\boldsymbol{W}^H \boldsymbol{W} \right]_{i,i} = 1, \tag{2.16}$$

by optimizing the power allocation to the users.

Treating interference as noise is simple but not optimal. A better approach is that the receivers are aware of the interference from other users, and each receiver jointly detects all user signals. However, this approach requires additional complexity, since the users need to know the channel information and the used precoder. We thus use the simple approach in this thesis and evaluate linear precoding performance as derived in (2.16).

2.2 Massive MIMO Advantages

In massive MIMO, the number of base station antennas, M, goes large. Many interesting and nice things start to happen. In this section, we review some key advantages of massive MIMO.

2.2.1 Large Increase in Capacity

Theoretically, MU-MIMO sum-rate capacity scales with $\min(M, K)$, the minimum of the number of base station antennas and the number of users. When both M and K become large in massive MIMO, the rank of $\boldsymbol{HH}^H$ grows, resulting in a large increase in the sum-rate capacity as derived in (2.14).

If we have a fixed number of users K and make the number of antennas $M \gg K$, array gain now becomes very large, and inter-user interference significantly reduces. This situation also leads to a large increase in sum-rate capacity, as discussed in the following.

2.2.2 Large Array Gain

With more antennas, we obtain more "samples" in the spatial domain, which means more degrees of freedom available for signal processing. If we coherently combine these "samples", i.e., the transmit or receive information signals, we can improve the SNR as compared to that in a single-antenna system. This power gain, achieved by using multi-antenna arrays, is known as *array gain*.

As M grows, the matrix $\boldsymbol{H}$ becomes long, and the value of $[\boldsymbol{H}\boldsymbol{H}^H]_{i,i}$, $i=1,2,\ldots,K$, also grows. As a result, in (2.7) with MF precoding, the signal strength for the targeted user becomes higher, and this is achieved without increasing the transmit power p_{dl}. The same effect happens also with ZF and MMSE. With ZF, the term $[(\boldsymbol{H}\boldsymbol{H}^H)^{-1}]_{i,i}$ in (2.11) becomes smaller as M grows, so $P_{\mathrm{ZF},i}$ can be larger, resulting in an increase in the user signal strength. For all linear schemes, the SINR in (2.15) will increase, thus higher rates can be achieved. In massive MIMO, the effect of array gain will be much more significant than in any of today's MIMO systems.

Large array gains improve link quality and coverage. Theoretically, higher SINRs will boost data rates, since higher-order modulation can be used. However, large dynamic range in signal strength and higher-order modulation require higher quantization precision in analog-to-digital converters (ADCs), and this may lead to more expensive hardware. With realistic low-cost terminals, only a certain SINR can be handled before the quantization noise starts to limit the performance. On the other hand, radio regulators set strict limitations on the effective power of radio devices, and this includes the antenna gain. Therefore, what we can do with such a large array gain in massive MIMO is to harvest it as reduced transmit power from both base stations and terminals. For example in papers II and III, we scale down the transmit power with the number of antennas, $p_{\mathrm{dl}} = \frac{\rho K}{M}$, as mentioned in Section 2.1. This is also why massive MIMO is a candidate for "green communications" [29]. Imagine $M \to \infty$, the transmit power can be made arbitrarily low. In practice, M cannot go to infinity, but the transmit power can still be reduced by at least one or two orders of magnitude, without sacrificing the performance.

2.2.3 Reduction of Inter-User Interference

The value of $[\boldsymbol{H}\boldsymbol{H}^H]_{i,i}$ becomes large as M grows. How about the off-diagonal elements, $[\boldsymbol{H}\boldsymbol{H}^H]_{i,j}$ where $i \neq j$? In massive MIMO, what happens is that the off-diagonal elements grow far slower than the diagonal elements.

Assume that $\boldsymbol{H}$ is an i.i.d. channel with complex Gaussian coefficients,

$CN(0,\sigma_{\rm h}^2)$, $\sigma_{\rm h}^2<\infty$. We examine $\frac{1}{M}\boldsymbol{H}\boldsymbol{H}^H$, where the diagonal elements are

$$\frac{1}{M}\left[\boldsymbol{H}\boldsymbol{H}^H\right]_{i,i}=\frac{1}{M}\sum_{m=1}^{M}|H_{i,m}|^2, \tag{2.17}$$

and the off-diagonal ones

$$\frac{1}{M}\left[\boldsymbol{H}\boldsymbol{H}^H\right]_{i,j}=\frac{1}{M}\sum_{m=1}^{M}H_{i,m}H_{j,m}^*, \quad i\neq j. \tag{2.18}$$

When $M\to\infty$, according to the central limit theorem [43], the distributions of both diagonal and off-diagonal elements converge to Gaussian distributions,

$$\frac{1}{M}\left[\boldsymbol{H}\boldsymbol{H}^H\right]_{i,i}\xrightarrow{d}N\left(\mu_0,\frac{\sigma_0^2}{M}\right), \tag{2.19}$$

and

$$\frac{1}{M}\left[\boldsymbol{H}\boldsymbol{H}^H\right]_{i,j}\xrightarrow{d}CN\left(\mu_1,\frac{\sigma_1^2}{M}\right), \quad i\neq j, \tag{2.20}$$

where $\mu_0=\mathbb{E}\{|H_{i,m}|^2\}$, $\sigma_0^2=\mathrm{var}\{|H_{i,m}|^2\}$, $\mu_1=\mathbb{E}\{H_{i,m}H_{j,m}^*\}$, and $\sigma_1^2=\mathrm{var}\{H_{i,m}H_{j,m}^*\}$. As $M\to\infty$, $\frac{\sigma_0^2}{M}\to 0$ and $\frac{\sigma_1^2}{M}\to 0$, variances of both distributions approach zero. On the diagonal, $|H_{i,m}|^2=\mathrm{Re}\{H_{i,m}\}^2+\mathrm{Im}\{H_{i,m}\}^2$, follows the chi-squared distribution with two degrees of freedom, and $\mu_0=\sigma_{\rm h}^2$. At the off-diagonal elements, $\mu_1=\mathbb{E}\{H_{i,m}\}\mathbb{E}\{H_{j,m}^*\}=0$, since channel coefficients are independent random variables. Finally, we have

$$\frac{1}{M}\boldsymbol{H}\boldsymbol{H}^H\to\sigma_{\rm h}^2\boldsymbol{I}, \tag{2.21}$$

as $M\to\infty$.

The nice thing happening here is that user channels become orthogonal. Inter-user interference vanishes, and the base station can communicate with the users simultaneously in maximum rates. More importantly, the maximum rates can now be achieved by using linear precoding/detection schemes.

2.2.4 Simple Precoding and Detection

Substituting (2.21) into (2.14), the sum-rate capacity achieved by DPC becomes

$$C_{\rm DPC}=\max_{\boldsymbol{P}_{\rm DPC}}\sum_{i=1}^{K}\log_2\left(1+\frac{p_{\rm dl}M\sigma_{\rm h}^2P_{{\rm DPC},i}}{\sigma_{\rm n}^2}\right) \quad \text{s.t.} \sum_{i=1}^{K}P_{{\rm DPC},i}=1, \tag{2.22}$$

where equal power allocation, $P_{\mathrm{DPC},i} = \frac{1}{K}$, is the optimal solution. DPC capacity in (2.22) thus is

$$C_{\mathrm{DPC}} = K \log_2 \left(1 + \frac{p_{\mathrm{dl}} M \sigma_{\mathrm{h}}^2}{K \sigma_{\mathrm{n}}^2}\right), \tag{2.23}$$

where we can see the multiplexing gain K and the array gain M.

With linear precoding, substituting (2.21) into (2.15), the interference term in the denominator in (2.15) becomes zero, for all $\boldsymbol{W}_{\mathrm{MF}}$, $\boldsymbol{W}_{\mathrm{ZF}}$ and $\boldsymbol{W}_{\mathrm{MMSE}}$. Then, solving the optimization in (2.16), we obtain the sum-rates achieved by MF, ZF and MMSE in this interference-free case,

$$C_{\mathrm{ZF}} = C_{\mathrm{MF}} = C_{\mathrm{MMSE}} = K \log_2 \left(1 + \frac{p_{\mathrm{dl}} M \sigma_{\mathrm{h}}^2}{K \sigma_{\mathrm{n}}^2}\right), \tag{2.24}$$

which are all equal to the DPC capacity in (2.23).

When the number of antennas grows large, user channel vectors become orthogonal, inter-user interference thus reduces. As a result of this effect, the maximum rates, achieved by complex non-linear DPC, can now be approached by using simple linear schemes.

2.2.5 Channel Hardening

From (2.19) and (2.20), we see that the fluctuation in the elements of $\frac{1}{M}\boldsymbol{H}\boldsymbol{H}^H$ decreases rapidly relative to their respective means, as M grows large. This effect is called *channel hardening*. Note that channel hardening does not mean the variation in the channel $\boldsymbol{H}$ becomes small, but is an effect that we obtain stable outputs after processing.

The consequences of channel hardening include:

- The effect of small-scale fading disappears. If we scale down the transmit power with the number of antennas, e.g., $p_{\mathrm{dl}} = \frac{\rho K}{M}$, then in (2.15), the receive SINRs at the users become more stable in the sense that they do not fluctuate with small-scale fading in the channel, for all the schemes $\boldsymbol{W}_{\mathrm{MF}}$, $\boldsymbol{W}_{\mathrm{ZF}}$ and $\boldsymbol{W}_{\mathrm{MMSE}}$.

- Resource allocations can be performed on a slower time scale. For example, the power allocation $\boldsymbol{P}$ that maximizes the sum-rate in (2.16) becomes stable, since $\boldsymbol{W}^H\boldsymbol{W}$ also hardens in all the precoding schemes. Therefore, power allocations only have to be updated when large-scale fading happens in the channel.

- The variation in sum-rates becomes small. The receive SINRs at the users do not vary with small-scale fading, as a result, so do the sum-rate in (2.16). The probability that we have a rate much lower than the ergodic rate becomes very small.

- Precoders and detectors become more stable. Due to interference reduction and channel hardening, for a given $\boldsymbol{P}$ in (2.3), the power variation in the precoded signal $\boldsymbol{z}$, i.e., the variation in $\|\boldsymbol{z}\|^2 = \|\boldsymbol{W}\sqrt{\boldsymbol{P}}\boldsymbol{x}\|^2$, becomes small and stable, when the transmit symbols in $\boldsymbol{x}$ vary.

In addition, the effects of channel hardening on transmission schemes and system performance have been studied, e.g., in [44, 45].

As the number of antennas increases, channel conditions that were random before, now start to be deterministic. We should also mention that if both $M, K \to \infty$ with a constant ratio $\frac{M}{K} < \infty$, the distribution of the eigenvalues of $\frac{1}{M}\boldsymbol{H}\boldsymbol{H}^H$ converges to the Marchenko–Pastur distribution [46].

2.2.6 Sharp Digital Beamforming

With an antenna array, we can perform *analog beamforming* that steers directional beams by adjusting the phases of RF signals at each antenna. Depending on the number of antennas and the size of the array, multiple beams can be formed to serve different users. In full-dimension MIMO (FD-MIMO) [47, 48], 3D beams can be formed to serve users in different azimuths and elevations. With more antennas, beams can be made narrower, resulting in a better separation of user signals. With analog beamforming, the number of simultaneous users is typically limited by the number of orthogonal beams that can be formed, and is fixed by the number of deployed RF chains.

Linear precoding, discussed in Section 2.1.1, works in a different way. It can be seen as *digital beamforming*, performed in the baseband by tuning the phases and amplitudes of transmit signals across all antennas. Without steering actual beams into the channel, signals add up in phase at the intended users and out of phase at other users, see Figure 2.3. With increasing number of antennas, this effect is more significant: the signal strength at the intended user location gets higher, while causing lower interference to the other users.

Digital beamforming in massive MIMO provides a more flexible and aggressive way of spatial multiplexing, as the number of users can vary and is less limited by the hardware. Another advantage of digital beamforming is that it does not require array calibration since reciprocity is used, but is typically needed in analog beamforming where the calibration complexity may grow with the number of antennas.

2.3 Massive MIMO Challenges

With the above theoretical advantages of massive MIMO, now, the question is what challenges we may face in practice, and to what extent the theoretical advantages can be harvested in reality.

2.3.1 Propagation Conditions

In Section 2.2, we assume i.i.d. Rayleigh channels where the number of base station antennas $M \to \infty$. This leads to interference-free transmission and optimal performance achieved by linear precoding and detection. In practice, however, the number of antennas are limited, and propagation channels are hardly i.i.d. Rayleigh. Channels of different base station antennas are often correlated, and so are channels to different users.

In massive MIMO literature, there is a commonly-used term called *favorable propagation* [49]. Many theoretical studies are based on this propagation condition, assuming that user channels become orthogonal as the number of antennas increases, see (2.21). The question is, however, under what conditions is the channel "favorable" and this assumption valid? I.i.d. Rayleigh channels are favorable, as seen in Section 2.2.3, but require very rich and complex propagation which does not always exist in real-life environments. To investigate propagation conditions in real channels, channel measurements using practical array setups are therefore needed.

Further questions are, does massive MIMO rely on favorable propagation, and how far we are from theoretical advantages if propagation is not entirely favorable? The major goal of the thesis work is to address the above questions, based on channel measurements in real propagation environments.

2.3.2 Hardware Complexity

A crucial challenge of massive MIMO is hardware complexity. As the number of antennas increases, the number of RF transceiver chains including components like RF amplifier, mixer and ADC/DAC, also grows on a much larger scale than in any of today's systems. To deal with large channel matrices, the complexity in baseband processing may significantly increase, as more operations are needed [50].

High hardware complexity often leads to low efficiency in terms of cost and energy. Antennas are usually cheap and easy to deploy, but RF chains can be relatively expensive. Due to large array gains, massive MIMO is energy efficient in terms of radiated transmit-power. However, energy consumption

in hardware can be quite high. Analog and RF components are expected to dominate massive MIMO energy consumption [50, 51].

To implement massive MIMO in practice, many studies are being conducted to simplify its hardware. Among those, antenna selection has been considered in this thesis, as a direct solution that reduces the number of RF chains without significant reductions in performance.

2.3.3 Hardware Imperfection

Since massive MIMO hardware tends to be very complex with many antennas and transceiver chains, it is important to make them as inexpensive as possible. However, the cheaper, the more imperfect, typically. With massive MIMO, we may allow many of the imperfections to be quite large, since the averaging effect due to many antennas helps to reduce the impact of imperfections on system performance [12]. This opens up the possibility to use inexpensive hardware, such as nonlinear amplifiers, high IQ-imbalance mixers, low-precision ADC/DACs, and so on.

Another issue is reciprocity calibration in TDD massive MIMO [50]. Ideally, precoding for the downlink transmission is computed on the basis of CSI estimated in the uplink. Propagation channels are reciprocal, however, transmit and receive RF front-ends are typically not. In order to make use of channel reciprocity, we need to estimate and compensate the difference in the responses between the transmit and receive RF chains. There are many calibration methods, e.g., in [32], mutual coupling among base station antennas is used.

2.3.4 Mutual Coupling in Antenna Arrays

Strong mutual coupling between antennas is good for reciprocity calibration [32]. However, mutual coupling may degrade massive MIMO performance, primarily, due to power loss, when many antennas are packed into a small physical space [7]. For example, the study in [52] points out that mutual coupling can result in substantially lower capacity and reduced degrees of freedom, as the number of antennas is increased for a fixed array aperture. In addition to power inefficiency, spatial correlation caused by small antenna spacings also limits massive MIMO performance [53].

The effect of mutual coupling, therefore, needs to be taken into account, when designing a massive MIMO antenna array, and when evaluating or predicting the performance of a massive MIMO system.

2.3.5 Channel Estimation

As discussed in Section 2.1, massive MIMO relies on CSI known at the base station to coherently process the signals, i.e., to perform precoding and detection. Related to CSI acquisition, there are several challenges as follows.

- Channel variations, due to the movement of users and scatterers, determine how often we need to update the CSI [54]. Accurate and timely CSI acquisition can be challenging, especially in high mobility scenarios.
- FDD massive MIMO induces training overhead, since channels from all base station antennas to all users need to be estimated and fed back [55]. TDD massive MIMO relies on channel reciprocity, but training may still occupy a large fraction of the coherence interval if the channel varies fast.
- Since the number of orthogonal pilot sequences is limited by the channel coherence interval, pilot sequences have to be reused from cell to cell. This causes *pilot contamination*, where channel estimates may contain interference from users transmitting data or the same pilot in other cells. This effect reduces massive MIMO performance [56].

2.4 Investigations in the Thesis

In this thesis work, we try to bridge massive MIMO from the "ideal" world of theory to the "non-ideal" reality, with a focus on real propagation channels. Channel measurements were designed and conducted, using practical antenna arrays and in typical propagation environments. Based on measured channel data, we address the following questions.

- Propagation conditions: Can we also harvest good channel orthogonality between users and high sum-rates in real channels, as in i.i.d. Rayleigh channels? (Papers I, II and III)
- Channel characterization: Do massive MIMO channels show different properties, as compared to conventional MIMO? How do these channel properties affect massive MIMO performance? (Papers II, IV and VI)
- Channel modeling: How do we capture massive MIMO channel properties and include them into a channel model? (Papers IV and V)
- Complexity reduction: Is there a way to greatly simplify massive MIMO systems without losing too much performance? (Papers VI)

In the following chapters, we overview these issues, and in Chapter 9, we summarize the thesis contributions and draw conclusions.

Chapter 3

Channel Measurements

Several measurement campaigns were carried out at Lund University to obtain real massive MIMO channel data. Each targeted a specific aspect of the massive MIMO study, e.g., comparisons of different array structures, and crowded scenarios with users being closely located. Measurements for massive MIMO channels require significant efforts, since we need to sample the spatial domain on a much larger scale than before. This applies both to the base station side, where arrays with many antennas are used, and to the user side, where many synchronized or unsynchronized terminals need to be considered.

In this chapter, let us overview the measurements performed during the thesis work, including the measurement setups at Lund University, and our capability of measuring channels in different scenarios that are interesting in the massive MIMO context. Before that, we start with a brief review of channel sounding principles.

3.1 Principles of Channel Sounding

What is a radio channel? It is the medium through which we transmit signals as electromagnetic waves at 3 kHz to 300 GHz. Propagation in a radio channel, governed by Maxwell's equations [57], is typically very complex as it not only happens in free space but is also affected by the phenomena of reflection, refraction, diffraction, scattering, etc. From a system perspective, the radio channel can be viewed as a linear filter [58], see Figure 3.1. We input sinusoidal signals, $\sin(2\pi f_0 t)$, and at the output we receive sinusoidal signals at the same frequency, $\alpha \sin(2\pi f_0 t + \vartheta)$, that have been attenuated due to propagation loss and phase-rotated due to delay and multipath superimposition, if ignoring

Figure 3.1: Radio channel can be viewed as a linear filter.

any additive noise. We thus bypass propagation composition in a channel, and characterize it by the input-output relation, in the complex baseband form, $\alpha e^{-j\vartheta}$, i.e., the channel response at frequency f_0 [58].

In most measurements, what we obtain are channel responses between transmit and receive antenna pairs, across space (antenna arrays and multiple terminal antennas), frequencies (system bandwidth) and time. Figure 3.2 illustrates a 4×4 MIMO channel sounding. The transmitter sends sounding signals that are known to the receiver, and the receiver captures linearly distorted versions of the signals. By comparing the transmit and receive signals, channel responses are estimated. Time and frequency synchronizations between the transmitter and receiver are important to correctly estimate channel responses. Effects of sounding equipment such as amplifiers, switches and cables need to be removed through a *calibration* process, so differences between the transmit and receive signals are only due to the propagation channel combined with antenna responses.

Different sounding methods are used by different sounding equipment and for different purposes [58]. In narrowband channel sounding, sinusoidal signals can be directly used. For wideband channels, the solution can be, e.g., correlative sounding using PN sequences, and frequency domain sampling using multi-tone signals or chirp signals (frequency modulated continuous wave, known as FMCW). In MIMO channel sounding, it is not always easy, or even possible, to measure all channels between transmit and receive antennas simultaneously. A popular solution is a *switched-array* architecture that measures one channel at a time and then switches to the next one.

Antennas and antenna arrays play an important role in channel measurements, as they determine how sounding signals are radiated into or received from propagation channels. Generally, which type of antennas and antenna arrays to use depends on the purpose of measurements. To evaluate the performance of a system in real channels, it is better to use antennas and antenna arrays designed for such a system. For channel characterization and modeling, omni-directional antennas are usually preferable as they have the least influence on propagation compared to directional antennas. Antenna arrays are needed to characterize directional information in the channels. In some scenarios, we also need to consider the effect of human bodies or hands on the radiation

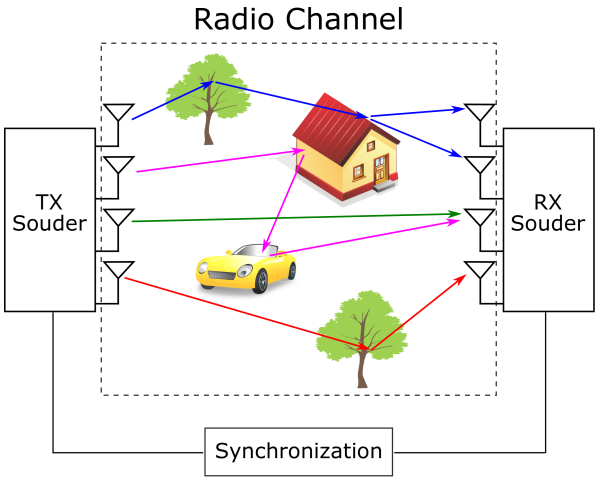

Figure 3.2: Sounding of a 4×4 MIMO channel. We bypass the propagation composition, and measure the channel by the input-output relation. The channel response includes the effect of antennas at both ends. Correct synchronization in both time and frequency is crucial to channel sounding [58].

pattern of terminal antennas, as often happens in real life.

3.2 Measurement Setups

In the following, we describe the measurement setups used during the thesis work. The description provides an overview of Lund University's capability of measuring massive MIMO channels.

3.2.1 Antenna Arrays

Two types of antenna arrays, a cylindrical and a linear array, were used in the measurements. We describe these two first, and introduce a planar array designed for a massive MIMO testbed later. The three array structures are compared regarding their potential use for massive MIMO.

Cylindrical Array

A cylindrical (faceted) array, operating in 2.5-2.7 GHz, is often used in channel measurements at Lund University. Figure 3.3 shows the cylindrical array on

Figure 3.3: The cylindrical array on a building roof at Lund University.

a roof top of the department building. It constitutes 64 dual-polarized patch antennas with two ports – a vertically-polarized and a horizontally-polarized port, giving a total of 128 elements. The 64 directive antennas are arranged in four circles of 16 each. Figure 3.4 illustrates the radiation pattern of the first patch (on the bottom circle), for both ports. The design parameters of the array can be found in [59].

Due to its circular structure and directive patch antennas, the cylindrical array can resolve the channel in all azimuth directions, and some range (about 120 degrees) in elevation. It was originally designed for the RUSK LUND channel sounder [60], rather than being specially designed for massive MIMO. Despite this, the large number of antennas (128 ports) and the compact size (30 cm in both diameter and height) make it a possible choice for a massive MIMO base station.

Since we pack many antennas in limited space, the effect of mutual coupling needs to be considered. As mentioned in Section 2.3, mutual coupling may have a substantial impact on massive MIMO performance. According to [59], mutual coupling between neighboring elements on the array is -11 dB at the maximum, which is not small. Using this array, we suffer from power loss due to coupling, and this may result in performance degradation as compared to using an "ideal" cylindrical array without coupling.

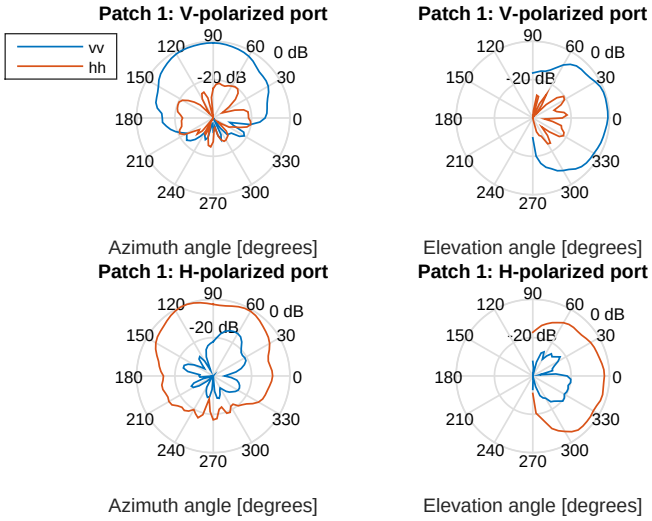

Figure 3.4: Radiation pattern of both ports of the first patch antenna, on the bottom circle of the array.

Virtual Linear Array

Practical antenna arrays, like the cylindrical array, usually require great efforts and long time in design, manufacture, test, and verification. With many antennas, many transceivers are required if we want to measure all antenna channels simultaneously, or an RF switch is needed if we switch over the array to measure the channels. These solutions can be expensive. Alternatively, virtual arrays are often used in channel measurements, where a single antenna with a single transceiver moves and measures at predefined positions.

Figure 3.5 shows the virtual linear array used in our measurements: a vertically-polarized omni-directional antenna (SkyCross SMT-2TO6MB-A type [61]), controlled by Labview [62] and a step motor, moves in 128 equidistant positions on a long rail. Thus, a 128-antenna linear array is formed in a virtual manner.

Using virtual arrays is a convenient way of measuring channels, however, it has some drawbacks compared to using real arrays. First, a virtual array does not contain the effect of mutual coupling as is naturally inherent in a real array. This may lead to an overestimation of system performance, if evaluations are based on measured channel data with a virtual array. Additionally, we may suffer from channel variation during one measurement, i.e., when measuring

Figure 3.5: Photos of the virtual linear array used during a measurement. An omni-directional antenna moves on a rail, and measures the channel at 128 equidistant positions with half-wavelength spacing at 2.6 GHz. This yields a large array that spans 7.4 m in one dimension.

from the first position to the last. With more positions to be measured, the chances that the channel varies during one measurement become higher. We therefore need to keep the channel as static as possible, when measuring with a virtual array. In that case, the dynamic properties of the channel cannot be captured.

Planar Array

A "T"-shaped planar array was designed for the Lund University massive MIMO testbed (LuMaMi) [21], see Figure 3.6. The array was built with 160 dual-polarized patch antennas, with half-wavelength spacing at 3.7 GHz. In total it has 320 ports, among which 100 are connected to the transceiver chains in the testbed. The "T" shape is designed to allow exploration of different array arrangements. For example, using more antennas horizontally results in higher angular resolution in azimuth, similarly, use more antennas vertically if we want to resolve elevation direction.

The planar array has not been used in this thesis work. Despite this, the planar arrangement of many antennas is an attractive deployment alternative at a massive MIMO base station, e.g., placing patch antennas on walls for indoor communications.

Comparison of Array Structures

The three arrays have very different structures, thus targeted different potential uses. Returning to Figure 1.3, we see examples of their possible deployments.

Placing a large number of antennas linearly results in a physically-large array. It is difficult to mount such an array in places with limited space.

Figure 3.6: Photo of the planar array designed for the LuMaMi testbed. The array has 160 dual-polarized antennas, giving a total of 320 ports.

The advantage is very high angular resolution due to a large aperture. In massive MIMO performance evaluations, e.g., in Paper II, we see that the large linear array is good at separating closely-located users, if the users or main scatterers are in the array's broadside direction. Moving to the end-fire direction, however, the angular resolution becomes worse.

A cylindrical array with directive antennas is more suitable in a practical deployment, due to its smaller aperture. Angular resolution becomes lower compared to a linear array, but instead of resolving only one dimension, the cylindrical array can resolve signals in both azimuth and elevation. All azimuth directions in an environment can be covered, making the array suitable for outdoor deployment, where users are located far apart in different directions.

A planar array can be placed on a wall or ceiling, so this structure is particularly suitable for indoor deployment. Outdoors, a planar array may not have as good coverage as a cylindrical array, since users at the opposite side of the array may have relatively low SNRs. Indoor propagation typically covers both azimuth and elevation, due to reflections on walls, ceilings and floors. In this situation, both horizontal and vertical spans of a planar array become useful to resolve the channels.

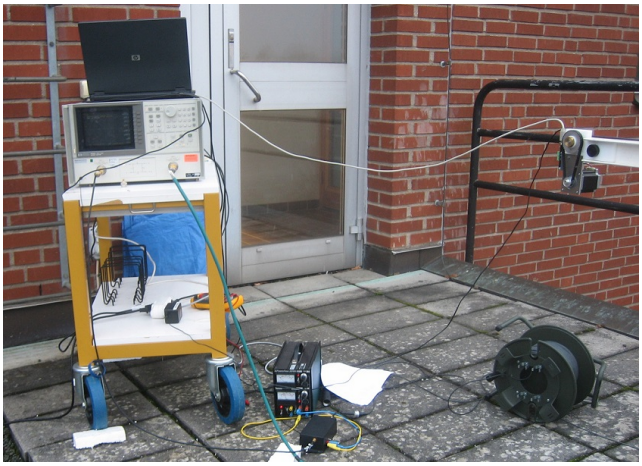

Figure 3.7: An HP 8720C VNA was used in the channel measurements with the virtual linear array. In the photo, on top of the VNA a laptop with Labview was used to control the measurement.

3.2.2 Measurement Equipment

The easiest way of measuring radio channels is to use a vector network analyzer (VNA), and typically with virtual arrays. Commercial channel sounders are specially designed for channel measurements, thus are faster and more flexible.

Vector Network Analyzer

Using a VNA, we can measure transmission and reflection characteristics of a device under test (DUT), through *scattering parameters* (*S-parameters*) [63]. In our case, the radio channel to be measured is the DUT. By sweeping the frequency of the sounding signal and measuring the *S21* parameter at each frequency, we obtain channel responses over a desired bandwidth. An HP 8720C VNA, see Figure 3.7, was used in our measurements with the virtual linear array.

The measurement system using the VNA is shown in Figure 3.8. Port 1 of the VNA was connected to the transmit equipment, including optical fiber cables, power amplifier and an omni-directional antenna used at the terminal side. The optical fiber has a length of 200 m, allowing the transmitter and receiver to be separated by a relatively large distance. Port 2 of the VNA (the receiver) was connected to the virtual linear array via a low-noise amplifier (LNA). A laptop with Labview was used to control the whole measurement.

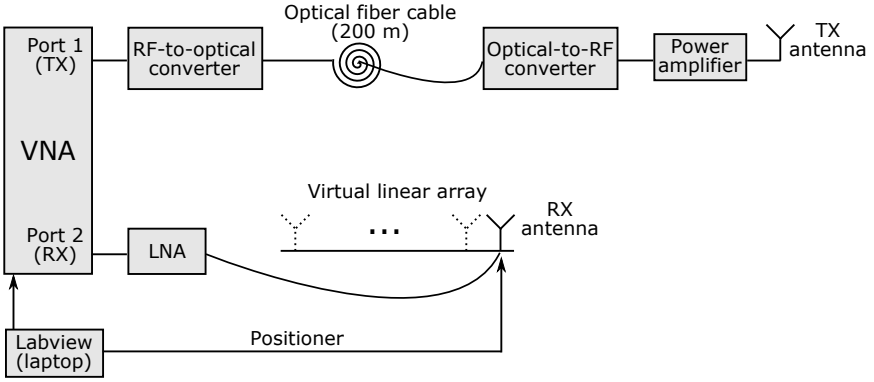

Figure 3.8: The measurement system using the VNA and the virtual linear array. An optical fiber cable was used to separate the transmit antenna (the user side) and the receive array (the base station side).

including positioning and movement of the antenna, activating and recording measurements across the predefined frequencies. In addition, a back-to-back measurement has to be taken to record the frequency response of the cables, converters and amplifiers, i.e., everything between port 1 and port 2 except for the antennas and propagation channel. After removing the effect of measurement equipment, we obtain the radio channel response.

When using the VNA, the measurement speed depends on the number of frequency samples and the chosen intermediate frequency (IF) bandwidth. The narrower the IF bandwidth, the longer the measurement time. On the other hand, a narrower IF bandwidth allows for a higher IF gain, resulting in better measurement SNRs. In our measurements, we set the IF bandwidth to be 300 Hz or 1 kHz, depending on the estimated SNR before starting a measurement.

Channel Sounder

The RUSK LUND channel sounder operates in the 300 MHz, 2 GHz and 5 GHz bands with a bandwidth of up to 240 MHz. It is based on periodic multi-carrier sounding signals (similar to OFDM signals) and real-time sampling at the receiver. This enables a high measurement repetition rate ensuring that we do not violate the Nyquist sampling criterion in time-variant MIMO channels. To completely characterize a time-variant channel, the required repetition rate f_{rep} is determined by the maximum expected Doppler shift $\Delta f_{\max}$, roughly

estimated as,

$$\Delta f_{\max} = \frac{\Delta v}{c} f_0, \tag{3.1}$$

where Δv is the maximum relative speed of the transmitter and receiver, c is the speed of light, and f_0 is the center frequency. According to the Nyquist sampling criterion, the repetition rate should satisfy [64]

$$f_{\text{rep}} \geq 2\Delta f_{\max}, \tag{3.2}$$

i.e., at least twice of the maximum Doppler shift.

The channel sounder does not measure channels between all transmit and receive antenna pairs simultaneously. It relies on a *switched-array* architecture at both transmit and receive sides. In this manner, one measurement snapshot means sounding and switching over all transmit and receive antennas. The sounding period of one antenna pair is determined by the estimated maximum excess delay, varying from environment to environment. Between successive antenna elements, the switching is very fast, less than 100 ns, and a time period is used to guarantee the switching and the processing at the receiver. The snapshot rate should still fulfill the Nyquist sampling criterion, when switching through all antennas. At the receive side, a 1-to-128 switch is used for the 128-port cylindrical array, while at the transmit side, a 1-to-32 switch is used when needed.

In MU-MIMO channel measurements, users need to be separated by some distance, typically, from a few wavelengths to tens of meters. To synchronize channel sounding of separated users, optical fibers can be used to connect the users (antennas) to the 1-to-32 switch at the transmit sounder. Figure 3.9 illustrates the measurement setup, used in the measurements for massive MIMO with nine synchronized users. There, only 9 of the switch ports are connected.

3.3 Measurement Scenarios

With the available measurement setups, the next question is, what scenarios are important in the massive MIMO context? In this thesis work, we focused on single-cell scenarios, using the linear and cylindrical arrays at the base station side. Both outdoor and indoor environments were covered, with users being closely located or well separated.

3.3.1 Semi-Urban Scenarios with Cylindrical and Linear Arrays

As discussed in Section 2.2, user channels become orthogonal as $M \to \infty$ in i.i.d. Rayleigh channels. Many massive MIMO advantages happen because of

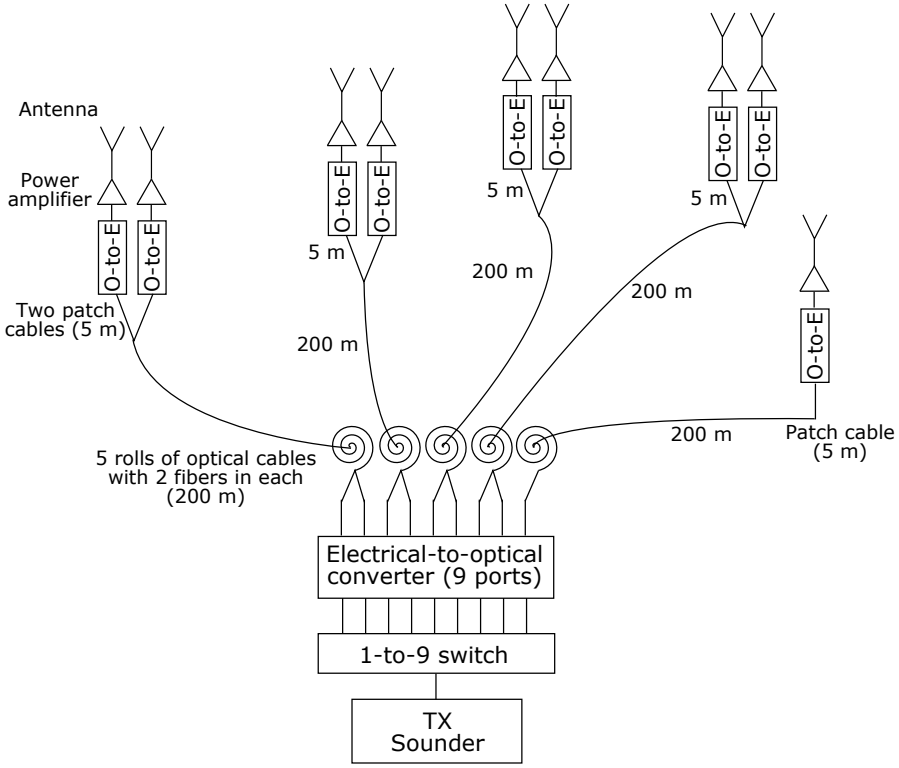

Figure 3.9: The measurement setup at the transmit side with the channel sounder. Nine terminal antennas are connected to the transmit sounder through optical fibers, allowing their channels to be measured in a synchronized manner.

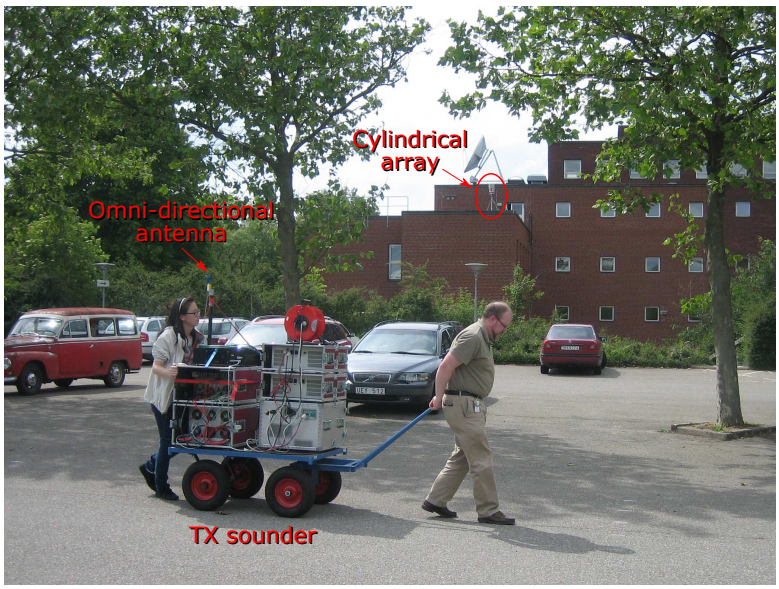

Figure 3.10: Outdoor-to-outdoor measurements with the cylindrical array. The transmit sounder with an omni-directional antenna was moved around, measuring the channels at different sites around the building where the cylindrical array was positioned on its roof. Dr. Zhu Meifang and Dr. Tommy Hult were helping with the measurement.

this property. Through channel measurements, the first thing we would like to investigate is, whether this claim also holds in real propagation environments.

In the summer of 2011, measurements for massive MIMO were performed at the campus of Lund University, an outdoor semi-urban environment, using the channel sounder and the cylindrical array. The measurements were taken at 2.6 GHz and over 50 MHz bandwidth. The measurement environment and scenarios are described in papers II and VI. Figure 3.10 shows a photo taken during the measurement.

In the autumn of 2011, measurements using the virtual linear array with the VNA were carried out in the same environment, also at 2.6 GHz and over 50 MHz bandwidth. The virtual linear array was positioned on the same building roof, and the same sites at the terminal side were measured using the same omni-directional antenna. This allows direct comparisons of the channel behavior and system performance, using the two types of arrays at massive MIMO base stations. The comparison results are presented in papers II and VI.

In the two measurements, channels of different user positions were not measured at the same time or in a synchronized manner. Channel data with "virtual users", may therefore not reflect the true channel orthogonality, especially for closely-located users where relative phase information between their channels is crucial.

3.3.2 Crowded Scenarios with Closely-Located Users

In 2014 and 2015, measurements were carried out targeting closely-located and synchronized users, using the cylindrical array and the setup shown in Figure 3.9. Closely-located users represent scenarios such as crowded squares, live concerts, sports events, open exhibitions and indoor conference centers. These scenarios are interesting in the massive MIMO context, as many users in a crowd are expected to be served simultaneously [65]. With user channels being measured in a synchronized manner, the dynamic properties of time-variant MU-MIMO channels can now be captured.

Both outdoor and indoor environments were measured at 2.6 GHz and over 40 MHz bandwidth. In the outdoor measurements, nine single-antenna users were confined in a circle of 5 or 10 m diameter, and sometimes with people around them acting as a crowd. For the indoor case, we measured in a large lecture hall, with users sitting closely together (see Figure 3.11) and the cylindrical array positioned at the front center or a corner of the hall. The measurement description can be found in Paper III and [66], where the initial results of performance evaluation and channel characterization based on the measurement data are also reported.

3.3.3 Other Interesting Scenarios

Indoor Base station in a Residential Area Before the above measurements designed for massive MIMO took place, measurement data targeting femto-cell systems were used for the massive MIMO study in Paper I. The receive sounder and the cylindrical array were placed indoor in a residential house. The transmit sounder and a 32-element planar array were moved in the residential area, placed indoor in other houses or outdoor. Indoor-outdoor-indoor and indoor-to-outdoor channels were measured [67]. For massive MIMO study, we select two antennas or two measurement positions at the transmit side, and investigate if they can be spatially separated by using the cylindrical array at the indoor base station.

Outdoor Base Station and Indoor Users Outdoor-to-indoor propagation is particularly interesting, since people spend most of their time indoors.

Figure 3.11: During the indoor measurements in a lecture hall, nine single-antenna users and some other people were sitting closely together.

Measurements were planed but not carried out during this thesis work. The issues to investigate are 1) spatial separability of indoor users by outdoor massive MIMO base stations, and 2) penetration loss through windows and walls. Indoor users can be located in the same room, different rooms on the same building floor, or on different floors. Measurements with users on different floors may target, e.g., urban scenarios with a dense distribution of high-rise buildings, where 3D coverage is required.

Chapter 4

Overview of Measurement Data Processing

With the obtained data from channel measurements, we can study massive MIMO channel behavior, evaluate system performance, design communication algorithms, and so on. How to process measurement data depends on what we would like to investigate. In this chapter, let us overview the data processing performed in this thesis.

From the perspective of MIMO channel characterization and modeling, it is important to understand directional properties and scatterer behavior in a channel. We estimate directional information in measured channels using various algorithms. We also extract multipath components (MPCs), and this provides a good picture of the propagation composition in the channel (cf. Figure 3.2). In cluster-based modeling approaches, the MPCs with similar properties are grouped into clusters. Channel behavior is then based on clusters rather than MPCs. This can be seen as a simplified way of modeling and simulating channels.

When evaluating massive MIMO performance, the obtained channel matrices can be used directly, e.g., calculating capacities and sum-rates, as derived in Section 2.1.2. However, channel power normalization has to be carefully dealt with, as normalization in massive MIMO can be performed across many dimensions – time, frequencies, users, and antenna elements.

4.1 Directional Estimation

Directional information is an important aspect of MIMO channels. If signals come from a narrow angle, i.e., having a relatively small angular spread, channel correlation between antennas can be relatively high. Large angular spread is preferable in a MIMO system.

In measured channels with the cylindrical array, azimuth angles of arrival can be roughly obtained through the power variation over the array, due to the circular structure and directive antenna arrangement. On the linear array, all antennas are omni-directional, so angles of arrival need to be estimated from the channel responses over the array. Simple estimation can be done through beamforming methods, but resulting in relatively low angular resolution. One of the high-resolution methods is the Space-Alternating Generalized Expectation (SAGE) maximization algorithm [68, 69], which estimates MPCs in terms of delay, direction, and complex amplitude.

4.1.1 Beamforming

The simplest directional estimation on a uniform linear array can be obtained by a Fourier transform of the receive signal vector $\boldsymbol{z}$ across the array. This is equivalent to steering beams and scanning certain directions ϕ. Through beamforming, we can obtain a continuous angular spectrum, by correlating the beamformer with the receive signal vector [70, 71],

$$P_{\mathrm{BF}}(\phi) = \frac{\boldsymbol{\varpi}^H(\phi)\, \boldsymbol{R}_{zz}\, \boldsymbol{\varpi}(\phi)}{\boldsymbol{\varpi}^H(\phi)\, \boldsymbol{\varpi}(\phi)}, \tag{4.1}$$

where $\boldsymbol{\varpi}(\phi)$ is the steering vector (beamformer) into the direction ϕ, and $\boldsymbol{R}_{zz} = \mathbb{E}\{\boldsymbol{z}\boldsymbol{z}^H\}$ is the covariance of the received signals. For a uniform linear array with omni-directional elements, and over which we assume plane wavefronts, the steering vector is

$$\boldsymbol{\varpi}(\phi) = \begin{bmatrix} 1 \\ e^{-jk_0\Delta_{\mathrm{a}}\cos(\phi)} \\ e^{-j2k_0\Delta_{\mathrm{a}}\cos(\phi)} \\ \vdots \\ e^{-j(N-1)k_0\Delta_{\mathrm{a}}\cos(\phi)} \end{bmatrix}, \tag{4.2}$$

where $k_0 = \frac{2\pi}{\lambda}$, Δ_{a} is the antenna spacing, and N is the number of antennas used for the directional estimation. Here ϕ is the angle between the incident wave and the array's end-fire direction.

Directional estimation through the above beamforming, however, has relatively low resolution. An often-used alternative is the Minimum Variance Method (MVM), also called Capon's beamformer [72–74]. The angular spectrum by the MVM is given as [72]

$$P_{\mathrm{MVM}}(\phi) = \frac{1}{\boldsymbol{\varpi}^H(\phi)\boldsymbol{R}_{zz}^{-1}\boldsymbol{\varpi}(\phi)}. \tag{4.3}$$

Instead of searching for the strongest correlation in directions with the received signals, the MVM minimizes the interference from other directions when estimating at the direction ϕ. The MVM provides better angular resolution than the classic beamforming method in (4.1).

The steering vector $\boldsymbol{\varpi}$ in (4.2) is formed based on the plane-wave approximation over a linear array. This approximation requires users and scatterers being located in the far field of the array, and typically holds for arrays with small apertures. When the array aperture becomes large, such as for our 7.4-m linear array, the plane-wave approximation does not hold, and spherical waves over the array need to be considered. As an important channel property in massive MIMO, spherical wavefronts with large arrays are discussed in Chapter 5 and Paper V. When estimating angles of arrival on the linear array using the two beamforming methods, we apply a sliding window on the array. The window contains, e.g., $N = 10$ consecutive antennas, across which we assume the plane-wave approximation to hold.

4.1.2 SAGE Algorithm

Using the beamforming methods, we can quickly obtain directional estimates over a linear array, however, the drawback is relatively low resolution. Among the high-resolution algorithms [68, 69, 75, 76], we use the Space-Alternating Generalized Expectation (SAGE) maximization algorithm [68, 69] to estimate the superimposed MPCs in a channel, with parameters such as delay, angle and complex amplitude.

The signal model used in the estimation is constructed under the plane-wave assumption. The channel response between the i-th receive and j-th transmit antenna pair, at time instant t and frequency f, is given as [77]

$$H_{i,j}(t,f) = \sum_{l=1}^{L} \begin{bmatrix} A^{\mathrm{v}}_{\mathrm{tx},j}(\phi_l^{\mathrm{tx}}, \theta_l^{\mathrm{tx}}) \\ A^{\mathrm{h}}_{\mathrm{tx},j}(\phi_l^{\mathrm{tx}}, \theta_l^{\mathrm{tx}}) \end{bmatrix}^T \begin{bmatrix} \gamma_l^{\mathrm{vv}} & \gamma_l^{\mathrm{vh}} \\ \gamma_l^{\mathrm{hv}} & \gamma_l^{\mathrm{hh}} \end{bmatrix} \begin{bmatrix} A^{\mathrm{v}}_{\mathrm{rx},i}(\phi_l^{\mathrm{rx}}, \theta_l^{\mathrm{rx}}) \\ A^{\mathrm{h}}_{\mathrm{rx},i}(\phi_l^{\mathrm{rx}}, \theta_l^{\mathrm{rx}}) \end{bmatrix} e^{-j2\pi f \tau_l} e^{j2\pi \nu_l t}, \tag{4.4}$$

where

- l represents the MPC index,

- ϕ_l^{tx} and θ_l^{tx} are the angles of departure in azimuth and in elevation, respectively, and ϕ_l^{rx} and θ_l^{rx} are the corresponding angles of arrival,
- $A_{\mathrm{tx},j}^{\mathrm{v}}(\phi_l^{\mathrm{tx}}, \theta_l^{\mathrm{tx}})$ and $A_{\mathrm{tx},j}^{\mathrm{h}}(\phi_l^{\mathrm{rx}}, \theta_l^{\mathrm{rx}})$ are the j-th transmit antenna response for the vertical and horizontal polarizations, and $A_{\mathrm{rx},i}^{\mathrm{v}}(\phi_l^{\mathrm{rx}}, \theta_l^{\mathrm{rx}})$ and $A_{\mathrm{rx},i}^{\mathrm{h}}(\phi_l^{\mathrm{rx}}, \theta_l^{\mathrm{rx}})$ are the response of the i-th receive antenna, the superscripts v and h indicate vertical and horizontal polarizations, respectively,
- γ_l^{vv} and γ_l^{hh} represent the complex amplitudes of the co-polarized parts in the l-th MPC, and γ_l^{vh} and γ_l^{hv} are the cross-polarized counterparts,
- τ_l is the delay of the l-th MPC, and
- ν_l the Doppler shift.

The measured channel, $H_{i,j}^{\mathrm{meas}}(t,f) = H_{i,j}(t,f) + n_{i,j}(t,f)$, contains additive noise $n_{i,j}(t,f)$. Given the channel data and antenna responses, we would like to estimate the unknown parameter set,

$$\boldsymbol{\psi}_l = \left[\tau_l, \phi_l^{\mathrm{tx}}, \theta_l^{\mathrm{tx}}, \phi_l^{\mathrm{rx}}, \theta_l^{\mathrm{rx}}, \gamma_l^{\mathrm{vv}}, \gamma_l^{\mathrm{vh}}, \gamma_l^{\mathrm{hv}}, \gamma_l^{\mathrm{hh}}, \nu_l\right]^T, \tag{4.5}$$

for all MPCs, $l = 1, 2, \ldots, L$. Assume that L is determined before the estimation, and $\boldsymbol{\psi} = [\boldsymbol{\psi}_1, \boldsymbol{\psi}_2, \ldots, \boldsymbol{\psi}_L]$, the maximum likelihood (ML) estimate is [78]

$$\hat{\boldsymbol{\psi}} = \arg\max_{\boldsymbol{\psi}} \mathcal{L}\left(\boldsymbol{\psi}; \boldsymbol{H}^{\mathrm{meas}}\right), \tag{4.6}$$

where $\mathcal{L}$ represents the *likelihood* function. Unfortunately, direct maximization of the likelihood is intractable due to many parameters in $\boldsymbol{\psi}$ when L is large. Thus we must resort to iterative methods, e.g., the SAGE algorithm [69].

The SAGE algorithm is used as a data processing tool throughout the thesis work, e.g., in papers II, IV and V, for channel characterization. In many measurements, only a part of the parameter set $\boldsymbol{\psi}$ is possible to estimate. Due to the use of single-antenna terminals, we cannot obtain directional information at this end. Using the linear array at the base station side, since it spans one dimension, we can only obtain angles of arrival in one dimension. With the cylindrical array, we can estimate directions in both azimuth and elevation. In addition, polarization information is not always under control. We usually know the polarimetric radiation patterns of the base station antennas, however, at the user side, it is hard to know the same for terminal antennas, when their radiation patterns are affected by human hands or bodies.

As an example of the SAGE results, Figure 4.1 shows the incoming angles and strength of the estimated MPCs, in an outdoor channel using the cylindrical array at the base station. In the figure, the direction with the strongest

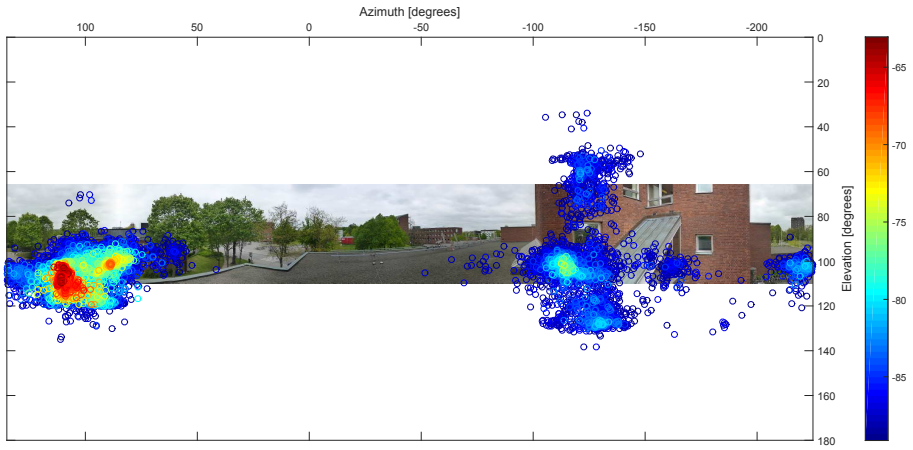

Figure 4.1: Panorama picture of an outdoor channel "seen" by the cylindrical array at the base station. The angles of arrival and strength of the estimated MPCs are shown. Color coding represents the MPC strength in dB.

MPCs (in dark red) is the LOS, and in other directions, the buildings form strong scattering.

The SAGE algorithm provides high angular resolution, where MPCs having a small difference in angles can be separated as long as their delays or Doppler frequencies differ sufficiently. However, it requires high computational complexity, and may converge to a local optimum. We also face the problem of estimation artifacts. This happens, e.g., when the contribution of an MPC is not completely extracted, and the residual power at the same delay and angle is relatively high.

The SAGE is good at estimating specular components, arising from specular reflections on smooth surfaces, but does not include diffuse multipath [79–81] in the estimation process. It has been reported, however, that the diffuse part can contribute significantly to the channel [82]. As an alternative to the SAGE, the RiMAX algorithm [76] takes both the specular and diffuse parts into consideration. It estimates components in the two alternately, and might therefore improve estimation performance. However, a comparison of estimation algorithms is beyond the scope of the thesis.

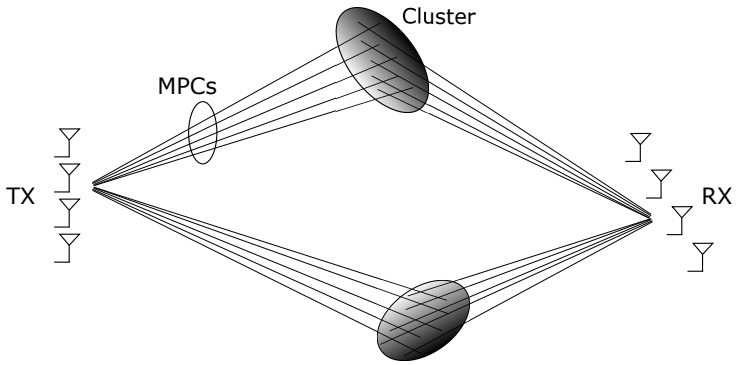

Figure 4.2: A cluster-based channel: MPCs depart from the transmitter and arrive at the receiver in groups.

4.2 Clustering and Tracking

MPCs tend to depart and arrive in groups, and from a channel characterization and modeling perspective, we group MPCs with similar delays and angles into clusters. Figure 4.2 illustrates a cluster-based channel representation. The analysis of a channel is now based on the behavior of clusters, such as cluster delay and angular spreads, cluster power variation over time, and so on. In this way, channel analysis is greatly simplified, while important properties can still be captured.

Before grouping estimated MPCs into clusters, we ask: What is a cluster? A general definition can be that, a cluster is a collection of objects that are similar to one another and are dissimilar to objects in other clusters [83]. When it applies to MPCs in a channel, there are different types of cluster concepts, depending on how we define the similarity of MPCs [84]. One concept is based on physical scatterers, e.g., a building wall, a tree, or a car (cf. Figure 3.2), and MPCs within a cluster have interacting points on the same physical scatterer. This cluster type is called *physical cluster*. Another cluster concept is based on the MPC parameter space, where MPCs within a cluster have similar delays and angles. This, however, does not guarantee the clusters match the physical scatterers in an environment, especially when multi-bounce propagation exists. We call this cluster type *parameter-based cluster*.

Physical clusters can be identified with assistance of ray-launching tools [85], however, this is out of the thesis scope. We identify parameter-based clusters based on estimated MPCs in measured channels. A comparison between physical and parameter-based clusters from a channel modeling perspective can be

found in [85].

4.2.1 Clustering

There are various automatic clustering algorithms used to identify parameter-based clusters, such as hierarchical, K-means and Gaussian mixture model (GMM) clustering [86, 87]. Each method introduces their own definitions of a cluster. In this thesis work, we use the KPowerMeans algorithm [88]. It is an extension of the K-means clustering and takes the power of MPCs into account. The idea is that MPCs with strong power should influence more on clustering than weak MPCs. Cluster centroids are thus pulled towards strong MPCs.

Similar to K-means, the KPowerMeans iteratively minimizes the total sum of power-weighted multipath component distances (MCD) [89]. The MCD is a measure of the distance between an MPC to a cluster centroid. In the u-th iteration, each MPC is assigned to the "nearest" cluster, then the cluster centroids are recalculated based on the latest assignment. The process can be formulated as [88]

$$\begin{aligned} I_l^u &= \arg\min_k \; P_l \cdot \mathrm{MCD}\left(\boldsymbol{x}_l, \boldsymbol{\mu}_k^u\right) \\ \boldsymbol{\mu}_k^{u+1} &= \frac{\sum_{I_l^u=k} P_l \boldsymbol{x}_l}{\sum_{I_l^u=k} P_l}, \end{aligned} \tag{4.7}$$

where $\boldsymbol{x}_l = [\tau_l, \phi_l^{\mathrm{tx}}, \theta_l^{\mathrm{tx}}, \phi_l^{\mathrm{rx}}, \theta_l^{\mathrm{rx}}]^T$ is the parameter space of the l-th MPC and a subset of (4.5), $P_l = |\gamma_l^{\mathrm{vv}}|^2 + |\gamma_l^{\mathrm{vh}}|^2 + |\gamma_l^{\mathrm{hv}}|^2 + |\gamma_l^{\mathrm{hh}}|^2$ is the MPC power, $\boldsymbol{\mu}_k^u$ is the k-th cluster centroid in the u-th iteration, and I_l^u is the cluster index that the l-th MPC is assigned to in this iteration. Based on the assignment, the new cluster centroids $\boldsymbol{\mu}_k^{u+1}$ are found. The algorithm iterates until convergence or reaching the allowed number of iterations. Regarding the MCD, there are different measures, and in this thesis work, we quantify it in the MPC parameter space, as defined in [84].

As an example, Figure 4.3 shows the clustering results based on the estimated MPCs shown in Figure 4.1. Different colors now represent different clusters. We see that some clusters well match the physical objects in the environment. However, the straight boundaries between clusters are artificial, caused by the used MCD measure.

4.2.2 Cluster Tracking

To characterize and model the time-variant nature of a radio channel, we study cluster behavior over time. Clusters thus have to be identified and also tracked. We use a joint clustering and tracking algorithm [84] in this work.

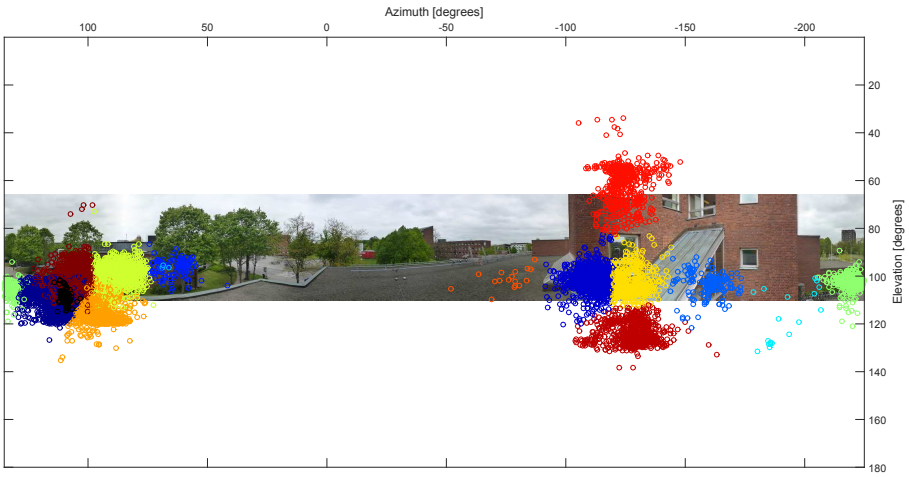

Figure 4.3: Panorama picture of an outdoor channel "seen" by the cylindrical array at the base station. MPCs with similar angles and delays are grouped into clusters. Color coding represents different clusters.

In the algorithm, the clustering results from the $(n-1)$-th snapshot are fed into the clustering initialization in the n-th snapshot. After applying the KPowerMeans algorithm, the identified clusters are associated with the "old" clusters in the previous snapshot. The cluster association is performed based on the *closeness function* defined in [84]. An old cluster that cannot be associated with any new cluster is considered "dead" and, similarly, a new cluster without an old counterpart is considered "newborn".

Cluster tracking is not only applied in the time domain, but can also be used in the spatial domain. Over our large linear array, we observe significant channel variations. MPC estimation, clustering and tracking are performed based on the 10-antenna sliding window mentioned in Section 4.1.1. We then study how cluster behavior varies over the array. The observations are reported in papers IV and V, and also summarized in Chapter 5. These include that 1) some clusters do not exist over the entire array, and 2) for clusters existing over the entire array, their power contributions may vary considerably over the array.

4.3 Channel Power Normalization

In evaluations of massive MIMO performance, raw channel data can be used directly, if measurement SNRs are good enough. Ideally, we do not need channel power normalization, since raw data reflects propagation conditions combined with antenna effects, such as pathloss and fading in a channel. To compare system performance in different scenarios, e.g., using different antenna arrays or when users are located at different places, we may need to normalize the channel power for fair comparisons. How to normalize channel power depends on what we would like to investigate, and the metric used for the investigation.

For MIMO channels, power normalization can be performed across time, frequencies, users and antenna elements. Typically, we would like to keep the power variation over time, i.e., the fading effects. Over frequencies, we also retain the power variation, as OFDM is used and on different subcarriers we have different channel attenuations. In the spatial domain, power variations over antenna arrays should be retained, as they affect MIMO performance. Antennas with higher channel gains contribute more to the system performance, compared to the ones with lower channel gains. This effect becomes significant in massive MIMO, due to large power variations over arrays, as discussed in Chapter 8 and Paper VI.

Channel normalization in this thesis is performed to equalize mean power between users. In MU-MIMO, users can be located near to or far from the base station. Thus they may have significant differences in pathloss and large-scale fading, resulting in very different SINRs in their links. To a certain extent, the differences can be compensated for by power control to pursuit fairness in rates among the users. When sum-rate maximization is the objective, as in (2.14) and (2.16), more power has to be allocated to the stronger users and less to the weak ones. In this case, it is difficult to relate MU-MIMO performance to the spatial orthogonality of user channels, i.e., the primary issue we would like to investigate in real massive MIMO channels. We therefore choose to normalize the imbalance in user channel attenuations. Such a normalization is formulated in papers II and III (with different notations) as

$$\boldsymbol{h}_{i,\ell,t}^{\text{norm}} = \sqrt{\frac{\widetilde{M}LT}{\sum_{t=1}^{T}\sum_{\ell=1}^{L}\left\|\boldsymbol{h}_{i,\ell,t}^{\text{raw}}\right\|^2}}\boldsymbol{h}_{i,\ell,t}^{\text{raw}}, \tag{4.8}$$

where $\boldsymbol{h}_{i,\ell,t}$ is the channel vector from the i-th user to all $\widetilde{M}$ base station antennas used in a measurement, on the ℓ-th subcarrier and at the t-th snapshot, L and T are the total numbers of subcarriers and snapshots, respectively. In

this thesis, $\widetilde{M} = 128$, since our cylindrical and linear arrays are used in measurements. The number of antennas, M, may vary in the range $K \leq M \leq \widetilde{M}$, for studying the same channel but with different numbers of antennas.

When using the singular value spread of a channel matrix to evaluate user orthogonality, we also perform the normalization in (4.8), see papers II and III. After the normalization, the singular value spread only reflects channel orthogonality, rather than in a mix with the attenuation imbalance between user channels.

We should note that the normalization in (4.8) have an effect of noise scaling. For user channels with lower measurement SNRs, the noise in the channel data is amplified relative to that in channels with higher measurements SNRs.

Chapter 5

Channel Characterization

After proper processing of measurement data, real massive MIMO channel behavior can be characterized. The general question to address is: What are the properties of real massive MIMO channels, as compare to i.i.d. Rayleigh and conventional MIMO channels? In this chapter, let us review the identified channel properties, both at the base station side, when different array types are used, and at the user side, when they are closely located or well distributed. The channel properties help us understand massive MIMO performance in real-life environments, and also provide us an insight into channel modeling.

5.1 Base Station Side

With increasing number of antennas, we may end up with a physically-large array such as our linear array, or we pack antennas into a compact space like the cylindrical array. Different array structures result in different channel behavior, and this will have an impact on massive MIMO performance.

5.1.1 Large Arrays

As the array aperture becomes large, the plane-wave approximation often used in conventional MIMO channels does not hold any more. This is because users or significant scatterers are, most likely, located within the *Rayleigh distance* of the array. The Rayleigh distance d_R, also known as the *Fraunhofer distance*, roughly defines the boundary of the near- and far-field regions of an antenna or antenna array [64],

$$d_R = \frac{2D_a^2}{\lambda}, \tag{5.1}$$

where D_a is the largest physical dimension of the antenna or antenna array and λ the wavelength. In the far field where the distance to the antenna or antenna array, d, fulfills $d \gg \lambda$ and $d \gg d_R$, wave propagation is approximated to have plane wavefronts. This approximation often holds for conventional MIMO where D_a is small. In massive MIMO with large D_a, the Rayleigh distance d_R becomes large. For example, with our 7.4-m linear array, $d_R \approx 950$ m, at 2.6 GHz. Users or significant scatterers are often located within this distance. Spherical wavefronts are thus experienced over the array.

As a comparison, Figure 5.1 illustrates plane and spherical wavefronts, over small and large arrays, respectively. With plane wavefronts, the phase difference between antenna elements only depends on the incident angle, for given array geometry and antenna patterns. With spherical wavefronts, the phase difference also relates to the propagation distance from a user or a scatterer to the array [90]. This property of spherical wavefronts allows spatial separation of user signals not only in angle but also in depth. With a small array, it can be particularly difficult to separate users being located at the same angle, while with a large array, it may be possible if users have different distances to the array.

In real channels, propagation is not as simple as illustrated in Figure 5.1. Users have line-of-sight (LOS) or none-line-of-sight (NLOS) conditions to the base station, and scatterers exist in the channels. Figure 5.2 shows the estimated angular power spectra (APS) over the linear array, in four LOS scenarios. Dominant components can be observed over the entire array or at most parts of the array. Contributions from strong scatterers can also be seen. Figure 5.3 shows the APS in four NLOS scenarios with rich scattering. In these APS, common characteristics are that the channel varies significantly over the array, and large-scale fading can be experienced - as large as 9 dB in the LOS scenarios and up to 6 dB in the NLOS. In measured channels, we observe very different propagation as compared to i.i.d. Rayleigh. Propagation in an i.i.d. Rayleigh channel is very rich and complex, while the measured channels show "sparsity" in the sense that significant power contributions only come from certain angles.

Spatial variation results in a different pattern of fading and correlation on a large array, as compare to a small array, see Figure 5.4. For conventional MIMO arrays, fading and correlation are often modeled by a Toeplitz structure,

$$\boldsymbol{T} = \begin{bmatrix} a_0 & a_1 & a_2 & \dots & a_{M-1} \\ a_1^* & a_0 & a_1 & \dots & a_{M-2} \\ a_2^* & a_1^* & a_0 & \dots & \vdots \\ \vdots & \vdots & \vdots & \ddots & a_1 \\ a_{M-1}^* & a_{M-2}^* & \dots & a_1^* & a_0 \end{bmatrix}, \tag{5.2}$$

where a_i^* is the complex conjugate of a_i. On average, there is no power variation

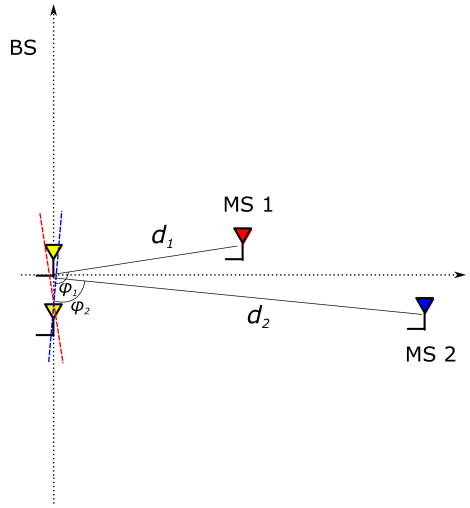

(a) Plane-wave approximation in the far field.

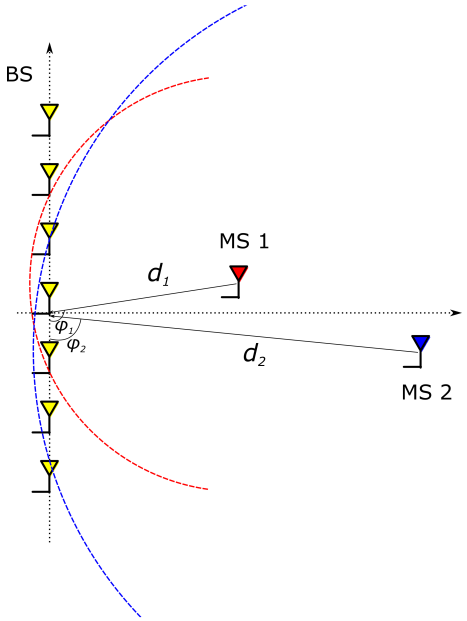

(b) Spherical-wave propagation in the near field.

Figure 5.1: Illustration of (a) plane wavefronts over a small array, and (b) spherical wavefronts over a large array.

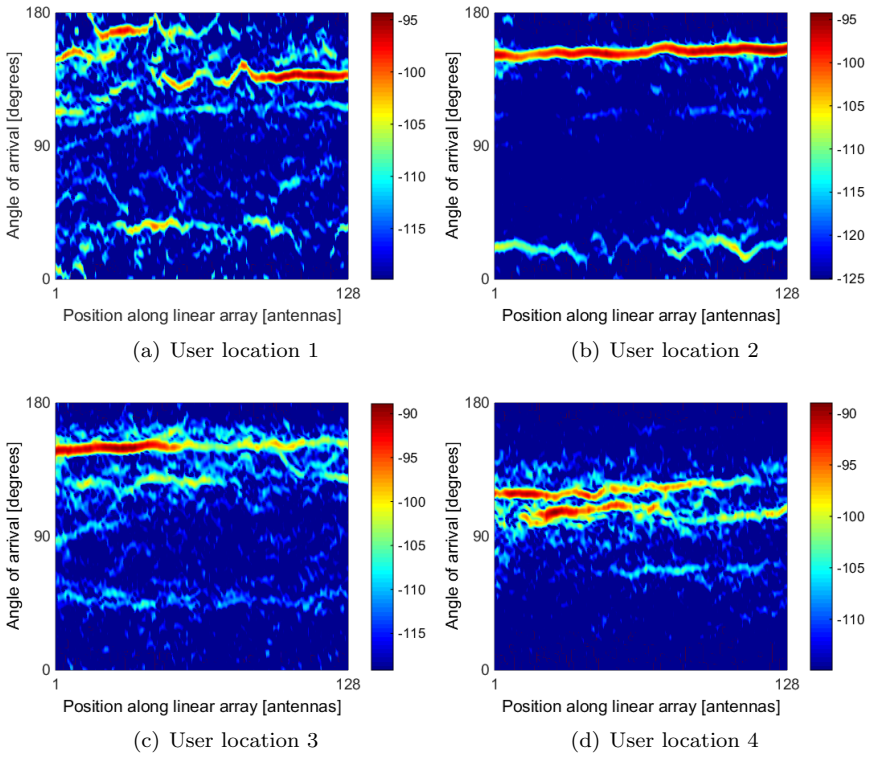

(a) User location 1

(b) User location 2

(c) User location 3

(d) User location 4

Figure 5.2: Angular power spectra (APS) over the 128-antenna linear array, from four user locations with LOS characteristics. Color coding represents power contribution in dB.

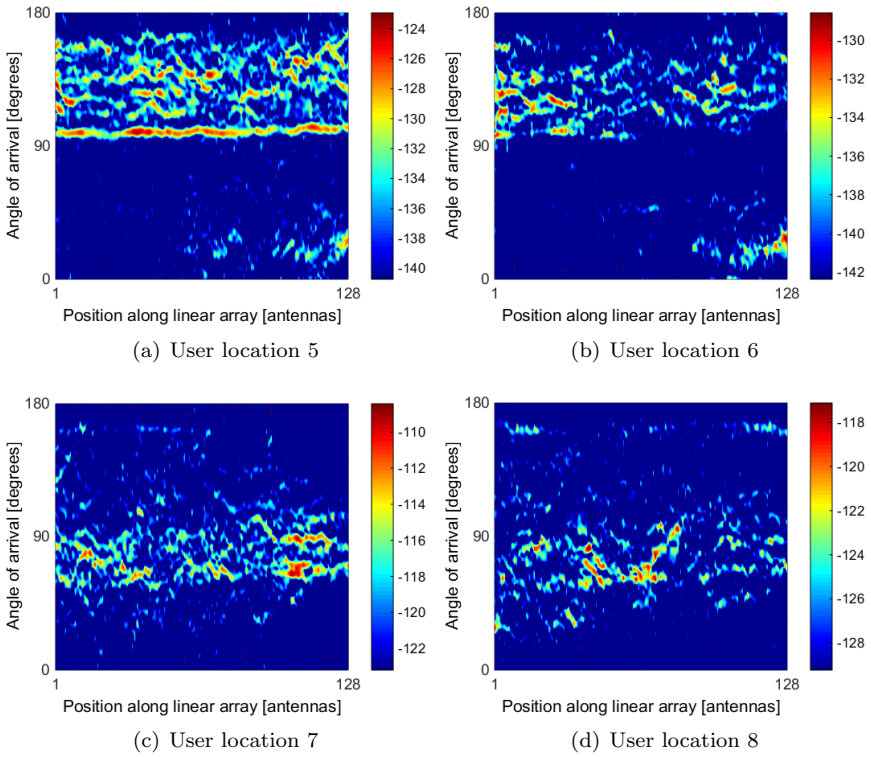

(a) User location 5

(b) User location 6

(c) User location 7

(d) User location 8

Figure 5.3: Angular power spectra (APS) over the 128-antenna linear array, from four user locations with NLOS characteristics. Color coding represents power contribution in dB.

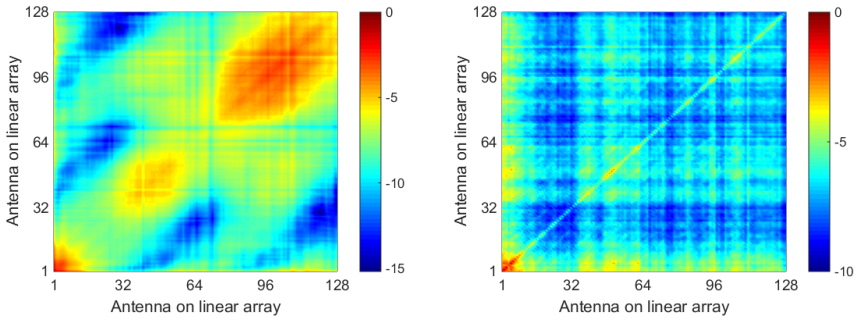

(a) A LOS scenario - user location 2 (b) An NLOS scenario - user location 5

Figure 5.4: Fading and correlation patterns on the 128-antenna linear array, in (a) a LOS scenario, and (b) an NLOS scenario.

over the array, and spatial correlation only depends on the distance between antennas. This structure holds when M is small. In massive MIMO with large M, however, fading and correlation structure is far from Toeplitz, as observed in Figure 5.4 and presented in [91].

5.1.2 Compact Arrays

To pack many antennas into a limited space, it is preferable to use rectangular or cylindrical array structures. We have to consider 3D propagation, when arrays extend in both horizontal and vertical dimensions, and also polarization characteristics, when polarized antennas are used to reduce spatial correlation on compact arrays. One example of such a compact array is our 128-element cylindrical array, about 30 cm in both diameter and height (cf. Figure 3.3).

Despite the compactness, the cylindrical array has a similar effect of channel variation over the array, as discussed in papers II and VI. This is, however, due to its circular structure and directive antenna arrangement. As a comparison, fading and correlation patterns on the cylindrical array are shown in Figure 5.5, for the same scenarios as in Figure 5.4 with the linear array. The patterns are, again, different from a Toeplitz structure.

5.2 User Side

The most important advantage of massive MIMO is that user signals can be separated in the spatial domain. Spatial separability of massive MIMO has

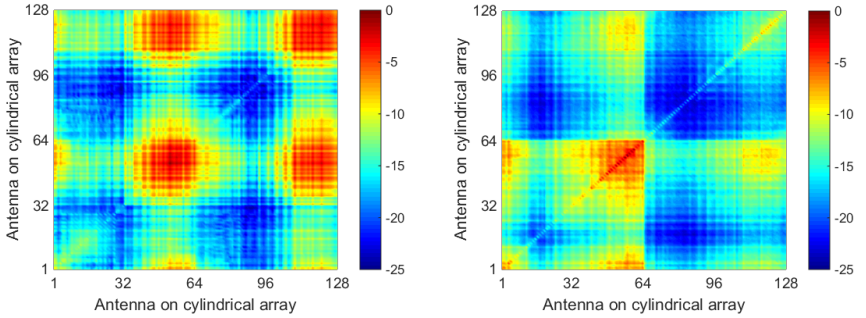

(a) A LOS scenario - user location 2 (b) An NLOS scenario - user location 5

Figure 5.5: Fading and correlation patterns on the 128-element cylindrical array, in (a) a LOS scenario, and (b) an NLOS scenario. The antennas are re-indexed as follows: the first 64 are vertically-polarized antennas and the last 64 are horizontally-polarized ones, antennas facing the same direction are ordered successively from bottom to top.

been evaluated and confirmed based on measured channels, as reported in papers I-III. Not only for users being located far apart, but closely-spaced users can also be separated even with compact arrays, as shown in Paper III where crowded scenarios are investigated. Propagation effects among closely-spaced users need to be investigated, as they have not been considered in conventional MU-MIMO.

For users being far apart, interacting with different scatterers in the propagation environment, it is relatively easy to spatially separate their signals. Closely-spaced users are most likely interacting with the same scatterers, but in different ways [66]. More precisely, closely-spaced users may interact with different structural details of a physical scatterer, resulting in MPCs with different angles, phases and amplitudes. Based on 3D ray tracing in an urban environment, the study in [92] investigated the duration of MPCs along a path. Figure 5.6 illustrates the propagation effect, where a transmitter is moving and a receiver is fixed, after some distance, the interaction point on a scatterer changes and a different MPC "arises". We call this distance *MPC lifetime*. Simulation results in [92] show that most MPCs last for less than 1 m, only a few last for above 10 m, and not much power is present in the long-lasting ones. The observation supports that closely-spaced users have different MPCs interacting with the same scatterer. However, this propagation effect needs to be further investigated using channel measurements.

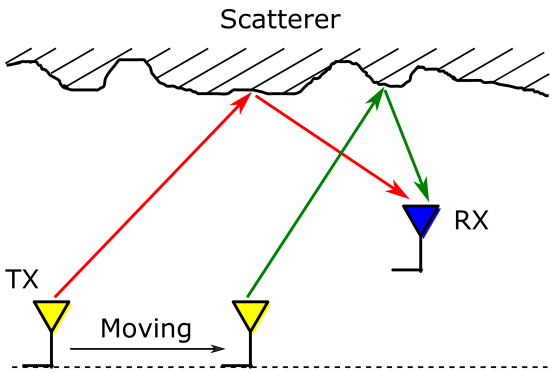

Figure 5.6: An illustration of the MPC duration along a path. After some distance, the interaction point on a scatterer changes.

5.3 Summary of Observed Channel Properties

In summary, propagation mechanisms in a radio channel are independent of antennas and systems, but some propagation properties become more pronounced in massive MIMO. We summarize these important properties influencing massive MIMO performance and that may need to be captured in channel models.

- Spherical wavefronts are experienced over large arrays, as users or significant scatterers are located in the near field of a large array.
- Channel variations over large arrays are significant, in terms of
  - variation in angular power spectrum (APS),
  - variation in power delay profile (PDP),
  - large-scale fading.
- Closely-spaced users often have MPCs interacting with different structural details of the same scatterer, resulting in different MPC parameters.
- 3D propagation becomes important when arrays extend in both horizontal and vertical dimensions.
- Polarization properties become important when polarized antennas are used.

Gaining an understanding of real massive MIMO channel behavior, we now move to the performance evaluation in the next chapter.

Chapter 6

Performance Evaluation in Measured Channels

In Chapter 5, we have seen that real massive MIMO channel characteristics are hardly i.i.d. Rayleigh and also very different from those in conventional MIMO. A major question we would like to address in the thesis is: Can we also harvest massive MIMO advantages in real channels as have been observed in i.i.d. Rayleigh channels?

We evaluate massive MIMO performance based on our measurement data, using metrics such as singular value spreads, capacities and sum-rates. Results from different measurements are presented in papers I-III. In this chapter, we overview the performance evaluation work. In conclusion, the message we would like to convey is: massive MIMO also works well in real propagation environments.

6.1 Singular Value Spreads

As discussed in Section 2.2, many theoretical advantages of massive MIMO arise because user channels become orthogonal. This happens in i.i.d. Rayleigh channels when $M \to \infty$, as concluded in (2.21). We would like to evaluate to what degree the claim also holds in measured channels. The evaluation metric we use is the singular value spreads of channel matrices, normalized using (4.8).

Performing singular value decomposition (SVD) of the $K \times M$ normalized channel matrix, for simplicity also denoted by $\boldsymbol{H}$,

$$\boldsymbol{H} = \boldsymbol{U}\boldsymbol{\Sigma}\boldsymbol{V}^H, \tag{6.1}$$

where $\boldsymbol{U}$ and $\boldsymbol{V}$ are unitary matrices containing the left and right singular vectors, we obtain the singular values $\sigma_1, \sigma_2, \ldots, \sigma_K$ on the diagonal of the matrix $\boldsymbol{\Sigma}$. The singular value spread is the ratio

$$\kappa = \frac{\max\limits_i \sigma_i}{\min\limits_i \sigma_i}, \tag{6.2}$$

of the maximum and minimum singular values. Since the imbalance in user channel attenuations has been removed by the normalization, κ contains information about how orthogonal the user channel vectors are. The best case is when $\kappa = 1$ ($20\log_{10}\kappa = 0$ dB) and all user vectors are orthogonal to each other. In this case, all users can be served simultaneously without inter-user interference. The value of κ gets large when user orthogonality is poor. If $\kappa \to \infty$, it means that at least two user vectors are aligned. By saying "at least", we mean that the rest of the users may enjoy good channel orthogonality, however, we cannot simply tell from the value of κ. For a detailed investigation, we need to look at all the singular values. Assume that K_0 ($K_0 \leq K$) singular values are large and among which the ratio of the maximum and minimum is small, while the other $K - K_0$ are small. This indicates that K_0 users have good channel orthogonality. In the evaluation of massive MIMO channels, we are hoping for small values of κ, so that all $K_0 = K$ users have good channel orthogonality.

Table 6.1 summarizes the statistical results of singular value spreads presented in Paper II [1], for $K = 4$ closely-located users, in the semi-urban measurements using linear and cylindrical arrays. When shifting from conventional MIMO ($M = 4$) to massive MIMO ($M = 128$), not only does the median of singular value spreads drop considerably, by 12-15 dB, in the measured channels, but also the dispersion measured by the inter-quartile range (IQR) shrinks to only 0.6-2 dB. The observations indicate that we also harvest improved user channel orthogonality and the effect of channel hardening in measured massive MIMO channels, like in i.i.d. Rayleigh.

6.2 Capacities and Sum-rates

Capacities and sum-rates are commonly-used metrics to evaluate system performance, since they indicate the maximum theoretical rates can be achieved in a system. We focus on MU-MIMO downlink capacities and sum-rates, achieved by using DPC and linear precoding schemes, as derived in Section 2.1.2.

In Paper I where a $K = 2$ user case is studied, we show that when users have good channel orthogonality, ZF and MMSE perform very close to DPC

[1] Note that the value of singular value spread in dB is calculated as $20\log_{10}\kappa$ in Paper II, but $10\log_{10}\kappa$ in Paper III.

Table 6.1: The median [dB] and inter-quartile range (IQR) [dB] of singular value spreads in i.i.d. Rayleigh and measured channels, for $K = 4$ co-located users, in conventional MIMO ($M = 4$) and massive MIMO ($M = 128$). The results are summarized from Paper II.

Scenarios	$M = 4$		$M = 128$	
and arrays	κ-median	κ-IQR	κ-Median	κ-IQR
I.i.d. Rayleigh	17	7	2	0.5
NLOS, linear array	17	7	2	0.6
NLOS, cylindrical array	23	8	7	2
LOS, linear array	23	9	9	0.8
LOS, cylindrical array	26	8	14	1.4

capacity. When users have very poor channel orthogonality, DPC capacity drops to the performance of single-user transmission, while ZF performs much worse than that. In this case, a time-sharing strategy between users can be used to achieve near-optimal performance. In the measured channels using the cylindrical array, ZF and MMSE can achieve as high as 98% of DPC capacity, with only 20 antennas, for the two-user case. The study indicates a potential of achieving near-optimal performance by using linear precoding in massive MIMO, and combining spatial multiplexing with time-sharing/user-scheduling strategies.

In Paper II, we investigate the measured channels with $K = 4$ and $K = 16$ users, in a semi-urban environment using the linear and cylindrical arrays. With $K = 4$ users, in the worst scenario where users are closely located in LOS conditions, the measured channels perform at 90% and 75% of the DPC capacities achieved in i.i.d. Rayleigh channels, when the number of antennas is above 40. With $K = 16$ users, in the worst scenario, more than 50% can be achieved, when using 128 antennas. The study shows that in real channels we can harvest a large fraction of the performance achieved in i.i.d. Rayleigh channels.

How about linear precoding performance in the measured channels in Paper II? Some unpublished results are shown in Figure 6.1 and Figure 6.2, for $K = 4$ co-located users in NLOS and LOS conditions, respectively. In the signal model, transmit power is scaled down as the number of antennas grows, $p_{\mathrm{dl}} = \frac{\rho K}{M}$. With increasing number of antennas, ZF sum-rates improve dramatically and get close to DPC capacities, while MF performance improves slowly in most cases and may also decrease if user orthogonality is poor. Table 6.2 summarizes DPC capacities and ZF sum-rates in these scenarios, when shifting

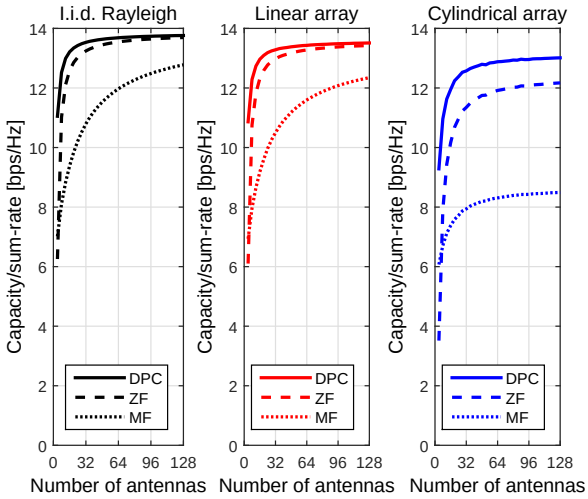

Figure 6.1: Capacities and sum-rates in i.i.d. Rayleigh channels and the measured channels presented in Paper II, for $K=4$ co-located users in NLOS conditions. Transmit power is scaled down linearly with the number of antennas, $p_{\mathrm{dl}}=\frac{\rho K}{M}$ where $\rho=10$ dB.

from conventional MIMO ($M=4$) to massive MIMO ($M=128$). While ZF is not a very efficient scheme in conventional MIMO, improved user orthogonality in real massive MIMO channels allows us to use ZF to achieve near-optimal performance. Also note that the improvement in sum-rates is achieved with reduced transmit power, by as much as 15 dB, from $M=4$ to $M=128$.

Paper III studies crowded scenarios with $K=8$ closely-spaced users. Users have LOS conditions to the cylindrical array at the base station, making spatial separation of their signals particularly difficult. Again, we observe a great improvement in ZF sum-rates, when shifting from conventional MIMO to massive MIMO. Further, we uncover the sum-rates and look at fairness in terms of per-user rates. Sum-rate maximization in (2.16) can result in large unfairness in per-user rates, and in the worst case some users have zero rates. We thus investigate how many of these closely-spaced users are actually "served", in the sense that they are allocated power and have non-zero rates. The results show that the total amount of transmit power plays an important role, and with the same amount of power available, massive MIMO can "serve" more users than conventional MIMO. This indicates that massive MIMO also achieves better fairness in user rates, thanks to the reduction of inter-user interference.

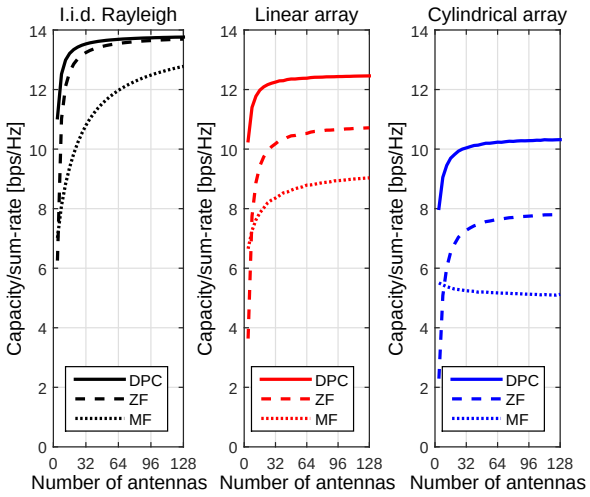

Figure 6.2: Capacities and sum-rates in i.i.d. Rayleigh channels and the measured channels presented in Paper II, for $K=4$ co-located users in LOS conditions. Transmit power is scaled down linearly with the number of antennas, $p_{\mathrm{dl}}=\frac{\rho K}{M}$ where $\rho=10$ dB.

Table 6.2: Average DPC capacities [bps/Hz] and ZF sum-rates [bps/Hz] in i.i.d. Rayleigh and the measured channels presented in Paper II, for $K=4$ co-located users, in conventional MIMO ($M=4$) and massive MIMO ($M=128$). Transmit power scheme is $p_{\mathrm{dl}}=\frac{\rho K}{M}$ where $\rho=10$ dB.

Scenarios and arrays	$M=4$		$M=128$	
	DPC	ZF	DPC	ZF
I.i.d. Rayleigh	11.1	6.3	13.8	13.7
NLOS, linear array	10.9	6.1	13.5	13.4
NLOS, cylindrical array	9.3	3.5	13	12.2
LOS, linear array	10.3	3.6	12.5	10.7
LOS, cylindrical array	8	2.3	10.3	7.8

6.3 Summary of Performance Evaluation

With all performance evaluation results, we come to the general conclusion that massive MIMO also works well in real propagation environments. Some factors have an important impact on massive MIMO performance. As a reference for system design and future work, let us summarize these ones, including comments on antenna arrays, linear precoding, antenna selection, user scheduling, and transmit energy.

- Antenna arrays.

  In most cases we have observed that the physically-large linear array is better at separating users than the cylindrical array. This is due to the linear array's large aperture and the resulting channel variations over the array (cf. Figure 5.2 and Figure 5.3). The cylindrical array, due to its circular structure, is good at separating well-distributed users in different directions. With dual-polarized antennas, the cylindrical array can also make use of polarization diversity offered by propagation environments. This becomes a great advantage since polarization at the user side is usually unknown.

- Linear precoding.

  In conventional MIMO, ZF may not be a good choice due to poor orthogonality of user channels. In massive MIMO, as channel orthogonality improves and becomes stable, ZF can achieve near-optimal performance and thus becomes an attractive choice for massive MIMO precoding. MF shows a slower convergence to the optimal performance, that is to say, more antennas are needed to achieve the same performance as ZF. Despite this, MF outperforms ZF in low-SNR scenarios.

- Antenna selection.

  As observed in measured channels, antennas on both the linear and cylindrical arrays typically have a significant imbalance in their channel gains. This results in, as discussed in Chapter 8 and Paper VI, some antennas contributing more to system performance than others. Antenna selection therefore becomes an effective strategy to reduce system complexity.

- User scheduling.

  Propagation conditions and user distributions have considerable impact on massive MIMO performance. Although massive MIMO greatly improves channel orthogonality, there are some "difficult" scenarios where not all users can be efficiently served at the same time. Some users may

suffer close to zero rates, especially when a lot of them are aggressively multiplexed in the spatial domain. The same effect is also observed when some users are close to the base station while others are far away, resulting in a large imbalance in their channel attenuations. User scheduling can be used as a strategy to guarantee user services and in the end reach better system performance.

- Transmit energy.

  As observed in measured channels, system performance can be greatly improved, at the same time transmit power can be lowered by an order of magnitude or more. However, reducing transmit power may not always be the best strategy to harvest large array gains. Guaranteeing good SNRs is also important, in the sense that ZF performs worse than MF in noise-limited scenarios. The situation with MF is different, where higher transmit power induces higher inter-user interference. After a certain point, the number of users that can be served simultaneously will actually decrease, as shown in Paper III.

To design communication schemes and evaluate system performance in an efficient way, we need realistic models that simulate channel statistics with the essential massive MIMO properties. We now move to channel modeling in the next chapter.

Chapter 7

Channel Modeling

As summarized in Chapter 5, several important propagation properties have been identified for real massive MIMO channels. These properties are different from those in conventional MIMO channels, and are also far from i.i.d. Rayleigh used in many theoretical studies. They determine the actual performance of a practical massive MIMO system.

To simulate realistic channels for the development and assessment of a massive MIMO system, an urgent task is to include the important channel properties into channel models. While channel modeling is a big and challenging topic, we overview the modeling work performed during this thesis study.

7.1 General Approaches

When developing a new wireless system, channel measurements, simulations, and field trials are important means to assess the actual performance of the new system. Measurements and trials, however, usually require a large investment in time and effort, as a new system needs to be tested in many propagation environments. Channel models, generating channel statistics with the essential propagation characteristics, is an efficient way of testing the system. Channel models are often implemented as channel simulators, so that various aspects of a system can be evaluated and optimized in a time- and cost-efficient manner.

Generally, physical propagation channels are independent of the systems that operate in them. Propagation mechanisms do not change, e.g., from narrowband to wideband systems, or from SISO to MIMO. The actual difference is in how different systems "resolve" different propagation effects. For example, delay dispersion becomes important in wideband systems, while angular

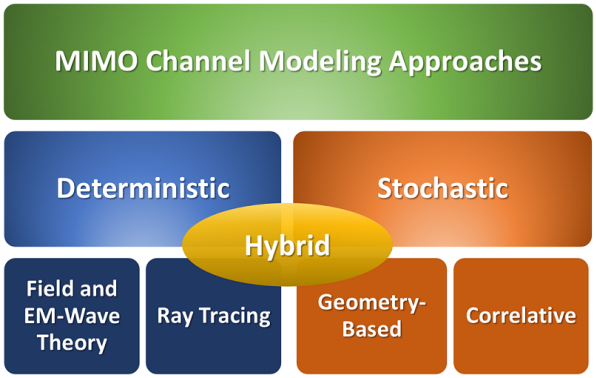

Figure 7.1: General approaches of MIMO channel modeling [58, 87].

dispersion is vital for MIMO. Channel models, on the other hand, do depend on the target systems for which a model is developed. Channel models are required to be only as complex as necessary, and can neglect propagation effects that do not have a significant impact on the system performance [93]. Hence, the goal of a channel model is to capture the propagation properties that are important to a specific system, while keeping the model simple to implement and use.

With the goal of channel models, different modeling approaches are applied depending on the target system and its intended use. Figure 7.1 shows a classification of the general approaches for MIMO channel modeling. The two main categories are *deterministic* and *stochastic* modeling approaches. Deterministic models are typically based on propagation mechanisms in a specific environment using, e.g., ray tracing or electromagnetic-wave theory. The site-specific feature of deterministic models makes them suitable for simulating systems in a specific environment. On the other hand, a physical model containing geographical and morphological information about the environment is required, which can be very complex depending on the environment and the desired modeling accuracy. Further, simulation factors such as the number of launched rays and the order of reflections will determine modeling accuracy and computational complexity.

Stochastic models aim at reproducing essential channel behavior in a statistical sense. Such modeling approaches do not attempt to predict the propagation in a specific environment, but rather to represent the statistical behavior of important propagation properties. A simple example is the Rayleigh fading model. In MIMO channel modeling, two approaches are often used: correlation-

based and geometry-based. Correlative models capture channel correlation properties between antenna elements at the transmitter and/or receiver. The Kronecker model [94] and the Weichselberger model [95] are two popular correlative models often used for analytical studies. A drawback is, however, their incapability of capturing the time-variant nature of propagation channels.

An alternative approach is used in geometry-based stochastic channel models (GSCMs) [96]. In this approach, the geometric location of interacting objects (IOs) and the interaction processes are characterized and modeled. Through very simple ray tracing based on these IOs, the parameters of MPCs can be obtained. An important modeling concept in GSCMs is clusters. As mentioned in Section 4.2, MPCs tend to depart and arrive in clusters. This effect arises because MPCs are created by the interaction with IOs in groups, e.g., a building can form a group of IOs. Based on clusters, GSCMs are simplified because the parameters of a cluster do not change when transmitter and/or receiver move over a relatively large area. In general, the advantages of GSCMs include that 1) directional properties can be easily modeled and implemented, 2) time variation in a channel can be captured through, e.g., the concept of cluster visibility regions, and 3) the influence of antennas can be decoupled from the propagation channel, making GSCMs able to simulate channels with different antenna types. Widely-known GSCMs include the series of the COST models (COST 259 [97, 98], 273 [99, 100] and 2100 [101]), the WINNER models [77], and the 3GPP Spatial Channel Model (SCM) [102].

In addition to deterministic and stochastic approaches, hybrid modeling is based on a combination of the two. For instance, a GSCM can be used together with ray tracing to determine cluster locations, while MPCs within a cluster are stochastic.

Among different approaches, the main modeling effort in this thesis is based on a cluster-based GSCM - the COST 2100 model [101]. The modeling work is presented in papers IV and V, attempting to extend the conventional COST 2100 model to cover massive MIMO. Modeling based on the Kronecker and Weichselberger models is also performed, and initial results can be found in [103].

7.2 Cluster Models

Among cluster-based GSCMs, the COST 2100 approach provides a generic and flexible framework, making it suitable for modeling multi-user, distributed MIMO and multi-base scenarios [101]. As discussed in Paper V, the COST 2100 framework is also easy to extend so that it captures the identify massive MIMO properties. We thus choose it as our modeling basis and extend it for massive

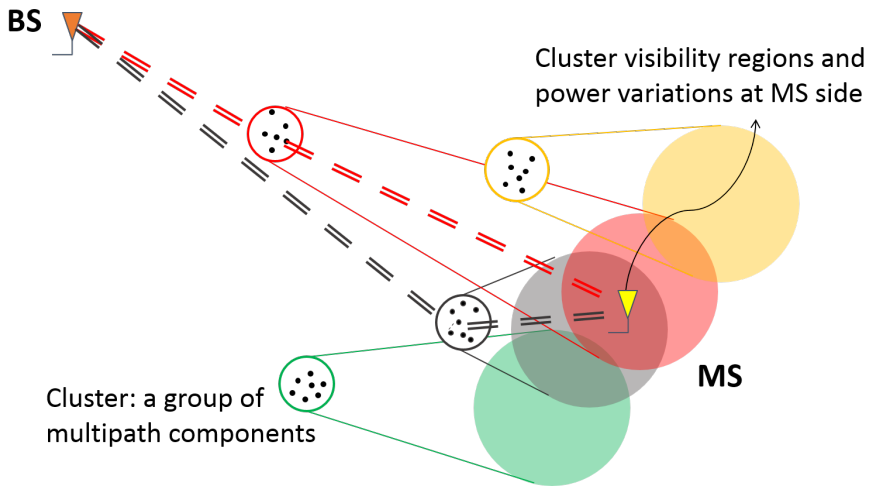

Figure 7.2: The COST 2100 MIMO channel model is based on the concepts of clusters and their visibility regions (VRs) [101]. In the conventional model, clusters have VRs at the terminal side. In the figure, the terminal is located in two cluster VRs, the corresponding clusters are thus "active" and contribute to the channel between the terminal and the base station.

MIMO. In the following, let us overview the COST 2100 extensions.

7.2.1 The COST 2100 Model Extensions

The COST 2100 channel model is a cluster-based GSCM that can simulate realistic channels over time, frequency and space. The propagation environment is simulated based on clusters and their visibility regions (VRs), as illustrated in Figure 7.2. Cluster VRs determine how cluster behavior varies when a terminal moves. The idea is that when a terminal moves into a cluster VR, this cluster becomes "active" and contributes to the channel between the terminal and the base station.

In the conventional model, only MIMO with small arrays is considered. When extending for massive MIMO, we attempt to include the channel properties summarized in Section 5.3 into the model. Figure 7.3 and Figure 7.4 illustrate the extensions for massive MIMO scenarios with large arrays and closely-spaced users, respectively.

- For scenarios with large arrays, as shown in Figure 7.3, we extend the concept of cluster VRs to the base station side. Now, a cluster has two VRs, one at the terminal side (MS-VR) and one at the base station side (BS-VR). A cluster is "active" in the channel between a terminal and a base station antenna, when the terminal moves into its MS-VR and the base station antenna is located within it BS-VR. Cluster power variation inside the BS-VR is also considered and modeled. In the extension, channel variation over a large array is captured, in the sense that different parts of the array can be located in different cluster BS-VRs, and within a BS-VR the cluster power contribution also varies. Spherical wavefronts are captured naturally due to the geometrical approach. This model extension is presented in Paper IV.

- For scenarios with closely-spaced users, the users may interact with different structural details of the same physical scatterer, as discussed in Section 5.2. Thus, closely-spaced users can experience different MPCs within the same cluster. In the conventional model, however, users have the same MPCs if they are within the same cluster MS-VRs. This leads to an overestimation of user correlation if they are closely located. In the extension, we introduce the concept of MPC gain function, as shown in Figure 7.4. We randomly assign peak locations for MPCs in a cluster MS-VR. The gain of an MPC to a specific user is determined by the distance of this user to the MPC's peak location. For now, we model the MPC gain as a 2D Gaussian function. When a user moves further away from an MPC's peak location, the MPC strength gets weaker and eventually vanishes. This model extension is presented in Paper V.

In addition, the model is also extended to include 3D propagation by introducing elevation angles. Polarization properties are captured by allowing each MPC to have both co-polarized and cross-polarized parts.

7.2.2 Validation of the Model Extensions

Validation against measurements is an essential step to check if the proposed extensions are capable of reproducing statistics in terms of the important massive MIMO properties. We simulate a set of channel data from the model, and compare its statistical behavior with that from measured channels. Ideally, the comparison should be performed without using the measurement data used to develop and parameterize the model. However, this requires more measurements performed in different environments, and so far we do not have such data. In the thesis, we therefore validate the model extensions against our measurements, as an initial validation step.

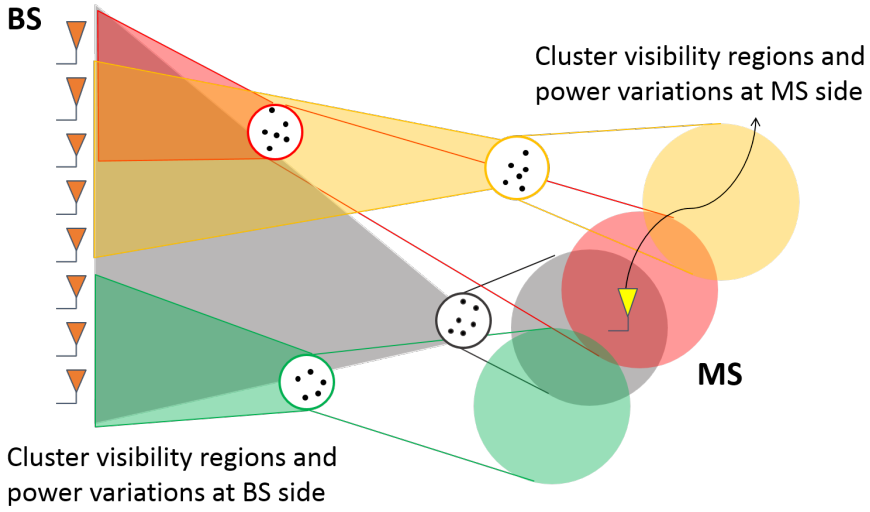

Figure 7.3: COST 2100 model extension for massive MIMO with large arrays in Paper IV. The modeling concept of cluster visibility regions is extended to the base station side.

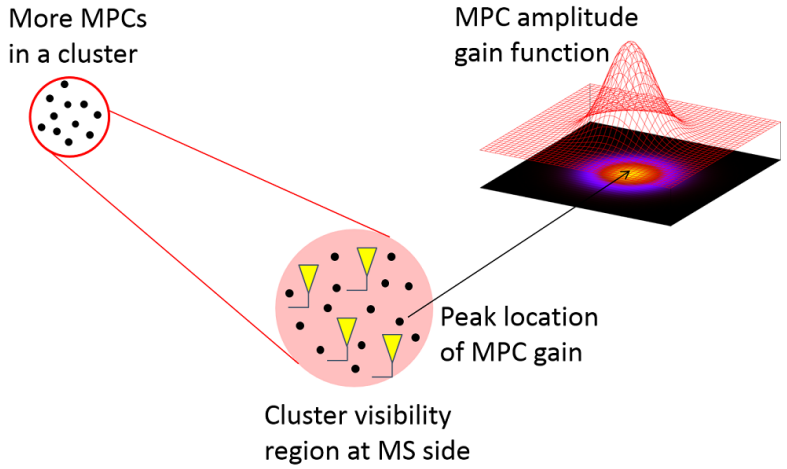

Figure 7.4: COST 2100 model extension for scenarios with closely-spaced users in Paper V. The modeling concept of MPC gain functions is introduced.

The most important aspect that we would like to validate for a massive MIMO channel model is user separability. This can be done by evaluating singular value spreads and sum-rates in the simulated channels and comparing the resulting statistics with that in the measured channels. On large arrays, fading and correlation properties produced by the model are also important to validate. For closely-spaced users, it is important to validate the temporal behavior of the channel, when a user is moving over a short distance. Initial validation for scenarios with closely-spaced users is presented in Paper V. The results show that the model extension is able to reproduce channel statistics in terms of singular value spreads, MF sum-rates and temporal behavior. However, statistics of ZF sum-rates from the simulated channels show a mismatch with those from the measured channels. Further validation and model improvements are therefore required.

7.3 Correlative Models

Due to the simplicity, correlative models are often used for MIMO analytical studies. The Kronecker model is particularly popular and also used in many massive MIMO investigations. In this thesis, we use our measurement data to validate two correlative models, the Kronecker and the Weichselberger, for massive MIMO.

A narrowband and spatially-correlated MIMO channel can be modeled as [58, 104]

$$\mathrm{vec}\left(\boldsymbol{H}\right) = \boldsymbol{R}_{\mathrm{full}}^{1/2}\mathrm{vec}\left(\boldsymbol{H}_{\mathrm{i.i.d.}}\right), \tag{7.1}$$

where $\mathrm{vec}(\cdot)$ is the vectorization of a matrix (stacking the columns of the matrix on top of one another), and $(\cdot)^{1/2}$ is the matrix square-root, $\boldsymbol{H}_{\mathrm{i.i.d.}}$ is an i.i.d. Rayleigh channel, and $\boldsymbol{R}$ is the full spatial correlation matrix between the transmitter and receiver,

$$\boldsymbol{R}_{\mathrm{full}} = \mathbb{E}\left\{\mathrm{vec}\left(\boldsymbol{H}\right)\mathrm{vec}\left(\boldsymbol{H}\right)^{H}\right\}. \tag{7.2}$$

The spatial structure of the MIMO channel is thus represented in $\boldsymbol{R}_{\mathrm{full}}$. This model, however, needs a large number of parameters, as the number of coefficients in $\boldsymbol{R}_{\mathrm{full}}$ is $MK \times MK$.

7.3.1 The Kronecker Model

The Kronecker model is based on the assumption that $\boldsymbol{R}_{\mathrm{full}}$ can be approximated as the Kronecker product [105],

$$\boldsymbol{R}_{\mathrm{full}} \approx \boldsymbol{R}_{\mathrm{TX}} \otimes \boldsymbol{R}_{\mathrm{RX}}, \tag{7.3}$$

of the correlation matrix at the transmit side, $\boldsymbol{R}_{\mathrm{TX}}$, and at the receive side, $\boldsymbol{R}_{\mathrm{RX}}$, given as

$$\begin{aligned} \boldsymbol{R}_{\mathrm{TX}} &= \frac{1}{\beta_{\mathrm{TX}}}\mathbb{E}\left\{\boldsymbol{H}^H\boldsymbol{H}\right\}^T \\ \boldsymbol{R}_{\mathrm{RX}} &= \frac{1}{\beta_{\mathrm{RX}}}\mathbb{E}\left\{\boldsymbol{H}\boldsymbol{H}^H\right\}, \end{aligned} \tag{7.4}$$

where β_{TX} and β_{RX} are power normalization scalars. The Kronecker model thus approximates the full-correlation model in (7.1) as

$$\boldsymbol{H} = \boldsymbol{R}_{\mathrm{RX}}^{1/2}\boldsymbol{H}_{\text{i.i.d.}}\left(\boldsymbol{R}_{\mathrm{TX}}^{1/2}\right)^T, \tag{7.5}$$

reducing the number of model parameters to M^2+K^2.

The approximation in (7.3) requires $\boldsymbol{R}_{\mathrm{TX}}$ and $\boldsymbol{R}_{\mathrm{RX}}$ to be independent. However, this only happens when scattering at the transmit side is independent from scattering at the receive side, e.g., when the distance between the transmitter and receiver is large. When the assumption is not valid, the Kronecker model causes artifact paths in the channel, since it forces the scattering at the two ends to be independent [106, 107]. The Kronecker model is found to consistently *underestimate* channel capacity [58]. The underestimation may become more severe in massive MIMO, as large arrays can resolve more scatterers, scattering at the two ends are more likely to be coupled than for small arrays.

7.3.2 The Weichselberger Model

The Weichselberger model extends the Kronecker one by introducing coupling between link ends [95]. A power coupling matrix $\boldsymbol{\Omega}$ is applied between the eigenbases of $\boldsymbol{R}_{\mathrm{TX}}$ and $\boldsymbol{R}_{\mathrm{RX}}$, given as [108]

$$\boldsymbol{\Omega} = \mathbb{E}\left\{\left(\boldsymbol{U}_{\mathrm{RX}}^H\boldsymbol{H}\boldsymbol{U}_{\mathrm{TX}}^*\right)\odot\left(\boldsymbol{U}_{\mathrm{RX}}^T\boldsymbol{H}\boldsymbol{U}_{\mathrm{TX}}\right)\right\}, \tag{7.6}$$

where $\odot$ is the Hadamard (element-wise) product of two matrices, and $\boldsymbol{U}_{\mathrm{TX}}$ and $\boldsymbol{U}_{\mathrm{RX}}$ are the eigenbases. The *coupling coefficient* $[\boldsymbol{\Omega}]_{i,j} = \mathbb{E}\{\|\boldsymbol{u}_{\mathrm{RX},i}^H\boldsymbol{H}\boldsymbol{u}_{\mathrm{TX},j}^*\|^2\}$ is the average power coupled between the i-th receive eigenvector and j-th transmit eigenvector. Introducing the coupling, the Weichselberger model becomes [58, 95, 108]

$$\boldsymbol{H} = \boldsymbol{U}_{\mathrm{RX}}\left(\sqrt{\boldsymbol{\Omega}}\odot\boldsymbol{H}_{\text{i.i.d.}}\right)\boldsymbol{U}_{\mathrm{TX}}^T, \tag{7.7}$$

where $\sqrt{(\cdot)}$ is the element-wise square-root of a matrix.

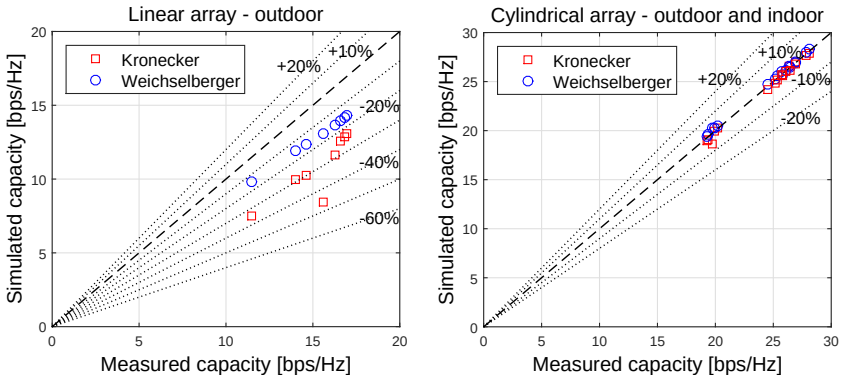

(a) Linear array.

(b) Cylindrical array.

Figure 7.5: Validation of the Kronecker and Weichselberger models based on measurements using the (a) linear and (b) cylindrical arrays. Users are located close to each other. Sum-rate capacity in the uplink is used as the validation metric.

7.3.3 Validation for Massive MIMO

Validation results based on our measurements are shown in Figure 7.5, for scenarios with closely-spaced users. With the 128-antenna linear array, the Kronecker model underestimates the sum-rate capacities achieved in the measured channels, and the mismatch is as high as 20-50%. The Weichselberger model performs better by introducing coupling, and the mismatch is below 20%. With the 128-element cylindrical array, it is interesting to observe that both the Kronecker and Weichselberger models have a good estimation of the capacities in the measured channels. This is possibly because only a small part of the cylindrical array contributes the most to the capacity, if users are closely located.

The validation gives us initial insights into analytical models for massive MIMO. More work is needed to understand the observations in Figure 7.5. When both M and K become large, the number of model parameters increases dramatically. How to reduce the number of parameters is a challenge. Potentially, the standard Kronecker and Weichselberger models can be modified for massive MIMO, but further analysis is required.

Chapter 8

Simplifying Hardware by Antenna Selection

When implementing a massive MIMO system, we face the challenge of hardware complexity. As mentioned in Section 2.3, the hardware complexity increases with the number of antennas and RF chains. This may result in a "massive" system with high cost and energy consumption. The question we address here is: Can we simplify massive MIMO hardware by removing RF chains, while largely maintaining the system performance? The proposed solution is antenna selection, and the investigations based on measured channels are presented in Paper VI and [110]. In this chapter, let us review massive MIMO antenna selection.

8.1 Antenna Selection

Cutting off RF chains is a direct way to simplify massive MIMO hardware, however, this leads to performance reductions. In order to make the performance reduction as small as possible, we can exploit the spatial domain and select the "best" antenna signals for further processing, while discarding the rest. In this way, high system performance may still be achieved with fewer than the full number of RF chains.

The effectiveness of antenna selection depends on channel properties. In i.i.d. Rayleigh, antennas contribute almost equally to the system performance, when averaging over a moderately-wide bandwidth. In other words, no specific antenna outperforms the others. In real massive MIMO channels, the situation is different. Inspired by Figure 5.4 and Figure 5.5 showing the fading and

correlation on the linear and cylindrical arrays, we believe some antennas do contribute more than others.

Paper VI investigates the effectiveness of antenna selection in measured massive MIMO channels, under different propagation conditions and with different numbers of users. Maximization of sum-rate capacity in the downlink is set as the objective for the antenna selection. Observations from this work are summarized as follows.

- Antenna selection is more effective when users are closely located, especially under LOS conditions. When users are well-distributed and under NLOS conditions, antenna selection is less effective but still performs better than in i.i.d. Rayleigh channels.
- Generally, antenna selection is more effective with the cylindrical array than with the linear array. With the linear array, the effectiveness significantly reduces as the number of users increases.
- In all investigated scenarios with up to $K = 40$ users, only 50-90 RF chains are required to achieve 90% of the full MIMO performance with 128 RF chains. This indicates that a large number of RF chains can be reduced with only 10% performance loss.
- Finding the antenna subset that maximizes the sum-rate is a relatively complex task. However, we have demonstrated in the measured channels that a simple selection scheme, based only on received signal power at each antenna, perform very close to the algorithm that maximizes the capacity. By only measuring received power on each antenna, this scheme can make a decision on antenna selection before any CSI estimation is performed and without complex processing.
- The capacity-maximizing algorithm finds a tradeoff between the channel gain at each antenna and the correlation among them. In massive MIMO, thanks to significant power variations over arrays, as discussed in Section 5.1, the simple power-based scheme performs close to the capacity-maximizing algorithm.

As a result, we consider antenna selection a promising and practical technique to reduce massive MIMO implementation complexity, and more importantly, this by using simple selection schemes.

8.2 Switching Networks

With fewer RF chains than the available antennas, an RF switch is required, as shown Figure 8.1. As numbers of antennas M and RF chains N grow large,

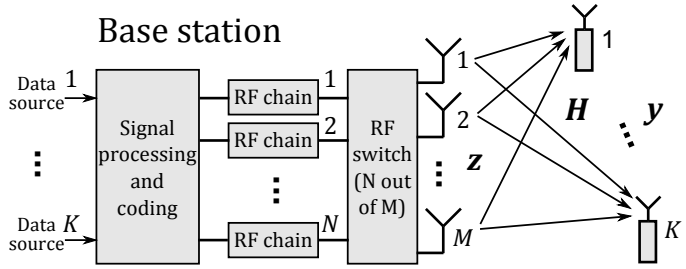

Figure 8.1: Antenna selection in an MU-MIMO system with M antennas and N RF chains at the base station. An RF switch is required to connect the antennas with the RF chains [110].

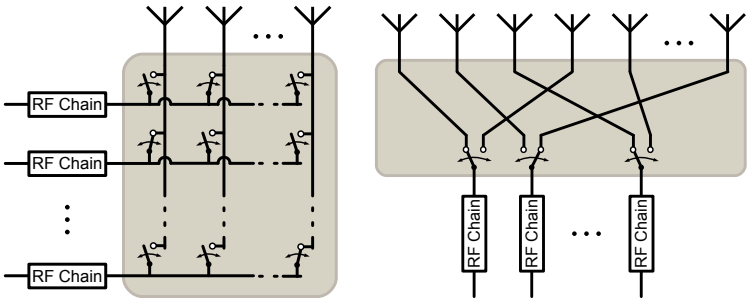

(a) Full switching network. (b) Binary switch network, $N = \frac{M}{2}$.

Figure 8.2: RF switching networks for antenna selection [110].

the RF switch may become very complex, and incur a loss in output signal quality due to insertion loss and cross talk. At the end, a complex RF switch may degrade antenna selection performance.

The study in [110] investigates a simpler solution for the RF switching network. The full switching, shown in Figure 8.2(a), is compared to a proposed binary-switching architecture, shown in Figure 8.2(b). In the comparison, we have used $N = \frac{M}{2}$ RF chains. The binary switching has lower complexity and thus better signal quality, but the number of possible antenna combinations is also much smaller than with full switching, i.e., $2^N \ll \binom{M}{N}$ when M and N are large. Thus the binary-switching network introduces a degradation in antenna selection performance. Despite this, [110] shows that the performance degradation due to binary switching is very small in our massive MIMO scenarios with an SNR loss less than 0.5 dB. The results indicate a potential for further simplifications of massive MIMO hardware.

Chapter 9

Summary and Contributions

This chapter summarizes the research contributions during the thesis work, draws general conclusions, and discusses future work.

9.1 Research Contributions

The contributions of the six papers included in this thesis are summarized here. Regarding the contributions from my side, I was responsible for designing and performing massive MIMO channel measurements, except for the measurements in Paper I. With the obtained measurement data, I was responsible for data processing, analysis, and evaluation of results. I was involved in implementing the used algorithms, including the SAGE algorithm as well as the clustering and tracking algorithm. I took the lead in writing the papers, except for Paper III.

9.1.1 Paper I: Linear Precoding Performance in Measured Very-Large MIMO Channels

This paper is the first paper that evaluates massive MIMO performance in real propagation channels. Theoretical investigations, based on i.i.d. Rayleigh channels with unlimited antenna numbers, have shown many advantages of massive MIMO, as discussed in Section 2.2. The most important phenomenon is that users tend to have orthogonal channels, with increasing number of base station antennas. In real channels, however, we need to know what benefits

we can get from very large, but limited, numbers of antennas. Measurement data obtained in a residential area with an indoor base station was used for the investigation.

The results in the paper show that user channel orthogonality improves with increasing number of antennas in the measured channels, and for two users there is very little improvement beyond 20 antennas. For the two-user case, DPC capacity and linear precoding sum-rates were derived and evaluated numerically. In the measured channels, linear precoding achieves sum-rates as high as 98% of DPC capacity, already at 20 base station antennas. The study points out that massive MIMO is a promising technique even in real channels with a limited number of antennas. This paper motivates further studies of massive MIMO in real propagation environments.

9.1.2 Paper II: Massive MIMO Performance Evaluation Based on Measured Propagation Data

This paper gives a deeper insight into how massive MIMO performs in real channels. Outdoor channel measurements targeting massive MIMO were performed, as described in Section 3.3.1. Two types of base station antenna arrays, a virtual linear and a switched cylindrical, both with 128 elements, were used in the measurements, allowing for performance comparisons. Propagation characteristics using the two arrays in representative scenarios were investigated and illustrated, through what we call *spatial fingerprints*. By studying propagation characteristics, massive MIMO performance in measured channels can therefore be better understood.

Compared to the two-user case in Paper I, this paper extends the number of users to four and sixteen. Based on the measured channels, singular value spreads and sum-rate capacities were investigated and compared to those obtained in i.i.d. Rayleigh channels. The results show that in the measured channels user orthogonality improves and the channel-hardening effect reinforces with increasing number of antennas, as in i.i.d. Rayleigh channels. The measured channels can achieve a large proportion of the sum-rate capacities achieved in i.i.d. Rayleigh channels, even when users are closely located.

This paper further brings massive MIMO from theory to reality, by showing that the theoretical advantages of massive MIMO can also be harvested in real-life environments.

9.1.3 Paper III: Spatial Separation of Closely-Spaced Users in Measured Massive Multi-User MIMO Channels

This paper focuses on a specific type of massive MIMO scenarios – users being closely located. It targets one of the 5G scenarios [65], for improving services in crowded places such as stadiums during sports events, open squares, open exhibitions, and festivals. From Paper II, we have observed that signals of closely-located users can be spatially separated by massive MIMO. The investigations there, however, assume "virtual users" created by combining measurements taken at different time instants and locations. In this paper, channel measurements were performed with multiple synchronized users, as discussed in Section 3.3.2. The measurements provide more accurate relative phases than assuming virtual users, and allows for studying the dynamic properties of the channel with user influence. Users were confined in a 5-m diameter circle and, in some measurements, with additional people around.

The performance evaluation results show that massive MIMO, indeed, is capable of separating closely-located users, even in LOS conditions. By increasing the number of antennas, many more users share a much higher sum-rate, as compared to conventional MIMO with up to 8 antennas. This paper indicates that massive MIMO has the potential to enhance the quality of service (QoS) in crowded scenarios.

9.1.4 Paper IV: Massive MIMO Channels – Measurements and Models

Papers I-III have shown very promising properties of massive MIMO in real channels. This paper focuses on channel characterization and modeling for massive MIMO with physically-large arrays. Key propagation characteristics were identified from measured channels, as discussed in Section 5.1. To model these characteristics, the COST 2100 MIMO channel model was adopted as a basis. An extension of the model was proposed to include important channel properties when large arrays are used at base stations. In the new model, the concept of cluster visibility regions (VRs) is extended to the base station side. New model parameters were introduced, and statistical models for those parameters were found based on measurement data.

This paper proposes a cluster-based modeling concept for extending a conventional MIMO channel model to include massive MIMO behavior. Although the model extension is not fully complete yet, in terms of parameterization and validation, it serves as a start of massive MIMO channel modeling.

9.1.5 Paper V: Massive MIMO Channel Modeling – the COST 2100 Extension

Following up on Paper IV, this paper gives a broader picture of massive MIMO channel modeling and the COST 2100 model extensions. Modeling approaches and scopes were discussed, and model extensions were suggested. The extensions include 3D propagation, polarization properties, cluster behavior at the base station side for scenarios with large arrays, and MPC gain functions for scenarios with closely-spaced users. Model parameters for these extensions were reported, and initial validation against measurements was also performed.

The validation results show that the extended model is capable of reproducing massive MIMO channel statistics, in terms of singular value spread, sum-rate and temporal behavior. The model still needs to be improved in terms of parameterization for more scenarios and further validation, but this paper is a step towards a complete massive MIMO channel model that can be used for simulations.

9.1.6 Paper VI: Massive MIMO in Real Propagation Environments: Do All Antennas Contribute Equally?

Inspired by the observed massive MIMO characteristics in real channels, this paper aims at exploiting the large spatial degrees of freedom to reduce system complexity. Antenna selection is considered a technique for that purpose. By selecting the "best" antenna channels, some RF chains can be switched off while largely maintaining a required performance level. Scenarios with different propagation conditions were investigated, for evaluating the effectiveness of antenna selection in real channels. While antenna selection is not an effective strategy in i.i.d. Rayleigh channels, results based on measured channels show that a substantial number of RF chains can be switched off without a significant performance loss. Furthermore, a simple selection scheme, based on measuring only received power at each antenna, was found to perform near-optimal, in terms of sum-rate capacity achieved by more complex selection schemes.

As complexity is one of the main challenges in massive MIMO implementation, this paper points out a promising technique to greatly simplify massive MIMO hardware, and more importantly, this by using very simple algorithms.

9.2 General Conclusions and Future Work

With the five years' thesis work presented in the included papers and reviewed in the previous chapters, let us draw some general conclusions here and look into topics for future work.

9.2.1 General Conclusions

From the studies of massive MIMO behavior and performance in real propagation environments, the following general conclusions are drawn.

- Theoretical advantages of Massive MIMO, as observed in i.i.d. Rayleigh channels, have been confirmed in real propagation channels using practical antenna arrays. These advantages include improved user orthogonality, channel hardening effects, improved spectral and transmit-energy efficiency, and near-optimal performance achieved by linear precoding/detection schemes.
- Through spatial multiplexing, many more users can be served in the same time-frequency resource, and they share a much higher data rate than in conventional MU-MIMO systems. Spatial multiplexing not only applies to users being located far apart, but also to closely-located users, e.g., in crowed scenarios.
- Important channel effects have been identified for massive MIMO scenarios. When large arrays are used at base stations, spherical wavefronts and spatial variations over arrays need to be considered. In scenarios with closely-spaced users, users interacting with different details on the same physical scatterer accounts for good spatial separability.
- The identified channel properties for massive MIMO have been modeled based on measurement data, and incorporated into a conventional MIMO channel model. Extensions of the COST 2100 MIMO channel model have been proposed for massive MIMO.
- Massive MIMO channel characteristics in real environments have been shown to allow for an efficient use of antenna selection. Hardware complexity in massive MIMO can therefore be greatly reduced without a significant performance loss. Fewer RF chains can be deployed together with simple RF switching networks, using simple antenna selection algorithms.

9.2.2 Future Work

As massive MIMO is still a relatively new research area in wireless communications, there are many topics for future work, including theoretical investigations, propagation measurements, antenna and system designs, and implementation issues. Related to the work in this thesis, I have considered the following topics for future studies.

- As massive MIMO is capable of serving many users simultaneously, it would be interesting to investigate the practical limits. How many users can be aggressively served through spatial multiplexing in a realistic propagation environment? This, of course, depends on propagation conditions, and user scheduling may also play an important role. There are visions that massive MIMO can be potentially combined with IoT, where enormous number of connected devices or sensors are the big challenge.

- As CSI acquisition is a challenge in massive MIMO, channel aging effects in the time and frequency domains are important to investigate. How often in time and how far apart in frequency do we need to sample the channel? To some extent, this is determined by the coherence time and coherence bandwidth from scenario to scenario.

- Regarding antenna arrays, cylindrical and linear arrays have been studied and compared in the thesis work. Other array structures, such as planar arrays, should also be studied. While array design is another topic, understanding massive MIMO channel behavior with different array geometries is important for performance evaluations, channel modeling, and finally, system deployments.

- The development of a complete massive MIMO channel model is an urgent task. The proposed extensions of the COST 2100 model need to be further improved, including the parameterization for more scenarios and the validation based on more measurements. In addition to the COST 2100 model, analytical models such as the correlative models may also be derived and validated for massive MIMO. A good massive MIMO channel model will make a big contribution to the research area.

- Regarding new channel measurements, outdoor-to-indoor scenarios are particularly interesting, as indoor coverage from outdoor base stations is a challenge for the operators. Scenarios with temporary blocking in a packet transmission interval, e.g., dynamic shadowing or a sudden change of scatterer behavior, should also be investigated, as enhanced QoS is one of the goals for the next generation networks.

- Due to the much higher resolution of massive MIMO in the spatial domain, compared to conventional MIMO systems, propagation environments are "sensed" or "scanned" on a much larger scale than before. When channel estimation is performed across users, antenna elements, time instants and frequencies, we obtain a large amount of channel data that can be stored and analyzed. We can view it as "big data" in wireless communications, and apply tools from that area, such as data mining,

machine learning, etc., to approach massive MIMO channels in a new way.

Massive MIMO is far from fully-exploited. With respect to propagation channels in real-life environments, there are many interesting aspects to study, and there are many new possibilities that have not been exploited yet. On "massive" uses of the spatial domain, personally, I foresee a promising future of this technology.

References

[1] E. Dahlman, S. Parkvall, J. Skold, and P. Beming, *3G Evolution, Second Edition: HSPA and LTE for Mobile Broadband*, 2nd ed. Academic Press, 2008.

[2] *Evolved Universal Terrestrial Radio Access (E-UTRA); User Equipment (UE) radio access capabilities*, 3GPP TS 36.306 V10.15.0, Dec. 2015.

[3] D. Astély, E. Dahlman, A. Furuskär, Y. Jading, M. Lindstrom, and S. Parkvall, "LTE: the evolution of mobile broadband," *IEEE Communications Magazine*, vol. 47, no. 4, pp. 44–51, Apr. 2009.

[4] D. Gesbert, M. Kountouris, R. W. Heath, C.-B. Chae, and T. Sälzer, "Shifting the MIMO paradigm," *IEEE Signal Processing Magazine*, vol. 24, no. 5, pp. 36–46, Sept. 2007.

[5] T. L. Marzetta, "Noncooperative cellular wireless with unlimited numbers of base station antennas," *IEEE Transactions on Wireless Communications*, vol. 9, no. 11, pp. 3590–3600, Nov. 2010.

[6] E. G. Larsson, O. Edfors, F. Tufvesson, and T. L. Marzetta, "Massive MIMO for next generation wireless systems," *IEEE Communications Magazine*, vol. 52, no. 2, pp. 186–195, Feb. 2014.

[7] F. Rusek, D. Persson, B. K. Lau, E. G. Larsson, T. L. Marzetta, O. Edfors, and F. Tufvesson, "Scaling up MIMO: Opportunities and challenges with very large arrays," *IEEE Signal Processing Magazine*, vol. 30, no. 1, pp. 40–60, Jan. 2013.

[8] H. Q. Ngo, E. G. Larsson, and T. L. Marzetta, "Energy and spectral efficiency of very large multiuser MIMO systems," *IEEE Transactions on Communications*, vol. 61, no. 4, pp. 1436–1449, Apr. 2013.

[9] H. Huh, G. Caire, H. C. Papadopoulos, and S. A. Ramprashad, "Achieving "massive MIMO" spectral efficiency with a not-so-large number of antennas," *IEEE Transactions on Wireless Communications*, vol. 11, no. 9, pp. 3226–3239, Sept. 2012.

[10] H. Q. Ngo, E. G. Larsson, and T. L. Marzetta, "The multicell multiuser MIMO uplink with very large antenna arrays and a finite-dimensional channel," *IEEE Transactions on Communications*, vol. 61, no. 6, pp. 2350–2361, June 2013.

[11] J. Hoydis, S. ten Brink, and M. Debbah, "Massive MIMO in the UL/DL of cellular networks: How many antennas do we need?" *IEEE Journal on Selected Areas in Communications*, vol. 31, no. 2, pp. 160–171, Feb. 2013.

[12] E. Björnson, J. Hoydis, M. Kountouris, and M. Debbah, "Massive MIMO systems with non-ideal hardware: Energy efficiency, estimation, and capacity limits," *IEEE Transactions on Information Theory*, vol. 60, no. 11, pp. 7112–7139, Nov. 2014.

[13] E. Björnson, L. Sanguinetti, J. Hoydis, and M. Debbah, "Optimal design of energy-efficient multi-user MIMO systems: Is massive MIMO the answer?" *IEEE Transactions on Wireless Communications*, vol. 14, no. 6, pp. 3059–3075, June 2015.

[14] X. Gao, F. Tufvesson, O. Edfors, and F. Rusek, "Measured propagation characteristics for very-large MIMO at 2.6 GHz," in *Proc. Asilomar Conference on Signals, Systems, and Computers (ASILOMAR)*, Nov. 2012.

[15] J. Hoydis, C. Hoek, T. Wild, and S. ten Brink, "Channel measurements for large antenna arrays," in *Proc. International Symposium on Wireless Communication Systems (ISWCS)*, Aug. 2012.

[16] S. Payami and F. Tufvesson, "Channel measurements and analysis for very large array systems at 2.6 GHz," in *Proc. European Conference on Antennas and Propagation (EuCAP)*, Mar. 2012.

[17] X. Gao, O. Edfors, J. Liu, and F. Tufvesson, "Antenna selection in measured massive MIMO channels using convex optimization," in *Proc. IEEE Global Communications Conference (GLOBECOM) Workshop on Emerging Technologies for LTE-Advanced and Beyond-4G*, Dec. 2013.

[18] A. O. Martínez, E. De Carvalho, and J. O. Nielsen, "Towards very large aperture massive MIMO: A measurement based study," in *Proc. IEEE*

Global Communications Conference (GLOBECOM) Workshop on Massive MIMO: From Theory to Practice, Dec. 2014.

[19] C. Shepard, H. Yu, N. Anand, E. Li, T. L. Marzetta, R. Yang, and L. Zhong, "Argos: Practical many-antenna base stations," in *Proc. Annual International Conference on Mobile Computing and Networking (MobiCom)*, 2012.

[20] C. Shepard, H. Yu, and L. Zhong, "ArgosV2: A flexible many-antenna research platform," in *Proc. Annual International Conference on Mobile Computing and Networking (MobiCom)*, 2013.

[21] J. Vieira, S. Malkowsky, K. Nieman, Z. Miers, N. Kundargi, L. Liu, I. Wong, V. Owall, O. Edfors, and F. Tufvesson, "A flexible 100-antenna testbed for massive MIMO," in *Proc. IEEE Global Communications Conference (GLOBECOM) Workshop on Massive MIMO: From Theory to Practice*, Dec. 2014.

[22] P. Harris, S. Zang, A. Nix, M. Beach, S. Armour, and A. Doufexi, "A distributed massive MIMO testbed to assess real-world performance and feasibility," in *Proc. Vehicular Technology Conference (VTC Spring)*, May 2015.

[23] J. G. Andrews, S. Buzzi, W. Choi, S. V. Hanly, A. Lozano, A. C. K. Soong, and J. C. Zhang, "What will 5G be?" *IEEE Journal on Selected Areas in Communications*, vol. 32, no. 6, pp. 1065–1082, June 2014.

[24] P. Pirinen, "A brief overview of 5G research activities," in *Proc. International Conference on 5G for Ubiquitous Connectivity (5GU)*, Nov. 2014.

[25] M. Iwamura, "NGMN view on 5G architecture," in *Proc. IEEE Vehicular Technology Conference (VTC Spring)*, May 2015.

[26] Ericsson, "Ericsson mobility report: on the pulse of the networked society," Nov. 2015.

[27] T. S. Rappaport, S. Sun, R. Mayzus, H. Zhao, Y. Azar, K. Wang, G. N. Wong, J. K. Schulz, M. Samimi, and F. Gutierrez, "Millimeter wave mobile communications for 5G cellular: It will work!" *IEEE Access*, vol. 1, pp. 335–349, May 2013.

[28] *Internet.org*, Facebook. [Online]. Available: http://internet.org/

[29] C.-L. I, C. Rowell, S. Han, Z. Xu, G. Li, and Z. Pan, "Toward green and soft: a 5G perspective," *IEEE Communications Magazine*, vol. 52, no. 2, pp. 66–73, Feb. 2014.

[30] Z. Gao, L. Dai, D. Mi, Z. Wang, M. A. Imran, and M. Z. Shakir, "MmWave massive-MIMO-based wireless backhaul for the 5G ultra-dense network," *IEEE Wireless Communications*, vol. 22, no. 5, pp. 13–21, Oct. 2015.

[31] L. Hanzo, Y. Akhtman, L. Wang, and M. Jiang, *MIMO-OFDM for LTE, Wi-Fi and WiMAX: Coherent versus Non-coherent and Cooperative Turbo Transceivers*. Wiley-IEEE Press, 2010.

[32] J. Vieira, F. Rusek, and F. Tufvesson, "Reciprocity calibration methods for massive MIMO based on antenna coupling," in *Proc. IEEE Global Communications Conference (GLOBECOM)*, Dec. 2014.

[33] E. Björnson, E. G. Larsson, and T. L. Marzetta, "Massive MIMO: 10 myths and one grand question," Mar. 2015, arXiv:1503.06854.

[34] N. Jindal and A. Goldsmith, "Dirty-paper coding versus TDMA for MIMO broadcast channels," *IEEE Transactions on Information Theory*, vol. 51, no. 5, pp. 1783–1794, May 2005.

[35] D. Tse and P. Viswanath, *Fundamentals of Wireless Communication*. Cambridge University Press, 2005.

[36] G. Caire and S. Shamai, "On the achievable throughput of a multiantenna Gaussian broadcast channel," *IEEE Transactions on Information Theory*, vol. 49, no. 7, pp. 1691–1706, July 2003.

[37] H. Weingarten, Y. Steinberg, and S. Shamai, "The capacity region of the Gaussian MIMO broadcast channel," in *Proc. International Symposium on Information Theory (ISIT)*, June 2004.

[38] M. Costa, "Writing on dirty paper," *IEEE Transactions on Information Theory*, vol. 29, no. 3, pp. 439–441, 1983.

[39] M. Joham, W. Utschick, and J. A. Nossek, "Linear transmit processing in MIMO communications systems," *IEEE Transactions on Signal Processing*, vol. 53, no. 8, pp. 2700–2712, Aug. 2005.

[40] C. B. Peel, B. M. Hochwald, and A. L. Swindlehurst, "A vector-perturbation technique for near-capacity multiantenna multiuser communication-part I: channel inversion and regularization," *IEEE Transactions on Communications*, vol. 53, no. 1, pp. 195–202, Jan. 2005.

[41] S. Boyd and L. Vandenberghe, *Convex Optimization*. Cambridge University Press, 2004.

[42] N. Jindal, W. Rhee, S. Vishwanath, S. A. Jafar, and A. Goldsmith, "Sum power iterative water-filling for multi-antenna Gaussian broadcast channels," *IEEE Transactions on Information Theory*, vol. 51, no. 4, pp. 1570–1580, Apr. 2005.

[43] J. A. Rice, *Mathematical Statistics and Data Analysis*. Duxbury Press, 2006.

[44] B. M. Hochwald, T. L. Marzetta, and V. Tarokh, "Multiple-antenna channel hardening and its implications for rate feedback and scheduling," *IEEE Transactions on Information Theory*, vol. 50, no. 9, pp. 1893–1909, Sept. 2004.

[45] T. L. Narasimhan and A. Chockalingam, "Channel hardening-exploiting message passing (CHEMP) receiver in large-scale MIMO systems," *IEEE Journal of Selected Topics in Signal Processing*, vol. 8, no. 5, pp. 847–860, Oct. 2014.

[46] A. M. Tulino and S. Verdú, *Random Matrix Theory and Wireless Communications*. Now Publishers, 2004.

[47] Y.-H. Nam, B. L. Ng, K. Sayana, Y. Li, J. Zhang, Y. Kim, and J. Lee, "Full-dimension MIMO (FD-MIMO) for next generation cellular technology," *IEEE Communications Magazine*, vol. 51, no. 6, pp. 172–179, June 2013.

[48] Y. Kim, H. Ji, J. Lee, Y.-H. Nam, B. L. Ng, I. Tzanidis, Y. Li, and J. Zhang, "Full dimension MIMO (FD-MIMO): The next evolution of MIMO in LTE systems," *IEEE Wireless Communications*, vol. 21, no. 3, pp. 92–100, June 2014.

[49] H. Q. Ngo, E. G. Larsson, and T. L. Marzetta, "Aspects of favorable propagation in massive MIMO," in *Proc. European Signal Processing Conference (EUSIPCO)*, Sept. 2014.

[50] "Distributed and centralized baseband processing algorithms, architectures, and platforms," MAMMOET D3.2 V1.0, Jan. 2016.

[51] C. Desset, B. Debaillie, and F. Louagie, "Modeling the hardware power consumption of large scale antenna systems," in *Proc. IEEE Online Conference on Green Communications*, Nov. 2014.

[52] R. Janaswamy, "Effect of element mutual coupling on the capacity of fixed length linear arrays," *IEEE Antennas and Wireless Propagation Letters*, vol. 1, no. 1, pp. 157–160, 2002.

[53] X. Artiga, B. Devillers, and J. Perruisseau-Carrier, "Mutual coupling effects in multi-user massive MIMO base stations," in *Proc. IEEE Antennas and Propagation Society International Symposium (APSURSI)*, July 2012.

[54] K. T. Truong and R. W. Heath, "Effects of channel aging in massive MIMO systems," *Journal of Communications and Networks*, vol. 15, no. 4, pp. 338–351, Aug. 2013.

[55] J. Choi, D. J. Love, and P. Bidigare, "Downlink training techniques for FDD massive MIMO systems: Open-loop and closed-loop training with memory," *IEEE Journal of Selected Topics in Signal Processing*, vol. 8, no. 5, pp. 802–814, Oct. 2014.

[56] J. Jose, A. Ashikhmin, T. L. Marzetta, and S. Vishwanath, "Pilot contamination and precoding in multi-cell TDD systems," *IEEE Transactions on Wireless Communications*, vol. 10, no. 8, pp. 2640–2651, Aug. 2011.

[57] S. J. Orfanidis, *Electromagnetic Waves and Antennas*. Rutgers University, 2014.

[58] N. Costa and S. Haykin, *Multiple-Input Multiple-Output Channel Models: Theory and Practice*. John Wiley & Sons, Inc., Hoboken, New Jersey, 2010.

[59] O. Işik, "Planar and cylindrical microstrip array antennas for mimo channel sounder applications," Master Thesis, Chalmers University of Technology, 2004.

[60] [Online]. Available: http://www.channelsounder.de/ruskchannelsounder.html

[61] [Online]. Available: http://www.skycross.com/

[62] [Online]. Available: http://www.ni.com/labview/

[63] P. H. Young, *Electronic Communication Techniques*. Prentice Hall, 2004.

[64] A. Molisch, *Wireless Communications*. Wiley-IEEE Press, 2005.

[65] A. Osseiran, F. Boccardi, V. Braun, K. Kusume, P. Marsch, M. Maternia, O. Queseth, M. Schellmann, H. Schotten, H. Taoka, H. Tullberg, M. A. Uusitalo, B. Timus, and M. Fallgren, "Scenarios for 5G mobile and wireless communications: the vision of the METIS project," *IEEE Communications Magazine*, vol. 52, no. 5, pp. 26–35, May 2014.

[66] "MaMi channel characteristics: Measurement results," MAMMOET D1.2 V1.0, June 2015.

[67] X. Gao, A. Alayon Glazunov, J. Weng, C. Fang, J. Zhang, and F. Tufvesson, "Channel measurement and characterization of interference between residential femto-cell systems," in *Proc. European Conference on Antennas and Propagation (EuCAP)*, Apr. 2011.

[68] J. A. Fessler and A. O. Hero, "Space-alternating generalized expectation-maximization algorithm," *IEEE Transactions on Signal Processing*, vol. 42, no. 10, pp. 2664–2677, Oct. 1994.

[69] B. H. Fleury, M. Tschudin, R. Heddergott, D. Dahlhaus, and K. Ingeman Pedersen, "Channel parameter estimation in mobile radio environments using the SAGE algorithm," *IEEE Journal on Selected Areas in Communications*, vol. 17, no. 3, pp. 434–450, Mar. 1999.

[70] B. D. Van Veen and K. M. Buckley, "Beamforming: a versatile approach to spatial filtering," *IEEE ASSP Magazine*, vol. 5, no. 2, pp. 4–24, Apr. 1988.

[71] K. W. Forsythe, "Utilizing waveform features for adaptive beamforming and direction finding with narrowband signals," *Lincoln Laboratory Journal*, vol. 10, no. 2, 1997.

[72] J. Capon, "High-resolution frequency-wavenumber spectrum analysis," *Proc. IEEE*, vol. 57, no. 8, pp. 1408–1418, Aug. 1969.

[73] P. Stoica, Z. Wang, and J. Li, "Robust Capon beamforming," *IEEE Signal Processing Letters*, vol. 10, no. 6, pp. 172–175, June 2003.

[74] R. G. Lorenz and S. P. Boyd, "Robust minimum variance beamforming," *IEEE Transactions on Signal Processing*, vol. 53, no. 5, pp. 1684–1696, May 2005.

[75] R. Roy and T. Kailath, "ESPRIT-estimation of signal parameters via rotational invariance techniques," *IEEE Transactions on Acoustics, Speech and Signal Processing*, vol. 37, no. 7, pp. 984–995, July 1989.

[76] A. Richter, "Estimation of radio channel parameters: Models and algorithms," Ph.D. dissertation, Technische Universität Ilmenau, 2005.

[77] P. Kyösti, J. Meinilä, L. Hentilä, X. Zhao, T. Jämsä, C. Schneider, M. Narandzić, M. Milojević, A. Hong, J. Ylitalo *et al.*, "WINNER II channel models," IST-4-027756 WINNER II D1.1.2 V1.2, 2008.

[78] S. M. Kay, *Fundamentals of Statistical Signal Processing: Estimation Theory*. Prentice Hall, 1993.

[79] S. M. Juds, *Photoelectric Sensors and Controls: Selection and Application*. Marcel Dekker, Inc., 1988.

[80] J. Poutanen, J. Salmi, K. Haneda, V. Kolmonen, F. Tufvesson, and P. Vainikainen, "Propagation characteristics of dense multipath components," *IEEE Antennas and Wireless Propagation Letters*, vol. 9, pp. 791–794, 2010.

[81] J. Poutanen, J. Salmi, K. Haneda, V. Kolmonen, and P. Vainikainen, "Angular and shadowing characteristics of dense multipath components in indoor radio channels," *IEEE Transactions on Antennas and Propagation*, vol. 59, no. 1, pp. 245–253, Jan. 2011.

[82] A. Richter, J. Salmi, and V. Koivunen, "Distributed scattering in radio channels and its contribution to MIMO channel capacity," in *Proc. European Conference on Antennas and Propagation (EuCAP)*, Nov. 2006.

[83] J. Han, M. Kamber, and J. Pei, *Data Mining: Concepts and Techniques*. Morgan Kaufmann, 2001.

[84] N. Czink, "The random-cluster model – a stochastic MIMO channel model for broadband wireless communication systems of the 3rd generation and beyond," Ph.D. dissertation, Technischen Universität Wien, 2007.

[85] M. Zhu, "Geometry-based radio channel characterization and modeling: Parameterization, implementation and validation," Ph.D. dissertation, Lund University, 2014.

[86] L. Rokach and O. Maimon, *Data Mining and Knowledge Discovery Handbook*. Springer US, 2005, ch. Clustering Methods, pp. 321–352.

[87] C. Gustafson, "60 GHz wireless propagation channels: Characterization, modeling and evaluation," Ph.D. dissertation, Lund University, 2014.

[88] N. Czink, P. Cera, J. Salo, E. Bonek, J. P. Nuutinen, and J. Ylitalo, "A framework for automatic clustering of parametric MIMO channel data including path powers," in *Proc. IEEE Vehicular Technology Conference (VTC Fall)*, Sept. 2006.

[89] M. Steinbauer, H. Özcelik, H. Hofstetter, C. Mecklenbräuker, and E. Bonek, "How to quantify multipath separation," *IEICE Transactions on Electronics*, vol. E85-C, no. 3, pp. 552–557, Feb. 2002.

[90] Z. Zhou, X. Gao, J. Fang, and Z. Chen, "Spherical wave channel and analysis for large linear array in LoS conditions," in *Proc. IEEE Global Communications Conference (GLOBECOM) Workshop on Massive MIMO: From Theory to Practice*, Dec. 2015.

[91] X. Gao, M. Zhu, F. Rusek, F. Tufvesson, and O. Edfors, "Large antenna array and propagation environment interaction," in *Proc. Asilomar Conference on Signals, Systems, and Computers (ASILOMAR)*, Nov. 2014.

[92] R. Zentner and A. Katalinic, "Dynamics of multipath variations in urban environment," in *Proc. European Wireless Technology Conference (EuWIT)*, Sept. 2010.

[93] A. F. Molisch and F. Tufvesson, "Propagation channel models for next-generation wireless communication systems," *IEICE Transactions on Communications*, vol. E97-B, no. 10, pp. 2022–2034, Oct. 2014.

[94] D. Chizhik, J. Ling, P. W. Wolniansky, R. A. Valenzuela, N. Costa, and K. Huber, "Multiple-input-multiple-output measurements and modeling in Manhattan," *IEEE Journal on Selected Areas in Communications*, vol. 21, no. 3, pp. 321–331, Apr. 2003.

[95] W. Weichselberger, "Spatial structure of multiple antenna radio channels," Ph.D. dissertation, Technischen Universität Wien, 2003.

[96] A. F. Molisch, A. Kuchar, J. Laurila, K. Hugl, and R. Schmalenberger, "Geometry-based directional model for mobile radio channels – principles and implementation," *European Transactions on Telecommunications*, vol. 14, no. 4, pp. 351–359, July 2003.

[97] A. F. Molisch, H. Asplund, R. Heddergott, M. Steinbauer, and T. Zwick, "The COST259 directional channel model-part I: Overview and methodology," *IEEE Transactions on Wireless Communications*, vol. 5, no. 12, pp. 3421–3433, Dec. 2006.

[98] H. Asplund, A. A. Glazunov, A. F. Molisch, K. I. Pedersen, and M. Steinbauer, "The COST 259 directional channel model-part II: Macrocells," *IEEE Transactions on Wireless Communications*, vol. 5, no. 12, pp. 3434–3450, Dec. 2006.

[99] H. Hofstetter, A. F. Molisch, and N. Czink, "A twin-cluster MIMO channel model," in *Proc. European Conference on Antennas and Propagation (EuCAP)*, Nov. 2006.

[100] N. Czink and C. Oestges, "The COST 273 MIMO channel model: Three kinds of clusters," in *Proc. IEEE International Symposium on Spread Spectrum Techniques and Applications*, Aug. 2008.

[101] L. Liu, C. Oestges, J. Poutanen, K. Haneda, P. Vainikainen, F. Quitin, F. Tufvesson, and P. D. Doncker, "The COST 2100 MIMO channel model," *IEEE Wireless Communications*, vol. 19, no. 6, pp. 92–99, Dec. 2012.

[102] G. Calcev, D. Chizhik, B. Göransson, S. Howard, H. Huang, A. Kogiantis, A. F. Molisch, A. L. Moustakas, D. Reed, and H. Xu, "A wideband spatial channel model for system-wide simulations," *IEEE Transactions on Vehicular Technology*, vol. 56, no. 2, pp. 389–403, Mar. 2007.

[103] X. You and Y. Wang, "Massive MIMO channel modeling," Master's thesis, Lund University, 2015.

[104] A. Paulraj, R. Nabar, and D. Gore, *Introduction to Space-Time Wireless Communications*. Cambridge University Press, 2003.

[105] J. P. Kermoal, L. Schumacher, K. I. Pedersen, P. E. Mogensen, and F. Frederiksen, "A stochastic MIMO radio channel model with experimental validation," *IEEE Journal on Selected Areas in Communications*, vol. 20, no. 6, pp. 1211–1226, Aug. 2002.

[106] H. Özcelik, M. Herdin, W. Weichselberger, J. Wallace, and E. Bonek, "Deficiencies of 'Kronecker' MIMO radio channel model," *Electronics Letters*, vol. 39, no. 16, pp. 1209–1210, Aug. 2003.

[107] H. Özcelik, N. Czink, and E. Bonek, "What makes a good MIMO channel model?" in *Proc. Vehicular Technology Conference (VTC Spring)*, May 2005.

[108] L. Wood and W. S. Hodgkiss, "Understanding the Weichselberger model: A detailed investigation," in *Proc. IEEE Military Communications Conference (MILCOM)*, Nov. 2008.

[109] R. Verdone and A. Zanella, Eds., *Pervasive Mobile and Ambient Wireless Communications: COST Action 2100*. Springer-Verlag London, 2012.

[110] X. Gao, O. Edfors, F. Tufvesson, and E. G. Larsson, "Multi-switch for antenna selection in massive MIMO," in *Proc. IEEE Global Communications Conference (GLOBECOM)*, Dec. 2015.

Part II

Included Papers

Paper I

Linear Precoding Performance in Measured Very-Large MIMO Channels

Wireless communication using very-large multiple-input multiple-output (MIMO) antennas is a new research field, where base stations are equipped with a very large number of antennas as compared to previously considered systems. In theory, as the number of antennas increases, propagation properties that were random before start to become deterministic. Theoretical investigations with independent identically distributed (i.i.d.) complex Gaussian (Rayleigh fading) channels and unlimited number of antennas have been done, but in practice we need to know what benefits we can get from very large, but limited, number of antenna elements in realistic propagation environments. In this study we evaluate properties of measured residential-area channels, where the base station is equipped with 128 antenna ports. An important property to consider is the orthogonality between channels to different users, since this property tells us how advanced multi-user MIMO (MU-MIMO) precoding schemes we need in the downlink. We show that orthogonality improves with increasing number of antennas, but for two single-antenna users there is very little improvement beyond 20 antennas. We also evaluate sum-rate performance for two linear precoding schemes, zero-forcing (ZF) and minimum mean squared-error (MMSE), as a function of the number of base station antennas. Already at 20 base station antennas these linear precoding schemes reach 98% of the optimal dirty-paper coding (DPC) capacity for the measured channels.

Xiang Gao, Ove Edfors, Fredrik Rusek, and Fredrik Tufvesson,
"Linear Pre-Coding Performance in Measured Very-Large MIMO Channels,"
in *Proc. IEEE Vehicular Technology Conference (VTC Fall)*, Sept. 2011.

1 Introduction

Multiple-antenna (MIMO) technology for wireless communications is becoming mature and has been incorporated into many advanced standards such as HSPA and LTE [1]. Basically the more antennas the transceivers are equipped with, the better performance can be obtained in terms of data rate and link reliability. The price to pay is increased complexity of hardware and signal processing at both ends. In classical point-to-point single-user MIMO systems (SU-MIMO), the multiplexing gain may disappear when the signal power is low, relative to interference and noise, or in propagation environmens with dominating line-of-sight or insufficient scatterers. SU-MIMO systems also require complex and expensive multiple-antenna terminals. Practical size limitations on terminals also limit the number of antennas that can be used and thereby the achievable multiplexing gains.

To overcome these drawbacks of SU-MIMO, multi-user MIMO (MU-MIMO) with single-antenna terminals and an unlimited number of base station antennas is investigated in [2]. This approach involves MU-MIMO operation with an infinite number of base station antennas in a multi-cell environment. It is shown that all the effects of uncorrelated noise and fast fading disappear, as does the intra-cell interference, and the only remaining impediment is the inter-cell interference due to pilot contamination. All of these motivate entirely new theoretical research on signal processing, coding and network design for such very-large MIMO systems. The vision put forward in [2] is that the base station array would consist of a very large number of small active antenna units, each of which uses extremely low power.

The assumption of an unlimited number of base station antennas in [2] greatly simplifies the theoretical analysis. In a practical system, however, the number of antennas cannot be arbitrarily large due to physical constraints. From a feasibility point of view, it is reasonable to ask how large the antenna array should be. The answer depends on the propagation environment, but in general, the asymptotic results of random matrix theory can be observed even for relatively small dimensions.

The analysis in [2] assumes that inner products between propagation vectors of different users grow at a lesser rate than inner products of propagation vectors with themselves, i.e., the user channels are asymptotically orthogonal. Experimental work is clearly of great importance to investigate the range of validity of this assumption. Therefore, in the initial phase of this new research in wireless communications, we study how well the measurements resemble the theoretical results and what benefits we can obtain at very-large, but limited, number of base-station antennas.

In the present paper, we study the linear precoding performance in mea-

sured very-large MIMO downlink channels. We consider a single-cell environment in which a base station with a very-large antenna array serves a number of single-antenna users simultaneously. The interference between cells and pilot contamination issues are therefore not addressed in this paper. Channel measurements were done with a 128-antenna base station in a residential area. To the best of the authors' knowledge, there are no other studies performed on this type of systems, with this high a number of antennas.

In Sec. 2 we describe our system model and define a number of measures. In Sec. 3 we describe the measurement setup and the residential-area environment where the measurements are performed. As a basis for our comparison of systems with more or less base station antennas we describe a number of precoding schemes in Sec. 4 – both the linear zero-forcing (ZF) and minimum mean squared-error (MMSE) precoders, as well as the optimal dirty-paper coding (DPC). System performance is then evaluated in Sec. 5 for different number of antennas and we show how the low-complex linear precoders perform in relation to the optimal DPC scheme. Finally, we summarize our contributions and draw conclusions in Sec. 6.

2 System Description

We consider the downlink of a single-cell MU-MIMO system: the base station is equipped with M antennas, and serves K single-antenna users. The total transmit power is constrained to an average of P_{t}. The composite received $K\times 1$ vector $\boldsymbol{y}$ at the users can be described as

$$\boldsymbol{y} = \sqrt{\rho}\boldsymbol{H}\boldsymbol{z} + \boldsymbol{n}, \tag{1}$$

where $\boldsymbol{H}$ is a composite $K\times M$ channel matrix, $\boldsymbol{z}$ is the transmitted vector across the M antennas, and $\boldsymbol{n}$ is a noise vector with unit variance. The variable ρ contains the transmit energy and channel energy so that the total power in $\boldsymbol{H}$ is K and $\boldsymbol{z}$ satisfies $\mathbb{E}\{\|\boldsymbol{z}\|^2\} = 1$. The $M\times 1$ transmit vector $\boldsymbol{z}$ contains a precoded version of the $K\times 1$ data symbol vector $\boldsymbol{x}$. Through precoding at the transmit side we have

$$\boldsymbol{z} = \boldsymbol{U}\boldsymbol{x}, \tag{2}$$

where $\boldsymbol{U}$ is a $M \times K$ precoding matrix including power allocation to the data symbols. The vector $\boldsymbol{x}$ comprises data symbols from an alphabet $\mathcal{X}$, and each entry has unit average energy, i.e. $\mathbb{E}\{|x_k|^2\} = 1$, $k = 1, 2, \ldots, K$. Taken together, the energy constraints on $\boldsymbol{x}$ and $\boldsymbol{z}$ yield an energy constraint on $\boldsymbol{U}$: $\mathrm{Tr}(\boldsymbol{U}^H\boldsymbol{U}) = 1$, where $\mathrm{Tr}(\cdot)$ is the trace-operator and $(\cdot)^H$ denotes the Hermitian transpose.

To facilitate analytical derivation of precoders and their performance, we will assume that the number of users is $K = 2$. The input-output relation of the

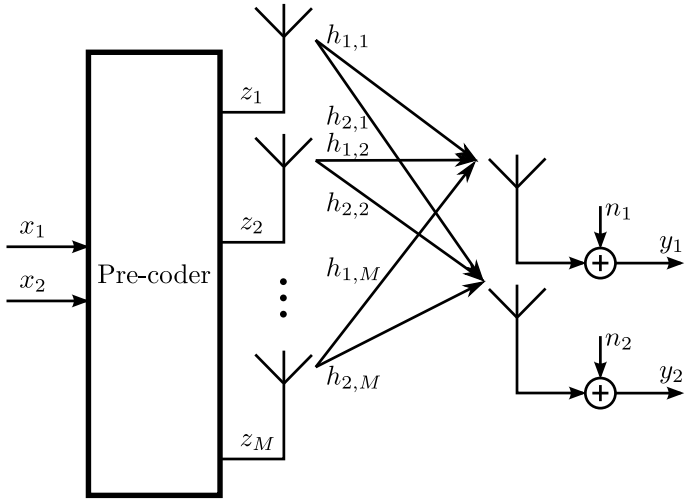

Figure 1: System model of a MU-MIMO system with an M-antenna base station and two single-antenna users.

channel for this two-user case is shown in Fig. 1. The Gram matrix associated with $\boldsymbol{H}$ can be expressed as

$$\boldsymbol{G} \triangleq \boldsymbol{H}\boldsymbol{H}^H = \begin{bmatrix} 1+g & \delta \\ \delta^* & 1-g \end{bmatrix}, \tag{3}$$

where g denotes the power imbalance between the two user channels, and δ is a factor measuring the correlation between the two channels. Since we can permute the rows of $\boldsymbol{H}$ at will, we can without loss of generality assume that $0 \leq g < 1$. The correlation between the channels to the two users can be expressed as $|\delta|/\sqrt{1-g^2}$. Further, we require $|\delta| < \sqrt{1-g^2}$ in order to have a positive definite matrix $\boldsymbol{G}$.

3 Measurement Scenario

The channel measurements were carried out in a residential area north of Lund city center, Sweden. Fig. 2 shows an overview of the measurement area, where the numbers indicate specific houses. The measurements were originally performed with the aim of studying channel properties for residential femto-cell systems [3]. However, the large receive array with 128 antenna ports also enables this study of very-large MIMO channels. The receive antenna array was

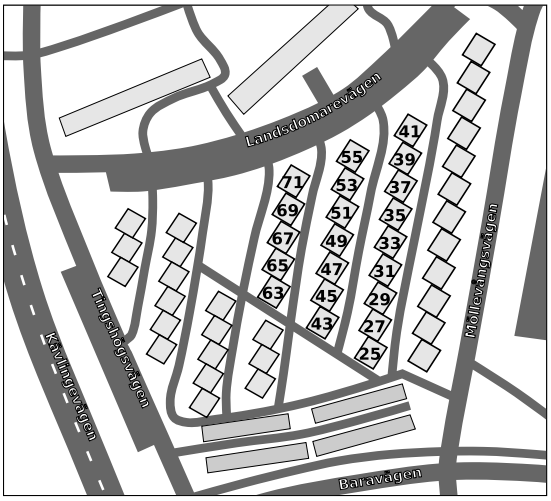

Figure 2: Overview of the residential measurement area. The numbers indicate specific houses.

placed upstairs in house 63, which is shown at street level in Fig. 3. This array is a cylindrical patch array having 16 dual polarized antennas in each circle and 4 such circles stacked on top of each other, giving in total 128 antenna ports. The left part of Fig. 4 shows this large antenna array. The diameter is 29.4 cm and the height is 28.3 cm. The distance between adjacent antennas is about 6 cm, half a wavelength at the 2.6 GHz carrier frequency used. The transmit antenna array was placed indoors and outdoors at different positions, therefore indoor-to-outdoor-to-indoor and outdoor-to-indoor channels were measured. The right part of Fig. 4 shows the transmit array which consists of a planar patch array having 2 rows of 8 dual polarized antennas, giving in total 32 antenna ports. The outdoor-to-indoor channels are selected for very-large MIMO study, as we consider the scenario in which the users are outdoors around the base station. The outdoor measurement positions were (to the west of) houses 29, 33, 37, 41, 43, 45, 47, 49, 51, and 53, respectively. The measurement data was recorded with the RUSK LUND channel sounder at a carrier frequency of 2.6 GHz and a signal bandwidth of 50 MHz. At each measurement position, the transmit antenna was moved along a 5-10 m straight line parallel to the direction of antenna array back-plane.

For this very-large MIMO study, we extract the measurement data to form MU-MIMO channels. The first antenna in the 32-antenna transmit array is selected to represent a single-antenna user terminal. Through all the measure-

Figure 3: Street level view of the measurement area, house 63, in which the receive antenna array was positioned.

Figure 4: Receive antenna array (left) and transmit antenna array (right).

ment positions, we can have several different users. In this paper we concentrate on the two-user case, where two different positions are selected randomly. The receive antenna array positioned in house 63 represents an indoor base station.

4 Precoding Schemes

In this section we derive closed form expressions for DPC capacity and linear precoding sum rates for two-user case, using the system model in Sec. 2.

4.1 Dirty-Paper Coding

The optimal sum rate in the downlink of a MU-MIMO system can be achieved by the interference pre-subtraction coding technique called dirty-paper coding (DPC), as long as the transmitter has perfect side information about the additive interference at the receiver [4]. The optimal DPC capacity for the two-user case is given as

$$C_{\mathrm{DPC}} = \max_{P_1,P_2} \log_2 \det\left(\boldsymbol{I} + \rho \boldsymbol{H}^H \boldsymbol{P} \boldsymbol{H}\right), \tag{4}$$

where $\boldsymbol{P}$ is a 2×2 diagonal matrix for power allocation with P_1 and P_2 on its main diagonal. The DPC capacity is maximized by optimizing over the power allocation under constraint that $P_1+P_2=1$. By substituting the Gram matrix $\boldsymbol{G}$ in (3) into (4), we find the optimal power allocation as

$$(P_1)_{\mathrm{DPC}}^{\mathrm{opt}} = \begin{cases} \frac{1}{2} + \frac{g}{\rho\left(1-g^2-|\delta|^2\right)}, & |\delta|^2 \le \delta_{\mathrm{th}} \\ 1, & |\delta|^2 > \delta_{\mathrm{th}}, \end{cases} \tag{5}$$

where $\delta_{\mathrm{th}} = 1-g^2-2g/\rho$. The corresponding DPC capacity becomes

$$C_{\mathrm{DPC}} = \begin{cases} \log_2\left[1+\rho+\frac{\rho^2\left(1-g^2-|\delta|^2\right)^2+4g^2}{4\left(1-g^2-|\delta|^2\right)}\right], & |\delta|^2 \le \delta_{\mathrm{th}} \\ \log_2\left[1+\rho\left(1+g\right)\right], & |\delta|^2 > \delta_{\mathrm{th}}. \end{cases} \tag{6}$$

If $|\delta|^2$ is higher than a certain threshold δ_{th}, all power will be allocated to the user with the stronger channel, and the DPC capacity becomes the same as the single-user transmission rate

$$C_{\mathrm{SU}} = \log_2\left[1+\rho\left(1+g\right)\right]. \tag{7}$$

Although optimal sum rate can be achieved, DPC is far too complex to be implemented in practice. We hence take the optimal DPC capacity as a benchmark for the sum rates achieved by the linear precoding schemes, ZF and MMSE, which are of more practical interest.

4.2 Linear Precoding Schemes

The precoding matrix $\boldsymbol{U}$ can be decomposed as

$$\boldsymbol{U} = \frac{1}{\sqrt{\gamma}}\boldsymbol{W}\sqrt{\boldsymbol{P}}, \tag{8}$$

where $\boldsymbol{W}$ represents a particular linear precoding algorithm, $\boldsymbol{P}$ is the power allocation matrix, and γ is used to normalize the total transmit power in $\boldsymbol{z}$ to unity. Therefore, from $\mathrm{Tr}(\boldsymbol{U}^H\boldsymbol{U})=1$, the power normalization factor γ should be

$$\gamma = \mathrm{Tr}\left(\boldsymbol{P}\boldsymbol{W}^H\boldsymbol{W}\right). \tag{9}$$

ZF Precoding Scheme. ZF precoding eliminates the interference by transmitting the signals towards the intended user with nulls in the "direction" of other users. The ZF precoder is given as

$$\boldsymbol{W}_{\mathrm{ZF}} = \boldsymbol{H}^{\dagger}, \tag{10}$$

where $\boldsymbol{H}^{\dagger}=\boldsymbol{H}^H(\boldsymbol{H}\boldsymbol{H}^H)^{-1}$ is the pseudoinverse of the channel matrix $\boldsymbol{H}$. Using ZF precoding, the signal model becomes

$$\boldsymbol{y} = \sqrt{\frac{\rho}{\gamma}}\boldsymbol{P}\boldsymbol{x} + \boldsymbol{n}. \tag{11}$$

Since perfect nulling makes this scheme interference free, the sum rate can be calculated as

$$C_{\mathrm{ZF}} = \max_{P_1,P_2}\sum_{i=1}^{2}\log_2\left(1+\frac{\rho P_i}{\gamma}\right), \tag{12}$$

subject to $P_1+P_2=1$. By substituting the ZF precoder and power allocation matrix into (9), and letting $P_2=1-P_1$ we obtain the normalization factor

$$\gamma = \frac{1+g-2P_1g}{1-g^2-|\delta|^2}. \tag{13}$$

Inserting this γ into (12), we find the optimal power allocation

$$(P_1)_{\mathrm{ZF}}^{\mathrm{opt}} = \begin{cases} \frac{1}{2}\left[1+g+\frac{2g\left(1-g^2\right)}{\rho\left(1-g^2-|\delta|^2\right)+2g^2}\right], & |\delta|^2 \le \delta_{\mathrm{th}} \\ 1, & |\delta|^2 > \delta_{\mathrm{th}}. \end{cases} \tag{14}$$

The resulting sum rate for ZF precoding becomes

$$C_{\mathrm{ZF}} = \begin{cases} \log_2\left[\frac{\left(2+\rho\left(1-g^2-|\delta|^2\right)\right)^2}{4\left(1-g^2\right)}\right], & |\delta|^2 \le \delta_{\mathrm{th}} \\ \log_2\left[1+\frac{\rho\left(1-g^2-|\delta|^2\right)}{1-g}\right], & |\delta|^2 > \delta_{\mathrm{th}}. \end{cases} \tag{15}$$

The ZF interference cancellation has significant signal power penalty if the two user channels are highly correlated. From (15) we can see that the capacity goes to zero when the channel correlation is high (low orthogonality), i.e. when $|\delta|$ approaches $\sqrt{1-g^2}$.

MMSE Precoding Scheme. MMSE precoding can trade interference suppression against signal power efficiency. The optimal MMSE precoder is given by [5]

$$\boldsymbol{W}_{\mathrm{MMSE}} = \boldsymbol{H}^H \left(\boldsymbol{H}\boldsymbol{H}^H + \alpha \boldsymbol{I}\right)^{-1}, \tag{16}$$

where $\alpha = K/\rho$, or in our case, $\alpha = 2/\rho$. At high SNRs (α small) the MMSE precoder approaches the ZF precoder, while at low SNRs (α large) the MMSE precoder approaches the matched filter (MF) precoder. In [6], the power allocation, i.e. the matrix $\boldsymbol{P}$, is also considered in minimizing the mean square error, but in this paper we optimize $\boldsymbol{P}$ to get the maximal sum rate.

The equivalent signal model of MMSE precoding scheme can be written as

$$\boldsymbol{y} = \sqrt{\frac{\rho}{\gamma}} \boldsymbol{G} \left(\boldsymbol{G} + \alpha \boldsymbol{I}\right)^{-1} \sqrt{\boldsymbol{P}} \boldsymbol{x} + \boldsymbol{n}, \tag{17}$$

where the normalization factor γ is

$$\begin{aligned} \gamma \;=\; & \frac{2P_1 g\left(\alpha^2 - 1 + g^2 + |\delta|^2\right)}{\left[(1+g+\alpha)(1-g-\alpha) - |\delta|^2\right]^2} \\ & + \frac{(1+g+\alpha)^2 (1-g) - (1+g+2\alpha)|\delta|^2}{\left[(1+g+\alpha)(1-g-\alpha) - |\delta|^2\right]^2}. \end{aligned} \tag{18}$$

Therefore, the two signal branches can be expressed by parameters ρ, g, δ and power allocations P_1 and P_2. We can calculate the SINR and then obtain the sum rate of the MMSE precoding scheme, subject to $P_1 + P_2 = 1$, as

$$C_{\mathrm{MMSE}} = \max_{P_1, P_2} \sum_{i=1}^{2} \log_2 \left(1 + \mathrm{SINR}_i\right), \tag{19}$$

where

$$\mathrm{SINR}_1 = \frac{\rho P_1 \left[(1+g)(1-g+\alpha) - |\delta|^2\right]^2}{\rho P_2 \alpha^2 |\delta|^2 + \gamma \left[(1+g+\alpha)(1-g+\alpha) - |\delta|^2\right]^2} \tag{20}$$

and

$$\mathrm{SINR}_2 = \frac{\rho P_2 \left[(1-g)(1+g+\alpha) - |\delta|^2\right]^2}{\rho P_1 \alpha^2 |\delta|^2 + \gamma \left[(1+g+\alpha)(1-g+\alpha) - |\delta|^2\right]^2}. \tag{21}$$

Closed form expressions of optimal power allocation and maximized sum rate can be reached but are far too long and complicated to be given here, but in the case of $g=0$, a simple expression of the sum rate is obtained as

$$C_{\mathrm{MMSE}}|_{g=0} = 2\log_2\left[1+\frac{\rho}{2}\left(1-\frac{\rho}{\rho+2}\,|\delta|^2\right)\right]. \tag{22}$$

5 Performance Comparison

Using the closed form sum rate expressions above, we first study how the DPC capacity and linear precoding sum rates are affected by correlation and power imbalance between user channels. We then let the number of base station antennas grow large, both for measured channels and simulated i.i.d. Gaussian channels, to see to what degree a realistic propagation environment decorrelates the user channels. Finally, we compare the linear precoding sum rates with the DPC capacity as the number of antennas increases.

5.1 Numerical Evaluation

It can be seen from the expressions above that if the channel correlation approaches zero, i.e., $|\delta|\approx 0$, ZF and MMSE precoding sum rates become equal to the DPC capacity,

$$C_{\mathrm{ZF,MMSE,DPC}} = \log_2\left[\frac{\left(2+\rho\left(1-g^2\right)\right)^2}{4\left(1-g^2\right)}\right]. \tag{23}$$

If the channel correlation grows very high, i.e. $|\delta|$ approaches $\sqrt{1-g^2}$, signal power would only be transmitted over the stronger user channel, and the other user would get zero capacity. In that case, C_{MMSE} and C_{DPC} become equal to the single user transmission rate in (7), while C_{ZF} tends to zero.

Fig. 5 shows the DPC capacity, linear precoding sum rates and single-user transmission rate as functions of the correlation-related factor $|\delta|^2$ for $\rho = 10$ dB and $g = 0.3$. We can see that the gap between DPC capacity and linear precoding sum rates becomes smaller when $|\delta|^2$ decreases. Eventually the linear precoding sum rates are the same as the DPC capacity when $|\delta|^2=0$, i.e, when the two user channels are orthogonal. When the channel correlation grows high, the ZF capacity decreases rapidly to zero and the DPC capacity decreases to the single-user capacity. It is interesting to notice that the MMSE sum rate first decreases and in fact becomes lower than the single-user capacity, but then increases after $|\delta|^2$ reaches a certain value, e.g. around 0.7-0.8 in this figure. By investigating the power allocation for MMSE, we find the power

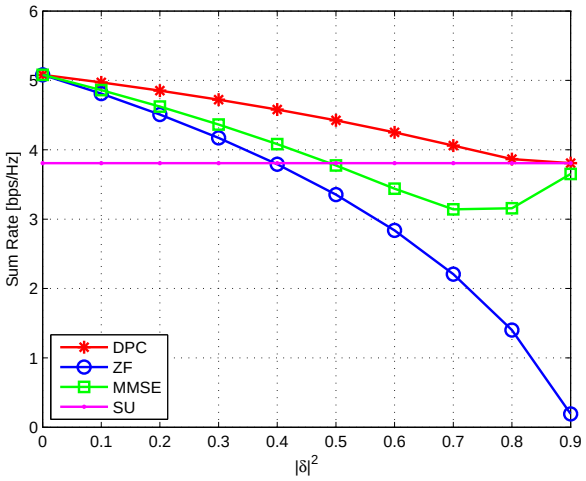

Figure 5: Sum rates for DPC, ZF, MMSE and single user transmission versus channel correlation-related factor $|\delta|^2$ when $\rho = 10$ dB, $g = 0.3$.

is only transmitted to the stronger user channel when $|\delta|^2 > 0.7$, hence, as the correlation gets higher, the MMSE precoding eventually approaches the single-user transmission.

The channel power imbalance factor g also has an effect on the capacity. Basically, as g grows, the channel power difference becomes large and thus the channel correlation $|\delta|/\sqrt{1-g^2}$ grows. Consequently, the ZF sum rate decreases rapidly while the MMSE sum rate and DPC capacity decrease first and then both become the same as single-user capacity. Furthermore, the DPC capacity and linear precoding sum rates are low when g is large. Hence, in order to have higher capacity, users with small channel power differences should be served at the same time according to some grouping strategies.

5.2 Measured Channels

As the number of base station antennas M increases, one hopes that the two user channels become less and less correlated. The ideal scenario would be that if the two users are spatially separated enough, the channels could be approximately orthogonal, i.e. $|\delta|^2$ approaches zero. In that case the DPC capacity could be achieved by linear precoding schemes. Here we verify whether it is true or not that the correlation decreases as M goes large for measured physical channels. Simulated i.i.d. Gaussian channels with the same dimension

and channel power imbalance as the measured channels are used as reference.

We select one representative group of user positions - the two users are positioned outside house 49 and 53 respectively. Fig. 6 plots the average channel correlation as a function of M. For each M, the averaging is performed over time and frequency, and also over different groups of antennas since the cylindrical structure of the array may cause receive power imbalances over the antennas. From Fig. 6 we can see that the channel correlation is higher in the measured channels than in the i.i.d. Gaussian channels. This is because the two user positions are close to each other and probably have common scatterers that make the channels similar [3]. However, in both i.i.d. Gaussian and measured channels, the average channel correlation decreases as M increases from 2 to 32. This suggests that the very-large array can decorrelate the user channels. Then we compare the linear precoding sum rates with the DPC capacity. Fig. 7 shows the ratio of the average linear precoding sum rates and the average DPC capacity as M grows. The SNR here is set to 20 dB and the total transmit power is kept unchanged. With the increase of M, the ratios for ZF and MMSE in both i.i.d. and measured channels is close to one. Therefore, the optimal DPC capacity can be achieved by ZF and MMSE precoding schemes when M is large.

We notice that the channel correlation in Fig. 6 decreases fast as the number of antennas increases from 2 to 8. Correspondingly, in Fig. 7 the ratios of linear precoding sum rates and DPC capacity grow very rapidly as the number of base station antennas increases. When the number of antennas increases to more than 20, the channel correlation as well as the sum rate ratios saturate. Actually, with 8 base station antennas, the linear precoding sum rates are already quite close to the DPC capacity. This shows that a relatively limited number of antennas is enough for the two-user case.

6 Summary and Conclusions

In this paper, linear precoding performance is studied for measured very-large MIMO downlink channels. We find that the user channels, in the studied residential-area propagation environment, can be decorrelated by using reasonably large antenna arrays at the base station. With linear precoding, sum rates as high as 98% of DPC capacity were achieved for two single-antenna users already at 20 base station antennas. This shows that even in realistic propagation environments and with a relatively limited number of antennas, we can see clear benefits with using an excessive number of base station antennas.

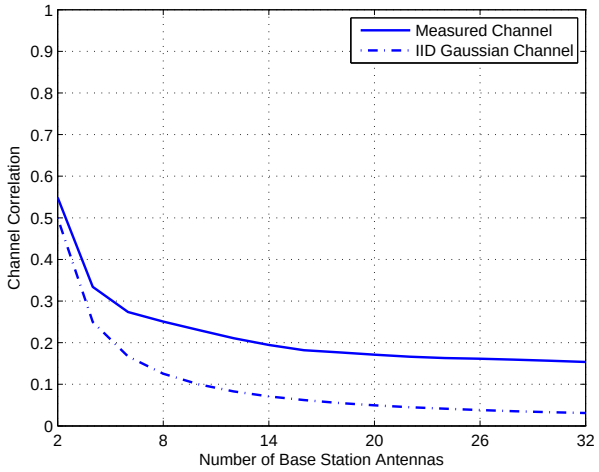

Figure 6: Average channel correlation $|\delta|^2/\left(1-g^2\right)$ as a function of the number of base station antennas. The two users are outside house 49 and 53 respectively.

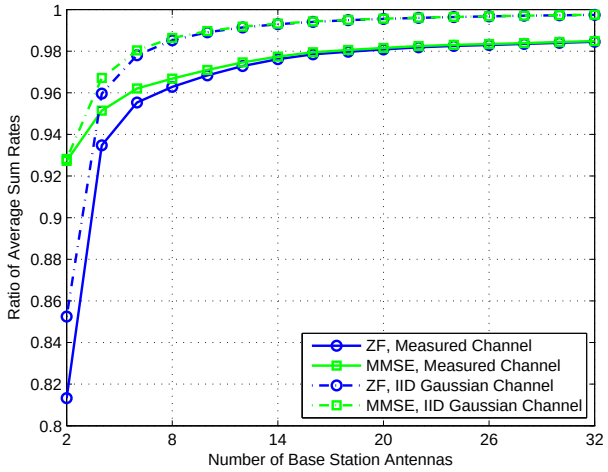

Figure 7: Ratio of average linear precoding sum rate and DPC capacity as a function of the number of base station antennas. The two users are outside house 49 and 53 respectively.

References

[1] E. Dahlman, S. Parkvall, J. Sköld, and P. Beming, *3G Evolution: HSPA and LTE for Mobile Broadband*. Academic Press, 2010.

[2] T. L. Marzetta, "Noncooperative cellular wireless with unlimited numbers of base station antennas," *IEEE Transactions on Wireless Communications*, vol. 9, no. 11, pp. 3590–3600, Nov. 2010.

[3] X. Gao, A. Alayon Glazunov, J. Weng, C. Fang, J. Zhang, and F. Tufvesson, "Channel measurement and characterization of interference between residential femto-cell systems," in *Proc. European Conference on Antennas and Propagation (EuCAP)*, Apr. 2011.

[4] A. Paulraj, R. Nabar, and D. Gore, *Introduction to Space-Time Wireless Communications*. Cambridge University Press, 2003.

[5] C. B. Peel, B. M. Hochwald, and A. L. Swindlehurst, "A vector-perturbation technique for near-capacity multiantenna multiuser communication - Part i: Channel inversion and regularization," *IEEE Transactions on Communications*, vol. 53, no. 1, pp. 195–202, Jan. 2005.

[6] S. Shi and M. Schubert, "MMSE transmit optimization for multi-user multi-antenna systems," in *Proc. IEEE International Conference on Acoustics, Speech, and Signal Processing (ICASSP)*, Mar. 2005.

Paper II

Massive MIMO Performance Evaluation Based on Measured Propagation Data

Massive MIMO, also known as very-large MIMO or large-scale antenna systems, is a new technique that potentially can offer large network capacities in multi-user scenarios. With a massive MIMO system, we consider the case where a base station equipped with a large number of antenna elements simultaneously serves multiple single-antenna users in the same time-frequency resource. So far, investigations are mostly based on theoretical channels with independent and identically distributed (i.i.d.) complex Gaussian coefficients, i.e., i.i.d. Rayleigh channels. Here, we investigate how massive MIMO performs in channels measured in real propagation environments. Channel measurements were performed at 2.6 GHz using a virtual uniform linear array (ULA) which has a physically large aperture, and a practical uniform cylindrical array (UCA) which is more compact in size, both having 128 antenna ports. Based on measurement data, we illustrate channel behavior of massive MIMO in three representative propagation conditions, and evaluate the corresponding performance. The investigation shows that the measured channels, for both array types, allow us to achieve performance close to that in i.i.d. Rayleigh channels. It is concluded that in real propagation environments we have characteristics that can allow for efficient use of massive MIMO, i.e., the theoretical advantages of this new technology can also be harvested in real channels.

Xiang Gao, Ove Edfors, Fredrik Rusek, Fredrik Tufvesson,
"Massive MIMO Performance Evaluation Based on Measured Propagation Data,"
in *IEEE Transactions on Wireless Communications*, vol. 14, no. 7, pp. 3899-3911, July 2015.

1 Introduction

Massive MIMO is an emerging technology in wireless communications, which has attracted a lot of interest in recent years. With massive MIMO, we consider multi-user MIMO (MU-MIMO) systems [1] where base stations are equipped with a large number (say, tens to hundreds) of antennas. As a comparison, the LTE standard only allows for up to 8 antennas at the base station [2]. In this way, massive MIMO scales conventional MIMO by an order or two in magnitude. Typically, a base station with a large number of antennas serves several single-antenna users in the same time-frequency resource.

It has been shown in theory that such systems have potential to remarkably improve performance in terms of link reliability, spectral efficiency, and transmit energy efficiency [3–6]. Massive MIMO can also reduce intra-cell interference between users served in the same time-frequency resource, due to its focus of transmitted power to desired users. The fundamental idea is that as the number of base station antennas grows large, channel vectors between users and base station become very long random vectors and, under "favorable" propagation conditions, these channel vectors become pairwise orthogonal. The term "favorable" is first defined in [6] as the mutual orthogonality among user channels, and "favorable" propagation is further investigated in theory in [7]. We can also interpret "favorable" propagation as a sufficiently complex scattering environment. Under these conditions, even simple linear precoding/detection schemes, e.g., zero-forcing and matched-filtering, become nearly optimal [3, 4, 8].

The attractive features of massive MIMO are, however, based on optimistic assumptions about propagation conditions in combination with available low-cost hardware making it possible to deploy large number of antennas. So far, investigations are mostly based on theoretical independent and identically distributed (i.i.d.) complex Gaussian, i.e., Rayleigh fading, channels and for antenna numbers that grow without limit. Bringing this new technology from theory to practice, we must ask to what degree the optimistic theoretical predictions can be maintained in real propagation environments when using practical antenna array setups. In attempts to answer this question, massive MIMO propagation measurements have been conducted and measurement data used to assess massive MIMO performance in real channels [8–12]. Channel measurements in [8], at 2.6 GHz with an indoor base station using a 128-port uniform cylindrical array (UCA) of patch antennas, showed that orthogonality of user channels improves significantly with increasing number of base station antennas. Already at 20 antennas, linear precoding schemes operating on measured channels achieve near-optimal performance for two users. From measurements using a 128-element virtual uniform linear array (ULA) at 2.6 GHz, presented

in [9] and [10], it was concluded that the angular power spectrum (APS) of the incoming waves varies significantly along the physically large ULA. This is a clear indication that large-scale/shadow fading across the array is an important mechanism when dealing with physically large arrays. As a comparison, the UCA studied in [8] is relatively compact and much smaller in size, but still a similar effect of variation in channel attenuations can be experienced over the array. In this case it is not primarily a large-scale/shadow fading effect, but rather a consequence of the circular array structure and directive patch antenna elements pointing in different directions. No matter the source of these power variations over the array, they can have a large influence on massive MIMO performance [13]. A measurement campaign independent of our investigations, with an antenna array consisting of up to 112 elements, is reported in [12]. Results obtained there, which to a large extent agree with our own experience [11], show that despite fundamental differences between measured and i.i.d. channels in terms of propagation characteristics, a large fraction of the theoretical performance gains of massive MIMO can be achieved in practice. A different approach to characterize massive MIMO performance has been presented in [14], where real propagation environment is replaced by simulation in a reverberation chamber.

In this paper, we aim for a deeper insight into how massive MIMO performs in real propagation environments. The investigations are based on outdoor-to-outdoor channel measurements using a 128-port UCA and a 128-port virtual ULA, as described in [11]. We study the channel behavior of massive MIMO under three representative propagation conditions, where users are: 1) closely located with line-of-sight (LOS) to the base station, 2) closely located with non-line-of-sight (NLOS) to the base station, and 3) located far from each other. When users are located close to each other, spatial multiplexing with good isolation between users can be particularly difficult, as compared to the case when users are located far from each other. LOS conditions may prove particularly difficult with highly correlated channels to different users, making spatial multiplexing less efficient. The more complex propagation in NLOS conditions is expected to decorrelate channels to different users to a larger extent. We investigate the corresponding performance obtained in these scenarios, by calculating sum-rates based on measured channel data and comparing with those obtained in i.i.d. Rayleigh channels. As a complementary tool, we also study the singular value spreads for the measured channels. This gives an indication of how large the difference is between the most favorable and least favorable channels. Small singular value spreads indicate stable channels to all users, while large spreads indicate that one or more users may suffer from significantly worse conditions than others.

In this investigation we compare two different large array structures. From a

practical point of view it is preferable to have a compact array, such as the UCA, since it is easier to deploy. However, if we make the array small, it will bring drawbacks such as higher antenna correlation and poor angular resolution. A two-dimensional structure like the UCA will, however, have the ability to resolve incoming waves in two dimensions. Using a much larger one-dimensional ULA with the same number of elements, we benefit from a higher angular resolution, but only in one dimension. Since both array structures have different characteristics, we can expect that they perform differently in a massive MIMO setting. Depending on how well the propagation environment suits each array type, one may be better than the other. To investigate this, we compare massive MIMO performance with the two arrays in the same propagation environments.

The rest of the paper is organized as follows. In Sec. 2, we describe our massive MIMO channel measurements and Sec. 3, outlines the system model and performance metrics used when evaluating the measured channels, including singular value spread and sum-rate capacity. Propagation characteristics in three measured scenarios are illustrated and discussed in Sec. 4. In Sec. 5 we evaluate singular value spreads and sum-rate capacities for the measured channels. Finally, in Sec. 6, we summarize our contributions and draw conclusions.

2 Channel Measurements

In this section, we present the measurement campaigns for massive MIMO channels, on which we base our study of propagation characteristics and evaluations of system performance. First we introduce the measurement setups, including antenna arrays and measurement equipment. Then we describe the semi-urban environment where measurements were performed under different propagation conditions.

2.1 Measurement Setups

Two channel measurement campaigns were performed with two different large arrays at the base station side. Both arrays are for the 2.6 GHz range and contain 128 antenna ports each, with antenna elements spaced half a wavelength apart. Fig. 1a shows the UCA having 64 dual-polarized patch antennas, with 16 antennas in each of the four stacked circles, giving a total of 128 antenna ports. This array is compact in size with both diameter and height around 30 cm. Fig. 1b shows the virtual ULA with a vertically-polarized omni-directional antenna moving along a rail, in 128 equidistant positions. In comparison, the ULA spans 7.4 m in space, which is more than 20 times the size of the UCA.

In both measurement campaigns, an omni-directional antenna with vertical polarization was used at the user side.

Channel data were recorded at center frequency 2.6 GHz and 50 MHz bandwidth. With the UCA, measurements were taken with the RUSK LUND channel sounder, while for the virtual ULA, an HP 8720C vector network analyzer (VNA) was used. With the virtual ULA and VNA, it takes about half an hour to record one measurement, when the antenna moves from the beginning of the array to the end. In order to keep the channel as static as possible during one measurement, we performed this campaign during the night when there were very few objects, such as people and cars, moving in the measurement area. To verify that channel conditions were static enough, some measurements were repeated directly after the full array length was measured. The two measurements done half an hour after each other were compared and found to match well[1].

Mutual coupling among antenna elements should also be mentioned, since it is a critical issue that may affect massive MIMO performance, if a large number of antennas are tightly placed [15,16]. Although the UCA is compact, the worst case of mutual coupling between the neighboring elements is -11 dB [17]. The virtual ULA, however, experiences no mutual coupling effect. This may lead to different performance of the virtual ULA, as compared to a practical ULA. However, a theoretical study in [18] shows that coupling has a major impact on MIMO capacity only when the element separation is below 0.2 wavelengths. Indeed, practical studies are also needed on the impact of coupling on massive MIMO performance. This is closely related to antenna array design, a topic not covered in this paper. We focus on the propagation aspects and investigate how different propagation conditions affect massive MIMO performance.

2.2 Measurement Environments

The channel measurements were carried out outdoors at the E-building of the Faculty of Engineering (LTH), Lund University, Sweden (N 55°42′37.96″, E 13°12′39.72″). Fig. 2 shows an overview of the semi-urban measurement area. The two base station antenna arrays were placed on the same roof of the E-building during their respective measurement campaigns. More precisely, the position of the UCA was on the same line as the ULA, near its beginning, and for practical reasons about 25 cm higher than the ULA.

[1]Comparing the two measured channels, i.e., the original one and the verification one, we found that the two transfer functions are very similar, however, there are minor differences due to channel variation and noise. Average amplitude correlation coefficients between the two measured transfer functions over all antenna positions are in the range of 0.95-0.99. Besides, we observed that the two measured channels give very similar angular power spectrum.

Figure 1: Two large arrays at the base station side: a) a UCA with 64 dual-polarized patch antenna elements, giving 128 ports in total, and b) a virtual ULA with 128 vertically-polarized omni-directional antennas.

At the user side, the omni-directional antenna was moved around the E-building at 8 measurement sites (MS) acting as single-antenna users. Among these sites, three (MS 1-3) have LOS conditions, and four (MS 5-8) have NLOS conditions, while one (MS 4) has LOS for the UCA, but the LOS component is blocked by the roof edge for the ULA, due to the slightly lower mounting. Despite this, MS 4 still shows LOS characteristic for the ULA, where one or two dominating multipath components due to diffraction at the roof edge cause a relatively high Ricean K-factor [19, 20]. At MS 4, besides the roof-edge diffraction to the ULA, there is also strong scattering from the building in the south. At each measurement site, 40 positions with about 0.5 m inter-spacing were measured with the UCA, and 5 positions with 0.5-2 m inter-spacing were measured with the ULA. The reason for having fewer positions with the ULA was due to the long measurement time.

For all the measurements with the ULA, the average signal-to-noise ratio (SNR) over all antenna elements was above 28 dB, while the lowest per-antenna SNR was above 23 dB. With the UCA, at MS 1-4 and MS 7, the average SNR over all antenna elements was above 33 dB, while the lowest per-antenna SNR was above 20 dB. At MS 5-6 and MS 8, the measurement SNR was lower but still good enough, i.e., for all antenna elements of the UCA, the SNR was about 10-25 dB. In the measured 50 MHz bandwidth, we observe a coherence bandwidth about 25 MHz in the LOS scenarios, and about 5 MHz in the NLOS scenarios.

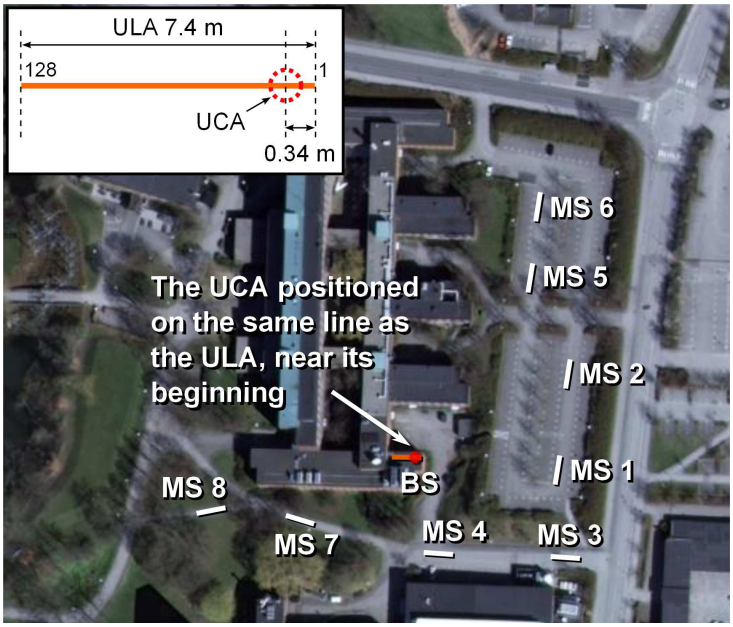

Figure 2: Overview of the measurement area at the campus of the Faculty of Engineering (LTH), Lund University, Sweden. At the base station side, the two antenna arrays were placed on the same roof of the E-building during their respective measurement campaigns. At the user side, the omni-directional antenna was moved around at MS 1-8 acting as single-antenna users.

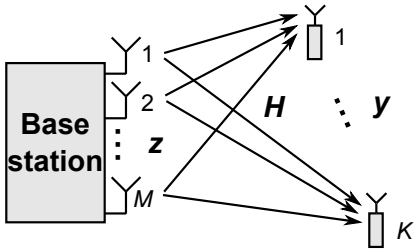

Figure 3: System model of the downlink of an MU-MIMO system with an M-antenna base station and K single-antenna users.

3 System Description

The acquired measurement data allows study of various aspects of massive MIMO systems. Before discussing channel behavior and evaluating performance of massive MIMO, we first define our system model.

3.1 Signal Model

We consider a single-cell multi-user MIMO-OFDM system with N subcarriers in the downlink. The base station is equipped with M antennas and simultaneously serves K ($K \leq M$) single-antenna users in the same time-frequency resource. We assume that the base station has perfect channel state information (CSI), and that the channel can be described as narrow-band at each OFDM subcarrier.

As shown in Fig. 3, the signal model of the considered narrow-band MU-MIMO downlink channel is

$$\boldsymbol{y}_\ell = \sqrt{\frac{\rho K}{M}} \boldsymbol{H}_\ell \boldsymbol{z}_\ell + \boldsymbol{n}_\ell, \tag{1}$$

where $\boldsymbol{H}_\ell$ is a $K \times M$ channel matrix at subcarrier ℓ, $\boldsymbol{z}_\ell$ the normalized transmit vector across M base station antennas, satisfying $\mathbb{E}\{\|\boldsymbol{z}_\ell\|^2\} = 1$, $\boldsymbol{y}_\ell$ the vector of received signals at the K users, and $\boldsymbol{n}_\ell$ a complex Gaussian noise vector with i.i.d. unit variance elements. The term $\rho K/M$ scales the transmit energy and ρ relates to the average per-user receive SNR[2]. From the term $\rho K/M$, we increase

[2]With the defined signal model and channel normalization, the average receive SNR at the users is smaller or equal to ρ, and different values can be obtained depending on used precoding scheme. For example, when user channels are not completely orthogonal and inter-user interference exists, the average receive SNR using dirty-paper coding would be higher than for zero-forcing precoding. Equality between average per-user receive SNR and ρ, both

the transmit power with the number of users and reduce it as the number of base station antennas grows. As K increases, we keep the same transmit power per user. With increasing M the array gain increases and we choose to harvest this as reduced transmit power instead of increased receive SNR at the users[3].

Let us now return to the channel matrix $\boldsymbol{H}_\ell$ in (1) and how it is formed. From our measurements, we have channel data obtained with 128 antenna ports at the base station and, at the user side, each measured position represents one single-antenna user. With the selection of K positions, we have a measured channel matrix of size $K \times 128$, which we denote $\boldsymbol{H}_\ell^{\text{raw}}$, at subcarrier ℓ. The channel matrix $\boldsymbol{H}_\ell$ is then formed by selecting M columns from a normalized version of $\boldsymbol{H}_\ell^{\text{raw}}$. Two different normalizations of $\boldsymbol{H}_\ell^{\text{raw}}$ are used in different investigations. The two channel normalizations are:

- **Normalization 1.** The measured channel vectors of each user, i.e., the rows of $\boldsymbol{H}_\ell^{\text{raw}}$, denoted as $\boldsymbol{h}_{i,\ell}^{\text{raw}}, i = 1, 2, \ldots, K$, are normalized such that the average energy over all 128 antenna ports and all N subcarriers is equal to one. This is achieved through

$$\boldsymbol{h}_{i,\ell}^{\text{norm}} = \sqrt{\frac{128N}{\sum_{\ell=1}^{N} \left\| \boldsymbol{h}_{i,\ell}^{\text{raw}} \right\|^2}} \boldsymbol{h}_{i,\ell}^{\text{raw}}, \tag{2}$$

  where the vector $\boldsymbol{h}_{i,\ell}^{\text{norm}}$ is the ith row of the normalized channel matrix $\boldsymbol{H}_\ell^{\text{norm}}$. With this normalization, the imbalance of channel attenuations between users is removed, while variations over antenna elements and frequencies remain.

- **Normalization 2.** The measured channel matrix is normalized such that the channel coefficients have unit average energy over all 128 antenna ports, K users and N subcarriers. This is achieved through

$$\boldsymbol{H}_\ell^{\text{norm}} = \sqrt{\frac{128KN}{\sum_{\ell=1}^{N} \| \boldsymbol{H}_\ell^{\text{raw}} \|_{\text{F}}^2}} \boldsymbol{H}_\ell^{\text{raw}}, \tag{3}$$

for DPC and ZF precoding is obtained when user channels are orthogonal, i.e., when the Gram matrix $\boldsymbol{H}_\ell \boldsymbol{H}_\ell^H$ is diagonal.

[3]With realistic low-cost terminals it can be expected that only a limited SNR can be handled by the terminals, before quantization noise and dynamic range start to limit performance. Further, sum-rate capacities in i.i.d. Rayleigh channels are closer to those in interference-free channels at lower SNRs [4]. For these reasons, we keep a constant interference-free SNR ρ at the users when the number of antennas M at the base station changes. This is to make fair and realistic comparisons of different settings.

where $\|\cdot\|_{\mathrm{F}}$ represents the Frobenius-norm of a matrix. Compared with Normalization 1, here we keep the difference in channel attenuation between users, as well as variations over antenna elements and frequencies.

Both normalizations are done for the originally measured channel matrix with 128 columns, rather than the matrix with M columns, obtained by selecting a subset of the 128 antennas. The reason for this is that we would like to maintain the imbalance of channel attenuations over the antenna arrays due to power variations over the antenna elements. These variations, caused by large-scale fading/shadowing and/or directive antennas with different orientation, are critical for performance evaluation of massive MIMO. When investigating singular value spreads of measured channels, we use Normalization 1. For capacity evaluation, Normalization 2 is used in scenarios where users are closely located, while Normalization 1 is used when users are far from each other and have large channel attenuation imbalance. The detailed reasons for using each normalization are given in the following.

3.2 Singular Value Spread

As mentioned in Sec. 1, by using a large number of antennas at the base station, massive MIMO has the potential to separate users so that all spatial modes are useful in such a system. However, this relies on "favorable" propagation where user channels become pairwise orthogonal with growing number of antennas, i.e., the off-diagonal terms of the Gram matrix $\boldsymbol{H}_\ell \boldsymbol{H}_\ell^H$ become increasingly small compared to the diagonal terms. As this phenomenon can be easily seen in i.i.d. Rayleigh channels, many theoretical studies are based on this assumption. We need to investigate to what degree real massive MIMO channels are "favorable". One way to evaluate joint orthogonality of all users is singular value spread of the normalized propagation matrix [21]. Here Normalization 1 applies, since the imbalance of channel attenuations between the users should be removed, so that the singular value spread does not contain the difference in channel norms, but only reflects the joint orthogonality of the users.

The propagation matrix $\boldsymbol{H}_\ell$ at subcarrier ℓ has a singular value decomposition (SVD) [22]

$$\boldsymbol{H}_\ell = \boldsymbol{U}_\ell \boldsymbol{\Sigma}_\ell \boldsymbol{V}_\ell^H, \tag{4}$$

where $\boldsymbol{U}_\ell$ and $\boldsymbol{V}_\ell$ are unitary matrices, and the $K \times M$ diagonal matrix $\boldsymbol{\Sigma}_\ell$ contains the singular values $\sigma_{1,\ell}, \sigma_{2,\ell}, ..., \sigma_{K,\ell}$. The singular value spread is defined as

$$\kappa_\ell = \frac{\max\limits_i \sigma_{i,\ell}}{\min\limits_i \sigma_{i,\ell}}, \tag{5}$$

i.e., the ratio of the largest and smallest singular values. A large κ_ℓ indicates that at least two rows of $\boldsymbol{H}_\ell$, i.e., the channel vectors of two users, are close to parallel and thus relatively difficult to separate spatially, while $\kappa_\ell = 1$, i.e., 0 dB, implies the best situation where all rows are pairwise orthogonal. The singular value spread can be an indicator whether the users should be served in the same time-frequency resource. It also has close connection with the performance of MIMO precoders/detectors [23–25].

With massive MIMO, as the number of antennas increases and becomes much larger than the number of users ($M \gg K$), we expect better orthogonality between user channels and thus smaller singular value spreads, as compared to conventional MIMO. More importantly, we expect the singular value spread to become more stable over channel realizations. The stability of singular value spread implies that bad channel conditions can be avoided and also leads to stability of MIMO precoders/detectors. While the above is true for i.i.d. Rayleigh channels, we investigate the measured channels in Sec. 5, in an attempt to find out if realistic channels also can provide sufficiently good and stable user orthogonality.

3.3 Dirty-Paper Coding Capacity

Through the singular value spread, we can investigate the potential of massive MIMO to spatially separate the users. However, singular value spread cannot fully quantify the performance of an MU-MIMO system, since it only offers an indication of the minimum quality of service that can be guaranteed for all users. We would also like to know the overall performance of a massive MIMO system in terms of sum-rate capacity. A small singular value spread leads to high capacity, as interference between all users is low and they can get relatively good quality of service. A large singular value spread, however, does not imply a low channel capacity. In this case, at least one user has relatively poor quality of service, but we do not know how many that still can get good quality of service. For example, in a rank-deficient channel with one singular value being zero, i.e., two user channels are aligned, the singular value spread goes to infinity, but the channel capacity can still be relatively high, depending on the remaining singular values. By combining the two metrics, singular value spread and sum-rate capacity, we can get a good understanding of massive MIMO performance.

Sum-rate capacity in the narrow-band MU-MIMO downlink channel is [26],

$$C_{\mathrm{DPC},\ell} = \max_{\boldsymbol{P}_\ell} \log_2 \det \left(\boldsymbol{I} + \frac{\rho K}{M} \boldsymbol{H}_\ell^H \boldsymbol{P}_\ell \boldsymbol{H}_\ell \right), \tag{6}$$

which is achieved by dirty-paper coding (DPC) [27]. The diagonal matrix $\boldsymbol{P}_\ell$

with $P_{\ell,i}, i = 1, 2, ..., K$ on its diagonal allocates the transmit power among the user channels and capacity is found by optimizing over $\boldsymbol{P}_\ell$ under the total power constraint $\sum_{i=1}^{K} P_{\ell,i} = 1$. This can be done using the sum-power iterative water-filling algorithm presented in [28].

In measured channels where users are far from each other, large variations in channel attenuations to different users can have a strong influence on sum-rate capacity. In order to maximize the downlink sum-rate, a large proportion of the transmit power will be allocated to users with low channel attenuation. These users will have relatively high date rates, compared to users with higher channel attenuation. We can imagine an extreme case where only one user has a very high data rate and the multi-user transmission is reduced to single-user transmission. When this happens, it is difficult to investigate the effect of user channel orthogonality on the system performance. To avoid large imbalance of channel attenuations, users with similar attenuation should be grouped and served simultaneously, while the user groups are, e.g., time multiplexed. Due to a limited number of measurement positions, we do not have enough data to analyze this situation. We therefore focus on orthogonality between channels to different users and remove attenuation imbalance between users that are far apart, when evaluating their sum-rate capacity, as described in Normalization 1. When users are closely located, the path losses can be expected to be similar and any attenuation imbalance is mainly due to small-scale and large-scale fading. From our measurements, we observe that attenuation imbalance between co-located users is very small. Thus, for capacity evaluation in this case, we apply Normalization 2 on the measured channels and keep the small attenuation imbalance among the users, as is the case in i.i.d. Rayleigh channels.

Ideally, in massive MIMO, as the number of base station antennas goes to infinity in "favorable" propagation conditions, the channels to different users become interference free (IF) [4] with per-user receive SNRs approaching ρ as given in our model (1). This leads to an asymptotic, interference free, sum-rate capacity

$$C_{\mathrm{IF}} = K \log_2 (1 + \rho), \tag{7}$$

to which i.i.d. Rayleigh channels converge, as the number of antennas grows. For the measured channels we would like to know how large a fraction of this capacity we can achieve. This is investigated and discussed in Sec. 5.

4 Propagation Characteristics

Before presenting numerical performance evaluation results, we focus on propagation characteristics in the investigated scenarios, as briefly outlined in Sec. 1. While not providing quantitative measures of massive MIMO performance,

this description gives an intuitive understanding of real massive MIMO propagation mechanisms, and also helps to understand the evaluation results of singular value spreads and sum-rate capacities, presented later in Sec. 5. By understanding these propagation mechanisms observed in massive MIMO, we also gain insight into what needs to be considered and included in a massive MIMO channel model [29, 30].

For a simple and clear illustration of massive MIMO propagation characteristics in each of the three scenarios, we start with four users ($K = 4$), which is the number of users supported in LTE MU-MIMO [2]. In two of the scenarios, the four users are located close to each other, with only 1.5-2 m inter-spacing, representing situations where the spatial separation of user signals can be expected to be particularly difficult. In the third scenario, the four users are located far from each other, with more than 10 m inter-spacing, representing situations where users are well distributed around the base station and we can expect good channel orthogonality. Combining difference in user inter-spacing with LOS/NLOS conditions, the three investigated scenarios are:

1. four users close to each other at MS 2, having LOS conditions to the base station,
2. four users close to each other at MS 7, with NLOS conditions,
3. four users far apart, at MS 1-4, respectively, all having channels with LOS characteristics.

With the aim of assisting understanding of the physical propagation channels, we estimate the APS at the base station side. The directional estimates for the ULA are obtained through the space-alternating generalized expectation maximization (SAGE) algorithm [31], which jointly estimates the delay, incidence azimuth, and complex amplitude, of multipath components (MPCs) in radio channels. The frequency-dependent SAGE algorithm is applied to a sliding window of 10 neighboring elements on the ULA and, for the measured channel within each window, 200 MPCs are estimated. The reason for estimating the MPC parameters based on 10-antenna windows is that the incoming waves can be considered planar if the array is small enough. This aperture corresponds to a Fraunhofer distance of about 5 m, making waves originating from reflections beyond that distance to appear planar. Using 10 antennas also provides a relatively high angular resolution for the directional estimation. Note that the range of azimuth estimation is 0-180 degrees for the ULA, due to inherent directional ambiguity problem when using this type of array structure [32].

Based on the SAGE estimates, we obtain the APS in azimuth at each position along the ULA. For each scenario, we compare the APS from different

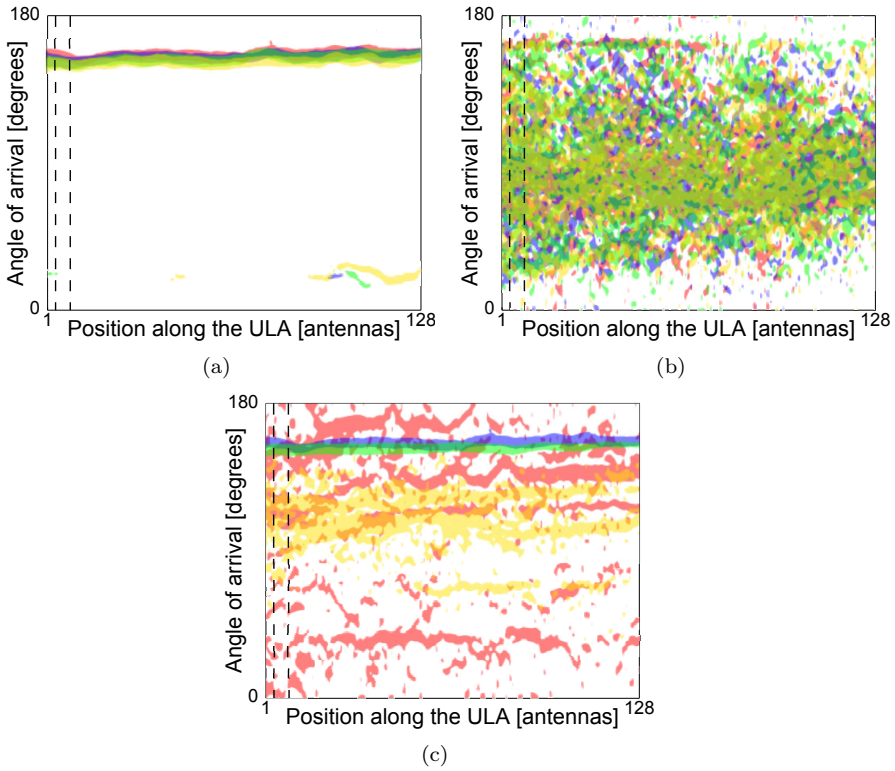

Figure 4: Spatial fingerprints (simplified forms of the angular power spectral density along the 128-element ULA), in (a) a LOS scenario where the four users are co-located at MS 2, (b) an NLOS scenario where the four users are co-located at MS 7, (c) a LOS scenario where the four users are far away from each other, at MS 1-4, respectively. The four different colors in each plot represent the spatial fingerprints of the four different users. Dashed vertical lines indicate where the UCA is located and which part of the ULA propagation channel it is exposed to. Distinct fingerprints, as in (b) and (c), indicate relatively good conditions for spatial separation of user signals, while similar fingerprints, as in (a), indicate that spatial separation may be more difficult.

users as seen at the base station. For the convenience of comparison, we simplify the APS from each user. Instead of showing the estimated power levels from all the azimuth directions, we only show from which directions the incoming energy is strongest. The colored patches show where 90% of the total energy across the whole array is concentrated. This simplified form of APS illustrates the directional pattern of the incoming energy from a specific user. Since it is a highly simplified form of the spatial properties of the channel from a specific user, we call it a "spatial fingerprint". In Fig. 4, for each scenario, we plot the four users' spatial fingerprints on top of each other. The four colors in each plot represent the spatial fingerprints of the four different users. Since the UCA was positioned at the beginning of the ULA, as indicated by the dashed lines in Fig. 4, we consider that it experiences the propagation channels at that particular part of the ULA, but with directional patch antennas oriented in different directions.

What can we learn from these spatial fingerprints? First, they provide an intuitive understanding of the distribution of incoming energy from different users in real channels under different propagation conditions. Secondly, by comparing fingerprints, we get an understanding of how much the APS changes between users in different scenarios. Through this we can acquire qualitative information about how difficult it is to do spatial separation of signals from different users. Distinct fingerprints indicate relatively good spatial orthogonality of the user channels, and we can expect that the user signals can be separated with rather simple means. In this case, the channels have relatively small singular value spreads and relatively high sum-rate capacities. Similar and overlapping fingerprints, on the contrary, represent a more difficult situation and spatial separation of user signals may be much harder. With incoming energy from largely the same directions, detailed knowledge about amplitude and phase is needed to fully assess the situation. Thirdly, these fingerprints allow for a direct comparison of the propagation channels experienced by massive and more conventional MIMO systems. This can be done by comparing fingerprints along the entire ULA with the local fingerprint somewhere along the ULA, that would be experienced by a smaller conventional MIMO array. Lastly, an attempt to develop a sophisticated geometry-based channel model for massive MIMO should likely take these spatial fingerprints into consideration. Our point of view is that if a channel model does not reflect the spatial properties observed through these fingerprints, it does not accurately model the nature of a massive MIMO propagation channel. We discuss these issues in the following.

First we turn our attention to propagation conditions and spatial separability of user channels in the three investigated scenarios. In Fig. 4a, we can see that in the LOS scenario with co-located users, incoming energy from all

users is concentrated around 160 degrees, which is the LOS direction. For some users, a significant amount of energy also comes from some scatterers at around 20 degrees at the end of the ULA. The overlap of the four users' fingerprints indicates that we may have a relatively high correlation[4] between their channels, making it difficult to spatially separate signals from the co-located users. However, as discussed above, amplitude and phase differences may still make users easier to separate than they appear from studying the fingerprints.

An entirely different situation is shown Fig. 4b, where the four users are still closely located but in an NLOS scenario with rich scattering. Incoming energy from all four users is distributed over a much larger angle across the whole array, reflecting a rich scattering environment. The four users' fingerprints are very complex and quite different from each other, as compared to the case in Fig. 4a. This indicates that the spatial correlation between channels to the users is relatively low, which should allow for a better spatial separation of user signals, even though they are still closely located.

Fig. 4c shows the scenario where four users are located far from each other, all having LOS propagation characteristics. Users at MS 2 and 3, whose fingerprints are in blue and green, respectively, have the strongest LOS characteristics with incoming energy concentrated to a certain direction along the entire array. This is in stark contrast to users at MS 1 and 4, whose fingerprints are in red and yellow. At MS 1, the LOS is at the end-fire direction of the ULA, and its power contribution is weakened due to the superposition with the ground reflection. At MS 4, besides the energy from the roof-edge diffraction to the ULA, strong scattering from the building in the south also contributes considerably. Since the users are located at different sites, their fingerprints should be very different from each other. Note that the signals from users at MS 2 and 3 appear to come from the same direction due to the inherent angular ambiguity of the ULA. However, as seen later in Sec. 5 it is possible to spatially separate the two users. A good spatial separation of all users can be expected in this scenario.

Now, let us turn our attention to propagation channels experienced by massive and more conventional MIMO systems. In the fingerprint plots, we can see that the ULA potentially experiences channels with much more spatial variations, as compared to small arrays spanning only a few wavelengths in space. Large spatial variations can help to decorrelate channels even when users are closely located, as in Fig. 4b. Fingerprints may overlap locally, but over longer distances along the array they are quite distinct. This indicates that, with small arrays users may have relatively low spatial correlation on average, e.g., over time, while with a physically large ULA decorrelation of user channels can

[4]The spatial correlation we talk about here is an instantaneous property between users, rather than an average property, e.g., over time realizations of the channels.

be instantaneous. However, strong LOS may reduce the ability of the ULA to spatially separate signals from co-located users, such as the situation shown in Fig. 4a. Since we do not consider the phase information over the array there, we later investigate this situation in more detail by evaluating both singular value spreads and sum-rate capacities.

For the compact UCA, experiencing only a small part of channels seen by the ULA, separation of user signals may be more difficult. When users are closely located and incoming energy is concentrated to similar and narrow directions, patch antennas oriented in "wrong" directions may have high channel attenuations and contribute little to spatial separation of signals from co-located users. Despite this, the UCA may still gain from its circular structure and provide good user decorrelation, when users are distributed around the base station, and incoming energy is distributed in different directions, as shown in Fig. 4c.

5 Performance Evaluation

To get a more quantitative understanding of how massive MIMO would perform in our measured channels, we turn our attention to singular value spreads and sum-rate capacities in the three measured scenarios. First we focus on the case of four users ($K = 4$), as we did in the propagation characteristics in Sec. 4. We then increase the number of users to sixteen ($K = 16$) and investigate the performance when more users are served simultaneously.

5.1 Four Users ($K = 4$)

In all three scenarios, over $N = 161$ subcarriers and 2000 random selections of antenna subsets, i.e., selections of M antennas out of the 128, we show a) the cumulative distribution functions (CDFs) of the singular value spreads in the channels, when using 4, 32 and 128 base station antennas, and b) the average DPC capacities including their 90% confidence intervals, as the number of base station antennas M grows from 4 to 128. Note that for $M = 128$ there is only a single choice of selecting the antenna subset, and the CDFs of the singular value spreads and the capacity confidence intervals are therefore computed over frequencies only. For $M < 128$, as the number of all possible antenna subsets can be extremely large, we randomly select 2000 subsets, and let the CDFs of the singular value spreads and the capacity confidence intervals also take the random antenna selections into account. As a reference, we also show simulated results for i.i.d. Rayleigh channels. We select the interference-free

SNR to $\rho = 10$ dB [5], and with four users the asymptotic capacity (7) becomes $4\log_2(1+10) = 13.8$ bps/Hz. In the following we discuss the singular value spreads and DPC capacities in the three scenarios.

Four Users Co-Located with LOS

As discussed in Sec. 4, this scenario represents a particularly difficult situation for spatial separation of user signals, which can be seen from the four users' similar fingerprints in Fig. 4a. First we study the CDFs of singular value spreads, as shown in Fig. 5. We observe that for i.i.d. Rayleigh channels, the median of the singular value spread significantly reduces from 17 dB to below 4 dB, as the number of antennas increases from 4 to 32 and 128. Singular value spreads also become much more stable around small values, as the CDF curves have no substantial upper tails.

For the measured channels, using either ULA and UCA, the singular value spreads are significantly larger than those of i.i.d. Rayleigh channels, for all three numbers of antennas. This indicates a much worse user channel orthogonality in the measured channels, due to co-location of users and strong LOS conditions in this scenario. Still, trends similar to those seen in i.i.d. Rayleigh channels can be observed in the measured channels. The median of the singular value-spread decreases by 14 dB with the ULA and 12 dB with the UCA, as the number of antennas increases from 4 to 128. Meanwhile, when using a large number of antennas, the substantial upper tails of the CDF curves reduce, and almost disappear in the case of 128 antennas. With only 4 antennas, the selections of antenna subsets and subcarriers can make a big difference on the user orthogonality. This means that with small arrays we may encounter propagation channels with very good conditions as well as very bad ones, depending on the choice of antenna positions and used subcarriers. When increasing the number of antennas to 32, user orthogonality improves and becomes much more stable over antenna selections and subcarriers. Thus, bad channel conditions can largely be avoided by adding more antennas at the base station. When using all 128 antennas, user orthogonality improves further and becomes more stable over subcarriers. The above observations tell us that despite a significant gap between measured and i.i.d. Rayleigh channels in this scenario, spatial separation of signals from co-located users can be greatly improved by using a large number of antennas, and more importantly, the results become more stable over both subcarriers and different antenna selections.

We now move to sum-rate capacities achieved by DPC, as shown in Fig. 6. As a reference, the average capacity in i.i.d. Rayleigh channels converges to the

[5] The performance of i.i.d. Rayleigh channels at different SNR levels has been derived in [4]. We select the interference-free SNR to be 10 dB since it is a middle-level SNR.

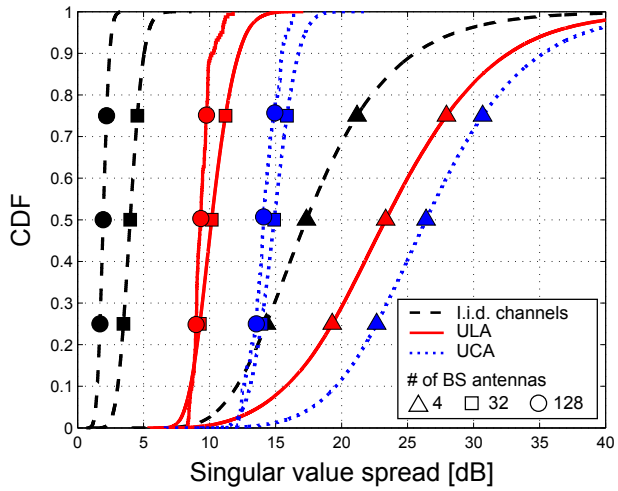

Figure 5: CDFs of singular value spreads when using 4, 32 and 128 antennas, in the scenario where the four users are closely located at MS 2, all having LOS to the base station antenna arrays.

asymptotic capacity value of 13.8 bps/Hz and the capacity variation becomes smaller as the number of antennas increases. In the measured channels, however, averages are significantly lower and variations are larger. Let us focus on the average capacities first, and discuss the variations later. The drops in average capacities for measured channels coincide with larger singular value spreads. Despite this, in this potentially difficult spatial separation situation, the ULA and UCA perform at 90% and 75% of the asymptotic capacity, respectively, when the number of antennas is above 40, i.e., when the number of antennas is 10 times the number of users.

Four Users Co-Located with NLOS

In this scenario we still have users closely located, but now in NLOS conditions. NLOS with rich scattering, as illustrated in Fig. 4b, where spatial fingerprints of users are complex and distinct, should improve the situation by providing more "favorable" propagation and thus allowing better spatial separation of user signals. The benefits of complex propagation are reflected in the CDFs of singular value spreads in Fig. 7. Singular value spreads in this scenario become significantly smaller, as compared to those in the corresponding LOS case. Especially for the ULA, the CDF curves are very close to those of i.i.d. Rayleigh

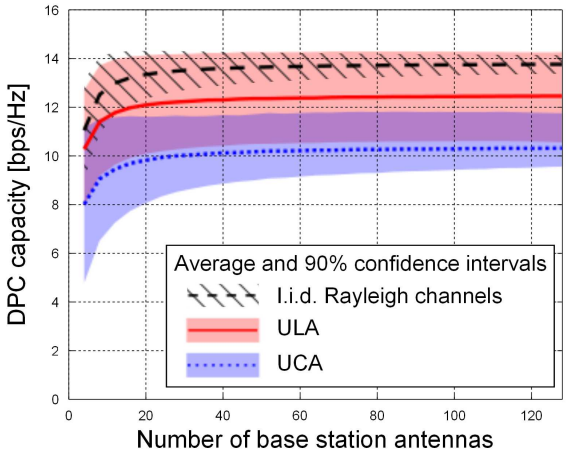

Figure 6: Sum-rate capacity in the downlink, achieved by DPC, in a scenario where four users are close to each other at MS 2, all having LOS to the base station antenna arrays.

channels. The substantial upper tails of the CDF curves observed when using a small number of antennas disappear when using all 128 antennas in the measured channels. This means that over the measured bandwidth the probability of seeing a singular value spread much larger than 2 dB for the ULA, and 7 dB for the UCA, is very low.

Correspondingly, the benefits brought by the NLOS condition with rich scattering can also be observed in DPC capacities, as shown in Fig. 8. Despite co-located users, the ULA here provides average performance very close to the asymptotic capacity achieved in i.i.d. Rayleigh channels, while the UCA reaches more than 90%, when the number of antennas is above 40.

Four Users Located Far From Each Other with LOS

In this scenario, despite LOS characteristics, increased inter-spacing between users should help to improve performance. As can be seen in Fig. 4c, the users' spatial fingerprints are reasonably different, which indicates a favorable decorrelation situation between user channels for the large arrays. In the CDFs of singular value spreads shown in Fig. 9, the ULA again performs very close to i.i.d. Rayleigh channels. The UCA has a significant improvement as compared to the two previous scenarios: the median of the singular value spread reduces to below 5 dB when using 128 antennas. Singular value spreads in the measured

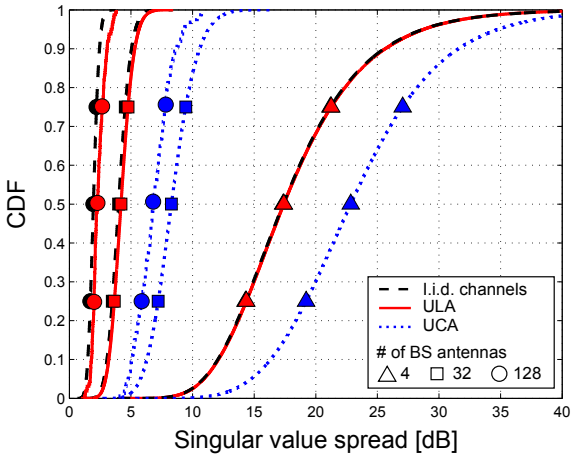

Figure 7: CDFs of singular value spreads when using 4, 32 and 128 antennas, in the scenario where four users are closely located at MS 7, with NLOS to the base station antenna arrays.

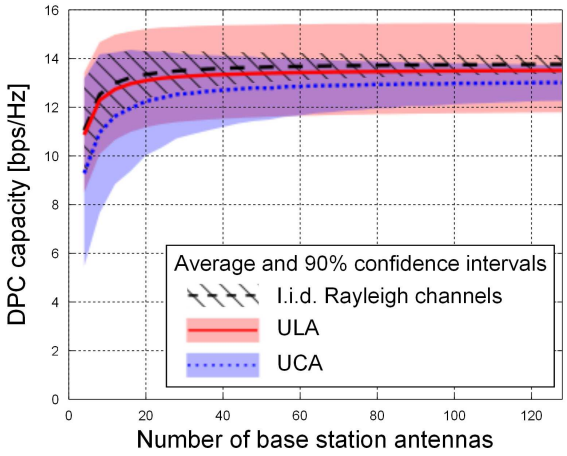

Figure 8: Sum-rate capacity in the downlink, achieved by DPC, in the scenario where the four users are close to each other at MS 7, with NLOS to the base station antenna arrays.

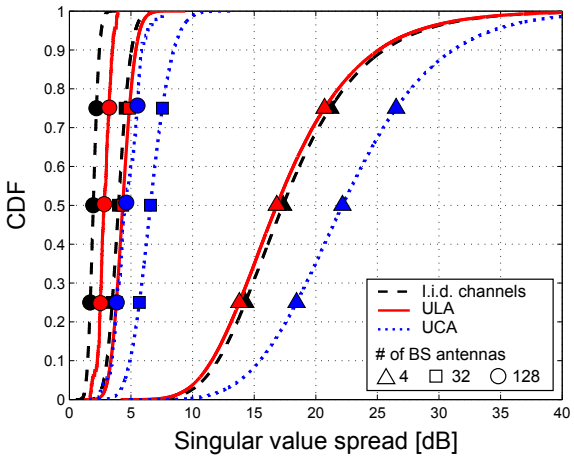

Figure 9: CDFs of singular value spreads when using 4, 32 and 128 antennas, in the scenario where four users are well separated at MS 1-4, respectively, with LOS characteristics.

channels again become quite stable when using a large number of antennas.

As can be seen in Fig. 10, both the ULA and the UCA perform very close to that of the asymptotic capacity achieved in i.i.d. Rayleigh channels, when having more than 40 antennas. The UCA shows slightly lower performance than the ULA.

Throughout the three scenarios discussed above and whose performances are shown in Fig. 5 - Fig. 10, we observe that the ULA performs better than the UCA. Due to its large aperture, the ULA experiences more spatial variations in the channels over the array, which provide better distinction between user channels and thus better spatial separation. In other words, the ULA has a very high angular resolution, which helps it resolve scatterers better than the compact UCA. The small aperture of the UCA and its patch antennas facing different directions make it difficult to resolve scatterers at similar azimuth angles, which is usually the case when users are located close to each other. When users are well distributed around the base station, the UCA can separate scatterers at different azimuth angles, and achieves better performance.

For the DPC capacities, we focused on averages in the previous discussions. Now we turn our attention to the variations over frequencies and random antenna selections. Comparing with i.i.d. Rayleigh channels, we notice that capacity variations in measured channels are much larger, and decrease much

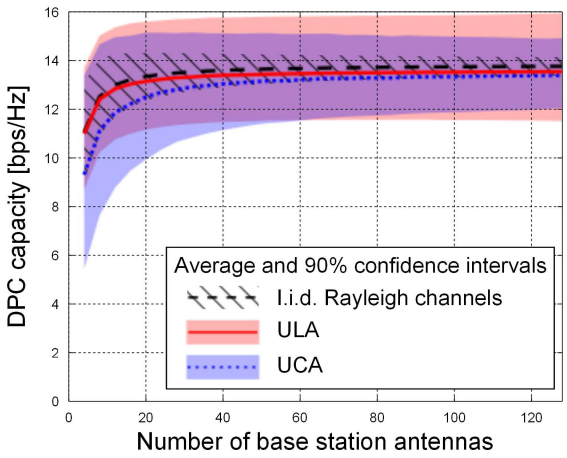

Figure 10: Sum-rate capacity in the downlink, achieved by DPC, in the scenario where the four users are well separated at MS 1-4, respectively, with LOS characteristics.

slower as the number of antennas increases. This is due to larger power variations over antenna elements and over frequencies in the measured channels. For the ULA, power variation over antenna elements is due to large-scale/shadow fading experienced across the array, as reported in [9,10], while for the UCA, it is mainly due to its circular structure with directional patch antennas oriented differently. With omni-directional antenna elements, the ULA has larger power variations over the measured bandwidth, as compared to the UCA with directional antenna elements. This gives the ULA larger capacity variations than the UCA, especially in the case of 128 antennas when the capacity variations are only across frequencies. Note that although the average capacity increases with the number of antennas, for some antenna selections a small number of antennas can perform better than a larger number of antennas. This can be observed from the upper part of the 90% confidence intervals of the UCA in Fig. 8. This is because in our signal model we reduce the transmit power with increasing number of antennas, while some antennas contribute more to the capacity than the others. It implies that we may gain by selecting the "right" antennas, as discussed in [13].

In all three scenarios with four users and the ULA, as few as 20 antennas gives very competitive performance, while slightly higher numbers are required for the UCA. However, when using more practical precoding schemes, such as zero-forcing (ZF) and matched-filtering (MF) precoding, sum-rate converges

slower, which means that more antennas are needed to achieve the required performance. This is shown in [5] and [11]. More antennas are also needed, if we want to serve more users in the same time-frequency resource.

5.2 Sixteen Users ($K = 16$)

While only four users are supported in LTE MU-MIMO, with more than one hundred antennas at the base station, massive MIMO can potentially serve many more users simultaneously. Here we increase the number of users to sixteen ($K = 16$), and again investigate singular value spreads and achieved sum-rate capacities. Due to limited number of measurement positions with the ULA, we concentrate on the UCA. In the two scenarios with co-located users, we simply increase the number of users from 4 to 16, and the inter-spacing between users is about 0.5 m. In the scenario where users are located far from each other, we select two users from each of the sites MS 1-8, with an inter-spacing larger than 10 m. Doing so, eight users have LOS conditions while the other eight have NLOS.

CDFs of singular value spreads in the three scenarios are shown in Fig. 11 - Fig. 13. In both measured channels and i.i.d. Rayleigh channels, singular value spreads are larger than those in the four user cases. This indicates, as expected, that with more users it is more difficult to spatially separate their signals. In the scenario where sixteen users are co-located with LOS, as shown in Fig. 11, singular value spreads are much larger than those in i.i.d. Rayleigh channels. The situation improves significantly in the NLOS scenario, as shown in Fig. 12. The gap in singular value spreads between measured and i.i.d. Rayleigh channels becomes smaller, which again indicates that NLOS with rich scattering provides more "favorable" propagation for the spatial separation of user signals, even when they are located close to each other. When sixteen users are located far from each other, the CDF curves of singular value spreads in the measured channels are closer to the ones for i.i.d. Rayleigh channels, as shown in Fig. 13. This implies that spatial separation of user signals improves even more. In all three scenarios, despite larger singular value spreads in the measured channels, trends similar to those for i.i.d. Rayleigh channels can be observed. The singular value spread becomes smaller and much more stable, as the number of base station antennas increases.

DPC capacities in the three scenarios are shown in Fig. 14. With sixteen users, asymptotic capacity given in (7) is $16 \log_2(1+10) = 55.4$ bps/Hz. Average performance in i.i.d. Rayleigh channels gets closer and closer to this asymptotic capacity, as the number of antennas increases. Performance in the measured channels is, however, significantly lower. Despite this, in the worst case where sixteen users are co-located with LOS, the average performance reaches about

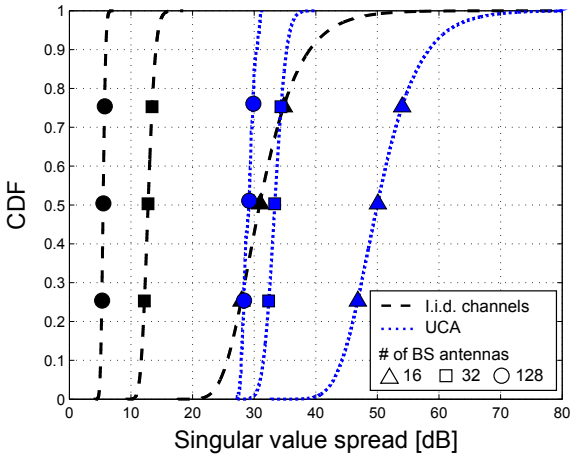

Figure 11: CDFs of singular value spreads when using 16, 32 and 128 antennas, in the scenario where sixteen users are closely located at MS 2, all with LOS to the UCA.

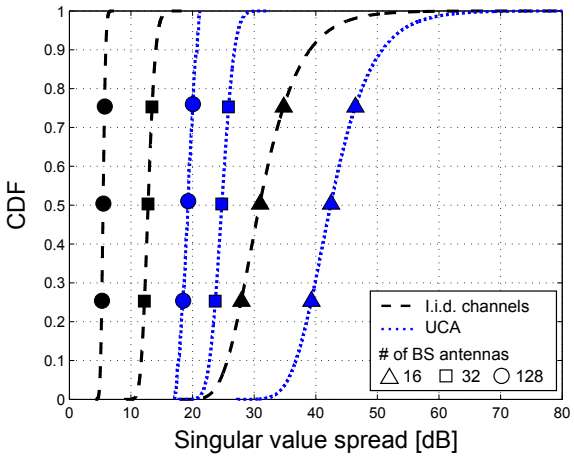

Figure 12: CDFs of singular value spreads when using 16, 32 and 128 antennas, in the scenario where sixteen users are located close to each other at MS 7, all with NLOS to the UCA.

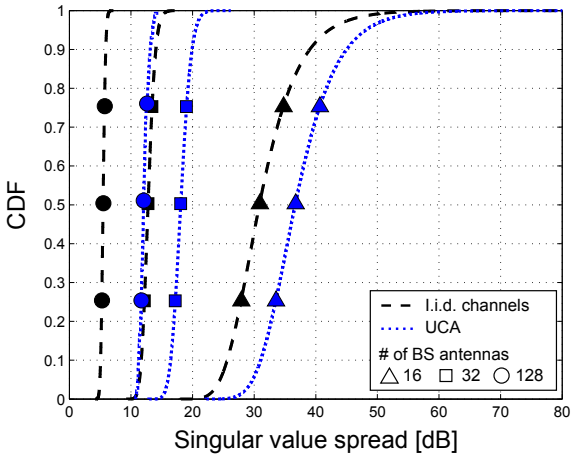

Figure 13: CDFs of singular value spreads when using 16, 32 and 128 antennas, in the scenario where sixteen users are located far from each other at MS 1-8, among which eight have LOS conditions and eight have NLOS to the UCA.

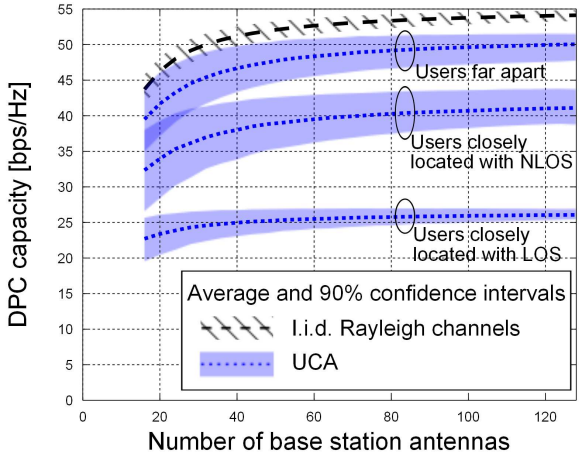

Figure 14: Sum-rate capacity in the downlink, achieved by DPC, in the scenario where sixteen users are located close to each other at MS 2 with LOS, MS 7 with NLOS, and are far from each other at MS 1-8, respectively.

50% of the asymptotic capacity when all 128 antennas are used, i.e., 8 times the number of users. The situations in the other two scenarios are better. With 128 antennas, the UCA performs at 75% and 90% of the asymptotic capacity, when sixteen users are co-located with NLOS and are far apart, respectively.

With more users and equal number of base station antennas, spatial separation becomes more difficult, but with the UCA we still obtain a large fraction of the i.i.d. Rayleigh performance, especially in NLOS conditions with rich scattering and when users are far apart. Although we lack measurement data for sixteen users with the ULA, we can expect that the ULA would provide better spatial separation also in this case, especially for co-located users, due to its higher angular resolution.

6 Summary and Conclusions

The presented investigation shows that in the studied real propagation environments we have characteristics that allow for efficient use of massive MIMO: the advantages of this new technology, as predicted by theory, can also be obtained in real channels. Based on channel measurements, using one practical UCA and one virtual ULA, both having 128 elements, we have illustrated the channel behavior of massive MIMO in three representative propagation scenarios and discussed corresponding singular value spreads and achieved sum-rate capacities.

In all scenarios, the singular value spread decreases considerably, and becomes more stable around a smaller value over the measured bandwidth, when using a large number of antennas. This indicates that massive MIMO provides better orthogonality between channels to different users and better channel stability than conventional MIMO. In the most difficult situation studied, i.e., closely located users with strong LOS to the base station, the singular value spread is significantly larger than that in i.i.d. Rayleigh channels, which indicates worse user orthogonality in the measured channels. Despite this gap, a large fraction of the asymptotic capacity achieved in i.i.d. Rayleigh channels can still be harvested in the measured channels. In the other studied scenarios, NLOS conditions with rich scattering provide more "favorable" propagation and allow better spatial separation of the users, even though they are closely located, while well distributed users also help to improve the performance. In the scenarios where users are in NLOS or in LOS but located far from each other, the measured channels with the ULA and the UCA achieve performance close to that in i.i.d. Rayleigh channels.

References

[1] D. Gesbert, M. Kountouris, R. W. Heath, C.-B. Chae, and T. Salzer, "Shifting the MIMO paradigm," *IEEE Signal Processing Magazine*, vol. 24, no. 5, pp. 36–46, Sept. 2007.

[2] "Requirements for further advancements for evolved universal terrestrial radio access (E-UTRA) (LTE-Advanced)," 3GPP TR 36.913 V8.0.1, Mar. 2009.

[3] T. L. Marzetta, "Noncooperative cellular wireless with unlimited numbers of base station antennas," *IEEE Transactions on Wireless Communications*, vol. 9, no. 11, pp. 3590–3600, Nov. 2010.

[4] F. Rusek, D. Persson, B. K. Lau, E. G. Larsson, T. L. Marzetta, O. Edfors, and F. Tufvesson, "Scaling up MIMO: Opportunities and challenges with very large arrays," *IEEE Signal Processing Magazine*, vol. 30, no. 1, pp. 40–60, Jan. 2013.

[5] E. Larsson, O. Edfors, F. Tufvesson, and T. L. Marzetta, "Massive MIMO for next generation wireless systems," *IEEE Communications Magazine*, vol. 52, no. 2, pp. 186–195, Feb. 2014.

[6] H. Q. Ngo, E. G. Larsson, and T. L. Marzetta, "Energy and spectral efficiency of very large multiuser MIMO systems," *IEEE Transactions on Communications*, vol. 61, no. 4, pp. 1436–1449, Apr. 2013.

[7] ——, "Aspects of favorable propagation in massive MIMO," in *Proc. European Signal Processing Conference (EUSIPCO)*, Sept. 2014.

[8] X. Gao, O. Edfors, F. Rusek, and F. Tufvesson, "Linear pre-coding performance in measured very-large MIMO channels," in *Proc. IEEE Vehicular Technology Conference (VTC Fall)*, Sept. 2011.

[9] S. Payami and F. Tufvesson, "Channel measurements and analysis for very large array systems at 2.6 GHz," in *Proc. European Conference on Antennas and Propagation (EuCAP)*, Mar. 2012.

[10] X. Gao, F. Tufvesson, O. Edfors, and F. Rusek, "Channel behavior for very-large MIMO systems – initial characterization," in *COST IC1004*, Sept. 2012.

[11] ——, "Measured propagation characteristics for very-large MIMO at 2.6 GHz," in *Proc. Asilomar Conference on Signals, Systems, and Computers (ASILOMAR)*, Nov. 2012.

[12] J. Hoydis, C. Hoek, T. Wild, and S. ten Brink, "Channel measurements for large antenna arrays," in *Proc. International Symposium on Wireless Communication Systems (ISWCS)*, Aug. 2012.

[13] X. Gao, O. Edfors, J. Liu, and F. Tufvesson, "Antenna selection in measured massive MIMO channels using convex optimization," in *Proc. IEEE Global Communications Conference (GLOBECOM) Workshop on Emerging Technologies for LTE-Advanced and Beyond-4G*, Dec. 2013.

[14] A. A. Glazunov, S. Prasad, and P. Handel, "Experimental characterization of the propagation channel along a very large virtual array in a reverberation chamber," *Progress In Electromagnetics Research B*, vol. 59, pp. 205–217, 2014.

[15] P. S. Taluja and B. L. Hughes, "Diversity limits of compact broadband multi-antenna systems," *IEEE Journal on Selected Areas in Communications*, vol. 31, no. 2, pp. 326–337, Feb. 2013.

[16] X. Artiga, B. Devillers, and J. Perruisseau-Carrier, "Mutual coupling effects in multi-user massive MIMO base stations," in *Proc. IEEE Antennas and Propagation Society International Symposium (APSURSI)*, July 2012.

[17] O. Işik, "Planar and cylindrical microstrip array antennas for mimo channel sounder applications," Master Thesis, Chalmers University of Technology, 2004.

[18] X. Liu and M. E. Bialkowski, "Effect of antenna mutual coupling on MIMO channel estimation and capacity," *International Journal of Antennas and Propagation*, vol. 2010, 2010, article ID 306173.

[19] D. Greenwood and L. Hanzo, *Characterisation of Mobile Radio Channels: 2nd.* John Wiley & Sons, 1999, ch. 2, pp. 91–185.

[20] A. Molisch, *Wireless Communications.* Wiley-IEEE Press, 2005.

[21] D. Gesbert, M. Shafi, D. shan Shiu, P. J. Smith, and A. Naguib, "From theory to practice: an overview of MIMO space-time coded wireless systems," *IEEE Journal on Selected Areas in Communications*, vol. 21, no. 3, pp. 281–302, Apr. 2003.

[22] A. Paulraj, R. Nabar, and D. Gore, *Introduction to Space-Time Wireless Communications.* Cambridge University Press, 2003.

[23] H. Artes, D. Seethaler, and F. Hlawatsch, "Efficient detection algorithms for MIMO channels: a geometrical approach to approximate ML detection," *IEEE Transactions on Signal Processing*, vol. 51, no. 11, pp. 2808–2820, Nov. 2003.

[24] J. Maurer, G. Matz, and D. Seethaler, "Low-complexity and full-diversity MIMO detection based on condition number thresholding," in *Proc. IEEE International Conference on Acoustics, Speech and Signal Processing (ICASSP)*, Apr. 2007.

[25] S. Mohammed, E. Viterbo, Y. Hong, and A. Chockalingam, "MIMO precoding with X- and Y-codes," *IEEE Transactions on Information Theory*, vol. 57, no. 6, pp. 3542–3566, June 2011.

[26] S. Vishwanath, N. Jindal, and A. Goldsmith, "Duality, achievable rates, and sum-rate capacity of Gaussian MIMO broadcast channels," *IEEE Transactions on Information Theory*, vol. 49, no. 10, pp. 2658–2668, Oct. 2003.

[27] M. Costa, "Writing on dirty paper," *IEEE Transactions on Information Theory*, vol. 29, no. 3, pp. 439–441, 1983.

[28] N. Jindal, W. Rhee, S. Vishwanath, S. A. Jafar, and A. Goldsmith, "Sum power iterative water-filling for multi-antenna Gaussian broadcast channels," *IEEE Transactions on Information Theory*, vol. 51, no. 4, pp. 1570–1580, Apr. 2005.

[29] X. Gao, F. Tufvesson, and O. Edfors, "Massive MIMO channels – measurements and models," in *Proc. Asilomar Conference on Signals, Systems, and Computers (ASILOMAR)*, Nov. 2013.

[30] K. Zheng, S. Ou, and X. Yin, "Massive MIMO channel models: A survey," *International Journal of Antennas and Propagation*, vol. 2014, 2014, article ID 848071.

[31] B. H. Fleury, M. Tschudin, R. Heddergott, D. Dahlhaus, and K. Ingeman Pedersen, "Channel parameter estimation in mobile radio environments using the SAGE algorithm," *IEEE Journal on Selected Areas in Communications*, vol. 17, no. 3, pp. 434–450, Mar. 1999.

[32] A. Manikas and C. Proukakis, "Modeling and estimation of ambiguities in linear arrays," *IEEE Transactions on Signal Processing*, vol. 46, no. 8, pp. 2166–2179, Aug. 1998.

Paper III

Spatial Separation of Closely-Spaced Users in Measured Massive Multi-User MIMO Channels

Fully-synchronous measurements of a massive multi-user multiple-input multiple-output (MU-MIMO) radio propagation channel are presented. We evaluate the ability of a massive MIMO system to spatially separate users located close to each other in line-of-sight (LOS) propagation conditions. The system consists of a base-station (BS) antenna array equipped with 64 dual-polarized antenna elements (128 ports) arranged in a cylindrical configuration, and eight single-antenna users. The users are confined to a five-meter diameter circle and move randomly at pedestrian speeds. The BS antenna array is located on top of a 20 m tall building and has LOS to the users. We examine user separability by studying singular value spread of the MU-MIMO channel matrix for several subsets of BS antenna array ports, along with sum-rate capacity and achievable sum-rates with both zero-forcing and matched-filtering linear precoders. We also analyze the performance of the user with the lowest rate. Finally, a comparison between the performance offered by the massive MIMO system and that of a conventional MU-MIMO system is provided. To the best of our knowledge, this is the first report of fully-synchronous dynamic measurements of a massive MIMO system. Our investigation shows that even users located close to each other in LOS propagation conditions can be spatially separated in a massive MIMO system.

Jose Flordelis, Xiang Gao, Ghassan Dahman, Fredrik Rusek, Ove Edfors and Fredrik Tufvesson,
"Spatial Separation of Closely-Spaced Users in Measured Massive Multi-User MIMO Channels,"
in *Proc. IEEE International Conference on Communications (ICC)*, June 2015.

1 Introduction

Massive MIMO is an emerging communication technology promising order-of-magnitude improvements in data throughput, link reliability, range, and transmit-energy efficiency [1–4]. These benefits arise from leveraging additional degrees of freedom provided by an excess of antenna elements at the BS side. A typical massive MIMO system can consist of one or more BSs equipped with many, say, $M = 100$, antenna elements serving K single-antenna users in the same time-frequency resource. K is in the order of 10 to 20 users, possibly more. Due to its potential to greatly increase spectral efficiency compared to today's systems, massive MIMO is considered as one of the main directions towards future 5G communication systems [5–7].

A key assumption when addressing massive MIMO systems is so-called *favorable* propagation conditions, meaning that propagation channels to different users are nearly orthogonal. Under this assumption, the scaled Gram matrix $\boldsymbol{G} = \boldsymbol{H}\boldsymbol{H}^H/M$, where $\boldsymbol{H}$ is the channel matrix, approaches a diagonal matrix as M goes to infinity. Hence, linear precoding and detection schemes such as zero-forcing (ZF) and matched-filtering (MF) become nearly optimal [1, 2, 8]. Nevertheless, in real propagation channels and with practical setups, the off-diagonal entries of $\boldsymbol{G}$ typically have non-zero values. User separation based on spatial channel properties is particularly difficult in situations where the users are located close to each other and experience LOS propagation conditions to the BS antenna array.

Several measurement campaigns have been conducted to study the performance of massive MIMO in real propagation environments. In [9–11], we reported outdoor massive MIMO channel measurements at 2.6 GHz with a linear array and a cylindrical array, both having 128 antenna elements. The investigations concluded that real propagation channels allow effective use of massive MIMO technology in the sense that a large fraction of the sum-rate capacity of MIMO channels with independent and identically distributed (i.i.d.) Rayleigh fading can be achieved in real propagation channels: as the number of BS antenna elements increases, the orthogonality among users' channels increases, and linear precoding schemes achieve a performance close to that of dirty-paper coding (DPC) [12]. This is also shown in [8] for indoor BS measurements. In [13] massive MIMO channel measurements using a scalable antenna array consisting of up to 112 elements were reported. The results in [13] further support the conclusions drawn in [8, 10, 11], that theoretical gains of massive MIMO can be achieved in practice. Altogether, the combined set of published experimental results on massive MIMO elevates it from a mere theoretical concept to a practical technology.

Here we present a new massive MIMO channel measurement campaign at

2.6 GHz. Similar to [8] and [11] we use a cylindrical array with 128 ports, although the presented campaign differs from those previously reported in two important ways:

- Instead of having virtual users, i.e., choosing users from different measurement positions, as in [8–11], we have fully-synchronous dynamic measurements to multiple users. This means that the channels from all users to the BS antenna array are measured simultaneously, and we can capture joint statistical properties of the multi-user channels and their evolution in time, i.e., the dynamics of the system. To the best of our knowledge, this is the first paper reporting such measurements for a massive MIMO system.
- With the obtained measurement data, we focus on investigating the spatial separation of closely-spaced users in LOS, which is a particularly difficult situation for conventional MIMO. For massive MIMO, it is expected that with a large-enough number of antenna elements at the BS, spatial multiplexing of closely-spaced users is possible. Our study is relevant to the scenario of outdoor live concerts or sports events, where user density can be relatively high.

2 Measurement Description

2.1 Measurement Setup

The measurement campaign was performed using a 128-port cylindrical array at the BS side, shown in Fig. 1, with 16 dual-polarized patch antenna elements in each circle and 4 such circles stacked on top of each other. The spacing of adjacent elements is half a wavelength at 2.6 GHz. At the user side, we use eight vertically-polarized omni-directional antennas[6], acting as eight simultaneous users. The eight antennas are connected through optical fibers to the transmit side of the RUSK LUND MIMO channel sounder [14].

Measurements were recorded using a center frequency of 2.6 GHz and 40 MHz bandwith. Each measurement took 17 seconds, and 300 snapshots were recorded during this time. The sounding signals were transmitted with 0.5 W output power. Values of the average measurement signal-to-noise ratio (SNR) between 14 dB to 16 dB have been estimated.

[6]The antennas, of type SkyCross SMT-2TO6MB-A, are omni-directional in azimuth when measured without users. The radiation pattern including the users is more complex and is dependent on the exact position of antenna and users.

Figure 1: (a) The cylindrical array with 128 ports. (b) View from site MS 2.

Figure 2: (a) A user holding the user equipment antenna with an inclination of 45°. (b) Users moving randomly within the five-meter diameter circle.

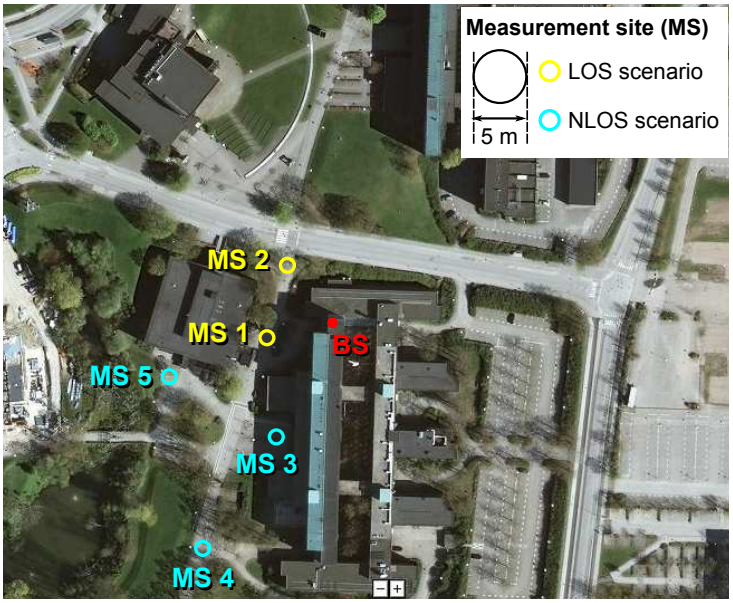

Figure 3: Overwiew of the measurement area.

2.2 Measurement Environment

The measurements were carried out outside the main entrace of the E-building of the Faculty of Engineering (LTH), Lund University, Lund, Sweden (55.711510 N, 13.210405 E). The cylindrical array at the BS side was placed on the roof of the E-building, as shown in Fig. 1. At the user side several sites were measured. MS 1 and 2 have LOS conditions to the BS array, while MS 3–5 have NLOS conditions[7] (see Fig. 3). At each site, we have a circle with a five-meter diameter and eight users moving inside it, representing a situation of high user density. During the measurements, the users were holding the antennas inclining them at about 45 degrees, so that we have both vertical and horizontal polarizations at the user side. The eight users were moving randomly at pedestrian speeds around 0.5 m/s, inside the 5 m circle. Note that, since the users were allowed to turn around, the LOS component to the BS can be blocked in some snapshots, by the user holding the antenna or by other users (see Fig. 2).

[7]In this work we are only concerned with sites in LOS, i.e. MS 1 and MS 2.

3 Signal Model

For the analysis, we consider the downlink of a single-cell MU-MIMO system. The system consists of K single-antenna users and a BS equipped with M antenna ports ($K \leq M$). Orthogonal frequency division multiplexing (OFDM) with L subcarriers is assumed. Let $\boldsymbol{s}_{\ell,n}$ be the $M \times 1$ vector signal transmitted by the BS at subcarrier ℓ and snapshot n, with $1 \leq l \leq L$ and $1 \leq n \leq N$. The composite received signal $\boldsymbol{y}_{\ell,n}$ can be written as

$$\boldsymbol{y}_{\ell,n} = \boldsymbol{H}_{\ell,n}\boldsymbol{s}_{\ell,n} + \boldsymbol{w}_{\ell,n}, \tag{1}$$

where $\boldsymbol{w}_{\ell,n}$ is the $K \times 1$ vector of the receiver noise with independent components distributed as $\mathcal{CN}(0,1)$, and $\boldsymbol{H}_{\ell,n} \in \mathbb{C}^{K \times M}$ is the narrow-band channel matrix of the radio propagation channel, satisfying $\mathbb{E}\{\|\boldsymbol{h}_{k,\ell,n}\|_{\mathrm{F}}^2\} = M$ where $\boldsymbol{h}_{k,\ell,n}$ is the kth row of $\boldsymbol{H}_{\ell,n}$. Furthermore, the transmit vector $\boldsymbol{s}_{\ell,n}$ has a covariance matrix satisfying the power constraint

$$\mathbb{E}\{\boldsymbol{s}_{\ell,n}^{\mathrm{H}}\boldsymbol{s}_{\ell,n}\} = P. \tag{2}$$

With these conventions, the mean received power per user in the MISO case with maximum ratio transmission (MRT) becomes $P\frac{M}{K}$, yielding a channel capacity

$$C_{\mathrm{MISO}} = \log_2\left(1 + P\frac{M}{K}\right). \tag{3}$$

In this work, we choose to harvest the array gain as reduced transmit power. Therefore, the total transmit power P is scaled according to

$$P = \rho\frac{K}{M}. \tag{4}$$

In this way, the mean SNR per user in the MISO case with MRT remains constant at some target level ρ.

3.1 Normalization

In order to compensate for gain imbalances across different MISO links, arising, e.g., from differences in the electronic components used in the measurement setup, channel normalization is applied. The normalization is such that the average energy of the user channels, when taken over all $L = 257$ subcarriers and $N = 300$ measurement snapshots, is equal to 128. This normalization can be obtained by defining

$$\boldsymbol{h}_{k,\ell,n}^{\mathrm{norm}} = \sqrt{\frac{128LN}{\sum_{n=1}^{N}\sum_{l=1}^{L}\left\|\boldsymbol{h}_{k,\ell,n}^{\mathrm{meas}}\right\|_{\mathrm{F}}^2}}\,\boldsymbol{h}_{k,\ell,n}^{\mathrm{meas}}, \tag{5}$$

where $\boldsymbol{h}_{k,\ell,n}^{\text{norm}}$ is the kth normalized MISO channel, i.e., the kth row of the normalized MU-MIMO channel matrix $\boldsymbol{H}_{\ell,n}^{\text{norm}}$, and $\boldsymbol{h}_{k,\ell,n}^{\text{meas}}$ represents the *measured* MISO channel from the BS antenna array to the kth user. With the normalization proposed, imbalances in the channel gain of different users are removed, while energy variations over BS antenna elements, subcarriers and measurement times are retained. In particular, the distance-dependent path loss of the radio propagation channel is removed, whereas the effects of small-scale and large-scale fading remain. The sub-indices ℓ and n will be dropped in the rest of the discussion. This will not cause any problem since, from this point on, all processing is done per time-frequency resource.

3.2 Antenna Array Size Reduction

The effect of the number of antenna elements M at the BS antenna array is a topic of interest for the design and implementation of practical massive MIMO systems. Thus, the 8×128 MU-MIMO channel matrices obtained from the measurements at different sites can be downsampled to a suitable size, $8 \times M$, and the influence of the parameter M can be investigated. Let $8 \leq M \leq 128$ be the reduced number of antenna elements at the BS antenna array, and $\pi_M = \{p(1), \ldots, p(M)\}$, with $1 \leq p(1) < \ldots < p(M) \leq M$, a set of indices selecting M antenna elements from a total of 128. Then, the normalized and π_M-reduced channel matrix $\boldsymbol{H}^{\text{norm},\pi_M}$ is obtained from

$$\boldsymbol{h}_k^{(\text{col) norm},\pi_M} = \boldsymbol{h}_{p(k)}^{(\text{col) norm}}, \tag{6}$$

where $\boldsymbol{h}_k^{(\text{col) norm},\pi_M}$ and $\boldsymbol{h}_i^{(\text{col) norm}}$ are the kth and ith columns of $\boldsymbol{H}^{\text{norm},\pi_M}$ and $\boldsymbol{H}^{\text{norm}}$, respectively.

The antenna elements of the sub-arrays have been selected in the following way: i) for $M = 128$, all antenna patches are used; ii) for $M = 64$, 8 evenly spaced antenna patches are chosen from each antenna ring, with the antenna patches in two adjacent antenna rings staggered by one element; iii) for $M = 32$, the antenna patches of the two middle rings for the case of $M = 64$ are chosen; iv) for $M = 16$, the antenna patches of the lower ring for the case of $M = 32$ are chosen; v) for $M = 8$, the four adjacent antenna patches pointing northwest in the same ring as for the case of $M = 16$ are chosen. In all cases, both ports from each selected antenna patch are used. With this choice, the sub-arrays for the cases of $M = 128, 64, 32$ and 16 are approximately isotropic, while the sub-array for the case of $M = 8$ shows a directional gain of 0.6 dB and 3.8 dB for sites MS 1 and MS 2, respectively. The case $M = 8$ resembles a conventional 8×8 MU-MIMO deployment and, hence, will serve as a baseline for evaluating the performance of massive MIMO.

3.3 Singular Value Spread

In this section we introduce the singular value spread of the channel matrix $\boldsymbol{H}$ as a measure of the degree of orthogonality among the users. The channel matrix $\boldsymbol{H}$ has a singular value decompostion

$$\boldsymbol{H} = \boldsymbol{U}\boldsymbol{\Sigma}\boldsymbol{V}^{\mathrm{H}}, \tag{7}$$

where $\boldsymbol{U} \in \mathbb{C}^{K\times K}$ and $\boldsymbol{V} \in \mathbb{C}^{M\times M}$ are unitary matrices and $\boldsymbol{\Sigma} \in \mathbb{C}^{K\times M}$ is a diagonal matrix containing the ordered singular values of the channel, $\sigma_1 \geq \ldots \geq \sigma_K \geq 0$. The singular value spread κ (*a.k.a.* condition number) is then defined as the ratio between the largest and the smallest singular values, as given by

$$\kappa = \frac{\sigma_1}{\sigma_K}. \tag{8}$$

It follows that $1 \leq \kappa \leq \infty$. Values of κ close to 1 indicate nearly full user orthogonality while, under the assumption (5), large values of κ imply a strong linear dependency of, at least, two of the rows in $\boldsymbol{H}$ and, thereupon, a relative difficulty in the spatial separation of the corresponding users.

3.4 Dirty-Paper Coding Capacity

The singular value spread is not very informative when it takes large values. For example, consider a radio propagation environment in which the transmit signals from the BS antenna array to two of the users, say user 1 and user 2, reach those users through certain common propagation paths. This situation may lead to almost parallel MISO channels $\boldsymbol{h}_1$ and $\boldsymbol{h}_2$ and, as a result, to large singular value spreads. However, the BS antenna array might nonetheless be able to separate the channels of the remaining users. Hence, multiplexing several data streams on the same time-frequency resource is possible even when the singular value spread is large. In this section, the sum-rate capacity of the MU-MIMO downlink channel is introduced as a second measure of the performance of the massive MIMO system.

The sum-rate capacity of the narrow-band MU-MIMO downlink channel with full channel state information (CSI) at the BS is given by [15]

$$\begin{aligned} C_{\mathrm{DPC}} &= \max_{\{\gamma_k\}} \log_2 \det\left(\boldsymbol{I}_M + \boldsymbol{H}^{\mathrm{H}}\boldsymbol{D}\boldsymbol{H}\right) \\ \text{subject to} \quad & \sum_{k=1}^{K} \gamma_k = P, \quad \gamma_k \geq 0, \quad \forall k, \end{aligned} \tag{9}$$

with $\boldsymbol{D} = \mathrm{diag}(\gamma_1, \ldots, \gamma_K)$ and P the total transmit power (2). Problem (9) is a convex problem and can be efficiently solved, for instance, by means of the sum-power iterative waterfilling algorithm described in [16].

3.5 Linear Precoding

The sum-rate capacity of the narrow-band MU-MIMO downlink channel can be achieved by dirty-paper coding (DPC) [12]. However, the high computational complexity of DPC renders it impractical even for a low number of users. As an alternative to DPC, we consider linear precoding schemes of the form

$$\boldsymbol{s} = \boldsymbol{W}\boldsymbol{x}, \tag{10}$$

where $\boldsymbol{W} \in \mathbb{C}^{M \times K}$ is the precoding matrix and $\boldsymbol{x}$ is the $K \times 1$ vector containing the user data streams. We look at the performance of the popular zero-forcing and matched-filtering linear precoders [17]. The ith column of the ZF precoding matrix, $\boldsymbol{w}_{\mathrm{ZF},i}$, is given by

$$\boldsymbol{w}_{\mathrm{ZF},i} = \frac{\boldsymbol{h}_i^{(\dagger)}}{\sqrt{\left\|\boldsymbol{h}_i^{(\dagger)}\right\|_{\mathrm{F}}^2}}, \tag{11}$$

where $\boldsymbol{h}_i^{(\dagger)}$ is the ith column of $\boldsymbol{H}^{\mathrm{H}}(\boldsymbol{H}\boldsymbol{H}^{\mathrm{H}})^{-1}$, the pseudo-inverse of the channel matrix. The ith column of the MF precoding matrix, $\boldsymbol{w}_{\mathrm{MF},i}$, is given by

$$\boldsymbol{w}_{\mathrm{MF},i} = \frac{\boldsymbol{h}_i^{\mathrm{H}}}{\sqrt{\|\boldsymbol{h}_i\|_{\mathrm{F}}^2}}. \tag{12}$$

where $\boldsymbol{h}_i$ is the ith row of $\boldsymbol{H}$. Optimal allocation of transmit power to the user data streams in $\boldsymbol{x}$, subject to the sum-power constraint (2), has been performed by means of numerical methods. For the ZF precoder, the product $\boldsymbol{H}\boldsymbol{W}_{\mathrm{ZF}}$ is diagonal and optimal power allocation can be achieved by the standard water-filling algorithm [18]. The MF precoding case, however, constitutes a non-convex problem and the numerical methods used in the preparation of this work do not guarantee the optimality of the transmit power allocations obtained.

4 Performance Evaluation

In this section, we evaluate the ability of massive MIMO at separating users located close to each other in LOS propagation conditions, and compare it with

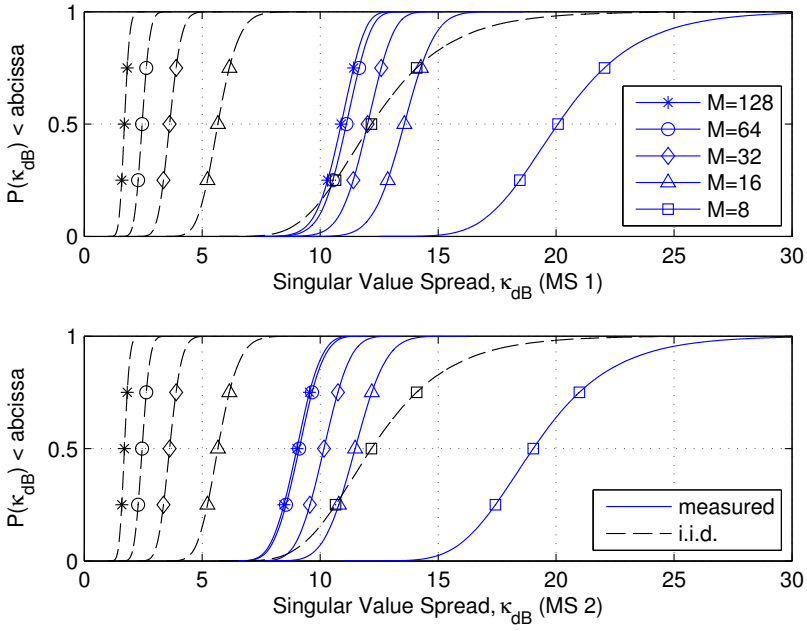

Figure 4: CDFs of the singular value spread in logarithmic units when using 128, 64, 32, 16 and 8 antenna elements at the BS. In this scenario, eight users are located close to each other within the area of a five-meter diameter circle and experience LOS to the BS antenna array. Plots are given for two different measurement sites, labeled as MS 1 (top) and MS 2 (bottom). For comparison purposes, CDFs of the singular value spread of i.i.d. Rayleigh channels with the same number of antenna elements are also given. Note that the legend is shared between both figures.

the performance of i.i.d. Rayleigh channels. First, we look at the singular value spread of the measured channels.

The cumulative distribution function (CDF) of the singular value spread in logarithmic units,

$$\kappa_{\mathrm{dB}} = 10 \log_{10} \frac{\sigma_1}{\sigma_K}, \tag{13}$$

when using 128, 64, 32, 16 and 8 antenna elements at the BS, can be seen in Fig. 4. CDFs of the singular value spreads of i.i.d. Rayleigh channels with the same number of transmit and receive antenna elements are also shown.

We can see from Fig. 4 that the measured user channels decorrelate as the number of antenna elements at the BS, M, increases. Furthermore, the slopes of the CDF curves become steeper with increasing values of M, demonstrating the hardening effect of the user channels. The median of the singular value spread for measured channels when using 128 antenna elements at the BS is 10.4 dB and 8.4 dB for sites MS 1 and MS 2, respectively. For both sites, the CDF of the singular value spreads for $M = 64$ is very similar to that of $M = 128$, while a moderate degradation by one to three dB is observed when M is reduced to 32 and 16. By contrast, the median of the singular value spread increases dramatically to 19.6 dB for site MS 1 and to 18.4 dB for site MS 2 when only 8 antenna elements are used at the BS — i.e. a 10 dB loss when comparing conventional MU-MIMO with massive MIMO; a similar increase of the variance is observed.

This information is summarized in Fig. 5, where the CDFs shown in Fig. 4 are represented as points in a coordinate system in which the abcissas correspond to the median of the distribution of the singular value spread, and the ordinates correspond to the inter-quartile range (IQR). In this representation, moving to the left (reduced median) and to the bottom of the figure (reduced IQR) means improved user orthogonality and channel hardening. We see that, for the case of $M = 128$, the median of the channel measured at site MS 1 lies in-between the median of i.i.d. Rayleigh channels with $M = 8$ and $M = 9$, whereas the IQR matches that of an i.i.d. Rayleigh channel with $M = 10$. Hence, one can say that, the measured 8×128 channel has an *effective* degree of orthogonality equivalent to an i.i.d. Rayleigh channel with M between 8 and 9, whereas its *effective* hardening corresponds to $M = 10$. In the same sense, for site MS 2, the behavior of the channel resembles that of an i.i.d. Rayleigh channel with 9–10 BS antenna elements, with a somewhat reduced dispersion ($M = 11$). The large gap between measured channels and synthetic i.i.d. channels can be partly explained by the cylindrical geometry of the BS antenna array: more than half of the antenna array elements cannot "see" the users at sites MS 1 and MS 2.

A further observation that we can make from Fig. 5 is that the improvement

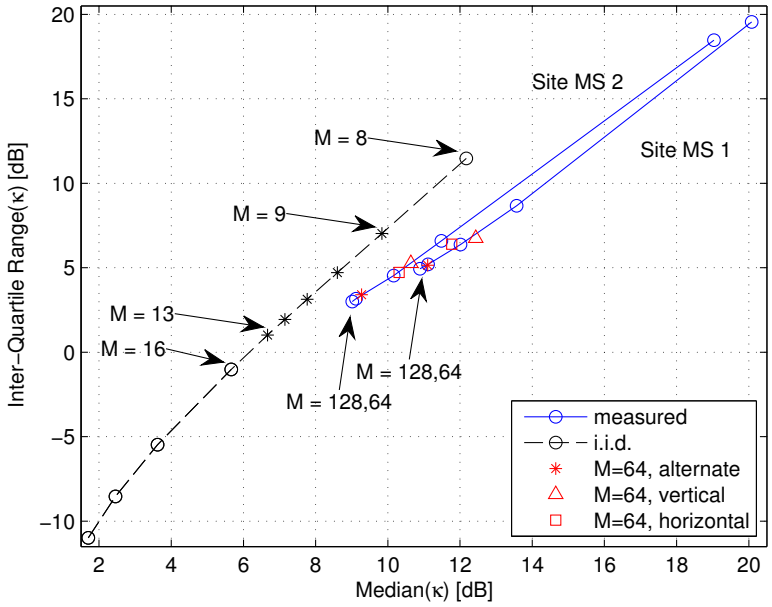

Figure 5: Median and inter-quartile range (IQR) of the singular value spread for the same cases as in Fig. 4. From left to right, circles represent the cases of $M = 128, 64, 32, 16$ and 8. For i.i.d. Rayleigh channels, dots are used to represent the cases $M = 13, 12, 11, 10$ and 9. Additionally, the medians and the IQRs for the cases of $M = 64$ and vertically-polarized antenna ports only (triangle), horizontally-polarized antenna ports only (square) and antenna ports including both polarizations (star) are also given.

in user channel orthogonality when increasing the number of antenna elements at the BS beyond 64 is marginal in comparison with that of i.i.d. Rayleigh channels. This fact might indicate that, for this specific scenario and array geometry, further gains in user spatial separation cannot be obtained by increasing the density of the spatial sampling at the BS. Rather, one must resort to dual-polarized antenna elements, as explained next. On top of the subsets of BS antenna elements thus far discussed, three extra BS antenna array subsets are considered: i) $M = 64$ with all elements vertically polarized, ii) $M = 64$ with all elements horizontally polarized, and iii) $M = 64$ with neighbour elements having alternate polarizations. With this choice, exactly one port from

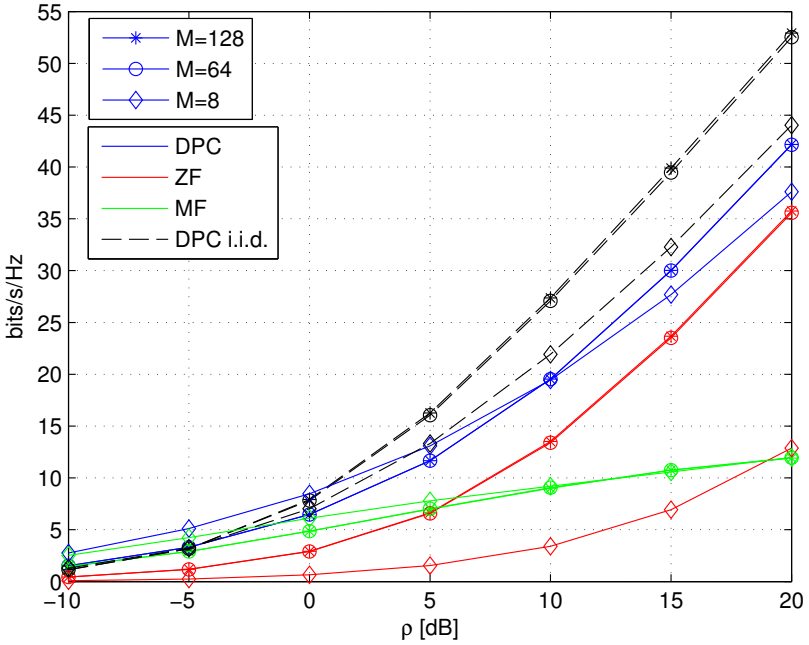

Figure 6: Ergodic sum-rate capacity at site MS 2 when using 128, 64 and 8 antenna elements at the BS. Transmit power reduction have been applied.

each of the 64 antenna patches of the BS array is selected, for all three subsets. The correponding median and IQR coordinates have been plotted in Fig 5. We see that, to fully extract the diversity offered by the environment, we need to use both vertically and horizontally polarized antenna elements. As a matter of fact (see Fig. 5), when only a single polarization is used the resulting system is roughly equivalent to one with 16 dual-polarized antenna patches ($M = 32$). In other words, if only one polarization mode is used, up to half of the antenna elements have a zero net contribution.

Let us now turn our attention to the sum-rates achievable through massive MIMO in the considered setup by linear precoding. The estimated ergodic sum-rate capacity and ergodic sum-rates for the ZF and MF precoders when using 128, 64 and 8 antenna elements at the BS are shown in Fig. 6 for several target values of ρ. Note that the cases $M = 32$ and $M = 16$ have been dropped since these values of M are not representative of typical massive MIMO deployments. We focus on the sum-rate results for site MS 2 (similar comments apply to site

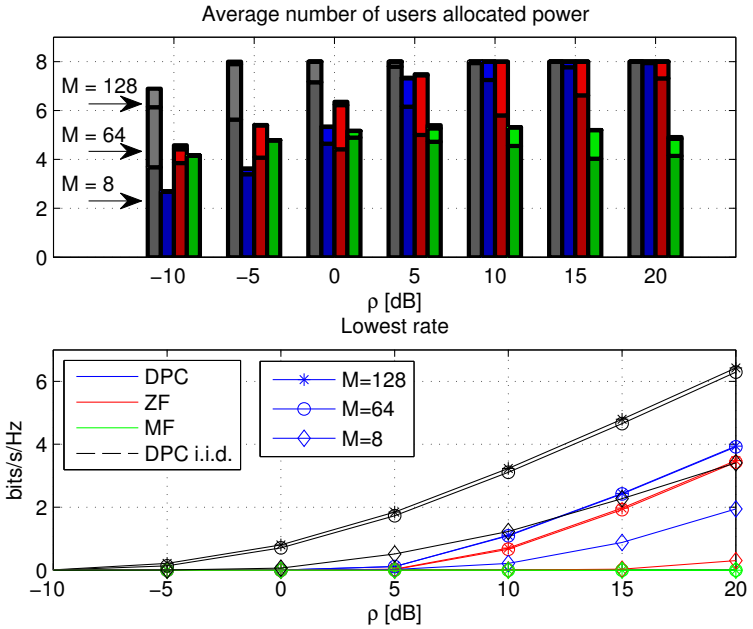

Figure 7: Average number of users allocated power (top) and lowest ergodic rate (bottom) at site MS 2 when using 128, 64 and 8 antenna elements at the BS. Transmit power reduction has been applied.

MS 1). Fig. 6 shows that, for moderate values of ρ, massive MIMO with ZF can achieve a large fraction of the DPC capacity. For instance, 69% of the DPC capacity (19.5 bits/s/Hz) is achieved when $\rho = 10$ dB, and this figure increases to 86% (of 42.2 bits/s/Hz) when $\rho = 20$ dB. On the other hand, the sum-rates achievable by the ZF precoder in a conventional 8×8 MU-MIMO setup fall much shorter: 18% and 34% (of 19.4 bits/s/Hz and 37.6 bits/s/Hz, respectively) for the same SNR points. It is important to recall that transmit power has been reduced as described in Sec. 3.2: In the case at hand, conventional 8×8 MU-MIMO radiates 38.4 times more power than massive MIMO with $M = 128$. If, rather, the massive MIMO array gain is leveraged to its full extent, an increase of the sum-rate capacity and ZF sum-rate by $K \log_2(\frac{M}{K})$ bits/s/Hz, i.e. 32 bits/s/Hz for $M = 128$, can be expected for moderate values of ρ and beyond.

Finally, we look into the issue of *fairness* in the allocation of the user data rates. As is known, maximizing the sum-rate might result in large imbalances in the data rates allocated to each of the users, with users experiencing advan-

Table 1: ZF sum-rate for site MS 2 (ρ=10 dB).

	$M=8$	$M=64$
Average number of users allocated power with ZF	6	8
Sum-rate shared among the users	3.4 bps/Hz	13.4 bps/Hz
Fraction of DPC capacity achieved	18%	69%
Total transmit power shared among the users	3.8 dB	-9.0 dB

tageous signal strength levels being allocated most of the available sum-rate, and users experiencing weak signal strengths being allocated little or no capacity. The top part of Fig. 7 shows the average number of users allocated power, i.e. the average number of users with $\gamma_k > 0$, at site MS 2 when using 128, 64 and 8 antenna elements at the BS, for DPC, ZF and MF. It can be seen that, with 8×64 massive MIMO and ZF, all 8 users are allocated power for values of $\rho = 10$ dB, or greater. By contrast, at the same SNR point, conventional 8×8 MU-MIMO with ZF allocates power to six users only. Hence, we see that massive MIMO can achieve higher sum-rates and, at the same time, schedule more users than conventional MU-MIMO. On the other hand, conventional MU-MIMO with MF offers a larger sum-rate (see Fig. 6) at the expense of a decrease in user fairness (five or less users scheduled). Additionally, the lowest user rate averaged over all time-frequency resources is shown at the bottom part of Fig. 7. As expected, the lowest user rate for the MF and ZF with conventional 8×8 MU-MIMO is (close to) zero bits/s/Hz.

5 Summary and Conclusions

Let us go back to the question that we tried to answer in this paper: Can massive MIMO spatially separate users that are confined to a circle with a five-meter diameter in LOS conditions? This question is not easy to give a satisfactory answer to, but in an effort to partly address it, we have conducted a measurement campaign which can be summarized as in Table 1.

In our view, we have demonstrated clear indications that massive MIMO indeed separates them, as, with massive MIMO, many more users can share a much larger sum-rate compared to the case of conventional MIMO. What is more, with massive MIMO, all users get a non-zero communication rate for reasonable SNR values when the sum-rate of the system is maximized. All in all, we think it is fair to say that the massive MIMO system is able to separate all the closely-located users.

References

[1] T. L. Marzetta, "Noncooperative cellular wireless with unlimited numbers of base station antennas," *IEEE Transactions on Wireless Communications*, vol. 9, no. 11, pp. 3590–3600, Nov. 2010.

[2] F. Rusek, D. Persson, B. K. Lau, E. G. Larsson, T. L. Marzetta, O. Edfors, and F. Tufvesson, "Scaling up MIMO: Opportunities and challenges with very large arrays," *IEEE Signal Processing Magazine*, vol. 30, no. 1, pp. 40–60, Jan. 2013.

[3] E. Larsson, O. Edfors, F. Tufvesson, and T. L. Marzetta, "Massive MIMO for next generation wireless systems," *IEEE Communications Magazine*, vol. 52, no. 2, pp. 186–195, Feb. 2014.

[4] H. Q. Ngo, E. G. Larsson, and T. L. Marzetta, "Energy and spectral efficiency of very large multiuser MIMO systems," *IEEE Transactions on Communications*, vol. 61, no. 4, pp. 1436–1449, Apr. 2013.

[5] J. G. Andrews, S. Buzzi, W. Choi, S. V. Hanly, A. Lozano, A. C. K. Soong, and J. C. Zhang, "What will 5G be?" *IEEE Journal on Selected Areas in Communications*, vol. 32, no. 6, pp. 1065–1082, June 2014.

[6] F. Boccardi, R. W. Heath, A. Lozano, T. L. Marzetta, and P. Popovski, "Five disruptive technology directions for 5G," *IEEE Communications Magazine*, vol. 52, no. 2, pp. 74–80, Feb. 2014.

[7] A. Osseiran, F. Boccardi, V. Braun, K. Kusume, P. Marsch, M. Maternia, O. Queseth, M. Schellmann, H. Schotten, H. Taoka, H. Tullberg, M. A. Uusitalo, B. Timus, and M. Fallgren, "Scenarios for 5G mobile and wireless communications: the vision of the METIS project," *IEEE Communications Magazine*, vol. 52, no. 5, pp. 26–35, May 2014.

[8] X. Gao, O. Edfors, F. Rusek, and F. Tufvesson, "Linear pre-coding performance in measured very-large MIMO channels," in *Proc. IEEE Vehicular Technology Conference (VTC Fall)*, Sept. 2011.

[9] S. Payami and F. Tufvesson, "Channel measurements and analysis for very large array systems at 2.6 GHz," in *Proc. European Conference on Antennas and Propagation (EuCAP)*, Mar. 2012.

[10] X. Gao, F. Tufvesson, O. Edfors, and F. Rusek, "Measured propagation characteristics for very-large MIMO at 2.6 GHz," in *Proc. Asilomar Conference on Signals, Systems, and Computers (ASILOMAR)*, Nov. 2012.

[11] X. Gao, O. Edfors, F. Rusek, and F. Tufvesson, "Massive MIMO performance evaluation based on measured propagation data," *IEEE Transactions on Wireless Communications*, vol. 14, no. 7, pp. 3899–3911, July 2015.

[12] M. Costa, "Writing on dirty paper," *IEEE Transactions on Information Theory*, vol. 29, no. 3, pp. 439–441, 1983.

[13] J. Hoydis, C. Hoek, T. Wild, and S. ten Brink, "Channel measurements for large antenna arrays," in *Proc. International Symposium on Wireless Communication Systems (ISWCS)*, Aug. 2012.

[14] R. S. Thoma, D. Hampicke, A. Richter, G. Sommerkorn, A. Schneider, U. Trautwein, and W. Wirnitzer, "Identification of time-variant directional mobile radio channels," *IEEE Transactions on Instrumentation and Measurement*, vol. 49, no. 2, pp. 357–364, Apr. 2000.

[15] S. Vishwanath, N. Jindal, and A. Goldsmith, "Duality, achievable rates, and sum-rate capacity of Gaussian MIMO broadcast channels," *IEEE Transactions on Information Theory*, vol. 49, no. 10, pp. 2658–2668, Oct. 2003.

[16] N. Jindal, W. Rhee, S. Vishwanath, S. A. Jafar, and A. Goldsmith, "Sum power iterative water-filling for multi-antenna Gaussian broadcast channels," *IEEE Transactions on Information Theory*, vol. 51, no. 4, pp. 1570–1580, Apr. 2005.

[17] A. Paulraj, R. Nabar, and D. Gore, *Introduction to Space-Time Wireless Communications*. Cambridge University Press, 2003.

[18] I. E. Telatar, "Capacity of multi-antenna Gaussian channels," *European Transactions on Telecommunications*, vol. 10, no. 6, pp. 585–595, 1999.

Paper IV

Massive MIMO Channels – Measurements and Models

Spatial multiplexing using Massive MIMO has been shown to have very promising properties, including large gains in spectral efficiency and several orders of magnitude lower transmit power, as compared to today's access schemes. The properties of massive MIMO have been studied mostly for theoretical channels with independent and identically distributed (i.i.d.) complex Gaussian coefficients. To efficiently evaluate massive MIMO in more realistic scenarios, we need channel models that capture important massive MIMO channel characteristics. We pursue this by analyzing measurement data from a measurement campaign in the 2.6 GHz frequency range, using a physically large array with 128 elements. Key propagation characteristics are identified from the measurements. We use the cluster-based COST 2100 MIMO channel model as a basis, and propose an extension to include those important propagation properties for massive MIMO. Statistical models of the total number of clusters, their visibility regions and visibility gains at the base station side are found based on the measurement data.

---

1 Introduction

Massive MIMO, also known as very-large MIMO or large-scale antenna systems, is an emerging technology in wireless communications. With massive MIMO, we consider multi-user MIMO (MU-MIMO) where a base station is equipped with a large number (say, tens to hundreds) of antennas, and is serving several single-antenna users in the same time-frequency resource.

It has been shown both in theory and in real propagation environments that massive MIMO has very promising properties, including large gains in spectral efficiency and several orders of magnitude lower transmit power [1–4], as compared to conventional MIMO systems with a small number of antennas at the base station. So far, theoretical studies of massive MIMO are mostly done in channels with i.i.d. complex Gaussian coefficients. However, to efficiently evaluate such a new technique in more realistic scenarios, new channel models are needed that capture important properties of real massive MIMO propagation channels.

Unlike conventional MIMO with small and compact antenna arrays, massive MIMO with a large number of antennas can have antenna arrays that span tens to hundreds of wavelengths in space. Over this type of large arrays, the propagation channel cannot be seen as wide-sense stationary (WSS) as is usually the case for conventional small MIMO. This has been observed in measured channels using a 128-element linear array, as reported in [5] and [6]. When we resolve the propagation channel into scatterers, we observe that some scatterers are not visible over the whole array, and for scatterers being visible over the whole array, their power contribution may vary considerably. Thus, large-scale/shadow fading can be experienced over this large array. The power variation caused by the large-scale/shadow fading over the antenna array can be critical to performance evaluation and algorithm design for massive MIMO. Therefore, it is important to model the non-WSS characteristic of the propagation channel over the array and include it in new channel models.

We start from a well-known MIMO channel model - the COST 2100 model [7], in which only small and compact MIMO arrays have been considered so far. Based on channel measurements using the 128-element linear array, we identify propagation properties of massive MIMO channels that are missing in the COST 2100 model. Then we propose an extension to include these massive MIMO properties. These propagation properties are also modeled statistically, using the measurement data.

The rest of the paper is organized as follows. In Sec. 2, we give a brief introduction on the COST 2100 MIMO channel model. In Sec. 3, we describe our massive MIMO channel measurements, measurement data processing, and propagation properties that are observed from the measured channels. Then

in Sec. 4 we propose an extension of the COST 2100 model to include massive MIMO channel characteristics. Finally we summarize this modeling work in Sec. 5.

2 COST 2100 MIMO Channel Model

The COST 2100 MIMO channel model is a geometry-based stochastic channel model (GSCM) that can reproduce the stochastic properties of MIMO channels over time, frequency, and space. It characterizes and models the radio channel in delay and directional domains, through the geometric distribution of scatterers, or clusters, i.e., groups of multipath components (MPCs), in the propagation environment. This cluster-based channel model describes the physical channel and is antenna-independent. The directional domain, when combined with antenna array responses at transmit and receive side, can be directly transformed into the spatial dimension for wideband MIMO channel simulations.

One advantage of cluster-based channel models is that they model the time-variant/spatially-variant nature of the radio channels. In the COST 2100 model, this is done by introducing cluster visibility regions, as one of the key modeling concepts. A visibility region (VR) is a region on the azimuth plane in the simulation area, which determines the visibility of a particular cluster. Each cluster is associated with at least one VR. When a mobile enters a VR, the related cluster becomes "visible", and contributes scattering through the corresponding MPCs in the radio channel between the mobile and the base station. The power level is controlled by a function called visibility gain, which describes the power variation of the scattering contribution within a VR. The mobile can be located in an area where multiple VRs overlap, and in this case, multiple clusters are "visible" simultaneously. The VRs are assumed to be uniformly distributed in the simulation area. When a mobile moves in the simulation area, it enters and leaves different cluster VRs. In this way, the time-variation/spatial-variation of the channel due to the movement is modeled by the variation of scattering contribution from different clusters. In the current COST 2100 model, the cluster VRs are only used at the mobile side, since the mobile terminal movement is one of the main causes of temporal and spatial variations of the channels. However, for a massive MIMO base station, when the antenna array becomes physically much larger than today's small and compact arrays, the effect of a spatially-variant channel can be experienced, but now over the large antenna array at the base station. This is shown and discussed when we analyze channel measurements in Sec. 3.

More details on the COST 2100 MIMO channel model, such as general

structure, parameterization, implementation and validation, can be found in [7–9].

3 Channel Measurements and Processing

In order to characterize and model massive MIMO channels, measurements with a large virtual array were performed. Since the cluster-based COST 2100 channel model is our modeling basis, we extract clusters from the measured channels and investigate the channel behavior of massive MIMO at a cluster level. Comparing with conventional small MIMO channels, we identify missing properties of massive MIMO in the current model. Channel measurements, measurement data processing, and observed channel behavior are presented in the following.

3.1 Channel Measurements

The measurements were carried out outdoors around the E-building of the Faculty of Engineering (LTH), Lund University, Sweden. An overview of the semi-urban measurement area is shown in Fig. 1 (left). The base station (receive) antenna array was placed on the roof of E-building. It is a 128-element virtual linear array and spans 7.4 m in space. The distance between adjacent antenna element positions is half a wavelength at 2.6 GHz. Fig. 1 (upper and lower right) shows this physically large array with an omni-directional antenna moving on a rail, giving 128 antenna positions. At the user (transmit) side, an omni-directional antenna was moved around 8 measurement sites (MS) acting as single-antenna users. Among these sites, three (MS 1-3) have line-of-sight (LOS) conditions, and five (MS 4-8) have non-line-of-sight (NLOS) conditions. At each site, 5 positions were measured.

The measurement data were recorded at a center frequency of 2.6 GHz and a signal bandwidth of 50 MHz, using an HP 8720C vector network analyzer. With the virtual linear array and vector network analyzer, it takes around half an hour to record one measurement, i.e., at the base station, the omni-directional antenna moves from the beginning of the array to the end. In order to keep the channel as static as possible during one measurement, this campaign was performed during the night when there were few objects, e.g., people and cars, moving around in the measurement area.

3.2 Measurement Data Processing

From the raw measurement data, i.e., the channel transfer functions, we need to investigate the massive MIMO channel behavior at a cluster level and iden-

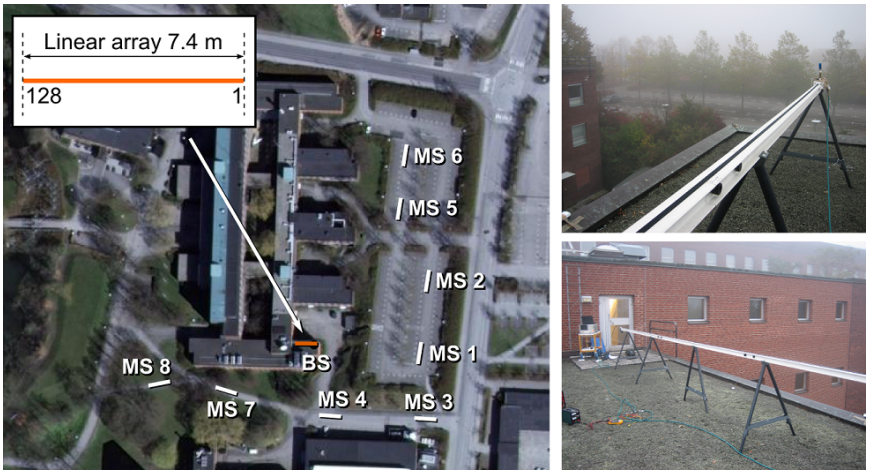

Figure 1: Left: overview of the measurement area at the campus of the Faculty of Engineering (LTH), Lund University, Sweden. A 128-element virtual linear array at the base station was placed on the roof of the E-building. 8 measurement sites (MS 1-8) around the E-building were measured. Upper right: an omni-directional antenna moving along a rail, forms the virtual linear array with 128 equidistant antenna positions. Lower right: another view of the same virtual linear array spanning 7.4 m.

tify propagation properties that are missing in the current model. For each measured position, in order to extract the clusters in the channel, we apply a sliding window with 10 neighboring antennas over the array. From the raw measurement data within each window, we estimate the MPCs with parameters of delay, angle of arrival (AoA) in azimuth and complex amplitude, through the space-alternating generalized expectation maximization (SAGE) algorithm [10]. Based on the estimated MPC parameters, joint clustering and tracking [11] is performed. Clusters are identified by grouping the MPCs through the KpowerMeans clustering algorithm [12] for each 10-antenna window, then the identified clusters are tracked over windows along the array. The reason we process the channel data based on 10-antenna windows is that the channel can be considered as wide-sense stationary (WSS) within such window. On the basis of these WSS sub-channels, we can study the spatial-variation of the whole channel over the array. Furthermore, when the SAGE algorithm estimates the directional information[8], 10 antennas can provide relatively high angular resolution.

Through the above processing of raw measurement data, we can investigate the channel behavior at a cluster level. Angular power spectrum from the SAGE estimates and corresponding cluster power variations over the array from joint clustering and tracking are shown in Fig. 2 as examples. Fig. 2(a) and 2(b) show the angular power spectrum over the array in one LOS scenario and one NLOS scenario, respectively. From here we can see the spatial-variation of the channel over the large array. For example, in Fig. 2(a), the LOS component from around 150 degrees is stronger at the beginning of the array and becomes shadowed at the end of array. The power contribution from 130 degrees only appears over a part of the array. In the NLOS scenario shown in Fig. 2(b), we can see that the scattering is more rich and many scatterers are only visible over a part of the array. The corresponding cluster power variations over the array in these two scenarios are shown in Fig. 2(c) and 2(d) (solid lines). Along with the cluster power variations, we can also see the distance along the array that each cluster is visible. Some clusters are visible over the whole array, while others are only visible for a part of the array. The above shows that the massive MIMO channel cannot be considered wide-sense stationary over the large array, and thus large-scale/shadow fading is experienced.

In comparison with massive MIMO with a large array, the shadowed regions in Fig. 2 indicate a channel that a conventional small MIMO would experience. A small and compact array which spans only a few wavelengths in space would experience a very small part of the channel that a large array sees. From the

[8]The range of directional estimation is 0-180 degrees for the linear array. This is due to the directional ambiguity problem inherent in this type of array structure [13], thus it does not affect the channel modeling for it.

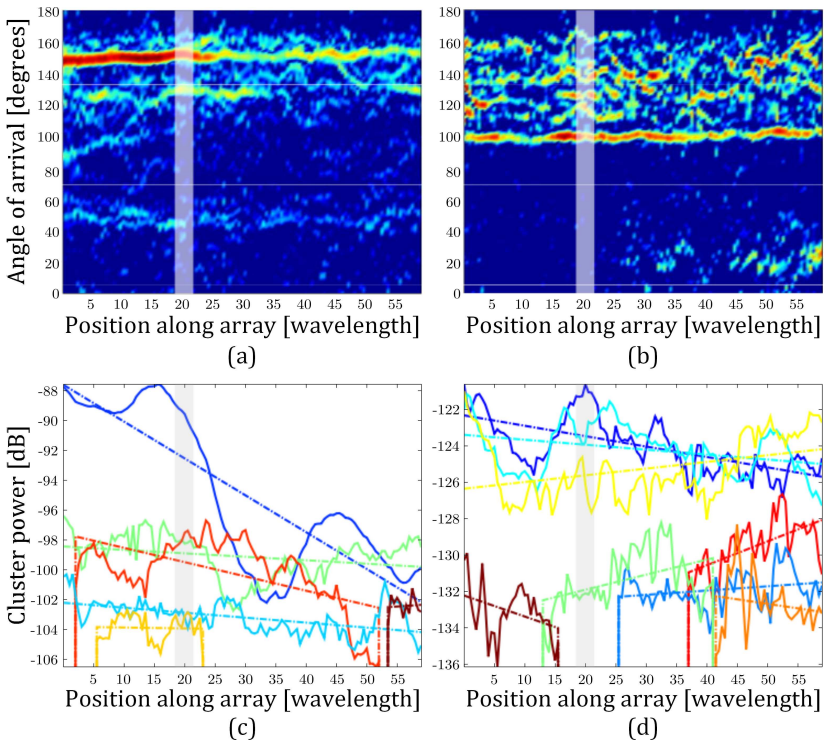

Figure 2: Angular power spectrum and cluster power variations over the large array at the base station. (a) and (c) are results from a LOS scenario when the user is at MS 3. (b) and (d) are results from a NLOS scenario when the user is at MS 7. For the cluster power variations shown in (c) and (d), different clusters are indicated by different colors, and the solid lines are the cluster power variations over the array, which are fitted by linear slopes, i.e., the dashed lines, in a least-squares sense. The shadowed regions in the four plots show examples of the channels that a conventional small MIMO array extending over a few wavelengths would experience.

shadowed regions in Fig. 2, we can see that the small MIMO channels do not have much spatial-variation: within the indicated range of the small array, the same clusters are visible and the cluster power has small variations.

4 Modeling for Large Array

From the observation of measured channel behavior discussed above, we know that massive MIMO channels can have significant spatial-variation over the large array. To extend the current COST 2100 model to support large arrays, this spatial-variation at the base station side needs to be modeled and included. A simple way for this is to extend the concept of cluster visibility regions, as discussed in Sec. 2, to the base station side. The idea is that each cluster should have two types of VRs, one at mobile station side (MS-VR), and one at base station side (BS-VR). Similar to how a mobile terminal moves in and out of MS-VRs on the mobile side, antenna elements along the large array are either inside or outside BS-VRs at the base station side. This is illustrated in Fig. 3, where colored regions imply visibility of different clusters along a large linear array.

After introducing the concept of cluster VRs on the base station side, we determine what needs to be modeled in the extension to include massive MIMO. First of all, the total number of clusters that are visible over a large array should be modeled. As can be seen from Fig. 2 and Fig. 3, more clusters are visible for a large array as compared to a small array, so the number of clusters in the current model is not suitable any more. Then, for each cluster, we assign BS-VR to it together with MS-VR, we therefore need to model the properties of BS-VRs, such as shape and size. It should be mentioned that the modeling of MS-VR in the current model cannot be directly used for BS-VR. This is because the mobile station and the base station usually have very different propagation environments in their vicinity. Mobile stations are usually moving on ground, while base stations are typically positioned on top of buildings. Another thing that should be taken into account is the cluster power variations within the BS-VRs. In the current model, the average power contribution of a cluster depends on the geometry of the cluster location in the simulated propagation environment. As an extension, what we need to model here is only the variation of cluster power, which is the cluster visibility gain at the base station side.

The modeling of the total number of clusters, cluster visibility region and visibility gain at the base station side are discussed in the following. We model them statistically based on the processed measurement data. As being done for the current model in [8], LOS and NLOS scenarios are modeled and parameterized separately, since they show different statistics from the measurement

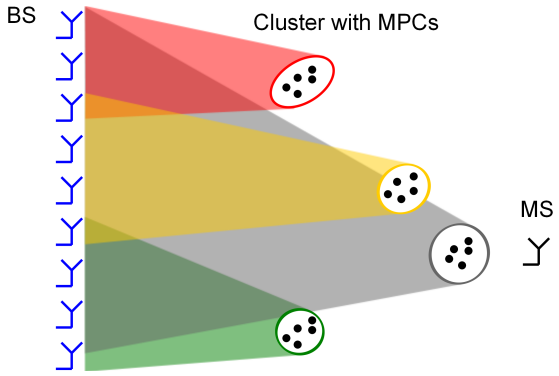

Figure 3: Extension of the concept of cluster visibility regions to the base station side. Each antenna sign represents a small MIMO array.

data. Here we show the modeling and parameterization for NLOS scenarios, based on the measurements at MS 4-8 (see Fig. 1), as an example. For LOS scenarios, the modeling and parameterization are done in the same way, but result in different values on the estimated distribution parameters.

4.1 Total Number of Clusters

Fig. 4 shows the statistics of the total number of clusters that are visible in the range of 7.4 m linear array in the NLOS scenarios. Since the data can only take on discrete values, we use a negative binomial distribution to model it, as can be seen in Fig. 4. The two parameters of the negative binomial distribution are obtained through maximum-likelihood estimation (MLE). Note that the clusters are extracted from the channel when the mobile is at one measurement position. It means that only clusters with MS-VRs overlapping that position are visible. If the movement of mobile station is considered, the total number of clusters in the environment should be even higher than what we observe in this measurement.

4.2 Cluster Visibility Region at the Base Station Side

In the current model, the MS-VRs are modeled as circular regions of a fixed size. However, a modification has been suggested in [8] to introduce variations in the VR size. In contrast to the MS-VRs which are two-dimensional regions on the azimuth plane, the BS-VRs have to be modeled as intervals for now, since the large linear array only spans one dimension. The lengths of these intervals

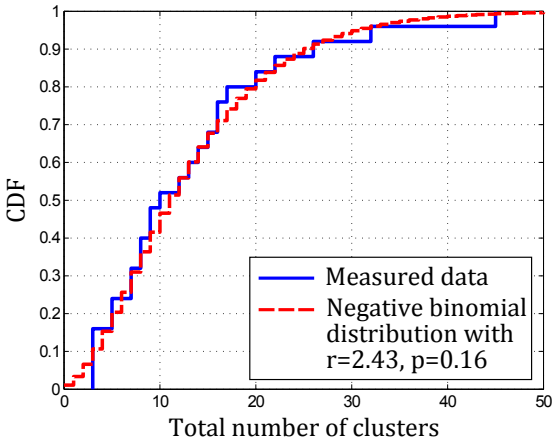

Figure 4: CDF of the total number of clusters, which is modeled as negative binomial distribution with the estimated parameters $r = 2.43$ and $\sigma = 0.16$.

are the BS-VR sizes, for which the modeling is discussed in the following.

As can be seen in Fig. 2, some clusters have BS-VRs entirely inside the array, and some clusters have BS-VRs that overlap one or both ends of the array. For the former case, the observed BS-VR length on the array is the cluster's true BS-VR length, while for the latter case, the true BS-VR length may be much longer than what is observed on the array. Since the physical size of the linear array is limited, we can only measure part of the length of many cluster BS-VRs. In order to model the true BS-VR lengths from the observed data, we derive the relationship between the true BS-VR length and the observed BS-VR length, depending on the BS-VR center position along the array. This relationship is illustrated in Fig. 5. For the three cases of the BS-VR being entirely inside the array, outside the array at one end and outside the array at both ends, we can write the observed BS-VR length Δ as a function of the true length α and the center position X_c. We assume that the cluster BS-VR center positions X_c are uniformly distributed along the line of the array in space, just as in the current model the MS-VRs are uniformly distributed in the simulation area. Then we can find the relationship between the distributions of Δ and α. The cumulative distribution function (CDF) of the observed BS-VR lengths, $K_\Delta(y)$, can be written as a function of the

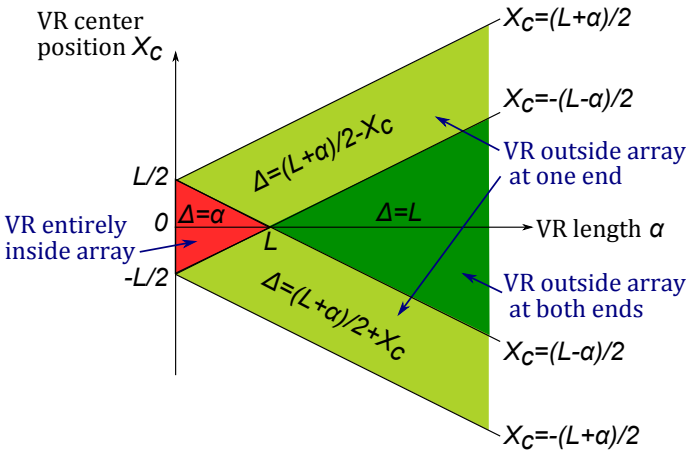

Figure 5: Illustration of the relationship between a cluster's true BS-VR length α and observed BS-VR length on the array Δ, depending on the BS-VR center position X_c. On the axis of BS-VR center position, the origin is at the center of the linear array, and L represents the length of the array.

probability density function (PDF) of the true BS-VR lengths, $f_\alpha(\nu)$, as

$$K_\Delta(y) = \begin{cases} K'_\Delta(y), & y \le L \\ 1, & y > L, \end{cases} \tag{1}$$

where

$$K'_\Delta(y) = \int_{\Delta_0}^{y} f_\alpha(\nu)\,\mathrm{d}\nu + 2y\int_{y}^{\infty} \frac{1}{L+\nu} f_\alpha(\nu)\,\mathrm{d}\nu - 2\Delta_0 \int_{\Delta_0}^{\infty} \frac{1}{L+\nu} f_\alpha(\nu)\,\mathrm{d}\nu, \tag{2}$$

L is the length of the array, and Δ_0 is the smallest observation of the BS-VR length on the array due to measurement data processing.

Having the relationship of the distributions of the observed BS-VR lengths and the true BS-VR lengths above, we can assume any particular distribution of the true BS-VR lengths, i.e., $f_\alpha(\nu)$, and find its parameters through an MLE approach based on the observed data. Here we select a log-normal distribution, judging from the shape of the empirical distribution seen in the measurements, and estimate its two parameters. The estimation result is shown in Fig. 6(a), where the true BS-VR length follows log-normal distribution with the estimated parameters. We can also see the fitting of the distribution of observed BS-VR lengths from the MLE result to the measured data, as shown in Fig. 6(b) and

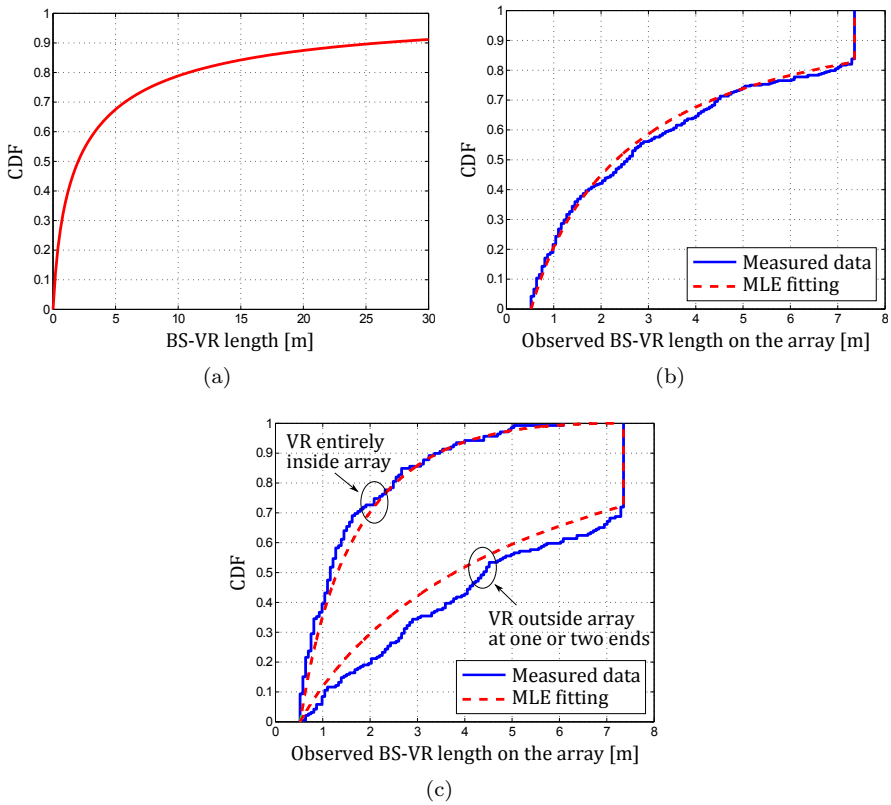

Figure 6: Distributions of the true BS-VR lengths and observed BS-VR lengths on the array. (a) CDF of the estimated true BS-VR lengths, which follows a log-normal distribution with the estimated parameters of logarithm mean $\mu = 0.7$ and logarithm standard deviation $\sigma = 2$. (b) CDF of the observed BS-VR lengths on the array and the fitting through the MLE approach. (c) CDFs of the observed BS-VR lengths and the fittings through the MLE approach, splitting into two groups: BS-VRs entirely inside the array and BS-VRs outside the array at one or both ends.

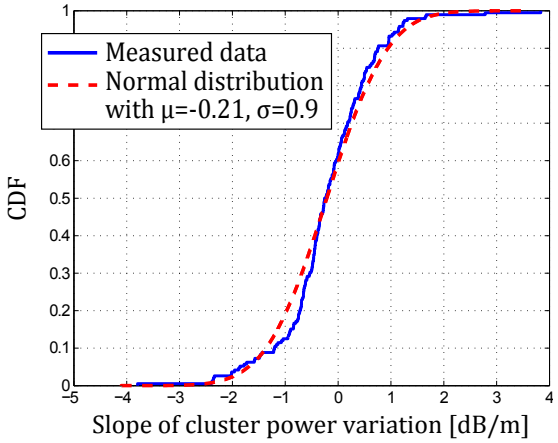

Figure 7: CDF of the slopes of cluster power variations in their BS-VRs. It follows normal distribution with the estimated parameters of the mean $\mu = -0.21$ and the standard deviation $\sigma = 0.9$.

Fig. 6(c). Fig. 6(c) shows the data of BS-VR entirely inside the array and the data of BS-VR outside the array separately. We can see that for the part that BS-VRs are entirely inside the array, the MLE result fits quite well, while for the part that BS-VRs are outside the array, the MLE fitting in the CDF plot is slightly higher than the measured data. Despite this, we can see in Fig. 6(b) the MLE fitting is quite good for the whole data set.

4.3 Cluster Visibility Gain at the Base station Side

For the cluster power variations within the BS-VRs, since the small-scale fading has already been modeled as the constructive and destructive effects of the MPCs in the current model, what we need to capture here is the large-scale fading along the array. For simplicity, we use linear slopes in dB to fit the cluster power variations, as shown in the dashed lines in Fig. 2(c) and (d). These linear slopes are estimated in a least-squares sense in the dB domain. The CDF of the slopes of these linear changes in dB are shown in Fig. 7. Note that for clusters with small observed BS-VRs, the estimation of the slopes may be unreliable. Thus in Fig. 7, the slopes for the clusters with observed BS-VRs larger than 25 windows, i.e., about 2 m, are shown and fitted well by the normal distribution.

5 Summary

In this paper, the ongoing work of cluster-based modeling for massive MIMO channel is presented. We start from the well-known COST 2100 MIMO channel model, in which only small and compact MIMO arrays have been considered so far. Based on channel measurements using a physically large array with 128 elements, we have studied the massive MIMO channel behavior and identified important propagation properties missing in the current COST 2100 model. The observation is that the channel cannot be seen as wide-sense stationary over the large array at the base station. Therefore, an extension of the current model to support large arrays is proposed. The concept of cluster visibility regions in the current model is extended to the base station side to model the spatial-variation of the channel over the large array. Then statistical models of the total number of clusters, their visibility regions and visibility gains at the base station side are found based on the measured data.

References

[1] F. Rusek, D. Persson, B. K. Lau, E. G. Larsson, T. L. Marzetta, O. Edfors, and F. Tufvesson, "Scaling up MIMO: Opportunities and challenges with very large arrays," *IEEE Signal Processing Magazine*, vol. 30, no. 1, pp. 40–60, Jan. 2013.

[2] E. Larsson, O. Edfors, F. Tufvesson, and T. L. Marzetta, "Massive MIMO for next generation wireless systems," *IEEE Communications Magazine*, vol. 52, no. 2, pp. 186–195, Feb. 2014.

[3] H. Q. Ngo, E. G. Larsson, and T. L. Marzetta, "Energy and spectral efficiency of very large multiuser MIMO systems," *IEEE Transactions on Communications*, vol. 61, no. 4, pp. 1436–1449, Apr. 2013.

[4] X. Gao, F. Tufvesson, O. Edfors, and F. Rusek, "Measured propagation characteristics for very-large MIMO at 2.6 GHz," in *Proc. Asilomar Conference on Signals, Systems, and Computers (ASILOMAR)*, Nov. 2012.

[5] S. Payami and F. Tufvesson, "Channel measurements and analysis for very large array systems at 2.6 GHz," in *Proc. European Conference on Antennas and Propagation (EuCAP)*, Mar. 2012.

[6] X. Gao, F. Tufvesson, O. Edfors, and F. Rusek, "Channel behavior for very-large MIMO systems – initial characterization," in *COST IC1004*, Sept. 2012.

[7] L. Liu, C. Oestges, J. Poutanen, K. Haneda, P. Vainikainen, F. Quitin, F. Tufvesson, and P. D. Doncker, "The COST 2100 MIMO channel model," *IEEE Wireless Communications*, vol. 19, no. 6, pp. 92–99, Dec. 2012.

[8] M. Zhu, G. Eriksson, and F. Tufvesson, "The COST 2100 channel model: Parameterization and validation based on outdoor MIMO measurements at 300 Mhz," *IEEE Transactions on Wireless Communications*, vol. 12, no. 2, pp. 888–897, Feb. 2013.

[9] R. Verdone and A. Zanella, Eds., *Pervasive Mobile and Ambient Wireless Communications: COST Action 2100*. Springer-Verlag London, 2012.

[10] B. H. Fleury, M. Tschudin, R. Heddergott, D. Dahlhaus, and K. Ingeman Pedersen, "Channel parameter estimation in mobile radio environments using the SAGE algorithm," *IEEE Journal on Selected Areas in Communications*, vol. 17, no. 3, pp. 434–450, Mar. 1999.

[11] N. Czink, "The random-cluster model – a stochastic MIMO channel model for broadband wireless communication systems of the 3rd generation and beyond," Ph.D. dissertation, Technischen Universität Wien, 2007.

[12] N. Czink, P. Cera, J. Salo, E. Bonek, J. P. Nuutinen, and J. Ylitalo, "A framework for automatic clustering of parametric MIMO channel data including path powers," in *Proc. IEEE Vehicular Technology Conference (VTC Fall)*, Sept. 2006.

[13] A. Manikas and C. Proukakis, "Modeling and estimation of ambiguities in linear arrays," *IEEE Transactions on Signal Processing*, vol. 46, no. 8, pp. 2166–2179, Aug. 1998.

Paper V

Massive MIMO Channel Modeling – the COST 2100 Extension

As massive MIMO is currently considered a leading 5G technology candidate, channel models that capture important massive MIMO channel characteristics are urgently needed. In this paper we present an attempt to model massive MIMO channels, based on measurement campaigns at 2.6 GHz in both outdoor and indoor environments, using physically-large arrays and with closely-spaced users. The COST 2100 MIMO channel model is adopted as a general framework. We discuss modeling approaches and scopes for massive MIMO, based on which we suggest extensions to the COST 2100 model. Extensions include 3D propagation, polarization, cluster behavior at the base station side for physically-large arrays, and multi-path component gain functions for closely-spaced users. Model parameters for these extensions in massive MIMO scenarios are reported. Initial validation against the measurements are also performed, which shows that the model is capable of reproducing channel statistics in terms of temporal behavior of the user separability, singular value spread and sum-rate.

Updated version of the Temporary Document (TD)
Xiang Gao, Jose Flordelis, Ghassan Dahman, Fredrik Tufvesson, Ove Edfors,
"Massive MIMO Channel Modeling – Extension of the COST 2100 Model,"
TD(15)W1025 in *COST IC1004*, Oct. 2015.

1 Introduction

Massive MIMO [1–4] is an emerging technology in wireless communications. With a large number of antennas at the base station, massive MIMO exploits a large number of spatial degrees of freedom in the propagation channels. It has been shown in both theory and experiments that massive MIMO can dramatically improve both spectral and transmit-energy efficiencies of conventional MIMO by orders of magnitude [5–10]. With the potential of offering higher data rates and serving more users simultaneously, massive MIMO is thus considered as a leading 5G technology candidate [11–15]. When massive MIMO is brought from theory to practice, channel measurements were performed to evaluate massive MIMO in real propagation environments [6–10], and real-time massive MIMO testbeds are also being implemented [16]. In order to efficiently design massive MIMO systems and test algorithms, channel models that include massive MIMO characteristics are now urgently needed.

So far, theoretical studies of massive MIMO are mostly done for channels with independent and identically distributed (i.i.d.) complex Gaussian coefficients, or based on correlative channel models, e.g., the Kronecker model. Channel models using an i.i.d. assumption do not consider channel correlations and power variations between users and between base station antennas, thus usually give more optimistic results than those obtained in real propagation channels. The Kronecker model is not suitable for physically-large arrays due to the assumption that the propagation at the transmitter and receiver sides are uncoupled, resulting in underestimation of the performance [17]. Another important aspect is the temporal behavior of the channels, which is crucial for studying massive MIMO channel estimation, however, many correlative models are unable to model time-variation.

In this paper, we present an attempt to model massive MIMO channels based on measurement campaigns at 2.6 GHz in both outdoor and indoor environments. The COST 2100 MIMO channel model is adopted as a general framework. The COST 2100 model is a geometry-based stochastic channel model (GSCM), and inherently it is able to capture and model important massive MIMO channel characteristics, i.e., the user separability and the temporal behavior of the channel. Most importantly, the COST 2100 modeling approach is generic, and the developed model is not specific to massive MIMO only, which means they can be consistent in both the spatial and frequency domain, i.e., capturing the propagation behavior over a few wavelengths to hundreds of meters, and supporting lower frequencies as well as higher frequencies. We suggest extensions of the COST 2100 channel model for massive MIMO. The extensions include 3D propagation, polarization, cluster behavior at the base station side for physically-large arrays, and variability of multi-path component (MPC)

gain for closely-spaced users.

The channel measurements on which we develop the massive MIMO channel model have been reported in [6–8, 18, 19]. The measurements were performed at 2.6 GHz and with 40 or 50 MHz bandwidth, using a physically-large linear array and a compact cylindrical array at the base station, both having 128 antenna elements. Scenarios with closely-spaced users were measured using the cylindrical array only, in an outdoor semi-urban environment emulating open exhibitions with a high user density, and in an indoor environment emulating crowded auditorium.

The rest of the paper is organized as follows. In Sec. 2 we review massive MIMO channel behavior that should be included in the new model, and we briefly discuss the limitations of current MIMO channel models. In Sec. 3 we discuss our modeling approach and scope, including model consistency and extensions to the COST 2100 model. We report initial parameters for the model extension in Sec. 4, and initial validation against measurements are presented in Sec. 5. Finally in Sec. 6 we summarize our work and draw conclusions.

2 Review of Massive MIMO Channel Behavior

Massive MIMO channel behavior including spherical wavefronts and large-scale fading over physically-large arrays have been reported in [18,20]. With closely-spaced users, massive MIMO channel characteristics have been observed and presented in [8,19]. Here we briefly review these new features of massive MIMO channels that have to be modeled, as compared to conventional MIMO channels.

2.1 New Features of Massive MIMO Channels

Compared to conventional MIMO channel, the radio channel of a massive MIMO system is of course the same, independent of system and antenna configuration used, but some propagation effects become more pronounced or more important when using physically-large arrays, when using many antenna elements at the base station, and when having many closely-located users. These effects are important and we need to capture detailed behavior that can explain, e.g., user separability, temporal behavior, as well as the possibilities for significant increases in spectral and transmit-energy efficiency. Among the important specific propagation effects for massive MIMO can be mentioned noticeable spherical wavefronts, variations of statistics over physically-large arrays, and the limited lifetime of individual MPCs when a user is moving.

When physically-large arrays are used at the base station, users or significant scatterers may be located inside the Rayleigh distance of the array, e.g., the 7.4 m linear array in [6] gives a Rayleigh distance of about 950 m. The plane-wave assumption does not hold for large arrays, and spherical wavefronts are observed [10]. Spherical wavefronts are important to model because then not only directions to users and scatterers are important, but also the distances to scatterers and users. The inherent beamforming capability of massive MIMO makes it possible to focus the signal energy to a specific point in the environment rather than just in a certain direction. Furthermore, if two users are in the same direction but at different distances from the base station, the spherical wavefronts can make it possible to separate those users, also in line-of-sight (LOS) [21]. This is typically not the case for conventional MIMO using smaller arrays.

The variations in statistics of the received signal from a specific user over physically-large arrays also contributes to user separation. The variations include, e.g., received signal power, angular power spectra, as well as power delay profile between different antenna elements [10], also in cases where they have identical antenna patterns aimed in the same direction. Variations of the angular power spectra can be characterized by the so-called spatial fingerprints [6]. The large-scale fading over the array can also be crucial for massive MIMO performance, as the antennas do not contribute equally to the performance [7].

When having many closely-spaced users, users interacting with different structural details of a scatterer needs to be considered when analyzing user separability. In conventional MIMO channel models, all the scatterers in a cluster are visible from all positions in the visibility region of the cluster. In practice this is, however, not the case. Each of the MPCs typically has a limited area inside the visibility region where they can be seen. In [22], the results show that duration of multipath components in urban scenarios is much shorter than commonly expected. Most of them last less than 1 m, and only a few last more than 10 m. This study suggests a modification of cluster-based models. Clusters provide a very effective way of modeling antenna correlation for a single user, but our observations show that conventional MIMO models tend to overestimate correlation between closely-spaced users in massive MIMO systems.

Other propagation effects that become important in massive MIMO scenarios include 3D propagation, because arrays with a large number of antennas may span more than one dimension.

2.2 Current MIMO Channel Models

Among MIMO channel models, the GSCMs provide a natural way to capture time-variation and describe correlation effects between users and between antenna elements in a straightforward way through the concept of clusters and their visibility regions.

Within the group of GSCMs there are two basic approaches having the same origin (the COST 259 model): the COST 2100 approach and the WINNER approach. In the COST 2100 [23] approach, scatterers have fixed physical positions in the simulated environment, whereas in the WINNER [24] approach the channel simulation is based on angles to the scatterers. From a massive MIMO perspective the latter has the drawback that the angles vary as long as we are not in the far field of the array; hence we need to include this in the model. Due to this reason and since we aim for a consistent model showing realistic correlations between users in a massive MIMO context, we use the COST 2100 modeling approach where the clusters and scatterers are described by their physical locations rather than their directions in the simulation area. The model extensions we propose are general and not specific to massive MIMO, as they realistically represent physical propagation mechanisms when taking wireless communication beyond the conventional cellular scenario with one or several base stations. The concepts introduced should, e.g., be useful also for peer-to-peer channels or when developing models for radio-based positioning. In this paper, however, we focus on the massive MIMO scenario with one base station equipped with many antennas and several mobile users with one or a few antennas.

It should also be mentioned that there are theoretical geometrical model proposals in the literature, e.g., in [25]. As we aim for a model connected to a physical environment those models are out of scope of our investigation, though these theoretical models can provide useful insights into, e.g., correlation characteristics. Ray-tracing based investigations and models can also provide useful insights for system design and performance evaluation, but those models rely heavily on a deterministic geometry and thus also out of scope of our investigation here.

3 Modeling Approach and Scope

In this section we introduce our modeling approach and scope, and suggest the extensions to the COST 2100 channel model.

3.1 Model Consistency

As explained above, the COST 2100 model is adopted in this work as a general framework, since it has the required flexibility to model different aspects of massive MIMO channels. Besides the requirement of capturing channel behavior in different spatio-temporal, angular, and delay domains, the developed channel model should also be consistent in both the spatial and frequency domains.

In the spatial domain, the channel model should be able to capture the propagation behavior over small distances in the range of a wavelength to very large distances (hundreds of meters), for both the user side and the base station side. The model should cover the cases where user terminals are closely-spaced to the cases where user terminals are far separated and the cases where the base station array is physically small to the cases where it is physically large. The consistency in the spatial domain makes it possible to compare massive MIMO with conventional MIMO.

In the frequency domain, the channel model should support low frequencies (below 6 GHz) as well as high frequencies (above 6 GHz). The consistency in the frequency domain has become more important due to the trend in 5G communications towards using higher frequency bands, i.e., the 6-100 GHz band. The COST 2100 model potentially can meet the consistency requirement in both spatial and frequency domains, as discussed above. We, however, limit the efforts here to the case below 6 GHz.

3.2 Extension of the COST 2100 Channel Model

The extensions are based on the performed measurement campaigns, and modeling aspects for physically-large arrays and closely-spaced users are implemented. In the case of having limitations preventing us from extracting some parameters of interest based on our measurement data, these parameters are implemented based on the 3GPP and WINNER channel models [24, 26]. The implemented extensions for the COST 2100 model are detailed below.

3D Extension

Supporting elevation angles for the MPCs is crucial in capturing the behavior of the channel, especially when base station arrays span more than one dimension. Besides that, the proximity of the base station and/or the user terminals to the interacting objects in the environment makes the effect of the elevation angles more pronounced. Therefore, the propagation in the COST 2100 model simulation has been extended to 3D, by including parameters such as intra-cluster angular spread in elevation for both base station and user sides. Due to limitations in extracting these parameters based on our measurements, the

parameter values of cluster angular spreads in elevation are thus adopted from the 3GPP 3D model [26].

Polarization Extension

One of the main results discussed in [8] is the significant effect of polarization on massive MIMO performance when serving closely-spaced users. Both vertical and horizontal-polarized antennas at the base station are useful for separating users. This is of great importance since the polarization at the user side is usually dual but unknown when having the hand and head effect on the antenna pattern. We also gain from the user diversity due to the difference in user polarizations and patterns. Therefore, the COST 2100 model has been extended by including polarization for the MPCs, i.e., in a single MPC, how much energy is from co-polarization (vertical to vertical and horizontal to horizontal), and how much is from cross-polarization (vertical to horizontal and horizontal to vertical).

In our measurements, however, due to lack of the polarization information at the user side, we adopt the cross polarization ratio (XPR) parameters reported in the WINNER II models. There, XPR for each MPC follows log-normal distribution $\kappa = 10^{\frac{X}{10}}$, where $X \sim N(\mu, \sigma)$. For the indoor office (A1) scenario, the means $\mu = 11$ dB for LOS and $\mu = 10$ dB for NLOS, and the standard deviation is $\sigma = 4$ dB. For the large indoor hall hotspot (B3), $\mu = 9$ dB for LOS and $\mu = 6$ dB for NLOS, $\sigma = 4$ dB and $\sigma = 3$ dB for LOS and NLOS, respectively. For the urban micro-cell (B1), $\mu = 9$ dB for LOS and $\mu = 8$ dB for NLOS, and $\sigma = 3$ dB.

Extension for Physically-Large Arrays

Dedicated measurement campaigns were performed for the scenarios with physically-large arrays at the base station [6, 18]. It has been observed that spherical wavefronts and large-scale fading are experienced across the large array. In order to capture the effect of having a physically-large array and be compatible with the conventional model, the simulation area at the base station side is determined by the size of the used array, and the cluster visibility region at the base station side is introduced, see Fig. 1. A cluster thus has two visibility regions, one at the user side (MS-VR) and one at the base station side (BS-VR), and the cluster contributes in the channel between a user and a base station antenna only when the user is within its MS-VR and the base station antenna is within its BS-VR. Based on the measurements, the size of BS-VRs and the power variation of a cluster within its BS-VR, i.e., the visibility gain, have been modeled and implemented. The number of clusters can be more

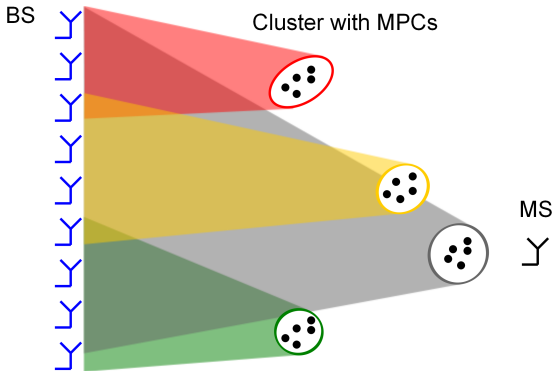

Figure 1: An illustration of the extension of cluster visibility regions to the base station side [27].

than in conventional MIMO channels, since physically-large arrays "see" the channel more in the spatial domain. This extension naturally captures the effect of the spherical wavefronts.

The extension for physically-large arrays is consistent with physically-compact arrays, since a small array falls in the same BS-VR. This allows direct comparison of physically-large and compact arrays in the simulation.

Extension for Closely-Spaced Users

Different measurement campaigns were performed for the scenarios with closely-located users, in both outdoor and indoor environments. The users were confined within a small area, i.e., 5 m diameter circle, therefore, we assume that all users stay within the same cluster visibility regions. When a user is moving within this confined area, the effects of changing its position, orientation and antenna tilt and the effect of the crowd around the user are captured as follows.

When a user is moving within a cluster visibility region, the power contribution of each MPC varies. This makes individual MPCs to have different patterns describing their contribution to the channel at each user position. This effect is captured by introducing MPC gain functions that have a symmetric Gaussian shape. Each MPC has its own gain function and it has a peak location randomly distributed within the corresponding cluster visibility region. The gain is thus determined by the distance d between the peak location and

the user location,

$$g_{\mathrm{MPC}}(d) = \exp\left(-\frac{d^2}{2\sigma_g^2}\right), \tag{1}$$

where the standard deviation σ_g determines the width of the gain function and controls the variability of the MPC gain. From our preliminary observation, the lifetime of MPCs is about 2 m, we therefore set $\sigma_g = 2.37$ which corresponds to a 3 dB power decay when $d = 2$ m.

The number of MPCs per cluster, $N_{\mathrm{MPC}}^{\mathrm{total}}$, the average number of effective MPCs per cluster, $N_{\mathrm{MPC}}^{\mathrm{effective}}$, the radius of cluster visibility region, R_c, and the radius of 3-dB power decay of the MPC gain function, r_g, fulfill the following relation

$$N_{\mathrm{MPC}}^{\mathrm{total}} = N_{\mathrm{MPC}}^{\mathrm{effective}} \frac{R_c^2}{r_g^2}. \tag{2}$$

According to the conventional models (COST 2100 and WINNER II), we choose the average number of effective MPCs per cluster to be 16. Hence, with $R_c =$ 10 m and $r_g = 2$ m, the total number of MPCs per cluster is 400. The large amount of MPCs with weak power can possibly be regarded as diffuse multipath components (DMC). Backward compatibility with the conventional model can be achieved by setting a large standard deviation for the gain functions.

The user antenna pattern that includes the interaction between the terminal antenna and the user body can capture the effect of changing the orientation, the tilt of the antenna and the shadowing by the users. The shadowing effect due to the crowd around the users possibly can be modeled as extra absorbing objects dropped within the simulation area. This, however, needs further investigations, and for now we do not include absorbing objects in the model.

4 Model Parameters

We report the initial parameters for the model extensions discussed above.

4.1 Scenario with Physically-Large Arrays

In Table 1, we list the parameters of the model extension for physically-large arrays. Details of the parameter extraction can be found in [18, 20, 27].

4.2 Scenario with Closely-Spaced Users

In Table 2, we list the initial parameters for the model extension with closely-spaced users. As marked in the table, some parameter values are adopted from

Table 1: Parameters of the COST 2100 model extension for physically-large arrays, extracted from the 2.6 GHZ measurements, semi-urban outdoor.

Parameter	LOS group	NLOS group
Total number of clusters		
r_N	-	2.43
p_N	-	0.16
Length of BS-VR [m]		
μ_α	-	0.7
σ_α	-	2
Slope of BS-VR gain [dB/m]		
μ_s	-	0
σ_s	-	0.9
Cluster power decay factor		
k_τ [dB/μs]	27.83	42.98
Cluster cut-off delay		
τ_B [μs]	0.87	0.91
Cluster shadowing factor		
σ_S [dB]	5.84	7.55
Number of MPCs per cluster		
N_MPC	30	31
Cluster delay spread		
m_τ [μs]	0.15	0.14
S_τ [dB]	3.20	2.85
Cluster angular spread		
m_{ψ_BS} [deg]	11.04	6.96
S_{ψ_BS} [dB]	2.93	2.39
Cluster spread cross-correlation		
$\rho_{\psi_\mathrm{BS}\tau}$	0.27	0.42
$\rho_{\psi_\mathrm{BS}\sigma_\mathrm{S}}$	0.09	0.04
$\rho_{\tau\sigma_\mathrm{S}}$	0.35	-0.09
LOS power factor		
μ_{K_LOS}	5.19	-
σ_{K_LOS} [dB]	3.47	-

a 300 MHz outdoor measurements for the COST model, and some are adopted from the 3GPP 3D channel model and the WINNER II channel models.

5 Validation Against Measurements

We validate the model extension for closely-spaced users in LOS scenarios. In order to validate the concept and use of MPC gain functions, in the simulation we place the clusters at the same positions and with the same cluster spreads as in the measurements. Randomness is obtained through cluster shadowing, MPC distribution within clusters, and LOS K-factors, etc. We simulate the user movements in straight lines but with random rotations (between $-\pi$ to π) of user antenna patterns in order to emulate the rotation of users during the movements. The user antenna pattern we use in the simulation is a measured pattern in the hand of an upper body phantom. The base station antenna pattern is the measured cylindrical array antenna pattern. In the validation we also add artificial noise to the simulated channels, according to the signal-to-noise ratio (SNR) in the measurements, i.e., about 16-20 dB. We compare the simulated channels with the measured channels in terms of user separability, linear precoding sum-rates as well as temporal behavior.

As explained earlier, closely-spaced users can be spatially separated because they "see" different MPCs, and this is modeled by the MPC gain function. We validate this model extension by evaluating the singular value spreads and the achieved sum-rates in the simulated channels, as compared with those in the measured channels. The model should also be consistent in spatial domain and be able to capture propagation behavior from small distances that are less than half-wavelength to distances that are at least a few wavelengths. We therefore validate the temporal behavior of the simulated channels from 0.01 m to 1 m through the auto-correlation functions when users are moving. We discuss these validations in the following.

5.1 User Orthogonality

As shown in Fig. 2, the singular value spreads of the simulated channels match well with those of the measured channels. However, in the simulated channels, the singular value spreads have larger variations. That means, in the simulated channels, we obtain relatively low singular value spreads as well as relatively high singular value spreads. The reason could be lack of statistics in the simulations due to 1) number of simulations, 2) randomness in user movements, 3) diversities in user antenna patterns. We also see similar trends that the singular value spreads become smaller when increasing the number of antennas,

Table 2: Parameters of the COST 2100 model extension for closely-spaced users, extracted from 2.6 GHz measurements, semi-urban outdoor.

Parameter	LOS scenario	NLOS scenario
Number of far clusters		
N_{C}	15	14
Radius of cluster visibility region		
R_{C} [m]	10	10
Radius of cluster transition region		
T_{C} [m]	2	2
Number of MPCs per cluster		
N_{MPC}	400	400
Cluster power decay factor		
k_τ [dB/μs]	79.6	20
Cluster cut-off delay		
τ_{B} [μs]	1.7	1.7
Cluster shadowing		
σ_{S} [dB]	5.8	5
Cluster delay spread		
m_τ [μs]	0.02	0.06
S_τ [dB]	0.01	0.01
Cluster angular spread in azimuth (at BS)		
$m_{\psi_{\mathrm{BS}}}$ [deg]	8.5	9.8
$S_{\psi_{\mathrm{BS}}}$ [dB]	1.9	2.2
Cluster angular spread in elevation (at BS)		
$m_{\theta_{\mathrm{BS}}}$ [deg]	7.0	8.9
$S_{\theta_{\mathrm{BS}}}$ [dB]	1.9	1.9
Cluster angular spread in azimuth (at MS)[1]		
$m_{\psi_{\mathrm{MS}}}$ [deg]	14.8	19
$S_{\psi_{\mathrm{MS}}}$ [dB]	2.68	2.03
Cluster angular spread in elevation (at MS)[2]		
$m_{\theta_{\mathrm{MS}}}$ [deg]	4	7.6
$S_{\theta_{\mathrm{MS}}}$ [dB]	1.6	1.6
Cluster spread cross-correlation		
$\rho_{\tau\sigma_{\mathrm{S}}}$	-0.5	-0.4
$\rho_{\psi_{\mathrm{BS}}\sigma_{\mathrm{S}}}$	-0.8	-0.8
$\rho_{\theta_{\mathrm{BS}}\sigma_{\mathrm{S}}}$	-0.8	-0.7
$\rho_{\psi_{\mathrm{BS}}\tau}$	0.6	0.4
$\rho_{\theta_{\mathrm{BS}}\tau}$	0.4	0.2
$\rho_{\psi_{\mathrm{BS}}\theta_{\mathrm{BS}}}$	0.7	0.7
Radius of LOS visibility region[1]		
R_{L} [m]	343	-
Radius of LOS transition region[1]		
T_{L} [m]	93	-
LOS power factor		
$\mu_{K_{\mathrm{LOS}}}$ [dB]	2.8	-
$\sigma_{K_{\mathrm{LOS}}}$ [dB]	0.8	-
XPR[3]		
μ_{XPR} [dB]	9	8
σ_{XPR} [dB]	3	3
MPC gain function		
σ_g	2.37	2.37

[1]Parameter values adopted from the 300 MHz outdoor measurements for the COST 2100 model [28].
[2]Parameter values adopted from the 3GPP 3D channel model [26].
[3]Parameter values adopted from the WINNER II channel models [24].

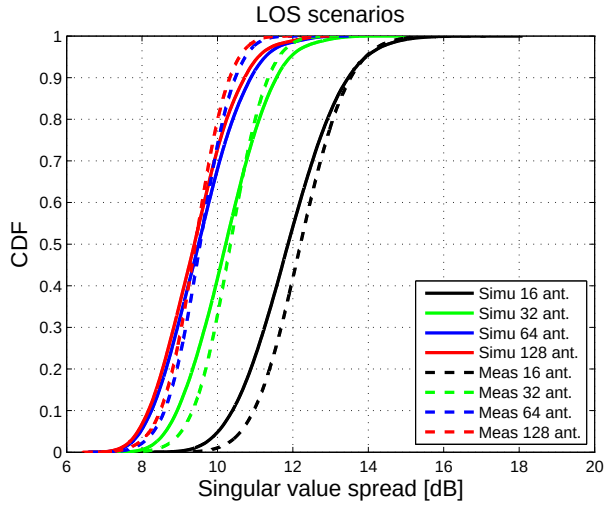

Figure 2: Singular value spreads of the simulated channels and measured channels.

and the difference is very small between the cases of 64 and 128 antennas. The simulation could be improved by introducing more randomness in user movements, and adding crowd effect to the user antenna patterns. This has been left for future work.

5.2 Linear Precoding Sum-Rates

Comparing the CDFs of MF and ZF sum-rates in the simulated and measured channels in Fig. 3, we clearly see larger variations in the simulated channels. This is more obvious in the ZF sum-rates than in the MF sum-rates. It can be explained by the fact that the ZF precoding is more sensitive to the user channel correlation than the MF. Again, it could be due to lack of randomness and statistics in the simulation.

5.3 Temporal Behavior

The temporal behavior of the simulated and measure channels, in terms of auto-correlation when one user is moving, are shown in Fig. 4. The auto-correlation is averaged over different users, snapshots and frequencies. The correlation

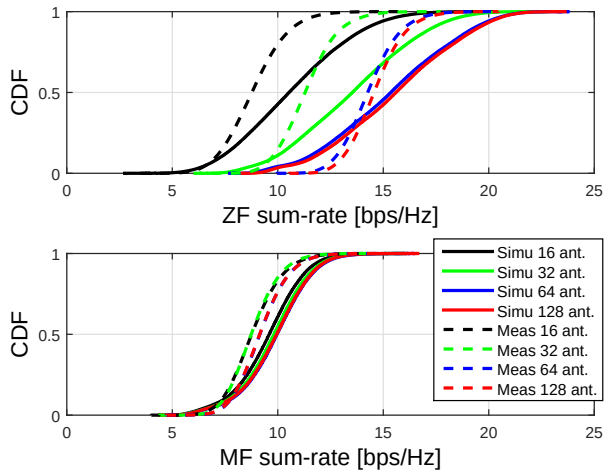

Figure 3: Downlink sum-rates by ZF and MF in the simulated channels and measured channels, when the average interference-free SNR at the users is 10 dB.

coefficient $c(\Delta_t)$ is calculated as below,

$$c(\Delta_t) = \frac{1}{L}\sum_{\ell=1}^{L}\frac{1}{K}\sum_{k=1}^{K}\frac{1}{T}\sum_{t=1}^{T}\left|\frac{\mathbf{h}_{t,k,\ell}\mathbf{h}_{t+\Delta_t,k,\ell}^{H}}{\|\mathbf{h}_{t,k,\ell}\|\,\|\mathbf{h}_{t+\Delta_t,k,\ell}\|}\right|, \tag{3}$$

where $\mathbf{h}_{t,k,\ell}$ is the $1\times M$ channel vector, M is the number of BS antennas, and t, k and ℓ represent snapshots, users and frequencies, respectively. Note that the averaging is performed on the amplitudes of the correlation coefficients in each realization. We see in Fig. 4 that from 0.01 m to 1 m the auto-correlation in the simulated channels matches with that in the measured channels, although the auto-correlation is slightly lower and the variation is larger in the simulated channels. This indicates that with the model extension we are able to capture the temporal behavior of the channels in a small distance.

6 Summary and Conclusions

Based on the massive MIMO channel measurements at 2.6 GHz, we have proposed and implemented a backwards compatible extension of the COST 2100 channel model for massive MIMO. The extension includes:

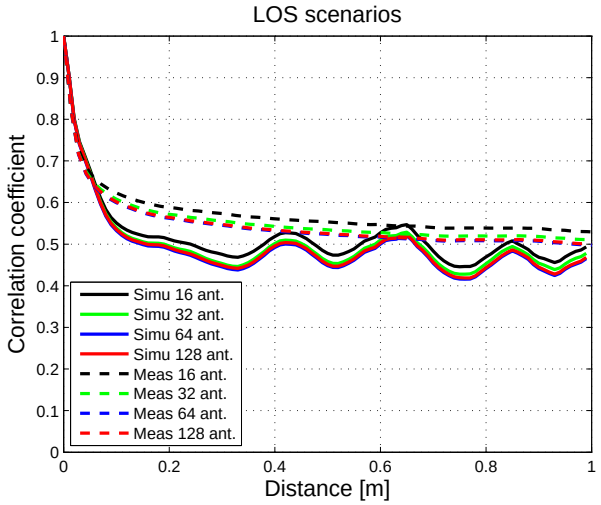

Figure 4: Auto-correlation in distance of the simulated channels and measured channels.

- 3D propagation, as the large arrays at the base station envisioned most likely will have the ability to resolve clusters both in azimuth and elevation;
- Polarization, as dual-polarization at the base station antennas will help to spatially separate the users;
- Cluster behavior at the base station, as spherical wavefronts and large-scale fading can be experienced over physically-large arrays;
- Individual gain functions of individual MPCs, as individual MPCs tend not to be visible in the entire cluster visibility region.

The initial validation showed that the proposed and implemented model extensions are capable of reproducing channel statistics in terms of user separability, MF sum-rates and temporal behavior. The COST 2100 model extension for massive MIMO can be a valuable input for 5G channel modeling. Future work include parametrization of more scenarios and more validations of the model.

References

[1] F. Rusek, D. Persson, B. K. Lau, E. G. Larsson, T. L. Marzetta, O. Edfors, and F. Tufvesson, "Scaling up MIMO: Opportunities and challenges with very large arrays," *IEEE Signal Processing Magazine*, vol. 30, no. 1, pp. 40–60, Jan. 2013.

[2] E. Larsson, O. Edfors, F. Tufvesson, and T. L. Marzetta, "Massive MIMO for next generation wireless systems," *IEEE Communications Magazine*, vol. 52, no. 2, pp. 186–195, Feb. 2014.

[3] T. L. Marzetta, "Massive MIMO: An introduction," *Bell Labs Technical Journal*, vol. 20, pp. 11–22, 2015.

[4] E. Björnson, E. G. Larsson, and T. L. Marzetta, "Massive MIMO: 10 myths and one grand question," Mar. 2015, arXiv:1503.06854.

[5] H. Q. Ngo, E. G. Larsson, and T. L. Marzetta, "Energy and spectral efficiency of very large multiuser MIMO systems," *IEEE Transactions on Communications*, vol. 61, no. 4, pp. 1436–1449, Apr. 2013.

[6] X. Gao, O. Edfors, F. Rusek, and F. Tufvesson, "Massive MIMO performance evaluation based on measured propagation data," *IEEE Transactions on Wireless Communications*, vol. 14, no. 7, pp. 3899–3911, July 2015.

[7] X. Gao, O. Edfors, F. Tufvesson, and E. G. Larsson, "Massive MIMO in real propagation environments: Do all antennas contribute equally?" *IEEE Transactions on Communications*, vol. 63, no. 11, pp. 3917–3928, Nov. 2015.

[8] J. Flordelis, X. Gao, G. Dahman, F. Rusek, O. Edfors, and F. Tufvesson, "Spatial separation of closely-spaced users in measured multi-user massive MIMO channels," in *Proc. IEEE International Conference on Communications (ICC)*, June 2015.

[9] J. Hoydis, C. Hoek, T. Wild, and S. ten Brink, "Channel measurements for large antenna arrays," in *Proc. International Symposium on Wireless Communication Systems (ISWCS)*, Aug. 2012.

[10] S. Payami and F. Tufvesson, "Channel measurements and analysis for very large array systems at 2.6 GHz," in *Proc. European Conference on Antennas and Propagation (EuCAP)*, Mar. 2012.

[11] J. G. Andrews, S. Buzzi, W. Choi, S. V. Hanly, A. Lozano, A. C. K. Soong, and J. C. Zhang, "What will 5G be?" *IEEE Journal on Selected Areas in Communications*, vol. 32, no. 6, pp. 1065–1082, June 2014.

[12] F. Boccardi, R. W. Heath, A. Lozano, T. L. Marzetta, and P. Popovski, "Five disruptive technology directions for 5G," *IEEE Communications Magazine*, vol. 52, no. 2, pp. 74–80, Feb. 2014.

[13] V. Jungnickel, K. Manolakis, W. Zirwas, B. Panzner, V. Braun, M. Lossow, M. Sternad, R. Apelfröjd, and T. Svensson, "The role of small cells, coordinated multipoint, and massive MIMO in 5G," *IEEE Communications Magazine*, vol. 52, no. 5, pp. 44–51, May 2014.

[14] A. Osseiran, F. Boccardi, V. Braun, K. Kusume, P. Marsch, M. Maternia, O. Queseth, M. Schellmann, H. Schotten, H. Taoka, H. Tullberg, M. A. Uusitalo, B. Timus, and M. Fallgren, "Scenarios for 5G mobile and wireless communications: the vision of the METIS project," *IEEE Communications Magazine*, vol. 52, no. 5, pp. 26–35, May 2014.

[15] C.-X. Wang, F. Haider, X. Gao, X.-H. You, Y. Yang, D. Yuan, H. Aggoune, H. Haas, S. Fletcher, and E. Hepsaydir, "Cellular architecture and key technologies for 5G wireless communication networks," *IEEE Communications Magazine*, vol. 52, no. 2, pp. 122–130, Feb. 2014.

[16] J. Vieira, S. Malkowsky, K. Nieman, Z. Miers, N. Kundargi, L. Liu, I. Wong, V. Owall, O. Edfors, and F. Tufvesson, "A flexible 100-antenna testbed for massive MIMO," in *Proc. IEEE Global Communications Conference (GLOBECOM) Workshop on Massive MIMO: From Theory to Practice*, Dec. 2014.

[17] X. Gao, M. Zhu, F. Rusek, F. Tufvesson, and O. Edfors, "Large antenna array and propagation environment interaction," in *Proc. Asilomar Conference on Signals, Systems, and Computers (ASILOMAR)*, Nov. 2014.

[18] X. Gao, F. Tufvesson, and O. Edfors, "Massive MIMO channels – measurements and models," in *Proc. Asilomar Conference on Signals, Systems, and Computers (ASILOMAR)*, Nov. 2013.

[19] "MaMi channel characteristics: Measurement results," MAMMOET D1.2 V1.0, June 2015.

[20] X. Gao, F. Tufvesson, O. Edfors, and F. Rusek, "Channel behavior for very-large MIMO systems – initial characterization," in *COST IC1004*, Sept. 2012.

[21] Z. Zhou, X. Gao, J. Fang, and Z. Chen, "Spherical wave channel and analysis for large linear array in LoS conditions," in *Proc. IEEE Global Communications Conference (GLOBECOM) Workshop on Massive MIMO: From Theory to Practice*, Dec. 2015.

[22] R. Zentner and A. Katalinic, "Dynamics of multipath variations in urban environment," in *Proc. European Wireless Technology Conference (EuWIT)*, Sept. 2010.

[23] L. Liu, C. Oestges, J. Poutanen, K. Haneda, P. Vainikainen, F. Quitin, F. Tufvesson, and P. D. Doncker, "The COST 2100 MIMO channel model," *IEEE Wireless Communications*, vol. 19, no. 6, pp. 92–99, Dec. 2012.

[24] P. Kyösti, J. Meinilä, L. Hentilä, X. Zhao, T. Jämsä, C. Schneider, M. Narandzić, M. Milojević, A. Hong, J. Ylitalo *et al.*, "WINNER II channel models," IST-4-027756 WINNER II D1.1.2 V1.2, 2008.

[25] S. Wu, C.-X. Wang, E.-H. Aggoune, M. Alwakeel, and Y. He, "A non-stationary 3-D wideband twin-cluster model for 5G massive MIMO channels," *IEEE Journal on Selected Areas in Communications*, vol. 32, no. 6, pp. 1207–1218, June 2014.

[26] *Study on 3D channel model for LTE*, 3GPP TR 36.873 V12.1.0, Mar. 2015.

[27] X. Gao, M. Zhu, F. Tufvesson, F. Rusek, and O. Edfors, "Extension of the COST 2100 channel model for massive MIMO," in *COST IC1004*, Jan. 2015.

[28] M. Zhu, G. Eriksson, and F. Tufvesson, "The COST 2100 channel model: Parameterization and validation based on outdoor MIMO measurements at 300 Mhz," *IEEE Transactions on Wireless Communications*, vol. 12, no. 2, pp. 888–897, Feb. 2013.

Paper VI

Massive MIMO in Real Propagation Environments: Do All Antennas Contribute Equally?

Massive MIMO can greatly increase both spectral and transmit-energy efficiency. This is achieved by allowing the number of antennas and RF chains to grow very large. However, the challenges include high system complexity and hardware energy consumption. Here we investigate the possibilities to reduce the required number of RF chains, by performing antenna selection. While this approach is not a very effective strategy for theoretical independent Rayleigh fading channels, a substantial reduction in the number of RF chains can be achieved for real massive MIMO channels, without significant performance loss. We evaluate antenna selection performance on measured channels at 2.6 GHz, using a linear and a cylindrical array, both having 128 elements. Sum-rate maximization is used as the criterion for antenna selection. A selection scheme based on convex optimization is nearly optimal and used as a benchmark. The achieved sum-rate is compared with that of a very simple scheme that selects the antennas with the highest received power. The power-based scheme gives performance close to the convex optimization scheme, for the measured channels. This observation indicates a potential for significant reductions of massive MIMO implementation complexity, by reducing the number of RF chains and performing antenna selection using simple algorithms.

Xiang Gao, Ove Edfors, Fredrik Tufvesson, Erik G. Larsson,
"Massive MIMO in Real Propagation Environments: Do All Antennas Contribute Equally?"
in *IEEE Transactions on Communications*, vol. 63, no. 11, pp. 3917-3928, Nov. 2015.

1 Introduction

Massive MIMO [1–5] is an emerging technology in wireless access. By using a large number (tens to hundreds) of antennas at the base station, and serving many users in the same time-frequency resource, massive MIMO can improve the spectral and transmit-energy efficiency of conventional MIMO by orders of magnitude [6–9], and simple signal processing schemes are expected to achieve near-optimal performance [10–12]. The basic premise of massive MIMO is that, as confirmed by several experiments [13–16], the propagation channel has a large number of spatial degrees of freedom. Massive MIMO is currently considered a leading 5G technology candidate [17–21]. Real-time massive MIMO testbeds are being implemented and demonstrations are also reported [22–25]. However, with a large number of antennas and associated transceiver chains, the challenges of massive MIMO include high system complexity and hardware power consumption [26–29].

This paper investigates whether all antennas in a massive MIMO system contribute equally to the overall performance or not. Experimental data from measurement campaigns at the 2.6 GHz band are used to demonstrate that in many cases, the antennas do *not* contribute equally. This observation paves the way for antenna selection algorithms and for hardware architectures where the number of activated radio-frequency (RF) transceiver chains is less than the actual number of antennas. Antenna selection algorithms for such architectures are then proposed and their performance is analyzed. The practical impact of the proposed techniques is that the overall energy efficiency of massive MIMO systems can be substantially improved, and the hardware complexity can be reduced.

The rest of the paper is organized as follows. In Sec. 2 we discuss the general background, and introduce the antenna selection concept. Sec. 3 outlines the approach we have chosen for the study. In Sec. 4 we describe the system model and present two antenna selection schemes. In Sec. 5 we describe the channel measurement setup used to obtain the experimental results. Then in Sec. 6 we present performance results with antenna selection, and discuss the effectiveness of the proposed algorithms and how many transceiver chains that are needed under different operating conditions. Conclusions are given in Sec. 7.

2 Background

In "ideal" independent and identically distributed (i.i.d.) Rayleigh fading channels, all the antennas can be expected to contribute equally to the system per-

formance. To see why, consider a multi-user MIMO-OFDM system with L subcarriers and suppose the base station has an array with M antennas that serves K users. Denote the $M \times 1$ channel vector for a given user k and a given subcarrier ℓ by $\boldsymbol{g}_k(\ell)$. In i.i.d. Rayleigh fading channels, all antennas are equally good in the sense that

$$\frac{1}{K}\sum_{k=1}^{K}\frac{1}{L}\sum_{\ell=1}^{L}|\boldsymbol{g}_{k,m}(\ell)|^2 \approx \text{constant} \qquad \text{for all } m, \tag{1}$$

where the constant is independent of the antenna index m. This means that provided the bandwidth is relatively large and the number of users is large, no antenna outperforms the others.

In real propagation channels, however, the situation is different. Here, all the antennas contribute, but some antennas contribute more than others. In the study based on measured channels at the 2.6 GHz band, using a linear array of omni-directional antennas and a cylindrical array of patch antennas, both having 128 elements, we have observed that over the measured 50 MHz bandwidth the average power variations across the two arrays can be significant [30–32]. As an example, the angular power spectrum (APS) and power variation over the 7.4 m linear array are shown in Fig. 1, for a line-of-sight (LOS) scenario and a non-line-of-sight (NLOS) scenario, respectively. Unlike in conventional MIMO (thought of here as up to 8 antennas as in LTE [33]), the characteristics of the propagation channel across the linear array vary significantly. In Fig. 1(a) and Fig. 1(b), some scatterers are not visible over the whole array, and for scatterers that are visible over the whole array, the power contributions vary considerably. Consequently, in Fig. 1(c) and Fig. 1(d), we observe large power variations over the array, about 7 dB in the LOS scenario and 4 dB in the NLOS scenario. Thus, large-scale fading is experienced over the array. The compact cylindrical array, which is smaller in size, experiences a similar effect of power variation over the array. This is, however, due to its circular structure and patch antenna arrangement, rather than large-scale fading. In contrast to i.i.d. Rayleigh fading channels, in real massive MIMO channels the large power variation makes some antennas more "useful" than others, and this power variation persists when averaging over frequency provided that the system is moderately wideband.

Since all antennas are not equally good in real propagation channels, it is possible to reduce the number of active antennas and transceivers, by selecting those that contribute the most and discarding the rest. Such antenna selection could simplify the design of a massive MIMO base station and lead to energy and cost savings. One possible implementation is to deploy a large number of antennas but fewer RF transceivers, exploiting the fact that antennas are

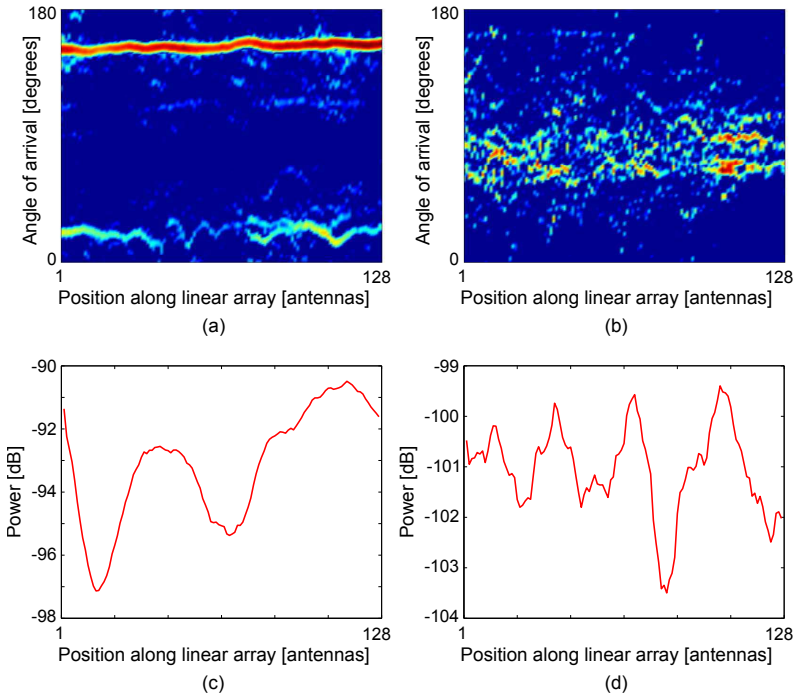

Figure 1: Angular power spectrum and power variation over a 7.4 m linear array, in the measured channels as reported in [30] and [32]. The four plots show: (a) angular power spectrum in a LOS scenario, (b) angular power spectrum in a NLOS scenario, (c) average power variation in the LOS scenario, (d) average power variation in the NLOS scenario.

relatively cheap while RF chains are expensive and energy consuming. In this case, we need an RF switch, which can be highly complex to implement and introduces losses in signal quality, especially when there are many antennas and transceivers. Another implementation option is to deploy an equal number of transceivers and antennas, and then simply turn on the transceivers corresponding to the selected antennas while turning off the rest. This implementation is illustrated in Fig. 2 and is more flexible as the number of active antennas can be variable. With power switches, the reduction in system complexity relies on simpler implementation of the baseband signal processing due to a reduced number of active antennas and RF chains. However, with a variable number of active antennas, the antenna selection algorithms will add extra complexity, e.g., in making a decision on the optimal number of antennas.

Antenna selection has been widely studied for conventional MIMO, see for example [34–42]. However, to the best of our knowledge, there are only few studies on antenna selection for massive MIMO available. In [43], antenna selection in massive MIMO was addressed for short-range wireless communications at 60 GHz. In [44], a simulation study using the Kronecker channel model [45] showed that significantly higher performance can be achieved with antenna selection than without. In [46], antenna selection for maximizing signal-to-noise ratio (SNR) was studied, and [47] considered antenna selection jointly with user scheduling for massive MIMO. The authors in [48] evaluated the characteristics of interference rejection with antenna sector selection in massive MIMO, based on measured channels in the 2 GHz band with 96 antenna elements. In the conference paper [49], we presented preliminary results on antenna selection in measured massive MIMO channels. The current paper extends [49] by studying in more depth how many RF chains that can be switched off while achieving a required performance, by considering more scenarios and propagation conditions, and by performing comparisons with suboptimal precoding schemes.

3 Approach

The aim of this paper is to obtain a deeper insight into how antenna selection in massive MIMO performs in real propagation channels. Specifically, we focus on how the number of users, the separation of users, and propagation conditions like LOS and NLOS affect the performance of antenna selection. Although the large power variation across antennas remains when averaging over frequencies, the effectiveness of the antenna selection can be reduced if the user channels to the base station are very distinct. This happens when users are located far apart and when many users are served. It is demonstrated that in the “worst

case", adaptive antenna selection does not perform significantly better than random selection, but in many cases adaptive selection substantially improves over random selection. All investigations use the measured channel data at 2.6 GHz described above, obtained with linear and cylindrical arrays.

In terms of algorithms, we select the set of active antennas that maximizes the downlink capacity. To find the optimal set, an exhaustive search can be used; however this is infeasible for massive MIMO in practice due to the huge number of possible selection alternatives. A number of antenna selection algorithms with lower complexity, notably greedy selection, have been proposed for conventional MIMO, and many of them can be applied to massive MIMO. We first examine a near-optimal scheme that uses convex optimization [49–51]. We then consider a very simple selection scheme that is based only on measurements of the received power at each antenna. Generally, this power-based selection scheme underperforms the convex-optimization based scheme that considers not only the received power but also the correlation between antenna channels. Yet, experiments with measured data show that the power-based scheme performs fairly well. This is so because the power variations over the array can be considerable in massive MIMO.

4 System Description and Antenna Selection Schemes

We first establish the system model that will be used in the rest of the paper. We also formally state the problem of antenna selection for downlink capacity maximization, and introduce the two selection schemes: a near-optimal scheme relying on convex optimization, and a simple scheme using only received signal power measurements.

4.1 System Model and Sum-Capacity

We consider a single-cell multi-user MIMO-OFDM system with L subcarriers in the downlink. As shown in Fig. 2, the base station has M antennas, and each antenna has an associated transceiver chain. With N antennas being selected, the N corresponding transceivers are switched on, while the other $M-N$ are switched off. This base station with N active antennas and transceivers serves K single-antenna users in the same time-frequency resource. With massive MIMO, we assume $M \gg K$ and allow N to be in the range from K to M.

The model for the downlink channel is

$$\boldsymbol{y}_\ell = \sqrt{\rho K}\boldsymbol{H}_\ell^{(N)}\boldsymbol{z}_\ell + \boldsymbol{n}_\ell, \tag{2}$$

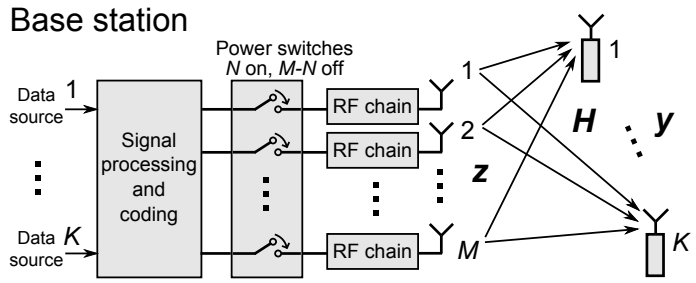

Figure 2: Multi-user MIMO system with transmit antenna selection. The base station has M available antennas and N active RF chains, and serves K single-antenna users in the same time-frequency resource. The switches indicate that entire RF chains are being switched on or off.

where $\boldsymbol{H}_\ell^{(N)}$ is a $K \times N$ channel matrix at subcarrier ℓ, and the superscript (N) indicates that antenna selection has been performed, i.e., the N columns of $\boldsymbol{H}_\ell^{(N)}$ are selected from the $K \times M$ full channel matrix $\boldsymbol{H}_\ell$. Normalization is performed such that the elements of $\boldsymbol{H}_\ell^{(N)}$ have unit energy, averaged over all L subcarriers, M antennas and K users, see [14] for more details. Then $\boldsymbol{z}_\ell$ is the $N \times 1$ transmit vector across the N selected antennas, and satisfies $\mathbb{E}\left\{\|\boldsymbol{z}_\ell\|^2\right\} = 1$, $\boldsymbol{y}_\ell$ is the received vector at the K users, and $\boldsymbol{n}_\ell$ is a noise vector with i.i.d. complex Gaussian, $CN(0,1)$, elements. The factor ρK represents the transmit power. With the conventions used in this paper, the transmit power per user is fixed. Hence, the total transmit power increases with K but is independent of N. The parameter ρ represents the normalized transmit SNR per user. With random antenna selection, the average per-user received SNR would be ρN,[9] which increases with the number of selected antennas N due to the increased array gain. When the number of users K varies, the average per-user received SNR is constant, and so is the average per-user rate (disregarding interference), if a fixed number N of RF transceivers are switched on. With adaptive antenna selection, the received SNRs are expected to be higher than those with random antenna selection, since the "best" antennas are selected.

[9]The received SNRs at the users in general depend on precoding scheme and the channel conditions. For example, in the single-user case, the received SNR is ρN. In the multi-user case with zero-forcing precoding, the per-user received SNR is $\rho K / \mathrm{Tr}\{(\boldsymbol{H}_\ell^{(N)}(\boldsymbol{H}_\ell^{(N)})^H)^{-1}\}$, where $\mathrm{Tr}\{\cdot\}$ represents the trace of a matrix. When the user channels are orthogonal, $\boldsymbol{H}_\ell^{(N)}(\boldsymbol{H}_\ell^{(N)})^H$ is diagonal, and the average per-user received SNR reaches the upper bound given by the single-user case, i.e., ρN. Under "favorable" propagation conditions [52], the user channels becomes orthogonal when the number of base station antennas grows, thus the average received SNR approaches this upper bound.

To avoid favoring users that have a better average channel, we normalize the channel matrix to remove the effects of the pathloss and the large-scale fading while retaining the effects of the small-scale fading. Specifically, when the users are far apart, we normalize the channel matrix according to Normalization 1 in [14], and when the users are closely located, Normalization 2 in [14] is applied. However, importantly, we do not normalize the channel variations per base station antenna, since these variations are critical for the antenna selection.

With the defined signal model, the downlink sum-capacity at subcarrier ℓ is given by [53]:

$$C_{\mathrm{DPC},\ell} = \max_{\boldsymbol{P}_\ell} \log_2 \det \left(\boldsymbol{I} + \rho K \left(\boldsymbol{H}_\ell^{(N)} \right)^H \boldsymbol{P}_\ell \boldsymbol{H}_\ell^{(N)} \right), \tag{3}$$

which is achieved using dirty-paper coding (DPC) [54]. In (3), $\boldsymbol{P}_\ell$ is a diagonal power allocation matrix with $P_{\ell,i}, i=1,2,...,K$ on its diagonal. Also, in (3), the optimization is performed subject to the total power constraint that $\sum_{i=1}^{K} P_{\ell,i} = 1$. This optimization problem is convex and can be solved, for example, by using the sum-power iterative waterfilling algorithm in [55].

DPC is highly complex to implement in practice. However, there are sub-optimal linear precoding schemes, such as zero-forcing (ZF) precoding that is much less complex and performs fairly well for massive MIMO [13, 56]. The sum-rate achieved by ZF precoding is [57]

$$C_{\mathrm{ZF},\ell} = \max_{\boldsymbol{Q}_\ell} \sum_{i=1}^{K} \log_2 \left(1 + \rho K Q_{\ell,i}\right), \tag{4}$$

where $Q_{\ell,i}$ represent received SNRs of the different users and the maximization is performed subject to the total power constraint

$$\sum_{i=1}^{K} Q_{\ell,i} \left[\left(\boldsymbol{H}_\ell^{(N)} \left(\boldsymbol{H}_\ell^{(N)} \right)^H \right)^{-1} \right]_{i,i} = 1. \tag{5}$$

In (4) and (5), $\boldsymbol{Q}_\ell$ is a diagonal matrix with $Q_{\ell,i}, i=1,2,...,K$ on its diagonal, and $[\cdot]_{i,i}$ indicates the i-th diagonal element of a matrix. The diagonal elements of $(\boldsymbol{H}_\ell^{(N)}(\boldsymbol{H}_\ell^{(N)})^H)^{-1}$ represent the power penalty of nulling out interference. The optimization in (4) can be solved using the standard waterfilling algorithm [58].

We choose to base the antenna selection algorithms on the DPC sum-capacity. However, performance of the resulting selection will be evaluated in terms of ZF sum-rate too, in relevant cases. Note that different antenna

combinations can be optimal on different subcarriers. However, in a practical MIMO-OFDM system, the same antennas need to be selected for all subcarriers. Therefore, our algorithms will find a set of N antennas that maximizes the DPC capacity averaged over all L subcarriers.

To select the N columns from the full MIMO matrix $\boldsymbol{H}_\ell$, we introduce an $M \times M$ diagonal matrix $\boldsymbol{\Delta}$, with binary diagonal elements

$$\Delta_i = \begin{cases} 1, & \text{selected} \\ 0, & \text{otherwise,} \end{cases} \tag{6}$$

indicating whether the ith antenna is selected, and satisfying $\sum_{i=1}^{M} \Delta_i = N$. Using Sylvester's determinant identity, $\det(\boldsymbol{I}+\boldsymbol{AB}) = \det(\boldsymbol{I}+\boldsymbol{BA})$, we can write the DPC sum-capacity in (3) in terms of $\boldsymbol{\Delta}$ as

$$\begin{aligned} C_{\mathrm{DPC},\ell} &= \max_{\boldsymbol{P}_\ell} \log_2 \det\left(\boldsymbol{I} + \rho K \boldsymbol{P}_\ell \boldsymbol{H}_\ell^{(N)} \left(\boldsymbol{H}_\ell^{(N)}\right)^H\right) \\ &= \max_{\boldsymbol{P}_\ell} \log_2 \det\left(\boldsymbol{I} + \rho K \boldsymbol{P}_\ell \boldsymbol{H}_\ell \boldsymbol{\Delta} \boldsymbol{H}_\ell^H\right), \end{aligned} \tag{7}$$

subject to $\sum_{i=1}^{K} P_{\ell,i} = 1$. The optimal $\boldsymbol{\Delta}$ (common to all subcarriers) is found by maximizing the average DPC capacity,

$$\boldsymbol{\Delta}_{\mathrm{opt}} = \arg\max_{\boldsymbol{\Delta}} \frac{1}{L} \sum_{\ell=1}^{L} \left\{\log_2 \det\left(\boldsymbol{I}+\rho K \boldsymbol{P}_\ell \boldsymbol{H}_\ell \boldsymbol{\Delta} \boldsymbol{H}_\ell^H\right)\right\}. \tag{8}$$

With the resulting antenna selection, we have the corresponding ZF sum-rate

$$C_{\mathrm{ZF},\ell} = \max_{\boldsymbol{Q}_\ell} \sum_{i=1}^{K} \log_2(1 + \rho K Q_{\ell,i}), \tag{9}$$

subject to

$$\sum_{i=1}^{K} Q_{\ell,i} \left[\left(\boldsymbol{H}_\ell \boldsymbol{\Delta}_{\mathrm{opt}} \boldsymbol{H}_\ell^H\right)^{-1}\right]_{i,i} = 1. \tag{10}$$

Note that $\boldsymbol{\Delta}_{\mathrm{opt}}$ may not be optimal for ZF. Despite this, the ZF sum-rate indicates the antenna selection performance when using a more practical precoding scheme than DPC.

As discussed in Sec. 1, exhaustive search of all possible combinations of N antennas will certainly give us the optimal $\boldsymbol{\Delta}$, however, it is extremely complex and infeasible for massive MIMO. We next introduce two practical selection schemes that will be used in our performance study in Sec. 4.2 and Sec. 4.3.

4.2 Antenna Selection Using Convex Optimization

Here we assume that the base station has perfect channel state information (CSI). The near-optimal selection scheme using convex optimization was introduced and used in [49]. We give a brief description in the following. As can be seen in (8), to maximize the average DPC capacity over subcarriers, we need to optimize over both $\boldsymbol{\Delta}$ and $\boldsymbol{P}_\ell$. This is a difficult task and we therefore divide the optimization into two steps: 1) we assume equal power allocation among the users, i.e., $P_{\ell,i} = 1/K$, and select the N antennas that maximize the average capacity; 2) with the selected N antennas, we optimize over $\boldsymbol{P}_\ell$ on each subcarrier, and thus obtain the maximum average capacity for the case of N antennas. Although this simplification does not ensure that we find the global optimum, it gives us a lower bound on the performance we can achieve by using adaptive antenna selection.

In Step 1, the optimization problem of antenna selection can be formulated as

$$\begin{aligned} \text{maximize} \quad & \frac{1}{L}\sum_{\ell=1}^{L}\left\{\log_2 \det\left(\boldsymbol{I} + \rho \boldsymbol{H}_\ell \boldsymbol{\Delta} \boldsymbol{H}_\ell^H\right)\right\}, \\ \text{subject to} \quad & \Delta_i \in \{0,1\} \\ & \sum_{i=1}^{M} \Delta_i = N. \end{aligned} \tag{11}$$

The objective function is concave in $\boldsymbol{\Delta}$ [59]. However, the variables Δ_i are binary integer variables, which makes the optimization problem NP-hard. In order to solve this optimization problem, as in [50, 51], we relax the constraint that each Δ_i must be binary integer to the weaker constraint that $0 \le \Delta_i \le 1$. The original problem thus becomes a convex optimization problem solvable in polynomial time. This relaxation yields a solution with non-integral values of Δ_i. From the relaxed solution, the N largest Δ_i are selected, and their indices represent the selected antennas. As discussed in [49–51], the relaxation gives near-optimal results, except for when we select a very small number of antennas, i.e., $N \ll M$. In a massive MIMO system, N should be relatively large and therefore we believe that the relaxation method is technically sound.

4.3 Antenna Selection Based on Received Power

Using only the received power per antenna as the basis for antenna selection results in a very simple scheme. We select the N antennas that have the highest received power from all K users, averaged over all L subcarriers. As compared to the convex-optimization based scheme, the power-based scheme has very

low complexity. By only measuring the received power at each antenna branch in the uplink (exploiting channel reciprocity), we can make a decision on the antenna selection for the downlink before any CSI estimation is performed and without complex signal processing. As discussed in Sec. 1, this simple selection scheme generally shows worse performance than the convex-optimization scheme. However, in situations when all antenna channels have relatively low correlation, e.g., in NLOS scenarios with rich scattering, the power-based selection scheme may become near-optimal. We compare the performance obtained through the two selection schemes with measured channels, for different propagation scenarios, in Sec. 6.

5 Measured Channels

The channel measurements used in this paper were first reported in [13, 14]. Here, we give a brief summary.

Measurements were taken over bandwidth of 50 MHz on the 2.6 GHz band, using two different large antenna arrays (cylindrical and linear) at the base station. Both arrays contain 128 antenna elements and have an adjacent element spacing of half a wavelength. Fig. 3(a) shows the cylindrical array, comprising 16 dual-polarized directional patch antennas in each circle with 4 such circles stacked on top of each other, giving a total of 128 antenna ports. This array is physically compact with physical dimensions (both diameter and height) of about 30 cm. Fig. 3(b) shows the virtual linear array with a vertically-polarized omni-directional antenna moving between 128 equidistant positions, along a rail. The linear array is 7.4 m long, which is more than 20 times the size of the cylindrical array. In both measurement campaigns, an omni-directional antenna with vertical polarization was used at the user side.

All measurements were carried out outdoors at the E-building of the Faculty of Engineering (LTH) of Lund University in Sweden. Fig. 4 shows an overview of the semi-urban measurement area. The two base station antenna arrays were placed on the same roof of the E-building during their respective measurement campaigns. More precisely, the cylindrical array was positioned on the same line as the linear array, near its beginning, and was for practical reasons mounted about 25 cm higher than the linear array. At the user side, the omni-directional antenna was moved between eight measurement sites (MS 1-8) around the E-building, emulating single-antenna users. Among these eight sites, three (MS 1-3) have LOS conditions, and four (MS 5-8) have NLOS conditions, while one (MS 4) has LOS for the cylindrical array, whereas the LOS component is blocked by the roof edge for the linear array. Despite this, MS 4 still has LOS characteristic for the linear array, where one or two dominating multipath

Figure 3: Two large antenna arrays at the base station side: a) a cylindrical array with 64 dual-polarized patch antenna elements, giving 128 ports in total, and b) a virtual linear array with 128 vertically-polarized omni-directional antennas.

components due to diffraction at the roof edge cause a relatively high Ricean K-factor [60].

The investigations in [13] and [14] showed that the linear array achieves higher average sum-rates than the cylindrical array, if we randomly select the same number of antennas on both arrays. The reason is that the linear array has very high angular resolution due to its large aperture, which helps to spatially separate the users, especially when users are closely located at the same measurement site. The cylindrical array has smaller aperture thus lower angular resolution, and due to its circular arrangement some antennas may face the "wrong" directions and contribute little. With a vertically-polarized antenna at the user side, the dual-polarization arrangement at the base station also degrades the performance of the cylindrical array, but only to a certain extent. In the measured channels, the received power ratios of the vertically-polarized and horizontally-polarized antenna ports are approximately log-normal distributed, with a mean value of 2.2 dB and a standard deviation of 8 dB in the dB domain. Note that the above investigations and comparisons are based on the spatial structure of the two arrays, when the two arrays have equal average channel gain due to the performed normalization, as discussed in Sec. 4. In reality, however, the cylindrical array may perform better than what we have seen, when the antenna gains of the patch elements are taken into account. Also, antennas at the user side are usually dual-polarized in reality, making both polarizations at the base station useful for user separation [16]. However, it is not a priori clear which array that performs better, if we adaptively select

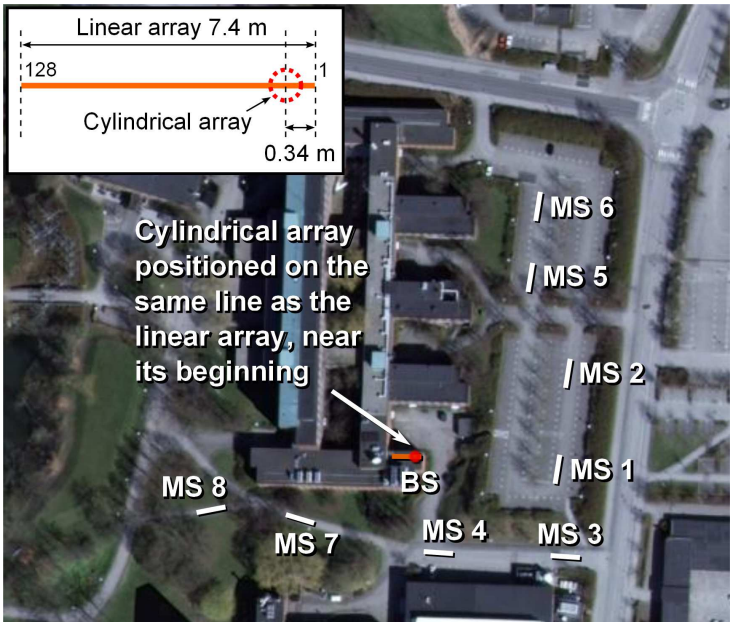

Figure 4: Overview of the measurement area at the Faculty of Engineering (LTH) campus at Lund University in Sweden. The two base station antenna arrays were placed on the same roof of the E-building. At the user side, eight sites (MS 1-8) around the E-building were measured.

antennas. We investigate this matter in the next section.

6 Performance Results in Measured Channels

With the obtained channel data, we apply antenna selection, as described in Sec. 4, for both arrays, in different propagation scenarios and for different number of users. Note that all results are obtained from the measured channels. First we focus on the convex-optimization scheme, since it gives us near-optimal results. We investigate how much we can gain by performing antenna selection, as compared to random selection, and how many RF transceivers we can switch off while maintaining 90% of full MIMO performance. Then we move to the simple selection scheme based on only received power measurements, and compare the corresponding performance with that of the convex-optimization scheme.

The parameter setting for evaluating antenna selection performance is as follows. We have $M = 128$ antennas at the base station, among which we select the N that works "best" across all $L = 161$ subcarriers, depending on which antenna selection scheme is used. We perform antenna selection for N growing from K to 128. When $N = 128$, we have the full MIMO performance. We study cases where the number of users, K, is 4, 16 and 40, respectively. In all cases, we set $\rho = -5$ dB, so that in the interference-free case and with random antenna selection the average per-user rate is in the range of 1.2-5.4 bps/Hz, as N grows to 128 and the array gain increases accordingly. The range of the per-user rate does not depend on the number of users, since we maintain the same transmit power per user, as discussed in Sec. 4. Next, we present and discuss the results.

6.1 Performance of Convex-Optimization Selection Scheme

To investigate the effectiveness of antenna selection in different propagation scenarios, we first focus on the case of four users ($K = 4$), which is the number of simultaneous users supported in multi-user MIMO transmission in LTE [33]. Then we increase the number of users to sixteen ($K = 16$) and forty ($K = 40$), and investigate the corresponding performance, as massive MIMO is capable of serving more users.

Four Users, $K = 4$

Combining user separation and LOS/NLOS condition, here we choose two reference scenarios to study, in which the four users are

- close to each other (1.5-2 m spacing), all at MS 2, having LOS conditions to the base station,
- well separated (larger than 10 m spacing), at MS 5-8, respectively, all having NLOS conditions to the base station.

We expect more effective use of antenna selection in the first scenario, since the channels are less frequency-selective and less distinct to different users. In the second scenario, there is higher frequency selectivity due to the NLOS conditions. Also, the users are more widely separated. Hence, it is expected that the combination of antennas that are optimal for a given user on a given subcarrier differs between the users and the subcarriers. Antenna selection, where the same antennas are used for all subcarriers and all users, will therefore be less effective in this scenario.

The resulting DPC capacities and ZF sum-rates by performing antenna selection are shown in Fig. 5 and Fig. 6, for the two scenarios, respectively. As a reference, we also show the antenna selection performance in i.i.d. Rayleigh channels. We can see that in i.i.d. Rayleigh channels the performance gain by applying adaptive antenna selection is very small, both in DPC capacity and ZF sum-rate, as compared to the average performance obtained from random selection of antenna combinations. This indicates that antenna selection is quite ineffective in i.i.d. Rayleigh channels, since all antennas are equally good, as discussed in Sec. 2.

In Fig. 5 where the four users are closely located with LOS, the measured channels provide significantly larger gain when performing antenna selection, for both arrays. With 40 RF transceivers, i.e., 10 times the number of users, for the linear array with antenna selection, the DPC capacity and ZF sum-rate increase by 11% and 18%, as compared to the performance of random selection. For the cylindrical array the gain is even higher, more than 30%, both in DPC capacity and ZF sum-rate. We can also see the performance loss when switching off RF transceivers. For the linear array, about 70 RF transceivers can achieve 90% of the full MIMO performance, with both DPC and ZF precoding. For the cylindrical array, only about 50 and 60 are needed, with DPC and ZF, respectively, thus more than half of the RF transceivers can be switched off. This can be explained that in this particular scenario many antennas on the cylindrical array do not "see" the users.

We next consider the scenario where the four users have NLOS conditions and are well separated. As shown in Fig. 6, the performance gain when performing adaptive antenna selection drops in the measured channels, compared to the previous scenario. The higher frequency selectivity due to NLOS conditions and the wider separation of users indeed reduce the effectiveness of antenna selection to some extent. Despite this, we still observe some gains in

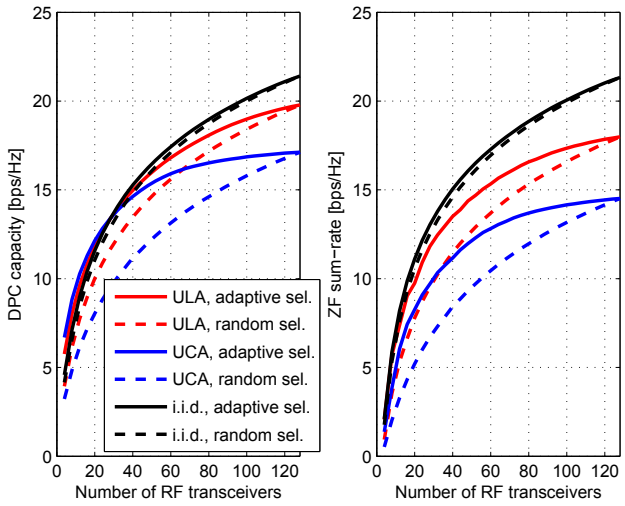

Figure 5: Performance of adaptive antenna selection using the convex-optimization scheme, as compared to performance of random selection, in the LOS scenario where four users are closely located at MS 2. "ULA" and "UCA" stand for uniform linear array and uniform cylindrical array, respectively.

the measured channels, as compared to i.i.d. Rayleigh channels. At 40 RF transceivers, using adaptive antenna selection, we increase both the DPC capacity and ZF sum-rate by 10% for the linear array, and 20% for the cylindrical array, as compared to random selection. Correspondingly, to achieve 90% of the full MIMO performance, a slightly higher number of RF transceivers are needed in this scenario. For the linear array, we need 80 RF transceivers, while for the cylindrical array, we need around 60, with both DPC and ZF. Still, a large number of RF transceivers can be switched off in this scenario.

From Fig. 6, another important observation in this scenario is that by using adaptive antenna selection, the measured channels with both arrays achieve higher performance than i.i.d. Rayleigh channels, except for when nearly all transceivers are active. With random selection, i.i.d. Rayleigh channels give better average performance than the measured channels, also reported in [14]. However, by exploiting the large number of spatial degrees of freedom in the measured channels through adaptive antenna selection, the transmit energy is fed to those "best" antennas with relatively high channel gains and relatively low correlation between each other, thus performance increases. Compare with the LOS scenario in Fig. 5; there the measured channels cannot outperform i.i.d. Rayleigh channels. The reason is that the spatial separation is particularly difficult for the closely-spaced users under LOS, therefore, even with adaptive antenna selection, the performance in the measured channels cannot surpass that of i.i.d. channels. In the NLOS scenario, however, the channel correlation between the well-separated users is relatively low, as in i.i.d. Rayleigh channels, hence, by selecting the antennas with relatively high channel gains, the measured channels outperform i.i.d. Rayleigh channels. Especially for the cylindrical array, the performance is significantly improved, and is higher than that of the linear array, for a large range of active transceiver numbers. Thus, adaptive antenna selection provides an opportunity for the cylindrical array to achieve higher performance. Taking practical deployments into consideration, this small and compact array is preferable to the physically large linear array.

From the above evaluation, adaptive antenna selection is effective in both scenarios. We gain significantly not only in DPC sum-capacity, which is our antenna selection criterion, but also in the sum-rate obtained by more practical ZF precoding. With four users, we can switch off 50-60 RF transceivers for the linear array, and 70-80 RF transceivers for the cylindrical array, while only losing 10% of full MIMO performance. However, if more users are served, more antennas and transceivers are required to spatially separate users. In this case, since more antennas are contributing, can we still switch off many RF transceivers? Next we increase the number of users to sixteen ($K = 16$) and forty ($K = 40$), and investigate the corresponding antenna selection performance.

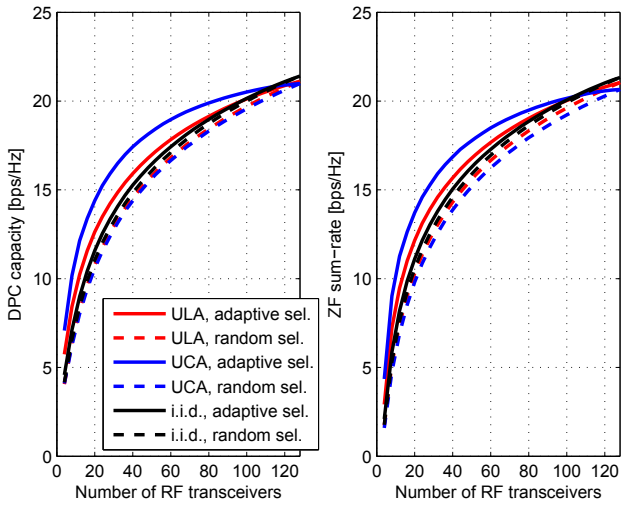

Figure 6: Performance of adaptive antenna selection using the convex-optimization scheme, as compared to performance of random selection, in the NLOS scenario where four users are well separated at MS 5-8. "ULA" and "UCA" stand for uniform linear array and uniform cylindrical array, respectively.

Sixteen and Forty Users, $K=16$ and $K=40$

Here we have sixteen or forty users distributed at MS 1-8. When $K=16$, two users are at the same site with 5 m spacing. When $K=40$, five users placed at each site with 0.5-2 m spacing. Users at different sites are spaced more than 10 m apart. Among these users, half have LOS conditions and half have NLOS conditions.

The antenna selection performance is shown in Fig. 7. The case of four users from Fig. 6 is also included for comparison. When the number of users increases, the DPC capacity increases. With ZF precoding, however, the sum-rate for more users can be lower, i.e., when the number of active transceivers is close to the number of users. For example, with 16 antennas, the sum-rate with 16 users is lower than with four users and with 40 antennas, the sum-rate for 40 users is also lower than with four users. This is due to high inter-user interference when the number of active antennas is not large enough to spatially separate the users. In this case, ZF has to waste a large amount of power on nulling the user interference. With more transceivers being switched on, user interference reduces and ZF sum-rate increases.

We now investigate how much we gain by adaptive antenna selection, as compared to random selection. If we draw a vertical line at 60 RF transceivers, we can see that for sixteen users and the linear array, we gain 6% with both DPC and ZF, while for the cylindrical array, we gain 14% and 17% with DPC and ZF, respectively. For forty users and the linear array, we gain 4% with both DPC and ZF, while for the cylindrical array, we gain 16% and 50% with DPC and ZF, respectively. With more users, we do not gain much by doing adaptive antenna selection for the linear array, however, for the cylindrical array, antenna selection helps significantly in improving the performance. With sixteen users, to reach 90% of full MIMO performance, the linear array needs more than 80 RF transceivers, while the cylindrical array needs more than 70. With forty users, 90 and 80 RF transceivers are needed for the linear and cylindrical arrays, respectively. Therefore, in the worst case, i.e., the linear array serving forty users, we can still switch off up to 40 RF transceivers.

In Fig. 7, we also observe that with adaptive antenna selection, the cylindrical array outperforms the linear array marginally for relatively small numbers of active RF transceivers, although linear array has better average performance in the case of random selection. With sixteen users, the cylindrical array achieves higher DPC capacity when less than 80 RF transceivers are switched on, while with forty users, the cylindrical array performs better with 40-60 active transceivers. Then, as the number of active transceivers increases, the linear array becomes more and more superior. The linear array can significantly gain from its high angular resolution, while the cylindrical array cannot.

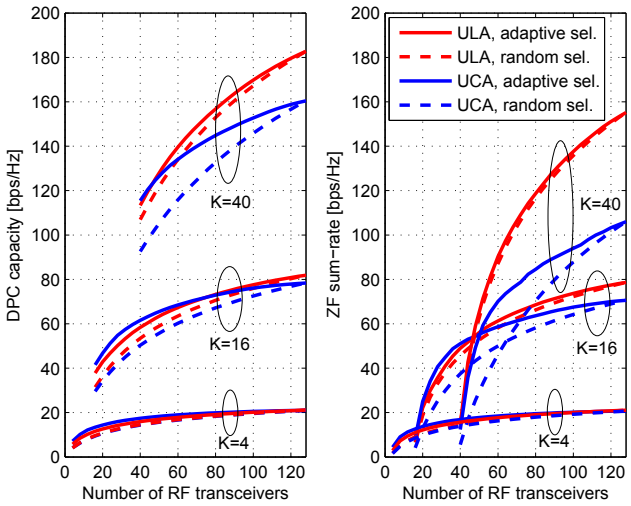

Figure 7: Performance of adaptive antenna selection using the convex-optimization scheme, as compared to performance of random selection, when four users are distributed at MS 5-8, and sixteen and forty users are distributed at MS 1-8. "ULA" and "UCA" stand for uniform linear array and uniform cylindrical array, respectively.

This can be clearly seen in the case of 40 users, where the linear array has much higher DPC capacity and ZF sum-rate than the cylindrical array. These observations indicate that the compact cylindrical array can perform better for relatively small number of users, while for larger number of users, a physically large array is preferable. The explanation is that for relatively small numbers of well-separated users and active antennas, the received SNRs at the users are more important for the performance than user channel decorrelation. Hence, we gain by selecting the antennas with high channel gains on the cylindrical array, pointing in the "right" directions. This effect is even more pronounced at very low SNRs. However, for relatively large numbers of users and active antennas, or at high SNRs, decorrelation of user channels becomes more important for the performance than the received SNRs. In this case, we need the high angular resolution provided by the linear array to spatially separate the users.

From the above investigations for different propagation conditions and different number of users, we see that quite many RF transceivers can be switched

Table 1: The performance gain by performing antenna selection, as compared to random selection.

No. of users	Scenario	Performance gain[1]	
		Linear array	Cylindrical array
4	Co-located, LOS	11-18%	>30%
	Far apart, NLOS	10%	20%
16	Mixed[2]	6%	14-17%
40	Mixed[2]	4%	16-50%

[1] The performance gain in terms of DPC and ZF sum-rates are at 40 RF transceivers for 4 users, and at 60 transceivers for 16 and 40 users.
[2] "Mixed" means that among the 16 or 40 users some are co-located at the same site, while users at different sites have large spacing. Half of the users are in LOS and half are in NLOS.

Table 2: The required number of RF transceivers to achieve 90% of full MIMO performance, with the convex-optimization selection scheme.

No. of users	Scenario	No. of RF transceivers	
		Linear array	Cylindrical array
4	Co-located, LOS	70	50-60
	Far apart, NLOS	80	60
16	Mixed[1]	80	70
40	Mixed[1]	90	80

[1] "Mixed" means that among the 16 or 40 users some are co-located at the same site, while users at different sites have large spacing. Half of the users are in LOS and half are in NLOS.

off to save energy consumption and simplify massive MIMO systems, even when serving a relatively large number of users. Table 1 and Table 2 summarize the performance gain of adaptive antenna selection and the required number of RF transceivers to achieve 90% of full MIMO performance. Next, we use these antenna selection results based on convex optimization as a benchmark, and evaluate how well the simple power-based selection scheme performs.

6.2 Performance of Power-Based Antenna Selection

For spatial multiplexing in multi-user MIMO systems, the goal is to have separated data streams to different users, it is thus not optimal to use the signals from two highly-correlated antennas, even if both have high SNRs. To obtain optimal antenna combinations, there is a trade off between antenna channel correlation and SNR, as what is done in the near-optimal convex-optimization selection scheme. In the power-based selection scheme, antenna correlation is not considered. The performance of this simple scheme thus depends on whether the antenna channels are highly correlated or not. In the scenario

where users are co-located with LOS, the correlation between antenna channels are higher, as compared to the NLOS scenario with well-separated users. We therefore expect the power-based scheme to work better in the latter case.

In Fig. 8, we show the performance loss by using the power-based selection scheme, relative to the performance of the convex-optimization scheme, in the two scenarios with four users, respectively. In the figure the vertical axis is the performance loss in DPC capacity or ZF sum-rate, and 100% loss means that the power-based scheme gives zero capacity/sum-rate, while a small loss, e.g., below 1%, indicates that the power-based scheme performs very close to the convex-optimization scheme. For co-located users with LOS, the performance losses in both DPC capacity and ZF sum-rate are quite high, when the number of RF transceivers is relatively small. However, the performance losses decrease as more RF transceivers are switched on. At around 70 RF transceivers, for both the linear and cylindrical arrays, the loss in DPC capacity goes below 1%. More RF transceivers, i.e., 90 have to be switched on to reduce the ZF sum-rate loss below 1%, for both arrays. For well-separated users with NLOS, as expected, the performance loss by using power-based scheme is much smaller, compared with the previous scenario. Already at 20 RF transceivers, the loss is below 1% in both DPC capacity and ZF sum-rate.

To better understand how the power-based scheme compares to the convex-optimization scheme, we compare the selected antenna indices when using the two schemes. Note that the selected antenna indices are presented for a single coherence interval, and the indices may change over time due to fading. The comparison is shown in Fig. 9 for both arrays, in the more "difficult" scenario where the four users are co-located with LOS. We can see why the power-based scheme performs worse for smaller number of active transceivers. With less than 60 RF transceivers, the antenna indices selected by the two schemes are quite distinct, for both arrays. With more RF transceivers, the difference becomes smaller and smaller, and eventually vanishes when all antennas are used.

We first focus on the differences on the linear array. Note that the shape of the selected antenna indices by the power-based scheme is similar to the power variation over the array shown in Fig. 1(c) where one user is at MS 2. The antennas at indices about 1-10, 40-50 and 80-110 are favored by the power-based scheme, due to the power contribution from the LOS component and the significant scatterers, as shown in Fig. 1(a). With about 20 to 60 active transceivers, the power-based scheme selects the neighboring antennas at index about 80-110 that have relatively high channel gain, while the convex-optimization scheme avoids selecting those neighboring ones at the same time due to their highly correlated channels. The convex-optimization scheme trades off between antenna correlation and channel gain, and selects the antennas at index around 40

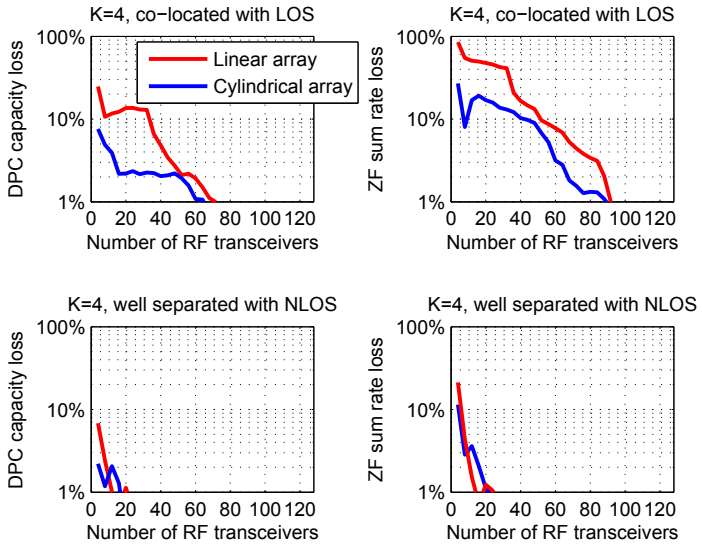

Figure 8: Performance loss of the power-based antenna selection scheme, relative to the near-optimal convex-optimization scheme, in the scenarios where four users are closely located at MS 2 with LOS conditions, and four users are well separated at MS 5-8 with NLOS conditions.

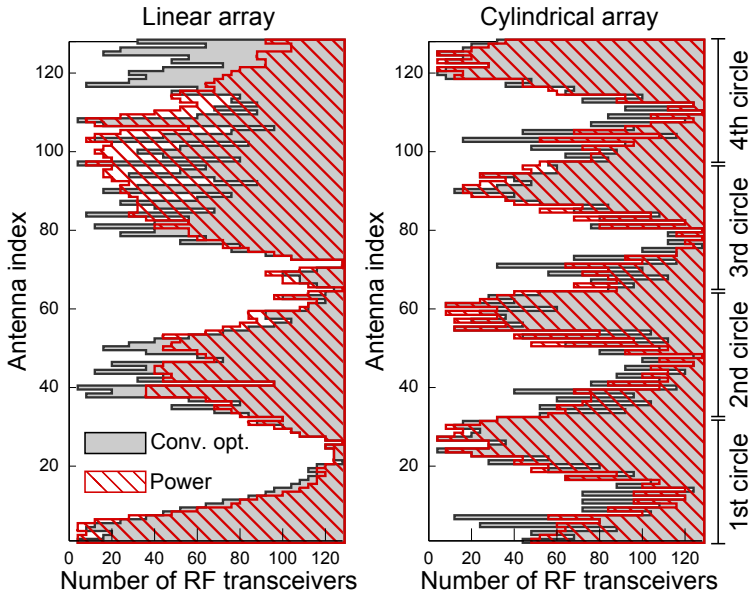

Figure 9: Comparison of the selected antenna indices using the convex-optimization selection scheme and the power-based selection scheme, as the number of active RF transceivers grows from 4 to 128. Four users are closely located at MS 2 and all have LOS conditions.

and 120 instead. Considering the influence on capacity from the two selections, capacity increases logarithmically with SNR and linearly with the number of orthogonal spatial dimensions. At a relatively high SNR, it is preferable to select uncorrelated channels, which contribute to all spatial dimensions. This effect can be observed in the performance loss of the power-based scheme with the linear array in Fig. 8. Above 30 RF transceivers the performance loss starts to decrease rapidly. This is because the power-based scheme starts to select antennas with index around 40 that have lower correlation with those at index 80-110, and the performance of the power-based scheme is boosted. We can also explain why ZF precoding needs more active transceivers to have a performance loss below 1%. ZF precoding is more sensitive to user interference than DPC, and the power-based scheme first selects antennas with high channel gain but high correlation, which is not preferable for reducing the user interference.

The antenna indices on the cylindrical array are ordered from the bottom circle (the 1st circle) to the top circle (the 4th circle) on the array. In each circle, the first antenna is pointing north (up in Fig. 4), and the antenna indices are ordered counter-clockwise. In Fig. 9, the selected antenna indices clearly show the four-circle structure, as well as the dual polarization since every other antennas are selected first. On each circle, the antennas pointing in the direction of MS 2, where the users are located, are selected first by the power-based scheme. This is clearly seen when there are about 20-50 RF chains. However, these antennas are closely spaced in elevation and thus experience higher channel correlation. This effect can be observed in Fig. 8 with the cylindrical array, where the performance loss decreases slowly between 20 and 50 RF transceivers. Above 50 RF transceivers, the antennas pointing in other directions and with lower correlations start to be selected, therefore, the performance loss drops quickly.

We move on to the cases of more users, shown in Fig. 10. For sixteen users and both arrays, we need to switch on 60 transceivers to make the performance loss below 1%, with DPC. With ZF, more than 80 transceivers are needed. The fluctuations in the performance loss for the linear array can be explained by the fact that above 60 RF chains the power-based scheme starts to select antennas with lower correlations, thus the performance loss drops quickly then. Moving up to forty users, an even larger number of transceivers has to be switched on. With the linear array, about 70 and 90 transceivers can make the performance loss below 1% in DPC capacity and ZF sum-rate, respectively. With the cylindrical array, up to 100 transceivers are needed with DPC, while 120 are needed with ZF precoding. This indicates that we need almost all the transceivers with the cylindrical array, for forty users, when using ZF. If we accept a bit lower sum-rate by the power-based selection scheme, e.g., allowing 5% loss, we can reduce the required number of transceivers to 100.

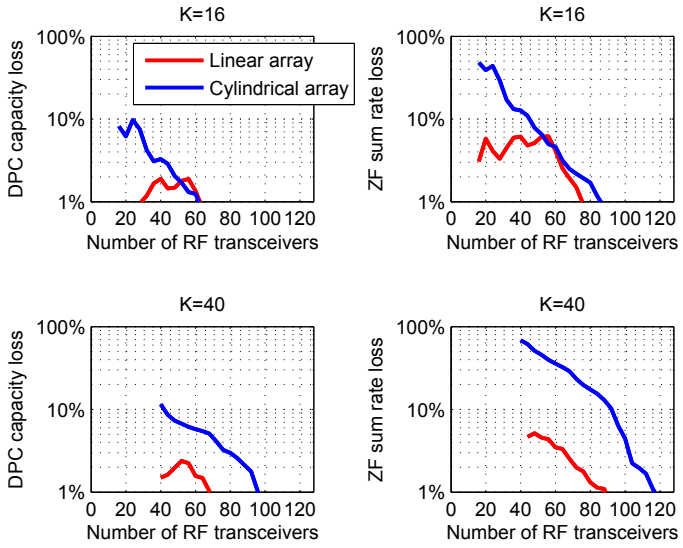

Figure 10: Performance loss of the power-based antenna selection scheme, relative to the near-optimal convex-optimization scheme, in the cases of sixteen and forty users.

Table 3: The required number of RF transceivers, with the simple power-based selection scheme and practical ZF precoding.

No. of users	Scenario	No. of RF transceivers	
		Linear array	Cylindrical array
4	Co-located, LOS	90	90
	Far apart, NLOS	80	60
16	Mixed[1]	80	80
40	Mixed[1]	90	120

[1] "Mixed" means that among the 16 or 40 users some are co-located at the same site, while users at different sites have large spacing. Half of the users are in LOS and half are in NLOS.

In Fig. 11, we show the difference in antenna indices selected by the two schemes, when there are 40 users. Again, the selected antenna indices are presented for a single coherence interval. For the linear array, the power-based scheme selects the antennas at index 1-60 due to high channel gain, while the convex-optimization scheme selects some antennas at index around 100 instead so that high antenna correlation can be avoided. When more than 70 transceivers are switched on, the power-based scheme starts to select antennas at index around 100, the performance gap between the two schemes drops below 1%, as shown in Fig. 10.

For the cylindrical array, the difference in the selected antenna indices is significant. The power-based scheme first selects antennas facing the user directions on each circle, however, those antennas have high correlation due to their small separation in both azimuth and elevation. The convex-optimization scheme tries to split them and selects antennas on the 1st and 4th circles instead, although some of the antennas are not pointing in the user directions. Due to the large number of users in this case, the power-based scheme needs more antennas to spatially separate the users and achieve performance close to the convex-optimization scheme, especially with ZF.

From all above observations, the power-based selection scheme gives very competitive results. Only in those "difficult" scenarios, such as closely-spaced users with LOS, and a relatively high number of users served by the cylindrical array, we need more antennas and transceivers to achieve performance close to the convex-optimization scheme. To summarize, Table 3 lists the number of required RF transceivers that achieves 90% of full MIMO performance, when using the simple power-based selection scheme and practical ZF precoding. From there, we see that generally a large number of RF transceivers can be switched off. This opens up an opportunity to apply this simple antenna selection scheme in massive MIMO.

The impact of SNR on antenna selection should be mentioned here. At very

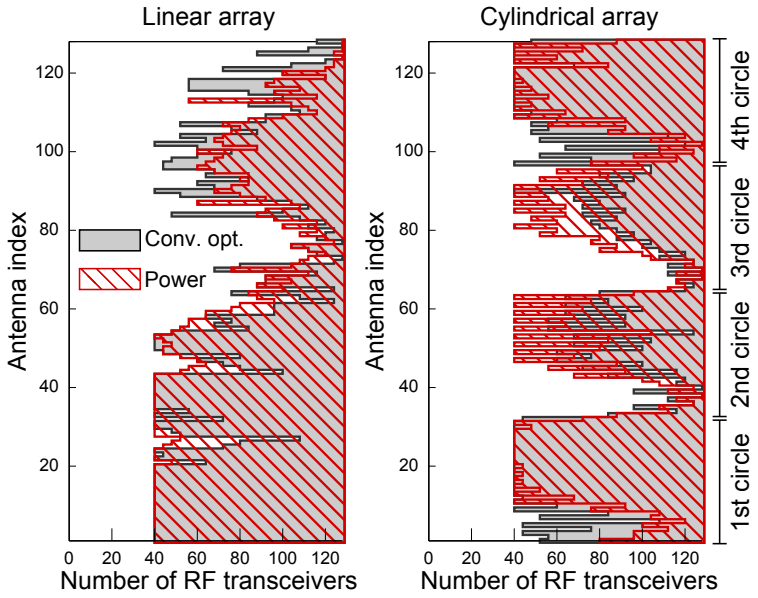

Figure 11: Comparison of the selected antenna indices using the convex-optimization selection scheme and the power-based selection scheme, as the number of active RF transceivers grows from 40 to 128. Forty users are distributed at MS 1-8.

low SNRs, it is more preferable to select antennas with high channel gains so that array gain can be achieved to boost the capacity, while at high SNRs, better user separation is more important for spatial multiplexing. Therefore, more RF transceivers should be switched on at very low SNRs than at higher SNRs. However, considering hardware power consumption, more active transceivers may decrease the overall energy efficiency of massive MIMO. It would be interesting to measure hardware power consumption at the base station, and investigate optimal amount of transmit power and optimal number of active transceivers that maximizes energy efficiency; however this has to be left for future work.

7 Summary and Conclusions

Unlike the situation in i.i.d. Rayleigh channels, where all antennas contribute equally, in real propagation channels, large-scale fading over the arrays or differences in antenna patterns, makes some antennas contribute more than others. Using channels measured at 2.6 GHz with a linear array with omni-directional elements and a cylindrical array with patch elements, we have illustrated that a significant performance gain can be achieved by performing adaptive antenna selection, as compared to random selection. A substantial number of RF transceiver chains can be turned off without a significant performance loss. Antenna selection based on a convex-optimization scheme gives near-optimal performance, however, a very simple selection scheme that is only based on received signal power measurements at each antenna also gives very competitive results.

The overall conclusion from our work is that antenna selection may be effectively used to reduce the implementation complexity, cost and hardware energy consumption of massive MIMO systems. The difference in characteristics between theoretical i.i.d. Rayleigh and real propagation channels also underlines the importance of developing new channel models for massive MIMO.

References

[1] T. L. Marzetta, "Noncooperative cellular wireless with unlimited numbers of base station antennas," *IEEE Transactions on Wireless Communications*, vol. 9, no. 11, pp. 3590–3600, Nov. 2010.

[2] F. Rusek, D. Persson, B. K. Lau, E. G. Larsson, T. L. Marzetta, O. Edfors, and F. Tufvesson, "Scaling up MIMO: Opportunities and challenges with

very large arrays," *IEEE Signal Processing Magazine*, vol. 30, no. 1, pp. 40–60, Jan. 2013.

[3] E. Larsson, O. Edfors, F. Tufvesson, and T. L. Marzetta, "Massive MIMO for next generation wireless systems," *IEEE Communications Magazine*, vol. 52, no. 2, pp. 186–195, Feb. 2014.

[4] L. Lu, G. Li, A. Swindlehurst, A. Ashikhmin, and R. Zhang, "An overview of massive MIMO: Benefits and challenges," *IEEE Journal of Selected Topics in Signal Processing*, vol. 8, no. 5, pp. 742–758, Oct. 2014.

[5] T. L. Marzetta, "Massive MIMO: An introduction," *Bell Labs Technical Journal*, vol. 20, pp. 11–22, 2015.

[6] H. Q. Ngo, E. G. Larsson, and T. L. Marzetta, "Energy and spectral efficiency of very large multiuser MIMO systems," *IEEE Transactions on Communications*, vol. 61, no. 4, pp. 1436–1449, Apr. 2013.

[7] H. Huh, G. Caire, H. C. Papadopoulos, and S. A. Ramprashad, "Achieving "massive MIMO" spectral efficiency with a not-so-large number of antennas," *IEEE Transactions on Wireless Communications*, vol. 11, no. 9, pp. 3226–3239, Sept. 2012.

[8] C. Guthy, W. Utschick, and M. L. Honig, "Large system analysis of sum capacity in the Gaussian MIMO broadcast channel," *IEEE Journal on Selected Areas in Communications*, vol. 31, no. 2, pp. 149–159, Feb. 2013.

[9] E. Björnson, M. Kountouris, and M. Debbah, "Massive MIMO and small cells: Improving energy efficiency by optimal soft-cell coordination," in *Proc. International Conference on Telecommunications (ICT)*, May 2013.

[10] X. Gao, O. Edfors, F. Rusek, and F. Tufvesson, "Linear pre-coding performance in measured very-large MIMO channels," in *Proc. IEEE Vehicular Technology Conference (VTC Fall)*, Sept. 2011.

[11] H. Yang and T. L. Marzetta, "Performance of conjugate and zero-forcing beamforming in large-scale antenna systems," *IEEE Journal on Selected Areas in Communications*, vol. 31, no. 2, pp. 172–179, Feb. 2013.

[12] J. Hoydis, S. ten Brink, and M. Debbah, "Massive MIMO in the UL/DL of cellular networks: How many antennas do we need?" *IEEE Journal on Selected Areas in Communications*, vol. 31, no. 2, pp. 160–171, Feb. 2013.

[13] X. Gao, F. Tufvesson, O. Edfors, and F. Rusek, "Measured propagation characteristics for very-large MIMO at 2.6 GHz," in *Proc. Asilomar Conference on Signals, Systems, and Computers (ASILOMAR)*, Nov. 2012.

[14] X. Gao, O. Edfors, F. Rusek, and F. Tufvesson, "Massive MIMO performance evaluation based on measured propagation data," *IEEE Transactions on Wireless Communications*, vol. 14, no. 7, pp. 3899–3911, July 2015.

[15] J. Hoydis, C. Hoek, T. Wild, and S. ten Brink, "Channel measurements for large antenna arrays," in *Proc. International Symposium on Wireless Communication Systems (ISWCS)*, Aug. 2012.

[16] J. Flordelis, X. Gao, G. Dahman, F. Rusek, O. Edfors, and F. Tufvesson, "Spatial separation of closely-spaced users in measured massive multi-user MIMO channels," in *Proc. IEEE International Conference on Communications (ICC)*, June 2015.

[17] J. G. Andrews, S. Buzzi, W. Choi, S. V. Hanly, A. Lozano, A. C. K. Soong, and J. C. Zhang, "What will 5G be?" *IEEE Journal on Selected Areas in Communications*, vol. 32, no. 6, pp. 1065–1082, June 2014.

[18] C.-X. Wang, F. Haider, X. Gao, X.-H. You, Y. Yang, D. Yuan, H. Aggoune, H. Haas, S. Fletcher, and E. Hepsaydir, "Cellular architecture and key technologies for 5G wireless communication networks," *IEEE Communications Magazine*, vol. 52, no. 2, pp. 122–130, Feb. 2014.

[19] F. Boccardi, R. W. Heath, A. Lozano, T. L. Marzetta, and P. Popovski, "Five disruptive technology directions for 5G," *IEEE Communications Magazine*, vol. 52, no. 2, pp. 74–80, Feb. 2014.

[20] A. Osseiran, F. Boccardi, V. Braun, K. Kusume, P. Marsch, M. Maternia, O. Queseth, M. Schellmann, H. Schotten, H. Taoka, H. Tullberg, M. Uusitalo, B. Timus, and M. Fallgren, "Scenarios for 5G mobile and wireless communications: the vision of the METIS project," *IEEE Communications Magazine*, vol. 52, no. 5, pp. 26–35, May 2014.

[21] V. Jungnickel, K. Manolakis, W. Zirwas, B. Panzner, V. Braun, M. Lossow, M. Sternad, R. Apelfröjd, and T. Svensson, "The role of small cells, coordinated multipoint, and massive MIMO in 5G," *IEEE Communications Magazine*, vol. 52, no. 5, pp. 44–51, May 2014.

[22] J. Vieira, S. Malkowsky, K. Nieman, Z. Miers, N. Kundargi, L. Liu, I. Wong, V. Owall, O. Edfors, and F. Tufvesson, "A flexible 100-antenna testbed for massive MIMO," in *Proc. IEEE Global Communications Conference (GLOBECOM) Workshop on Massive MIMO: From Theory to Practice*, Dec. 2014.

[23] C. Shepard, H. Yu, N. Anand, E. Li, T. L. Marzetta, R. Yang, and L. Zhong, "Argos: Practical many-antenna base stations," in *Proc. Annual International Conference on Mobile Computing and Networking (MobiCom)*, 2012.

[24] C. Shepard, H. Yu, and L. Zhong, "ArgosV2: A flexible many-antenna research platform," in *Proc. Annual International Conference on Mobile Computing and Networking (MobiCom)*, 2013.

[25] H. Suzuki, R. Kendall, K. Anderson, A. Grancea, D. Humphrey, J. Pathikulangara, K. Bengston, J. Matthews, and C. Russell, "Highly spectrally efficient Ngara rural wireless broadband access demonstrator," in *Proc. International Symposium on Communications and Information Technologies (ISCIT)*, Oct. 2012.

[26] E. Björnson, J. Hoydis, M. Kountouris, and M. Debbah, "Massive MIMO systems with non-ideal hardware: Energy efficiency, estimation, and capacity limits," *IEEE Transactions on Information Theory*, vol. 60, no. 11, pp. 7112–7139, Nov. 2014.

[27] S. K. Mohammed, "Impact of transceiver power consumption on the energy efficiency of zero-forcing detector in massive MIMO systems," *IEEE Transactions on Communications*, vol. 62, no. 11, pp. 3874–3890, Nov. 2014.

[28] E. Björnson, L. Sanguinetti, J. Hoydis, and M. Debbah, "Optimal design of energy-efficient multi-user MIMO systems: Is massive MIMO the answer?" *IEEE Transactions on Wireless Communications*, vol. 14, no. 6, pp. 3059–3075, June 2015.

[29] W. Liu, S. Han, and C. Yang, "Is massive MIMO energy efficient?" May 2015, arXiv:1505.07187.

[30] X. Gao, F. Tufvesson, and O. Edfors, "Massive MIMO channels – measurements and models," in *Proc. Asilomar Conference on Signals, Systems, and Computers (ASILOMAR)*, Nov. 2013.

[31] X. Gao, M. Zhu, F. Rusek, F. Tufvesson, and O. Edfors, "Large antenna array and propagation environment interaction," in *Proc. Asilomar Conference on Signals, Systems, and Computers (ASILOMAR)*, Nov. 2014.

[32] X. Gao, F. Tufvesson, O. Edfors, and F. Rusek, "Channel behavior for very-large MIMO systems – initial characterization," in *COST IC1004*, Sept. 2012.

[33] *Requirements for Further Advancements for Evolved Universal Terrestrial Radio Access (E-UTRA) (LTE-Advanced)*, Mar. 2009.

[34] A. F. Molisch and M. Z. Win, "MIMO systems with antenna selection," *IEEE Microwave Magazine*, vol. 5, no. 1, pp. 46–56, Mar. 2004.

[35] A. F. Molisch, M. Z. Win, Yang-seok. Choi, and J. H. Winters, "Capacity of MIMO systems with antenna selection," *IEEE Transactions on Wireless Communications*, vol. 4, no. 4, pp. 1759–1772, July 2005.

[36] S. Sanayei and A. Nosratinia, "Antenna selection in MIMO systems," *IEEE Communications Magazine*, vol. 42, no. 10, pp. 68–73, Oct. 2004.

[37] ——, "Capacity of MIMO channels with antenna selection," *IEEE Transactions on Information Theory*, vol. 53, no. 11, pp. 4356–4362, Nov. 2007.

[38] T. Gucluoglu and T. M. Duman, "Performance analysis of transmit and receive antenna selection over flat fading channels," *IEEE Transactions on Wireless Communications*, vol. 7, no. 8, pp. 3056–3065, Aug. 2008.

[39] M. Sadek, A. Tarighat, and A. H. Sayed, "Active antenna selection in multiuser MIMO communications," *IEEE Transactions on Signal Processing*, vol. 55, no. 4, pp. 1498–1510, Apr. 2007.

[40] R. Chen, J. G. Andrews, and R. W. Heath, "Efficient transmit antenna selection for multiuser MIMO systems with block diagonalization," in *Proc. IEEE Global Communications Conference (GLOBECOM)*, Nov. 2007.

[41] M. Mohaisen and K. Chang, "On transmit antenna selection for multiuser MIMO systems with dirty paper coding," in *Proc. IEEE International Symposium on Personal, Indoor and Mobile Radio Communications (PIMRC)*, Sept. 2009.

[42] P.-H. Lin and S.-H. Tsai, "Performance analysis and algorithm designs for transmit antenna selection in linearly precoded multiuser MIMO systems," *IEEE Transactions on Vehicular Technology*, vol. 61, no. 4, pp. 1698–1708, May 2012.

[43] K. Dong, N. Prasad, X. Wang, and S. Zhu, "Adaptive antenna selection and Tx/Rx beamforming for large-scale MIMO systems in 60 GHz channels," *EURASIP Journal on Wireless Communications and Networking*, vol. 2011, no. 1, p. 59, Aug. 2011.

[44] T.-W. Ban and B. C. Jung, "A practical antenna selection technique in multiuser massive MIMO networks," *IEICE Transactions on Communications*, vol. E96-B, no. 11, pp. 2901–2905, Nov. 2013.

[45] J. P. Kermoal, L. Schumacher, K. I. Pedersen, P. E. Mogensen, and F. Frederiksen, "A stochastic MIMO radio channel model with experimental validation," *IEEE Journal on Selected Areas in Communications*, vol. 20, no. 6, pp. 1211–1226, Aug. 2002.

[46] M. Gkizeli and G. N. Karystinos, "Maximum-SNR antenna selection among a large number of transmit antennas," *IEEE Journal of Selected Topics in Signal Processing*, vol. 8, no. 5, pp. 891–901, Oct. 2014.

[47] M. Benmimoune, E. Driouch, W. Ajib, and D. Massicotte, "Joint transmit antenna selection and user scheduling for massive MIMO systems," in *Proc. IEEE Wireless Communications and Networking Conference (WCNC)*, Mar. 2015.

[48] R. Kataoka, K. Nishimori, N. Tran, and T. Imai, "Performance evaluation by antenna selection using real propagation channel on massive MIMO," in *Proc. IEEE International Workshop on Electromagnetics (iWEM)*, Aug. 2014.

[49] X. Gao, O. Edfors, J. Liu, and F. Tufvesson, "Antenna selection in measured massive MIMO channels using convex optimization," in *Proc. IEEE Global Communications Conference (GLOBECOM) Workshop on Emerging Technologies for LTE-Advanced and Beyond-4G*, Dec. 2013.

[50] A. Dua, K. Medepalli, and A. J. Paulraj, "Receive antenna selection in MIMO systems using convex optimization," *IEEE Transactions on Wireless Communications*, vol. 5, no. 9, pp. 2353–2357, Sept. 2006.

[51] S. Mahboob, R. Ruby, and V. C. M. Leung, "Transmit antenna selection for downlink transmission in a massively distributed antenna system using convex optimization," in *Proc. International Conference on Broadband, Wireless Computing, Communication and Applications (BWCCA)*, Nov. 2012.

[52] H. Q. Ngo, E. G. Larsson, and T. L. Marzetta, "Aspects of favorable propagation in massive MIMO," in *Proc. European Signal Processing Conference (EUSIPCO)*, Sept. 2014.

[53] S. Vishwanath, N. Jindal, and A. Goldsmith, "Duality, achievable rates, and sum-rate capacity of Gaussian MIMO broadcast channels," *IEEE Transactions on Information Theory*, vol. 49, no. 10, pp. 2658–2668, Oct. 2003.

[54] M. Costa, "Writing on dirty paper," *IEEE Transactions on Information Theory*, vol. 29, no. 3, pp. 439–441, 1983.

[55] N. Jindal, W. Rhee, S. Vishwanath, S. A. Jafar, and A. Goldsmith, "Sum power iterative water-filling for multi-antenna Gaussian broadcast channels," *IEEE Transactions on Information Theory*, vol. 51, no. 4, pp. 1570–1580, Apr. 2005.

[56] E. Björnson, E. G. Larsson, and T. L. Marzetta, "Massive MIMO: 10 myths and one grand question," Mar. 2015, arXiv:1503.06854.

[57] A. Wiesel, Y. C. Eldar, and S. Shamai, "Zero-forcing precoding and generalized inverses," *IEEE Transactions on Signal Processing*, vol. 56, no. 9, pp. 4409–4418, Sept. 2008.

[58] T. Cover and J. Thomas, *Elements of Information Theory.* Wiley, New York, 1991.

[59] S. Boyd and L. Vandenberghe, *Convex Optimization.* Cambridge University Press, 2004.

[60] A. Molisch, *Wireless Communications.* Wiley-IEEE Press, 2005.